SINGLE-PHASE HEAT TRANSFER AND PRESSURE DROP OF WATER COOLED AT A CONSTANT WALL TEMPERATURE INSIDE HORIZONTAL CIRCULAR SMOOTH AND ENHANCED TUBES WITH DIFFERENT INLET CONFIGURATIONS IN THE TRANSITIONAL FLOW REGIME

Jonathan Albert Olivier

University of Pretoria

Department of Mechanical and
Aeronautical Engineering

UNIVERSITEIT VAN PRETORIA
UNIVERSITY OF PRETORIA
YUNIBESITHI YA PRETORIA

Submitted in partial fulfilment of the
requirements for the degree

Philosophiae Doctor (Mechanical Engineering)

in the Faculty of Engineering,
Built Environment and Information Technology,
University of Pretoria, Pretoria,
South Africa

August 2009

Promoters:
Prof Josua P. Meyer
Prof Leon Liebenberg

draft date: August 2009.

Typeset by the author with the LaTeX 2ε Documentation System.

To God,
my wife, Talita,
and children, Jean and Adèle

Abstract

It is common practice to design water chiller units and heat exchangers in such a way that they do not operate within the transition region. This is mainly due to the perceived chaotic behaviour as well as the paucity of information in this region. Due to design constraints or change of operating conditions, however, exchangers are often forced to operate in this region. This is even worse for enhanced tubes as much less information within this region is available. It is also well known that the entrance has an influence on where transition occurs, adding to the woes of available information.

The purpose of this study is thus to obtain heat transfer and friction factor data in the transition region of fully developed and developing flows inside smooth and enhanced tubes, using water as the working fluid, and to develop correlations from these results. The use of different inlets, tube diameters and enhanced tubes was also investigated with regards to the commencement of transition.

Heat transfer and pressure drop data were obtained from six different types of tubes with diameters of 15.88 mm (5/8″) and 19.02 mm (3/4″). Low fin enhanced tubes with a fin height to diameter ratio of 0.4 and helix angles of 18° and 27° were investigated. Heat transfer was obtained by means of an in-tube heat exchanger with the cooling of water being used as the test fluid. Reynolds numbers ranged between 1 000 and 20 000 while Prandtl numbers were in the order of 4 to 6. Uncertainties in heat transfer coefficient and friction factors were on average below 2.5% and 10% respectively.

Adiabatic friction factor results showed that the use of different inlets influenced the commencement of transition. The smoother the inlet profile the more transition was delayed, confirming previous work done. The effect of increasing tube diameters had a slight delay in transition. Enhanced tubes caused transition to occur at lower Reynolds numbers which was accounted for by the fin height and not the helix angle. Heat transfer results showed that transition occurred at approximately the same Reynolds number for all the different inlets and enhanced tubes. This was attributed to the secondary flow forces influencing the growing hydrodynamic boundary layer. These secondary flow forces also influenced the laminar heat transfer and diabatic friction factors with both these parameters being higher. Turbulent enhanced tube heat transfer results were higher than those of the smooth tube, with the tube with the greatest helix angle showing the greatest increase. Correlations were developed for all the tubes and their inlets and predicted all the data on average to within 3%.

UNIVERSITEIT VAN PRETORIA
UNIVERSITY OF PRETORIA
YUNIBESITHI YA PRETORIA

Acknowledgements

I would like to acknowledge the following people and institutions for their help and support:

- Professor Josua Meyer for his ongoing support and belief in my abilities. Thank you for being there when the times were tough. You were a true mentor to me and you taught me most of what I know about experimental systems today, especially about being patient.
- Professor Leon Liebenberg for your moral support. At times it was really helpful and it was much appreciated.
- Professor Afshin Ghajar from Oklahoma State University, Stillwater, OK. Your comments and recommendations made me rethink some preconceived ideas and were invaluable.
- Professor John Thome from the École Polytechnique Fédérale de Lausanne, Switzerland. Your comments and support were much appreciated.
- To "The American Society of Heating, Refrigerating and Air-Conditioning Engineers" (ASHRAE) who were the main sponsors of this project. This document also forms part of the ASHRAE-sponsored project 1280-RP.
- My wife Talita for all your ongoing support throughout the years. You were always supportive of my work and I thank you for all your patience.
- To my Father, Brother and Father-in-law. Thanks for the great discussions and support during this period. It helped me put things into perspective.
- The following institutions and organisations are also thanked for their financial support:
  - University of Pretoria
  - The Technology and Human Resources for Industry Programme (THRIP) - AL631
  - Tertiary Education Support Programme (TESP) from Eskom
  - National Research Foundation
  - SANERI and the Centre for Renewable and Sustainable Energy Studies, University of Stellenbosch
  - National Aerospace Centre of Excellence, University of the Witwatersrand
  - EEDSSM Hub, University of Pretoria
- To the technical and support staff: Jan Brand, Tersia Evans, Danie Gouws, Willem Ras and Willie Vos. Your help and advice were invaluable.

Contents

List of Figures

List of Tables

Nomenclature

A	Area	m^2
A_c	Actual tube flow cross-sectional area	m^2
A_{ce}	Enhanced tube cross-sectional area	m^2
A_{cn}	Nominal cross-sectional area based on root diamater	m^2
A_{core}	Core flow area $(A_n\,(1-2e/D_r)^2)$	m^2
A_{cs}	Smooth tube cross-sectional area	m^2
A_{fin}	Inner-fin flow area $(A_c - A_{core})$	m^2
A_i	Inner-tube inner heat transfer area	m^2
A_o	Inner-tube outer heat transfer area	m^2
A_{i_c}	Inner-tube cross-sectional area	m^2
$a_{1...2}$	Constants	
amd	Arithmetic mean deviation	
amd_{max}	Maximum arithmetic mean deviation	
$c_{1...6}$	Constants	
c_{pi}	Specific heat of inner-tube fluid	J/kgK
D	Diameter	m
D_h	Hydraulic diameter	m
D_{ho}	Annulus hydraulic diameter	m

D_i	Tube inner-wall diameter	m
D_o	Tube outer-wall diameter	m
D_r	Root diameter	m
e	Fin, dimple or roughness height	m
eb	Energy balance	
h_{iin}	Inner-tube inlet enthalpy	J/kg
h_{iout}	Inner-tube outlet enthalpy	J/kg
h_{oin}	Annulus inlet enthalpy	J/kg
h_{oout}	Annulus outlet enthalpy	J/kg
$\Im$	Term used in Eq. (3.21)	
K_∞	Excess pressure drop in hydrodynamic developed region	
k_{cu}	Thermal conductivity of copper tube	W/mK
k_o	Thermal conductivity of annulus fluid	W/mK
L	Tube length	m
$L_{\Delta p}$	Length between pressure taps	m
L_{eh}	Thermal entrance length	m
L_{hx}	Heat transfer length	m
l_c	Characteristic length	m
l_{csw}	Characteristic length modified for swirling flow	m
$\dot{m}_i$	Mass flow rate within inner tube	kg/s
$\dot{m}_o$	Mass flow rate within annulus	kg/s
N	Number of data points, Eq. (4.5) and (4.6)	
N_t	Number of tubes	
n	Number of fins / Slope of Nu vs Re curve in turbulent regime, Eq. (2.1)	
P	Perimeter	m

P_{pe}	Pumping power for an enhanced tube	W
P_{ps}	Pumping power for a smooth tube	W
p	Pressure	Pa
p_f	Fin pitch	m
$\dot{Q}_i$	Inner-tube heat transfer rate	W
$\dot{Q}_o$	Annulus heat transfer rate	W
$R_{1...5}$	Performance enhancement criteria	
R_w	Tube-wall thermal resistance	K/W
rms	Root mean square	
s	Average fin thickness	m
$\bar{T}_{Cu}$	Mean temperature of copper tube	K
$\bar{T}_i$	Mean inner-tube fluid temperature	°C
$\bar{T}_i(x)$	Local inner-tube fluid temperature	°C
$\bar{T}_{iin}$	Inner-tube inlet temperature	°C
$\bar{T}_{iout}$	Inner-tube outlet temperature	°C
T_{lmtd}	Logarithmic mean temperature difference	°C
$\bar{T}_{oin}$	Annulus inlet temperature	°C
$\bar{T}_{oout}$	Annulus outlet temperature	°C
$\bar{T}_{wi}$	Mean inner-tube inner-wall temperature	°C
$\bar{T}_{wo}$	Mean inner-tube outer-wall temperature	°C
$\bar{T}_{woo}$	Mean annulus outer-wall temperature	°C
U	Overall heat transfer coefficient	W/m^{2}K
u	Average fluid velocity	m/s
u_e	Enhanced tube average fluid velocity	m/s
u_i	Inner-tube average fluid velocity	m/s

u_s	Smooth tube average fluid velocity	m/s
x	Axial distance	m

Dimensionless Groups

f	Fanning friction factor
f_{app}	Apparent Fanning friction factor
f_e	Enhanced tube Fanning friction factor
f_{exp}	Experimental Fanning friction factor
f_L	Laminar Fanning friction factor
f_{Cr_L}	Laminar Fanning friction factor at the critical Reynolds number
f_{Le}	Enhanced tube laminar Fanning friction factor
f_{pred}	Predicted Fanning friction factor
f_s	Smooth tube Fanning friction factor
f_T	Turbulent Fanning friction factor
f_{Te}	Enhanced tube turbulent Fanning friction factor
f_{Tle}	Enhanced tube Fanning friction factor for lower turbulent Reynolds numbers
f_t	Transition Fanning friction factor
f_{Tt}	Turbulent-transition Fanning friction factor
f_{te}	Enhanced tube transition Fanning friction factor
f_pRe	Constant value of fRe according to the Poiseuille relation
Gr	Grashof number
Gr_f	Grashof number calculated at average of bulk and wall temperature
Gz	Graetz number
j	Colburn j-factor, $j = StPr^{2/3} = f/2\phi_w$
Nu	Nusselt number of inner tube
Nu_0^0	Nusselt number when $RePr \to 0$ in Eq. (2.4)

Nu_e	Enhanced tube Nusselt number
Nu_{exp}	Nusselt number from experimental results
Nu_∞^∞	Nusselt number for large Re and large Pr in Eq. (2.4)
Nu_∞^0	Nusselt number for large Re and low Pr in Eq. (2.4)
Nu_L	Laminar Nusselt number
Nu_{Cr_L}	Laminar Nusselt number at the critical Reynolds number
Nu_{pred}	Predicted Nusselt number
Nu_s	Smooth tube Nusselt number
Nu_T	Turbulent Nusselt number
Nu_t	Transition Nusselt number
Nu_{Te}	Turbulent Nusselt number for the enhanced tubes
Nu_{te}	Enhanced tube transition Nusselt number
$Nu_{Te_{38}}$	Turbulent Nusselt number for the enhanced tubes for Reynolds numbers between 3 000 and 8 000
Nu_{Tt}	Turbulent-transition Nusselt number
Pr	Prandtl number of inner tube
Pr_f	Prandtl number calculated at average of bulk and wall temperature
Pr_o	Annulus Prandtl number
Ra	Rayleigh number
Re	Reynolds number of inner tube
Re_{Cr}	Critical Reynolds number
Re_{Cr_L}	Laminar critical Reynolds number
Re_e	Enhanced tube Reynolds number
Re_o	Annulus Reynolds number
Re_s	Smooth tube Reynolds number

St	Stanton number	
St_{10}	Stanton number evaluated at $Re = 10\ 000$, Eq. (2.1)	
St_{Cr}	Stanton number at critical Reynolds number	
z^+	Dimensionless distance as used in Eq. (3.20) and (3.21)	

Greek Symbols

α_e	Enhanced tube heat transfer coefficient	W/m^2K
α_i	Inner-tube heat transfer coefficient	W/m^2K
α_o	Annulus heat transfer coefficient	W/m^2K
α_s	Smooth tube heat transfer coefficient	W/m^2K
β	Helix angle	$^\circ$
γ	Fin apex angle	$^\circ$
Δ	Used in Eq. (3.21)	
ε	As defined by Eq. (2.8)	
μ	Dynamic viscosity of the fluid in the inner tube	Pa.s
μ_o	Dynamic viscosity of annulus fluid	Pa.s
μ_w	Dynamic viscosity at tube wall	Pa.s
ν	Kinematic viscosity	m^2/s
ρ	Density	kg/m^3
ρ_i	Inner-tube fluid density	kg/m^3
σ	Standard deviation	
σ_α	Standard deviation of heat transfer coefficient	
σ_f	Standard deviation of Fanning friction factor	
σ_T	Standard deviation of temperature measurement	
τ_w	Shear stress of fluid at the tube wall	Pa
$\phi\,(Re)$	Function of Reynolds number as defined by Eq. (2.3)	

ϕ_w	Function of flow conditions, geometry and Prandtl number, Eq. (4.9)
χ	Defined as $(x/D)/Re$ in Eq. (5.1)

Chapter 1

Introduction

> The most exciting phrase to hear in science, the one that heralds new discoveries, is not 'Eureka!' (I found it!) but 'That's funny...'.
>
> *Isaac Asimov (1920 - 1992)*

1.1 Introduction

Throughout the years extensive studies were performed on fluids flowing within tubes. These studies started as far back as 1883 when Osborne Reynolds introduced a dye flowing in water to distinguish between two distinct regimes he called "direct" and "sinuous" (Reynolds, 1883) or, in modern terms, laminar and turbulent regimes. It was this groundbreaking work which led other researchers to pursue and demystify the true nature of these flow regimes.

In 1839 and 1840, Hagen and Poiseuille, respectively, studied hydrodynamically fully developed viscous/laminar isothermal flows within tubes (White, 1991). They showed that the pressure drop within a tube is directly proportional to the shear stress at the tube wall and inversely proportional to the diameter of the tube. This shear stress is non-dimensionalised with respect to the dynamic pressure to obtain a friction factor, one known as the Fanning friction factor and the other the Darcy friction factor. These friction factors are widely used in the design of piping systems as well as heat exchangers to determine the pumping power consumption required for the system.

Friction factors for pipe flow can be found on a Moody chart, relating friction factors with Reynolds numbers. The chart is divided into four regions; laminar, critical, transitional and turbulent regimes. The laminar regime extends up to a Reynolds number of somewhere between 2 000 and 3 000 within which there is a strong discontinuity at a Reynolds number of approximately 2 200. The discontinuity lies in the critical zone, which is defined up to a Reynolds number of approximately 6 000, after which it moves naturally into the transition zone and then into the fully turbulent region. The discontinuity, though, is a major problem

for designers due to the paucity of data.

An extensive amount of research work has been done regarding heat transfer in laminar flow. Typical results obtained in most heat transfer texts are those for a uniform wall heat flux and for a constant wall temperature boundary condition. For a uniform heat flux boundary condition, it can be shown that the Nusselt number reaches a constant value of 4.364, while for a constant wall temperature boundary condition, a value of 3.662 is obtained (Mills, 1999).

These values are, however, only obtained for the very special case where the flow is fully developed (hydrodynamically as well as thermally) and any buoyancy-induced secondary flows are neglected. In 1883, Graetz solved the problem for thermally developing low Prandtl number flows and in 1885 for high Prandtl number flows with the solutions being in the form of an infinite series (White, 1991). Studies on different laminar flow problems such as combined hydrodynamically and thermally developing flows for different boundary conditions and different tube geometries are given in elaborate detail by Shah and London (1978). Numerous research projects in the laminar regime have been undertaken pertaining to mixed convection (combined forced and natural convection)by Kern and Othmer (1943), Jackson *et al.* (1961), Oliver (1962), Petukhov *et al.* (1969) and Shannon and Depew (1969) are to name but a few.

Turbulent flow research within tubes has also enjoyed substantial attention. The first researchers to come up with a practical correlation were Dittus and Boelter (1985), who in 1930 stated that the heat transfer coefficient is proportional to, and a strong function of, the Reynolds number, as well as the Prandtl number to a lesser degree. By making use of the Reynolds analogy, Colburn (1933) generated a very similar result. Research into turbulent flow heat transfer within tubes is of such an extent that its effects can be predicted with fair accuracy.

Transition from laminar to turbulent flow inside pipes is accepted in most textbooks to occur at a Reynolds number of approximately 2 100. However, many researchers have shown that this critical value varies. Osborne Reynolds' experiments showed this value to be between a Reynolds number of 2 000 and 40 000, depending on the smoothness of the tube and the inlet, while Pfenniger was able to reach values as high as 100 000 Mullin and Peixinho (2006). Tatsumi (1952) showed, by means of a stability analysis of the boundary layer, that critical Reynolds numbers of nearly 10 000 can be reached.

From the 1990's up to the present date, Ghajar and co-workers at Oklahoma State University have been doing extensive research into transitional flow inside horizontal smooth tubes. Their extensive work can be found in the following citations: Ghajar and Zurigat (1990), Ghajar and Tam (1991), Ghajar and Madon (1992), Ghajar and Tam (1994), Ghajar and Tam (1995), Tam and Ghajar (1997), Tam and Ghajar (1998), Ghajar *et al.* (2004), Tam and Ghajar (2006) and Tam *et al.* (2008). Their experimental database covered a Reynolds number range of approximately 500 to 50 000 with water and a mixture of water and ethylene glycol as the working fluid. Their main focus was to investigate the effect different inlet configurations had on heat transfer and pressure drop with regard to transition. They found that the different inlet configurations influenced the commencement of transition; the smoother the inlet the more transition was delayed.

The effect of heating also had an effect on the laminar friction factors; the greater the

heating rate the greater the increase in friction factor was for a given Reynolds number. This was attributed to the increase in the strength of the buoyancy induced secondary flows within the tube. These secondary flow effects also accounted for an increase in laminar heat transfer due to the increase in mixing it induces.

To increase the performance of heat exchangers, augmentation techniques are implemented. Two main types of techniques are employed namely passive and active techniques. A detailed description of these techniques is given by Webb (1994). Active techniques are listed as an augmentation method by which external energy is added to enhance the heat transfer. An example of such a technique is the vibration of tubes. Passive techniques have more to do with changing the heat transfer surface in such a way that it enhances the heat transfer. Many examples of such techniques exist, namely finned tubes (increase the heat transfer surface area), twisted tape inserts (generate a swirl flow) and helical micro-fin tubes (capillary forces cause thin film layer during two-phase flow). Research in this field is quite extensive with regard to laminar and turbulent flow. Table 1.1 lists some of the research performed in these regimes. The effect of augmentation on transition have also been studied by a few researchers, also listed in the table.

Extensive augmentation work in the turbulent regime was performed between Reynolds numbers of 2 000 and 150 000 mostly with water, although some data is on air and glycol-water mixtures. Most of the research was performed by heating the fluid, although there are some researchers who performed the experiments on the cooling of the liquid. The augmentation techniques used were internally finned tubes, some with single-helix ridging, others with multi-helix ridging, micro-finned tubes, V-nozzle turbulators and finned inserts.

For augmentation in the laminar flow regime, most of the experiments were conducted with twisted tape inserts with only a few on micro-finned tubes. Reynolds numbers ranged between 15 and 30 000 with water and oil being the main fluids. These experiments were also mostly conducted on the heating of the fluid with only a few performing heating and cooling experiments.

In the transition regime, the experiments were performed on the heating of the fluid, except for those conducted by Manglik and Bergles (1993), who also investigated flow in the transition region by means of the cooling of the fluid. Most of the augmentation techniques involved the inserts of tapes and wire-coils. No helical finned-type tubes have yet been tested in this region. The fluids used were a mixture of water and ethylene/propylene glycol.

Due to the efficiency needs of the future, though, more surface is added to exchangers, with the implications that flow rates per tube drops. These efficiency requirements also imply reduced compressor and pumping power, with the overall trend being that many heat exchangers will start to operate in the transition region of flow. Predictive methods for enhanced tubes in the transition region, however, is unavailable.

A few predictive methods in the transition region have been given for smooth tubes, with the earliest being in a form of a *resumé* graph proposed by Colburn (1933). The work of Ghajar and co-workers have delivered heat transfer and pressure drop correlations for different inlet profiles. However, it is limited to smooth tubes with uniform heat flux heating.

Table 1.1 Heat transfer augmentation studies.

Author	Reynolds Range	Fluid	Condition	Augmentation
Turbulent Flow				
Watkinson *et al.* (1972)	10 000 - 150 000	Water	Heating	Internally Finned Tubes
Carnavos (1980)	10 000 - 100 000	Water	Heating	Internally Finned Tubes
Withers (1980a)	10 000 - 120 000	Water	Heating	Single-Helix Ridging
Withers (1980b)	10 000 - 120 000	Water	Heating	Multiple-Helix Ridging
Said and Trupp (1984)	25 000 - 150 000	Air	Heating	Internally Finned Tubes
Sethumadhavan and Raja Rao (1986)	5 000 - 80 000	Water & 50% Glycerol	Heating	Single & Multistart Spirally Enhanced Tubes
Takahashi *et al.* (1988)	10 000 - 100 000	Water	Heating	Three-Dimensional Spiral Ribs
Al-Fahed *et al.* (1993)	10 000 - 30 000	Water	Heating	Internal Micro-fins
Chiou *et al.* (1995)	8 000 - 30 000	Water	Heating	Micro-fin
Wang *et al.* (1996)	2 000 - 40 000	Water	Cooling	Micro-fin
Brognaux *et al.* (1997)	2 500 - 50 000	Water	Heating	Micro-fin
Copetti *et al.* (2004)	2 300 - 20 000	Water	Heating	Micro-fin
Han and Lee (2005)	3 000 - 40 000	Water	Cooling	Micro-fin tubes
Eiamsa-ard and Promvonge (2006)	8 000 - 18 000	Air	Heating	V-nozzle Turbulators
Tijing *et al.* (2006)	4 500 - 40 000	Water	Cooling	Internal Fin Inserts
Laminar Flow				
Marner and Bergles (1989)	15 - 575	Polybutene 20	Cooling & Heating	Twisted Tape Inserts & Internally Finned Tubes
Bandyopadhyay *et al.* (1991)	35 - 1756	Oil	Heating	Twisted Tape Inserts
Manglik and Bergles (1993)	300 - 30 000	Water & EG[a]	Cooling & Heating	Twisted Tape Inserts
Al-Fahed *et al.* (1999)	230 - 2 300	Oil	Heating	Micro-fin & Twisted Tape Inserts
Saha *et al.* (2001)	45 - 1150	Oil	Heating	Twisted Tape Inserts
Sivashanmugam and Suresh (2006)	200 - 3 000	Water	Heating	Helical Screw Inserts
Sivashanmugam and Nagarajan (2007)	200 - 2 000	Water	Heating	Helical Screw Inserts
Transition Flow				
Manglik and Bergles (1993)	100 - 20 000	Water & EG	Cooling & Heating	Twisted Tape Inserts
Vicente *et al.* (2002a)	200 - 100 000	Water & EG	Heating	Helical Dimpled Tubes
Vicente *et al.* (2004)	100 - 90 000	Water & EG	Heating	Corrugated Tubes
García *et al.* (2005)	80 - 90 000	Water & PG[b]	Heating	Wire Coil Inserts
García *et al.* (2007a)	10 - 2 500	Water & PG	Heating	Wire Coil Inserts

[a]Ethylene Glycol
[b]Propylene Glycol

1.2 Objectives

In the light of the previous discussion, the main objectives of this thesis will be:

- to obtain heat transfer and friction factor data for Reynolds numbers between 1 000 and 20 000, spanning the laminar, critical, transitional and turbulent flow regimes for smooth and enhanced tubes using water as the working fluid. Though some of the measurements for smooth tubes have already been made by others, it is necessary in this study to have accurate smooth tube measurements for comparison purposes with the enhanced tubes. Thus, while taking smooth tube measurements, the opportunity will be used to make contributions and improvements to the existing body of knowledge on smooth tubes.
- to determine the transitional threshold for the enhanced tubes at the upper end of the laminar regime and lower end of the turbulent regime;
- to study hysteresis in the transition region;
- to investigate the effect various inlets have on the critical Reynolds number in enhanced tubes;
- to investigate the effect enhanced tubes have on the transition region with respect to the various inlets;
- to investigate the effect tube diameters have on the results;
- to develop new correlations for the transitional region of flow for smooth and enhanced tubes with the cooling of the test fluid.

These objectives will be met by means of an experimental system specifically designed for capturing the required information. The system will be such that various inlets as well as various types of tubes can be tested.

1.3 Work of Ghajar and co-workers

In this chapter it has already been highlighted that Ghajar and co-workers have done a substantial amount of work on different types of inlets for smooth tubes. In Chapter 2 more detail is given of all the work that they have done. To summarise, they have investigated the heat transfer and pressure drop characteristics for different types of inlets. In their work they used (1) constant heat flux heating inside a (2) smooth tube only, investigating only a (3) single diameter (15.84 mm) tube, (4) measured local heat transfer and pressure drop data and (5) used a combination of water and glycol as their working fluid.

In this study the following very important distinctions are made to the work of Ghajar and co-workers. Firstly, the ultimate goal is to investigate the influence of different types of inlets

on enhanced tubes. However, for validation and comparison purposes accurate smooth tube data are needed and collected and where contributions and/or improvements can be made to the present body of knowledge on smooth tubes, this is done.

Secondly, tubes are not heated with a constant heat flux but cooled with a constant wall temperature (at low Reynolds numbers) as is what typically happens in chillers. The result is that different values of laminar heat transfer will be obtained, as noted in most heat transfer textbooks for uniform heat flux and constant wall temperature conditions (Lienhard and Lienhard, 2003). Further, the cooling of a fluid was shown to have different characteristics to that of a fluid being heated. This was shown by Petukhov *et al.* (1969) who developed a turbulent heat transfer correlation for both instances, but found that the results for the fluid being cooled reacted differently to the heating data. It should also be noted that the effect of viscosity is also different. For the case where the fluid is being heated, the viscosity near the wall is lower than the bulk, while for a fluid being cooled it is higher. Thus, higher shear stress at the wall can be expected for a cooling fluid, relating to a possible higher pressure drop.

Thirdly, as the limitation of this cooling method is that it is not possible to accurately determine the bulk temperature along the axial length of tubes, average heat transfer and pressure drop measurements are taken along the full length of a 5 m length tube. This is of practical importance to many design engineers as most large chillers are manufactured using these tube lengths.

Fourthly, only water was used, except in Chapter 4 where limited glycol measurements were made to support the results obtained with water. Water was used for all the tests, from the lowest to the highest Reynolds numbers, thus keeping the Prandtl number relatively constant throughout. This is unlike other work where a high Prandtl number fluid is used at low flow rates due to the limited range of the pumps and due to pressure drops being higher, improving their uncertainty during measurements.

1.4 Layout of the Thesis

The thesis starts off with a look into the state of the art regarding transitional flow. This forms part of the literature survey in Chapter 2. Next, the experimental system is discussed in Chapter 3. Included in this section is the method for calculating friction factors and heat transfer coefficients. The results of the uncertainty analysis will be shown, with the validation of the system with regard to these methods also being shown.

The results will be discussed in a span of four chapters. The chapters are separated in terms of smooth and enhanced tubes and the different types of inlets. Thus, Chapter 4 will discuss the fully developed smooth tube results, while Chapter 5 will discuss the smooth tube results with regards to the various inlet profiles. Chapter 6 will then contain the results of the fully developed enhanced tubes, while Chapter 7 will contain the results for the enhanced tubes with the various inlet profiles.

Each chapter will start off with adiabatic friction factor results. This is followed by the heat

transfer results, after which the diabatic friction factor results will be discussed. If necessary, a correlation will be developed after each of these sections. Only Chapter 6 will contain a section regarding the performance of the enhanced tubes with respect to their smooth tube counterparts.

The last chapter will contain the final conclusions of this thesis. Two of the appendices attached contain the full uncertainty analysis of the system and the results of the Wilson Plot technique used as part of the validation process.

1.4.1 Notation

Throughout this document all values are given in S.I. units. All dimensionless parameters will be in terms of the inner-tube inside/root diameter. Thus, these dimensionless parameters will not contain the subscript D as is customary. Any reference to parameters other than the inner-tube inside diameter will be indicated. All references to the inner-tube inside diameter will be indicated by the symbol D without any subscripts. Only in Chapter 3 will subscripts be added to distinguish between the different diameters used.

Chapter 2

Literature Survey

> If we knew what we were doing it wouldn't be research.
>
> *Albert Einstein (1879 - 1955)*

2.1 State of the Art

It is accepted in literature that transition from laminar to turbulent flow inside tubes occurs at a Reynolds number of approximately 2 300. Although this is an accepted value, transition in reality occurs in the range of Reynolds numbers between 2 300 and 10 000 (Tam and Ghajar, 1997). It is normally advised when designing heat exchangers to remain outside these limits due to the uncertainty and flow instability of this region. Large pressure variations are also encountered in this region since the pressure gradient required to move the fluid in laminar and turbulent flow could vary by an order of magnitude.

It was as early as 1883 when Reynolds (1883) showed that transition occurred at a critical value which depends on the surrounding disturbances. This value was a function of the fluid velocity, tube diameter and viscosity, also now known as the Reynolds number. Reynolds described the onset of turbulence always occurring at considerable distance from the entrance, with the turbulence moving towards the inlet as the velocity was increased. Reynolds also found that just above the critical value, turbulence would occur in flashes at a fixed point down the length of the tube. These flashes are also known as turbulent bursts, and was also visually observed by Lindgren (1953). Lindgren found that the transition occurred in a gradual manner with fluctuating bursts of turbulence. The frequencies of these bursts were found to be a function of the fluid velocity and the distance from the inlet. It was also shown that the critical Reynolds number increased with an increase in distance from onset, with visual observation confirming this.

Kalinin and Yarkho (1966) found with heat transfer experiments that the wall temperatures start to fluctuate in the transition region. Ede (1961) also detected the fluctuations although

it was blamed on a technical issue. Kalinin and Yarkho (1966) found that these fluctuations increased in amplitude and frequency as the fluid velocity was increased until the critical Reynolds number was reached, after which the fluctuations started to settle. It was found that the critical Reynolds number decreased with increasing axial distance, with the amplitude of these fluctuations becoming larger. This is in stark contrast to the work of Lindgren (1953), although understandable. Lindgren worked with an isothermal fluid while the work of Kalinin and Yarkho applied constant heat flux to the fluid along the length of the tube, hence increasing its temperature and decreasing its viscosity. The critical Reynolds number should, however, actually increase, but it is not clear from their paper how the Reynolds numbers were defined, e.g. whether inlet, outlet or bulk temperatures were used to obtain the Reynolds number as this would explain their observations.

Inlet profiles were found to have a profound influence on the transition Reynolds number. Nagendra (1973) found that the greater the disturbance, the earlier transition occurs. Ghajar and Madon (1992) performed an extensive study into the effect of three different types of inlets on the critical Reynolds number during isothermal fully developed flow. The three inlets tested were a *square-edged* (sudden contraction), *re-entrant* (tube-protruding square-edged inlet) and a *bellmouth* inlet (smooth, gradual contraction). It was found that transition from laminar to turbulent flow occurred at Reynolds numbers of 1 980 - 2 600 for the re-entrant, 2 070 - 2 840 for the square-edged and 2 125 - 3 200 for the bellmouth inlet. A study performed by Smith (1960) indicated that transition occurred in the inlet length of the tube and not in the fully developed Poiseuille region. This, combined with the work of Ghajar and Madon, shows that the inlet acts as a disturbance to the flow, which they also concluded. Results published in later work by Tam and Ghajar (1997) showed transition to occur at different Reynolds numbers (much higher) than previous results. The transition for the re-entrant inlet started and ended at 2 900 - 3 500, the square-edged at 3 100 - 3 700 and the bellmouth at 5 100 - 6 100. Once again, though, it is clear that the inlet disturbance influences the critical point where transition occurs.

Heat transfer results by Ghajar and Tam (1994) showed that transition varied from inlet to outlet, starting and ending at a Reynolds number of 2 000 and 6 400, respectively, near the inlet of the tube (three diameters from the inlet) and 2 000 and 8 000 near the exit (192 diameters from the inlet). For the square-edged inlet these limits were 2 200 to 7 500 and 2 200 to 8 100 while for the bellmouth, they were 3 800 to 9 500 and 3 900 to 10 000. Ghajar and Tam (1991) explained this variation from inlet to outlet to the variation in fluid properties. Since the tube was under a uniform heat flux boundary, the fluid was heated along the axial length with the effect of the viscosity decreasing and hence an increase in Reynolds number.

Heat transfer also had an effect on the laminar friction factor, increasing with the amount of heat being added (Tam and Ghajar, 1997). This effect was also observed by Nunner (1956) performing heat transfer experiments. The increase (as much as 100%) was attributed to the buoyancy-induced secondary flows altering the velocity profile, which in turn influences the shear stress at the tube wall.

Mori *et al.* (1966) performed tests with two types of inlets; one with a disturbance at the inlet

that generated turbulence and the other without. The tests with the disturbance revealed that as the Rayleigh number (accounting for buoyancy forces) was increased, the critical Reynolds number increased. The reason for this is that the secondary flow suppresses the turbulence being created by the disturbance. For tests with no disturbance, it was found that the critical Reynolds number decreased with an increase in Rayleigh number due to the secondary flow actually generating the turbulence.

Transition is also affected by the type of tube augmentation. Nunner (1956) found that transition was accelerated by the severity of the augmentation. Nunner inserted different types of circular rings at different distances along the length of the tube. For the same diameter tubes, laminar heat transfer results of the augmented tubes were not significantly higher than those of the smooth tube. Obot *et al.* (1990) analysed the results of previous research performed on transition flow. Specifically by reanalysing the results of Nunner (1956) and Koch (1960), it was found that the main contributing factor concerning transition was the roughness height. On average, it was found that greater heat transfer coefficients were obtained the earlier transition occurred.

As was the case of Mori *et al.* (1966) with secondary flow suppressing turbulence, Manglik and Bergles (1993) experimented with twisted tape inserts and found that the swirling motion induced by these inserts actually delayed transition. Transition also occurred in a gradual way without any sudden discontinuities as found for the smooth tube. Vicente *et al.* (2002a) found the opposite to be true for helical dimpled tubes, which accelerated transition to Reynolds numbers as low as 1 400. The main mechanism contributing to transition was also the roughness height, similar to the observation of Obot *et al.* (1990). Heat transfer results also revealed that the critical value remained unchanged from the isothermal results. It should be noted, however, that these transition results were measured in the fully developed region, neglecting the effect of the thermal entrance region.

Results obtained by García *et al.* (2005) for wire-coil inserts found that transition for isothermal flow occurs as low as $Re \approx 700$. It was shown that transition occurred in a gradual manner without the sudden discontinuities found in the smooth tube or the dimpled tubes of Vicente *et al.* (2002a). Similar results were found for twisted tape inserts by Manglik and Bergles (1993) due to the rotating component.

Vicente *et al.* (2002a) conducted heat transfer experiments in the entrance region and found that secondary flow did not have any effect on the heat transfer performance. Only after the flow became thermally fully developed, was the performance noticeable. This was also shown by Ghajar and Tam (1991) stating that a considerable starting length is required for secondary flows to become established, and hence to have any enhancing effects on heat transfer. Secondary flow did, according to Vicente *et al.* (2002a), have an effect on the thermal entrance length, shortening this length when compared to pure forced convection. With a shortened thermal entrance length implies that a greater region of the tube is under the influence of secondary flows and thus heat transfer coefficients, on average, are higher during mixed convection than for pure forced convection.

The heat transfer results of García *et al.* (2005) showed that the wire coils did not present

any enhancement in the laminar region since the main heat transfer mechanism was natural convection and not the wire coils.

2.2 Correlations

Of the authors mentioned above, only a few have developed correlations for the transition region. One of the first attempts to correlate the entire laminar-transition-turbulent regimes was proposed by Colburn (1933) in the form of a resumé chart. This chart was meant to be applied as a tool to obtain heat transfer and pressure drop values for a given Reynolds number. Laminar and turbulent data were combined by some scarce experimental results for the transition regime. This section will discuss some of the more modern correlations that are available regarding transitional flow inside smooth and enhanced tubes.

2.2.1 Heat Transfer

Petersen and Christiansen (1966) developed a heat transfer correlation for the combined transition-turbulent ($Re > 2\ 100$) flow regimes for non-Newtonian fluids. For Newtonian fluids they recommend using

$$Nu = RePrSt_{10}\left[\frac{St_{Cr}}{St_{10}}\right]^{\phi(Re)}\left(\frac{Re}{10\ 000}\right)^{n}\left(\frac{10\ 000}{2\ 100}\right)^{n\phi(Re)} \tag{2.1}$$

with n being the slope on a log-log plot of

$$St = St_{10}\left(\frac{Re}{10000}\right)^{n} \tag{2.2}$$

for turbulent flow and $\phi(Re)$ being given by

$$\phi(Re) = 1.635\log\left[\frac{1}{1.133}\frac{Re-710}{Re-1\ 800}\right] \tag{2.3}$$

It was recommended that this correlation not be used for liquids or gasses for which the Prandtl number is less than 2. The subscripts, 10 and Cr, imply that the properties should be evaluated at a Reynolds number of 10 000 and at the critical Reynolds number, respectively.

Churchill (1977) gives the first general equation describing all three flow regimes. This correlation was based on a method developed by him and a colleague (Churchill and Usagi, 1972). The correlation is given by

$$Nu = \left(Nu_L^{c_4} + \left\{Nu_t^{c_3} + \left[\left(Nu_0^0\right)^{c_2} + \left(\left(Nu_\infty^0\right)^{c_1} + \left(Nu_\infty^\infty\right)^{c_1}\right)^{c_2/c_1}\right]^{c_3/c_2}\right\}^{c_4/c_3}\right)^{1/c_4} \tag{2.4}$$

with c_1, c_2, c_3, and c_4 being constants. Nu_0^0 has a value of 6.3 or 4.8 for uniform heat flux and uniform wall temperature boundaries, respectively when $RePr \rightarrow 0$. For the transition regime, it was suggested that a correlation similar to, but not as complex as that proposed by Petersen and Christiansen (1966), rather be used. This correlation has the arbitrary form

$$Nu_t = Nu_{L_{Cr}} \, e^{(Re-2200)/730} \tag{2.5}$$

The laminar Nusselt number, Nu_L, is suggested to have a constant value of 3.657 and 4.364 for uniform wall temperature and uniform heat flux boundaries, respectively. These values do, however, neglect the effects of mixed convection often found in laminar flows. Churchill (1977) states, though, that more appropriate correlations can be used for the situation at hand.

The final equation, using values for exponents and correlations suggested by Churchill (1977), is given by

$$Nu = \left(Nu_L^{10} + \left[\frac{e^{(2200-Re)/365}}{Nu_{L_{Cr}}^2} + \left(Nu_0^0 + \frac{0.079 Re\sqrt{f} Pr}{\left(1 + Pr^{4/5}\right)^{5/6}} \right)^{-2} \right]^{-5} \right)^{1/10} \tag{2.6}$$

The author compared this correlation with a relatively large database obtained from various sources, with the correlation claiming to predict this data within the uncertainties of these sources.

A report of the Engineering Sciences Data Unit (ESDU, 1993) recommends using a linear interpolation of Nusselt values for the laminar and turbulent flow over the transition region for Reynolds numbers between 2 000 and 8 000. The equation given is

$$Nu = \varepsilon Nu_L + (1 - \varepsilon) \, Nu_T \tag{2.7}$$

$$\varepsilon = 1.33 - \frac{Re}{6000} \tag{2.8}$$

Ghajar and Tam (1994) developed a transition correlation for a smooth tube with a uniform heat flux boundary condition for $3 < x/D < 192$. This correlation takes on the same form as that proposed by Churchill (1977) and is given by

$$Nu_t = \left(Nu_L + e^{(c_1 - Re)/c_2} + Nu_T^{c_3} \right)^{c_3} \tag{2.9}$$

where the constants and limitations are given in Table 2.1. The laminar and turbulent Nusselt numbers were derived from their experimental data and are, respectively, given by

$$Nu_L = 1.24 \left[(RePrD/x) + 0.025 \, (GrPr)^{0.75} \right]^{1/3} \left(\frac{\mu}{\mu_w} \right)^{0.14} \tag{2.10}$$

with

Table 2.1 Constants and limitations for Eq. (2.9) (Ghajar and Tam, 1994).

Inlet	c_1	c_2	c_3	Limitations
Re-entrant	1 766	276	-0.955	$1\,700 \leq Re \leq 9\,100$ $5 \leq Pr \leq 51$ $4000 \leq Gr \leq 2.1 \times 10^5$ $1.2 \leq \mu/\mu_w \leq 2.2$
Square-edged	2 617	207	-0.950	$1\,600 \leq Re \leq 10\,700$ $5 \leq Pr \leq 55$ $4\,000 \leq Gr \leq 2.5 \times 10^5$ $1.2 \leq \mu/\mu_w \leq 2.6$
Bellmouth	6 628	237	-0.980	$3\,300 \leq Re \leq 11\,100$ $13 \leq Pr \leq 77$ $6\,000 \leq Gr \leq 1.1 \times 10^5$ $1.2 \leq \mu/\mu_w \leq 3.1$

$$3 \leq x/D \leq 192, \quad 280 \leq Re \leq 3\,800,$$
$$40 \leq Pr \leq 160, \quad 1\,000 \leq Gr \leq 2.8 \times 10^4,$$
$$1.2 \leq \mu/\mu_w \leq 3.8$$

and

$$Nu_T = 0.023 Re^{0.8} Pr^{0.385} \left(\frac{x}{D}\right)^{-0.0054} \left(\frac{\mu}{\mu_w}\right)^{0.14} \tag{2.11}$$

with

$$3 \leq x/D \leq 192, \quad 7\,000 \leq Re \leq 49\,000,$$
$$4 \leq Pr \leq 34, \quad 1.1 \leq \mu/\mu_w \leq 1.7$$

This correlation is valid for $3 \leq x/D \leq 192$ and predicted their data to within $\pm 10.5\%$. It should be noted, though, that the laminar correlation is valid only for Prandtl numbers greater than 40 and less than 160, while for the turbulent correlation it is greater than 4 and less than 34. It should be mentioned that this correlation is intended for local values, while the correlations of Petersen and Christiansen (1966) is independent on tube length while that of Churchill (1977) is based on the total heated length of the tube. Ghajar *et al.* (2004) developed

a more accurate correlation by means of artificial neural networks using their data, although this correlation is much more complicated to implement.

Figure 2.1 shows a comparison of the different heat transfer correlations mentioned regarding transition. The comparison is based on a Prandtl number of 7, Reynolds numbers from 1 000 to 100 000, tube diameter and length of 15 mm and 2.8 m respectively and a Grashof number of 1×10^5. Since the correlation of Ghajar and Tam (1994) is for local values, this comparison uses the arithmetic averaged value calculated over a length of 50 mm to 2.8 m. It should be noted that the comparison falls outside the valid range for the laminar correlation of Ghajar and Tam (1994) due to the choice of the Prandtl number. The laminar correlation of Oliver (1962) was used in conjunction with the correlation of Churchill (1977) to incorporate mixed convection effects.

The comparison shows that transition is predicted over a relatively wide range of Reynolds numbers, ranging from 2 000 to 8 000. This is mainly due to assumptions made by authors due to a lack of data in this region. The predictions of Ghajar and Tam (1994) are to be accepted as the most accurate. This data shows the influence inlet geometry has on transitional Nusselt numbers, with a smooth inlet (such as the bellmouth) being able to delay transition to much higher Reynolds numbers than for the other two inlets.

Ghajar and Tam (1995) also present correlations for predicting the lower and upper bound critical Reynolds number for the different inlets. These are given in terms of linear equations as a function of the axial distance. The critical Reynolds number varies with axial distance due to the fluid properties that change due to heating. As the fluid is being heated, the local wall and bulk temperatures increase, implying that the local fluid viscosity decreases. This has the effect that the local Reynolds number increases. These correlations, however, cannot be expected to be valid for a fluid that is being cooled, as the effect is totally opposite. However, due to the paucity of information regarding critical Reynolds numbers, it is only fitting to present these correlations.

Re-entrant

$$\begin{aligned} \text{Lower Bound: } & Re = 2\ 157 - 0.65\,(192 - x/D) \\ \text{Upper Bound: } & Re = 8\ 475 - 9.28\,(192 - x/D) \end{aligned} \tag{2.12}$$

Square-edged

$$\begin{aligned} \text{Lower Bound: } & Re = 2\ 524 - 0.82\,(192 - x/D) \\ \text{Upper Bound: } & Re = 8\ 791 - 7.69\,(192 - x/D) \end{aligned} \tag{2.13}$$

Bellmouth

$$\begin{aligned} \text{Lower Bound: } & Re = 3\ 787 - 1.80\,(192 - x/D) \\ \text{Upper Bound: } & Re = 10\ 481 - 5.47\,(192 - x/D) \end{aligned} \tag{2.14}$$

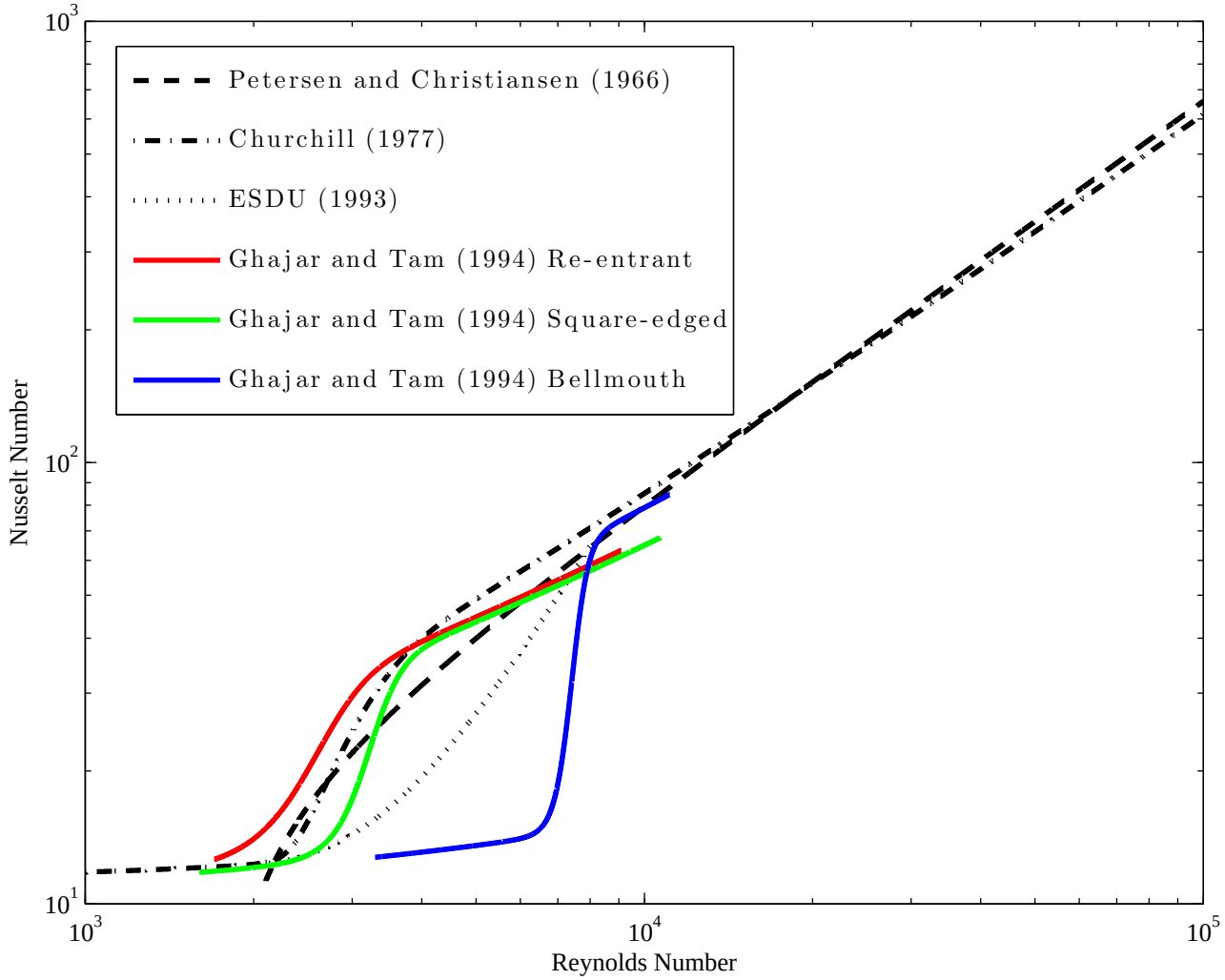

Figure 2.1 Comparison of different heat transfer correlations for transitional flow. $D = 15\ mm,\ L = 2.8\ m,\ Pr = 7,\ Gr = 1 \times 10^5$.

Ghajar and Tam (1995) note, though, that these correlations do not include the effects of mixed convection as the secondary flow would influence the start of transition. These correlations were obtained from data near the entrance of the tube where the influence of mixed convection is negligible as it needs a considerable length to develop.

Hrycak and Andrushkiw (1974) also presented a method for determining the critical Reynolds numbers of an isothermal fluid on the principle of entropy generation. This method showed that for circular tubes transition starts and ends at a Reynolds number of 2 000 and 2 200, respectively. It was also deduced that the effect of heat transfer would have little effect on these critical values.

2.2.2 Friction Factors

A few friction factor correlations were also developed for the transition region of flow for smooth tubes. Churchill (1977) suggested an asymptotic correlation, having the form

$$f = \left(\left[\left(\frac{8}{Re} \right)^{10} + \left(\frac{Re}{36\ 500} \right)^{20} \right]^{-0.5} + (2.21 \ln (Re/7))^{10} \right)^{-1/5} \tag{2.15}$$

Hrycak and Andrushkiw (1974) suggests using an interpolation formula obtained from experimental data. This is given as

$$f = 3.1 \times 10^{-3} + 7.125 \times 10^{-6} Re - 9.7 \times 10^{-10} \tag{2.16}$$

Bhatti and Shah in Kakaç *et al.* (1987) recommend the following correlation for all three regimes:

$$f = A + B/Re^{1/m} \tag{2.17}$$

with the constants A, B, and m listed in Table 2.2

Table 2.2 Values for the constants in Eq. (2.17).

	A	B	m
$Re < 2\ 100$	0	16	1
$2\ 100 < Re \leq 4\ 000$	0.0054	2.3×10^{-8}	$-2/3$
$Re > 4\ 000$	1.28×10^{-3}	0.1143	3.2154

Ghajar and Madon (1992) developed a similar correlation as that of Hrycak and Andrushkiw (1974) for different inlet configurations. This correlation is only valid for isothermal, fully developed flow, hence ignoring any entrance region effects, but considers the effect of the inlet disturbance. However, the correlation was extended into the laminar and turbulent regime as to extend its applicability in these regions, ensuring that there is a smooth transition between the two regimes. The correlation for the different inlets is given as

Re-entrant, $1\ 950 < Re < 2\ 650$

$$f = -9.88 \times 10^{-3} + 1.15 \times 10^{-5} Re - 1.29 \times 10^{-9} Re^2 \tag{2.18}$$

Square-edged, $2\ 055 < Re < 3\ 140$

$$f = -2.56 \times 10^{-2} + 2.49 \times 10^{-5} Re - 4.25 \times 10^{-9} Re^2 \tag{2.19}$$

Bellmouth, 2 075 $< Re <$ 3 450

$$f = -8.03 \times 10^{-3} + 1.05 \times 10^{-5} Re - 1.47 \times 10^{-9} Re^2 \tag{2.20}$$

These correlation predicted their data with an average absolute standard deviation of less than 2% and a maximum of less than 5%.

Tam and Ghajar (1997) showed that, as heating was applied to the fluid, there is a significant change in the laminar and transition friction factors. They found that as the heat flux was increased, the laminar friction factors were increased while transition was delayed to higher Reynolds numbers. The increase in laminar friction factors was attributed to the secondary flows which influence the velocity profile and hence the wall shear stress. The reason given for the delay in transition is due to the heating of the fluid stabilising the flow.

Due to the effect heating has on the laminar and transition friction factors, Tam and Ghajar (1997) developed correlations to predict these effects. For the laminar regime, the correlation is given by

$$f = \frac{16}{Re}\left(\frac{\mu}{\mu_w}\right)^{1.65-0.013 Pr^{0.84} Gr^{0.17}} \tag{2.21}$$

$$1\ 100 < Re < 7\ 400$$
$$17\ 100 < Gr < 95\ 600$$
$$1.25 < \mu/\mu_w < 2.40$$
$$6 < Pr < 36$$

This correlation predicted the authors' data to within ±12.6%. To predict the transitional friction factors, the following equation is recommended:

$$f = \left[1 + \left(\frac{Re}{c_1}\right)^{c_2}\right]^{c_3}\left(\frac{\mu}{\mu_w}\right)^{c_4} \tag{2.22}$$

with the values of c_1, c_2, c_3 and c_4 being given in Table 2.3.

These correlations predicted the data to within ±9.5% with an absolute average standard deviation of 3.4%. It should be mentioned that these correlations were developed in the fully developed region, thus ignoring any entrance effects. It should be noted that the power of the Pr-term in the above equations was set to a negative, as these correlations do not work when they are as given in the original paper.

Figure 2.2 shows a comparison of the aforementioned models. The same conditions were selected as for the heat transfer comparison. The comparison includes the friction factors with heating of Tam and Ghajar (1997). The simulation shows, unlike the case for the heat transfer simulation, that there is a quite good agreement between the different models. The

Table 2.3 Values to be used in Eq. (2.22) for different inlets (Tam and Ghajar, 1997).

Inlet	c_1	c_2	c_3	c_4	Limitations
Re-entrant	5 840	-0.0145	-6.23	$-1.1 - 0.46\,Gr^{-0.133}\,Pr^{-4.1}$	$2\,700 < Re < 5\,500$ $16 < Pr < 35$ $7\,410 < Gr < 158\,300$ $1.13 < \mu/\mu_w < 2.13$
Square-edged	4 230	-0.16	-6.57	$-1.13 - 0.396\,Gr^{-0.16}\,Pr^{-5.1}$	$3\,500 < Re < 6\,900$ $12 < Pr < 29$ $6\,800 < Gr < 104\,500$ $1.11 < \mu/\mu_w < 1.89$
Bellmouth	5 340	-0.0990	-6.32	$-2.58 - 0.42\,Gr^{-0.41}\,Pr^{-2.46}$	$5\,900 < Re < 9\,600$ $8 < Pr < 15$ $11\,900 < Gr < 353\,000$ $1.05 < \mu/\mu_w < 1.47$

prediction of Churchill (1977) and Ghajar and Tam (1994) using the bellmouth inlet are in excellent agreement. This is quite understandable since both of these correlations are based on fully developed flow data. The fully developed correlation is based on the fact that the flow has developed from a uniform velocity profile at the entrance. This uniform velocity profile is achieved by making use of a smooth contraction at the inlet (White, 1991), which is similar to the bellmouth used by Ghajar and Tam (1994).

The correlations of Ghajar and Tam (1994) and Tam and Ghajar (1997) clearly show the effect inlet geometry has on transition. What is of interest is the effect heating has on the transition values, increasing the critical Reynolds numbers significantly.

2.2.3 Enhanced Tubes

Very little data exists regarding enhanced tubes and transition. The correlations that do exist are mostly for Reynolds numbers greater than 2 300. Some excellent results are given by Vicente *et al.* (2002b), Vicente *et al.* (2004), García *et al.* (2005), García *et al.* (2007a) and García *et al.* (2007b) regarding work done in the laminar, transitional and turbulent regimes for helical dimpled tubes, corrugated tubes and tubes with wire coil inserts.

Regarding transition, what is of interest is the fact that from all the different tubes that were investigated, the critical Reynolds numbers were only a function of the disturbance height and not of any other enhancement parameter. For corrugated and helical dimpled tubes, the above mentioned authors suggest the use of the following correlation to predict the critical

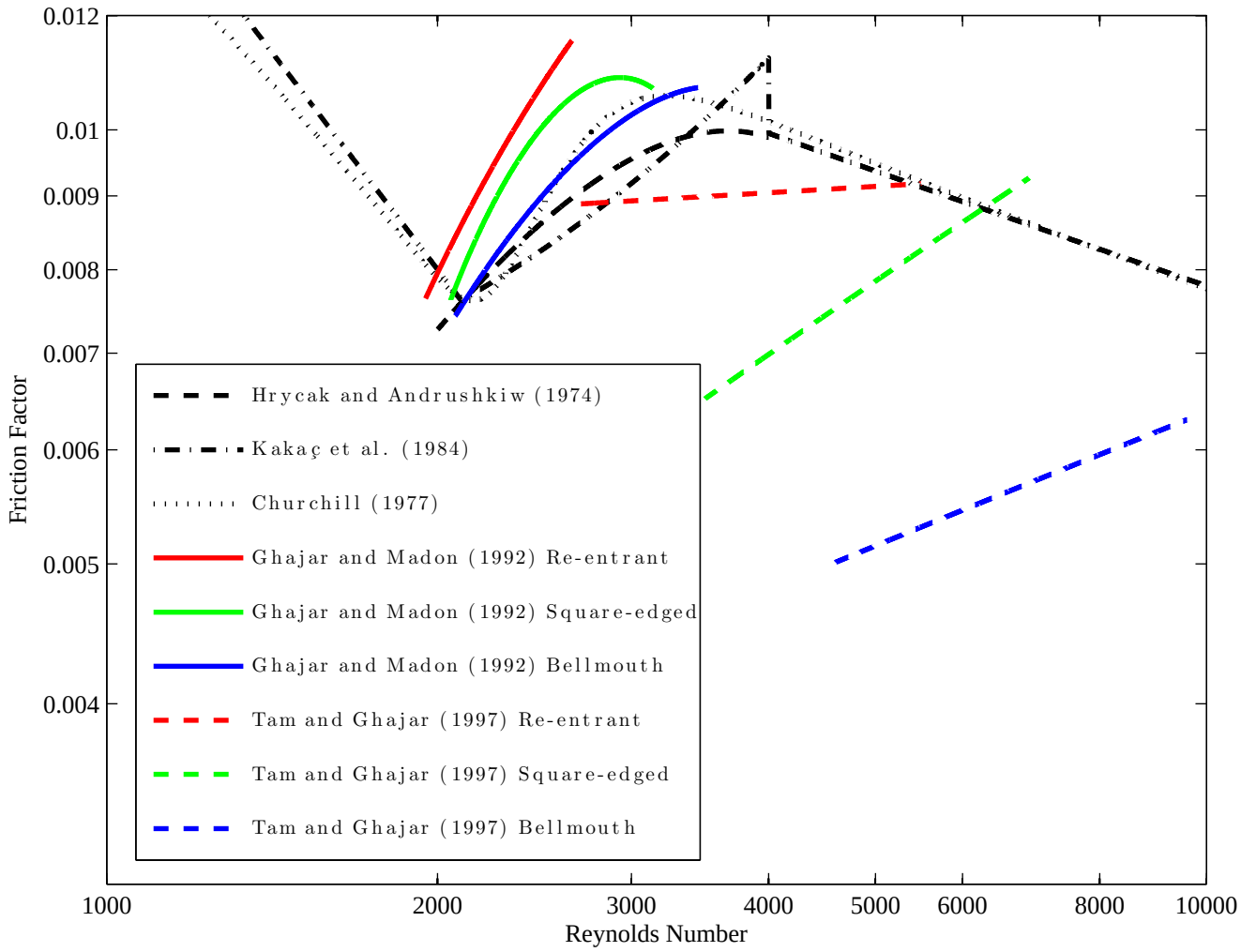

Figure 2.2 Comparison of different friction factor correlations for transitional flow. $D = 15\ mm,\ L = 2.8\ m,\ Pr = 7,\ Gr = 1 \times 10^5$.

Reynolds number:

Corrugated tube

$$Re_{Cr} = 2\ 100\left[1 + 1.18 \times 10^7\,(e/D)^{3.8}\right]^{-0.1} \tag{2.23}$$

Helical dimpled tube

$$Re_{Cr} = 2\ 100\left[1 + 7.9 \times 10^7\,(e/D)^{-6.54}\right]^{-0.1} \tag{2.24}$$

with e being the dimple height. These correlations predicted the authors' data to within 15%. These correlations are, however, only valid for fully developed flow, neglecting any entrance disturbance effects.

No correlations in the literature were found to predict heat transfer and pressure drop in the transition region for enhanced tubes with different inlet geometries.

2.3 Conclusion

An investigation into the literature revealed many aspects which influence transition in circular tubes. Inlet geometries as well as the effect of tube augmentation influence not only the onset of transition, but also the way in which the flow changes from laminar to turbulent flow.

Correlations were presented describing heat transfer as well as friction factors in the transition region. These correlations were accompanied by some comparisons, showing the overall trends of these prediction methods. The comparisons showed that prediction of the transition region for heat transfer and friction factors can vary widely. This is mainly due to the paucity of data which was available at the time of the development of these correlations. More accurate correlations showed the effect inlet geometries have on transition. The smoother the inlet, the more transition is delayed. The effects of heat transfer also delayed transition considerably.

Correlations for predicting critical Reynolds numbers in enhanced tubes showed that the critical values were affected by the roughness height and not by any of the other enhancement parameters. These predictions were only valid for fully developed isothermal fluids. No correlations in the literature were found to predict heat transfer and friction factors for finned (low-finned, helical finned or micro-finned) tubes in the transition region.

Thus, for chiller-unit applications, it is of great interest to obtain data for finned enhanced tubes that is being cooled (and not heated) in the transition region of flow and to develop correlations for prediction purposes. Of further interest would be to study the effect entrance geometries have on the enhanced tubes.

Chapter 3

Experimental Set-up, Data Analysis and Validation

> Nothing tends so much to the advancement of knowledge as the application of a new instrument. The native intellectual powers of men in different times are not so much the causes of the different success of their labours, as the peculiar nature of the means and artificial resources in their possession.
>
> *Sir Humphrey Davy (1778 - 1829)*

3.1 Introduction

This chapter discusses the experimental set-up. It gives an overview of the components of the set-up, the experimental test section and the instruments used. Further, the equations used to experimentally obtain heat transfer coefficients and friction factors are given. The experimental procedure and data reduction with these equations are discussed with the results being validated against those published in literature. The validation of the heat transfer coefficients compares three methods with each other as well as with well-known laminar and turbulent flow heat transfer models. The pressure drop validation compares adiabatic pressure drop results with well-known laminar and turbulent flow equations. Lastly, the uncertainties for all the measurements are given.

3.2 Experimental Set-up

The experimental test section, being one of the components in an experimental test facility as shown in Figure 3.1, consisted of a tube-in-tube heat exchanger in a counterflow configuration.

Distilled water was used as the working fluid for both streams, with the inner-fluid being hot and the annulus fluid being cold. The result is that the inner-fluid is being cooled as is found in chiller units. This differs from most other experimental set-ups where the fluid in the inner-tube is being heated at a constant heat flux (Allen and Eckert, 1964; Ghajar and Zurigat, 1990; Petukhov *et al.*, 1969).

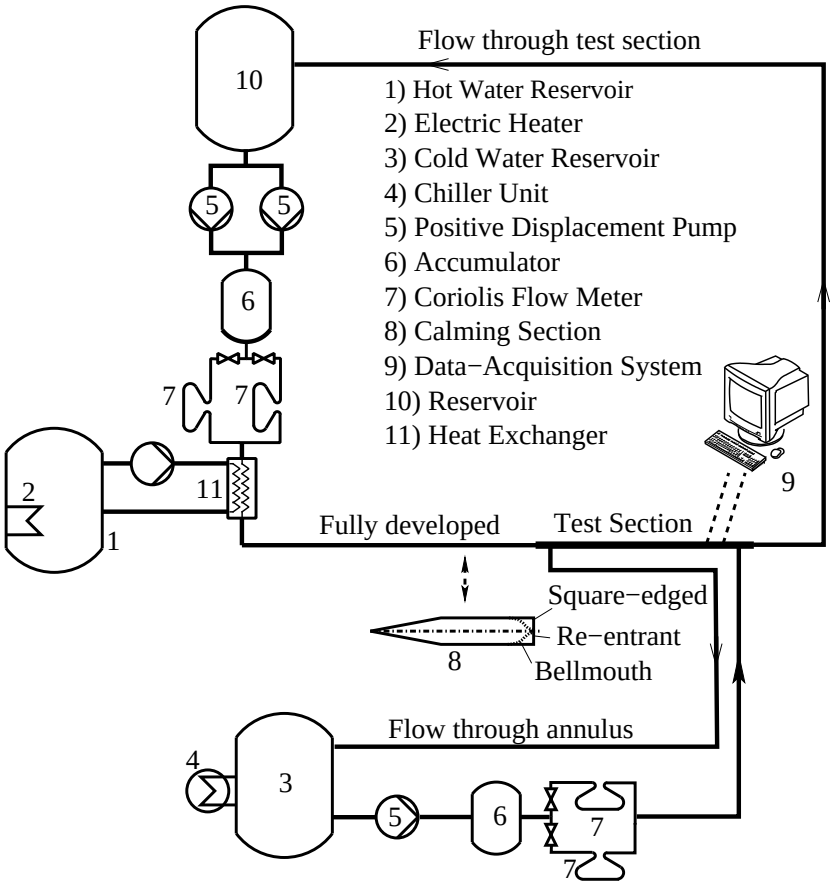

Figure 3.1 Schematic layout of the experimental test facility.

The test fluid in the inner-tube was heated to a temperature of 40-45°C by means of a counterflow heat exchanger. The hot water for the heating was received from a 1 000 *litre* reservoir with temperature maintained at approximately 60°C by means of a 12 kW electric heater. The reason for not using the hot water directly was to ensure that rust from the mild-steel reservoir did not enter the experimental set-up. The 200 *litre* reservoir containing the test fluid was made of plastic.

The test fluid was pumped through the system with two electronically controlled positive displacement pumps. The two pumps were installed in parallel and were used in accordance

with the flow rate requirements. The pumps were of similar capacity, each having a maximum flow rate of 270 *litre*/h.

The cold water loop consisted of a 1 000 *litre* reservoir which was connected to a water chiller having a cooling capacity of 15 kW. The temperature inside the reservoir was maintained at 20°C to prevent the risk of condensate forming on the test section if lower temperatures were used. The water was circulated through the system via an electronically controlled positive displacement pump which had a maximum flow rate of 2 670 *litre*/h. This flow rate ensured that the variation in wall temperature was never greater than 3°C over the whole length of the tube during laminar flow. The wall temperature during turbulent flow could not be maintained constant at turbulent Reynolds numbers, although this has a negligible effect on the results in this regime.

With the use of positive displacement pumps, comes the added pulsations introduced into the system. This has an unfavourable effect on the stability of the flow, which is crucial when studying transition flow. To decrease pulsations, a 70 *litre* accumulator was installed prior to the flow meters and the test section. The accumulators were fitted with bladders filled with air that dampened these fluctuations with the result that the pressure remained much more constant. A test was conducted to determine the effect of the accumulators on the flow rate. It was found that without them the flow rate fluctuations varied between 0.3 and 0.6%, while with the accumulators installed the flow fluctuations never varied more than 0.05%. These accumulators also ensured that stable flow could be achieved at low Reynolds numbers.

From the accumulators, the water flowed through a set of Coriolis flow meters that measured the mass flow rate. A total of four flow meters of different capacities were used, two in parallel per fluid-side, used according to the flow rate requirements. After the flow meters, the fluids flow through the experimental test section and then back into the reservoirs. Depending on the experiments performed, the flow would first move through a calming section before entering the test section. Further, although Figure 3.1 depicts the system in a counterflow configuration, it could also be operated in a parallel flow configuration.

Flow rates were controlled by means of frequency drives which were connected to the positive displacement pumps. In turn, the frequency drives were connected to a personal computer via the data-acquisition system from which the frequencies could be set. The computer would give a voltage output which the drives converted to a representative frequency. The finest voltage increments were in the order of 0.02 V, which in terms of Reynolds numbers was in the order of $\Delta Re = 20$.

3.2.1 Calming Section

Prior to the flow entering the test section, for three of the four different types of test sections, the flow first went through a calming section. The calming section was made from a clear acrylic plastic. This helped in detecting air bubbles that might have entered the system. The purpose of the calming section was two-fold; firstly, to remove any unsteadiness within the flow and to ensure a uniform velocity distribution and, secondly, to house the three different types

of inlets to be investigated. Figure 3.2 gives a schematic view of the calming section.

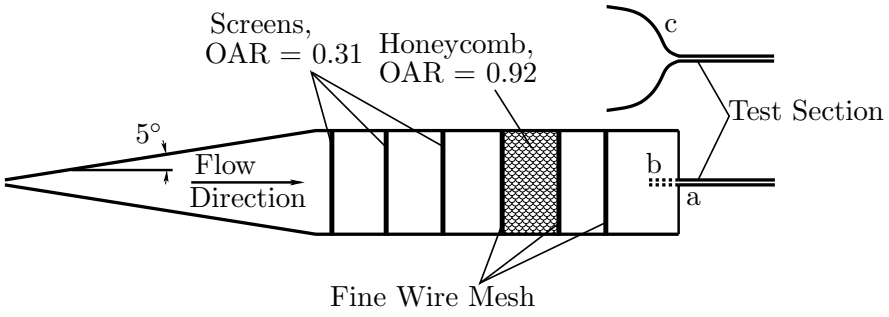

Figure 3.2 Schematic view of the calming section with three different inlet configurations; a) Square-edged, b) Re-entrant and c) Bellmouth. (OAR = Open Area Ratio).

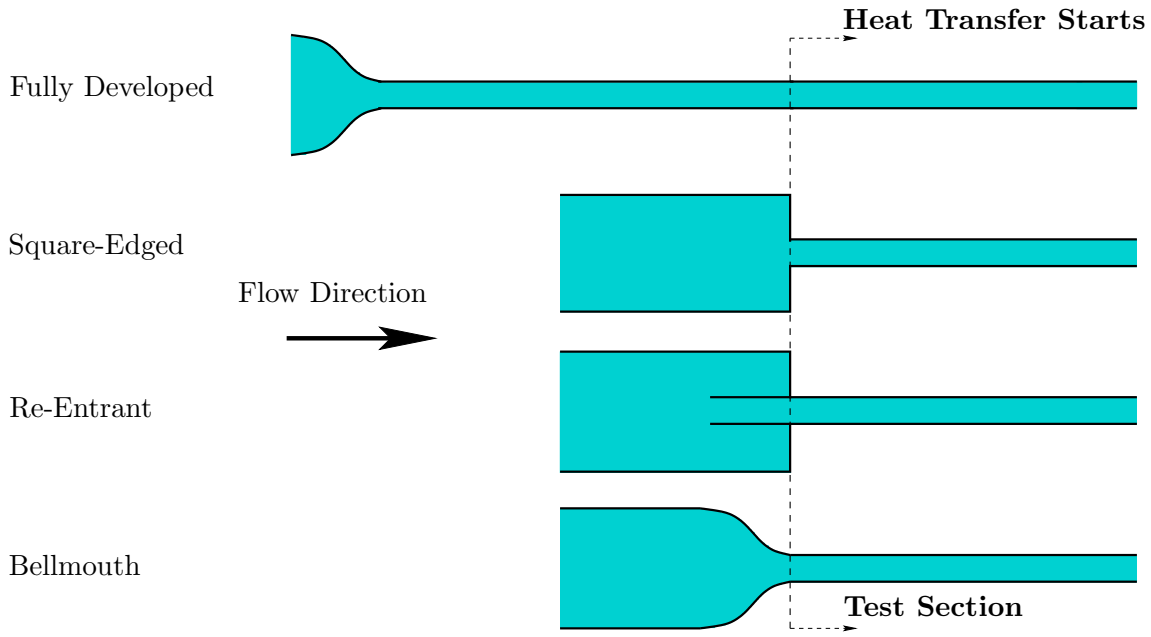

Figure 3.3 The four different inlets viewed relative to the test section.

The calming section was based on work conducted by Ghajar and Zurigat (1990) and consisted of a 5° diffuser which increased from a diameter of 15 mm to 140 mm. This angle was chosen such to prevent flow separation from the diffuser wall. Seventy millimetres after the diffuser were three screens separated 105 mm apart. These screens had an *open area ratio*

(OAR) of 0.31 (60 holes each with a diameter of 10 mm). The OAR is the ratio of the area occupied by the holes to the total area that the whole screen occupies. Located 155 mm from these screens, was a honeycomb which had an OAR of 0.92 and a length of 100 mm. Prior to and after the honeycomb, was a wire mesh with the wires having a diameter of 0.8 mm and the OAR being 0.54. Another fine wire mesh was inserted prior to the inlet nozzles situated 170 mm from the honeycomb. This mesh had a wire diameter of 0.3 mm and an OAR of 0.17.

Bleed valves were positioned at the top of the calming section at several axial positions. This allowed the bleeding of any air that might have entered the section.

Three different inlets could be housed on the calming section, namely a *square-edged*, *re-entrant* and a *bellmouth* inlet. These inlets are also shown in Figure 3.2 as items a, b and c, respectively. The calming section was designed such that the inlets could easily be interchanged. Figure 3.3 shows a basic schematic of each inlet with respect to the test section, from which point heat transfer was initiated.

The length of the fully developed inlet was determined in terms of the suggestion by Durst *et al.* (2005) which required a minimum length of 120-tube diameters. This is assuming that the flow is uniform at the inlet. A uniform inlet was obtained by placing the bellmouth prior to fully developed inlet. To ensure this minimum was met, the length of the inlet was chosen as 160-tube diameters. The square-edged inlet is characterised by a sudden contraction of the flow (from 140 mm to 14.8 mm or 17.7 mm, depending on the tube being tested). This is a typical situation encountered in a shell-and-tube exchanger. The re-entrant inlet makes use of the square-edged inlet except that the tube slides into the inlet by approximately one tube diameter. The third type of inlet is the bellmouth. The bellmouth is characterised by a smooth contraction, the profile being similar in shape to a bell. It has a contraction ratio of 8.8. The shape of the bellmouth was calculated with the method suggested by Morel (1975).

3.2.2 Test Section

The test section consisted of a counterflow, tube-in-tube heat exchanger. All the test sections were manufactured from hard-drawn copper tubes which were insulated with 25 mm thick insulation having a thermal conductivity of 0.034 W/mK. The estimated relative heat loss to the environment, based on a simple one-dimensional heat transfer calculation, was less than 1% of the lowest heat transfer rate obtained. The total length of each test section was approximately 5 m. Six tubes were tested, three having an outer-diameter of 15.88 mm and three with an outer-diameter of 19.02 mm. Each diameter set consisted of a smooth tube for referencing purposes and two enhanced tubes (18° and 27° helix angles). The geometric properties of these tube are summarised in Table 3.1. The cross-sectional and heat transfer area for enhanced tubes was determined by the method proposed by Lambrechts (2003) and is repeated in Appendix A. Figure 3.4 shows a cross-sectional and a close-up view of the enhanced tubes and its fins, respectively, with detail of the fin height, helix angle, etc. given in Table 3.1.

The annulus outer-diameters were chosen such that the space between the annulus and the inner-tube was small, ensuring high flow velocities and thus turbulent flow within the annulus.

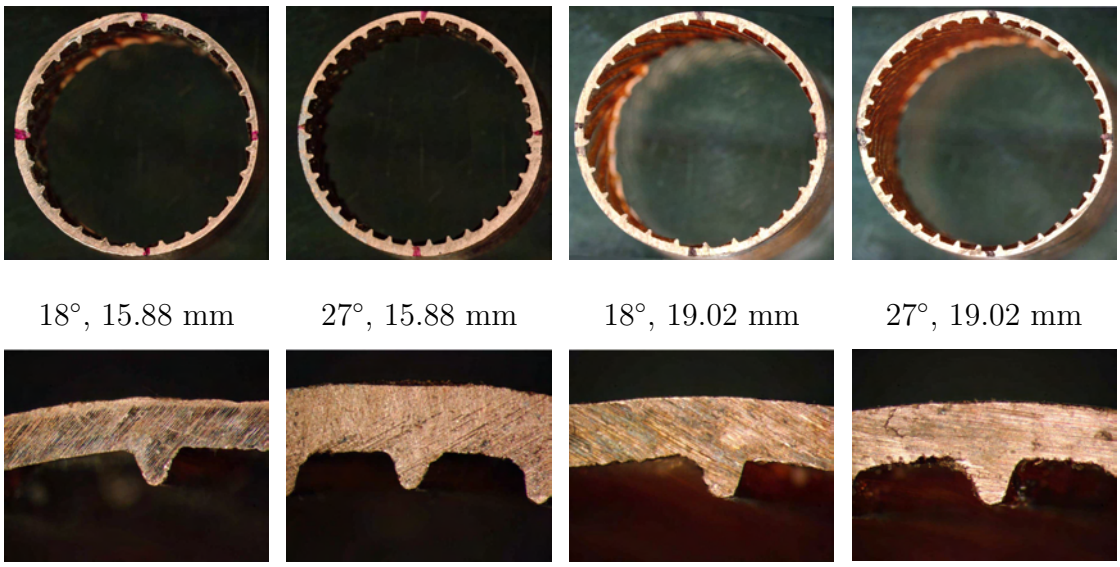

Figure 3.4 Cross-sectional view of the enhanced tubes (top) and close-up views of the fins (bottom).

A 20.7 mm inside diameter annulus was used for the 15.88 mm diameter tube and a 26.3 mm inside diameter for the 19.02 mm tube. The respective hydraulic diameters were 4.81 mm and 7.21 mm. To prevent sagging and the outer-tube touching the inner-tube, capillary tube was wound around the outer-surface of the inner-tube at a constant pitch of approximately 60°. This further promoted mixing inside the annulus. Figure 3.5 shows the test section under construction, with the capillary tube being visible.

Figure 3.6 gives a schematic layout of the test section. The test section was instrumented with a total of 53 thermocouples and two pressure taps. The overall heat transfer lengths were in the order of 5.1 m to 5.4 m while the pressure drop lengths were in the order of 5.13 m to 5.42 m.

The thermocouples were soldered to the tube by first drilling a 1 mm depression into the tube. Flux and solder were then inserted into this depression and heated. As soon as the solder melted, the thermocouple was inserted into the depression and the heat removed, allowing the tube to cool down. Each thermocouple was then checked to ensure that good contact with the tube was made.

The pressure taps were installed by drilling a 1 mm hole through the copper tube at the desired locations. These diameters for the taps were chosen so that they were smaller than 10% of the tube's inner-diameter (Rayle, 1959). This ensured that the taps did not cause any flow obstruction within the tube, which could lead to a localised eddy forming within the tap resulting in an error in pressure readings. After the holes were drilled, care was taken to ensure that any burrs that may have formed were removed, since burrs can cause a local increase in

Table 3.1 Geometric properties of the tubes tested.

Tube	D_o [mm]	D_i/D_r [mm]	D_h [mm]	L_{hx} [m]	$L_{\Delta p}$ [-]	n
R_1[a]	15.889	14.482	14.482	5.406	5.415	-
E_1	15.806	14.648	11.291	5.081	5.140	25
E_2	15.859	14.557	10.201	5.081	5.140	35
R_2	19.062	17.651	17.651	5.095	5.140	-
E_3	19.160	17.658	13.400	5.095	5.138	25
E_4	19.089	17.816	13.111	5.095	5.130	35

Tube	e [mm]	γ [°]	β [°]	A_{i_c} [m$^2 \times 10^6$]	A_i [m$^2 \times 10^3$]
R_1	-	-	-	164.72	245.95
E_1	0.399	46.97	18	166.80	319.44
E_2	0.395	43.93	27	164.22	348.11
R_2	-	-	-	244.70	282.50
E_3	0.480	38.49	18	242.89	391.97
E_4	0.467	41.92	27	247.12	407.56

[a] R_1 and R_2 are reference smooth tubes. E_1 to E_4 refer to the enhanced tubes.

pressure with the consequence being an incorrect reading. Lastly, a bush with a tap was then inserted over these holes and soldered to the copper tube. Nylon tubing was used to connect the pressure taps to the differential pressure transducer.

To obtain a representative inner-tube wall temperature, 36 of the 53 thermocouples were placed along the length of the inner-tube's outer-wall at nine, equally spaced stations; four thermocouples per station spaced at 90° intervals around the periphery. Five thermocouples were spaced along the length of the outer-wall of the annulus to obtain a representative annulus fluid temperature distribution.

The remaining thermocouples were placed at the in- and outlets of the test section; only three thermocouples positioned at 120° intervals around the periphery per in- and outlet were used due to the limited amount of available channels. The average of the three thermocouples was then used as a representative inlet and outlet temperature. These thermocouples were placed on a copper tube other than the test section itself, separated by rubber hosing. This was to prevent axial conduction from the test section, which may influence the temperature measurements. A detailed analysis of the axial conduction influence is given by Dobson (1994).

Due to thermal stratification which could occur at low Reynolds numbers, a static mixer

was inserted prior to the inner-tube's outlet-temperature measuring point. The static mixer was manufactured from a 22 mm copper tube with five fins inserted on the inside. This design was adapted from work done by Galaktionov *et al.* (2003). Each of the tapes was twisted with an angle of approximately 140° and then placed in series with each other; the trailing edge of the one being perpendicular to the leading edge of the other. This had the effect of splitting the thermal layer in half, mixing it, splitting it again and mixing it again, etc., so that in the end the flow was well mixed and the temperature throughout the cross-section of the tube was uniform.

3.3 Data Reduction

To achieve the objectives of this project, it is necessary to obtain representative heat transfer and friction factors for a smooth and enhanced inner-tube. This section will discuss the methodology used to obtain these two coefficients. The main method used to calculate the heat transfer coefficients is discussed in Section 3.3.1, while two alternative methods are also considered. For clarity purposes, the main method will be referred to as the *LMTD* method

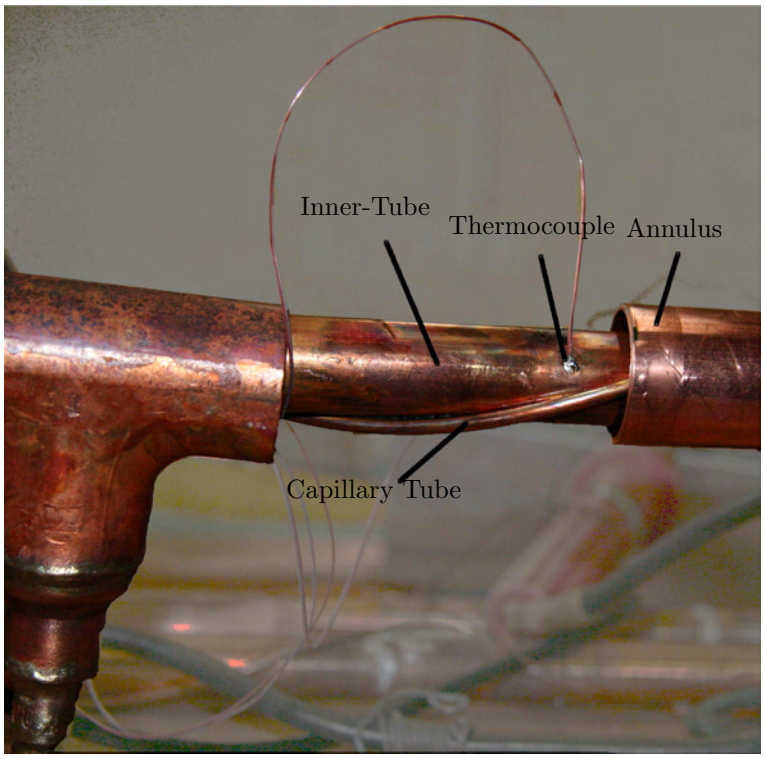

Figure 3.5 Test section under construction.

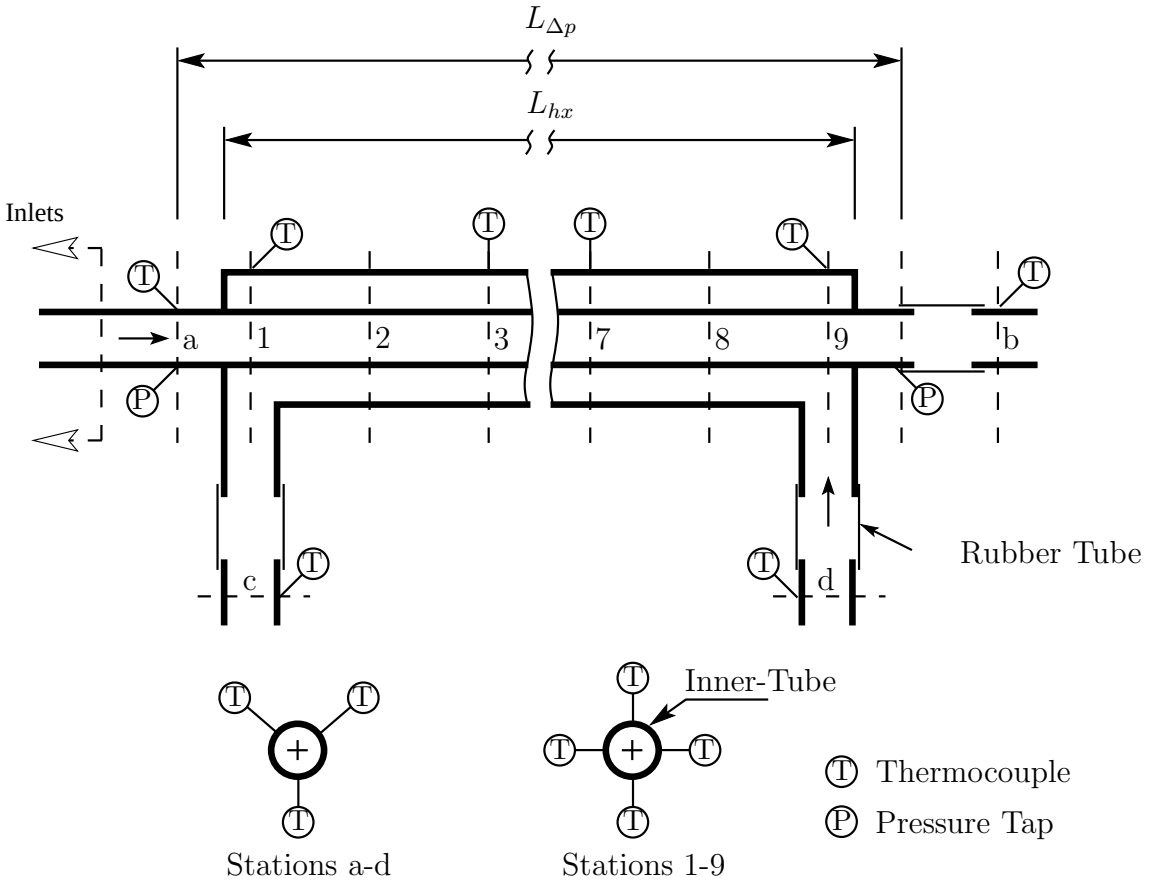

Figure 3.6 Schematic layout of the experimental test section in a counterflow, tube-in-tube configuration with pressure tap and thermocouple positions.

due to the Log Mean Temperature Difference being used to obtain the heat transfer coefficient. This reference will only be used in this chapter and Appendix B. Throughout the remainder of the document, however, the results of this method will be referred to as *Experimental Data*. In Section 3.3.2, the method used to obtain friction factors is discussed

3.3.1 Heat Transfer Coefficient

LMTD Method

The inner-tube's average heat transfer coefficient was obtained by making use of the overall heat transfer coefficient and the sum of the resistances as shown in Figure 3.7, where

$$\alpha_i = \frac{1}{A_i}\left[\frac{1}{UA} - R_w - \frac{1}{\alpha_o A_o}\right]^{-1} \tag{3.1}$$

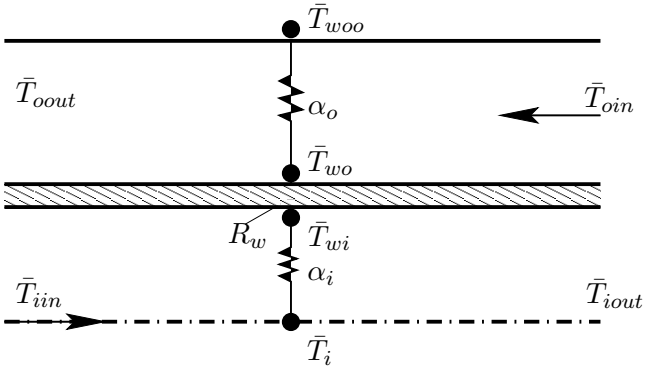

Figure 3.7 Schematic of the resistances inside an in-tube heat exchanger.

UA can be obtained by making use of the heat transfer as well as the log mean temperature difference, as

$$UA = \frac{\dot{Q}_i}{T_{lmtd}} \tag{3.2}$$

where $\dot{Q}_i$ is given by

$$\dot{Q}_i = \dot{m}_i \left(h_{iin} - h_{iout}\right) \tag{3.3}$$

and similarly the heat transfer in the annulus by

$$\dot{Q}_o = \dot{m}_o \left(h_{oout} - h_{oin}\right) \tag{3.4}$$

with the enthalpies obtained from IAPWS (2003), which is directly related to the local specific heat and temperature values.

The heat transfer in the inner-tube was compared with that in the annulus by means of an energy balance, given by

$$eb = \frac{\dot{Q}_i - \dot{Q}_o}{\left(\dot{Q}_i + \dot{Q}_o\right)/2} \times 100 \tag{3.5}$$

Although good energy balances were obtained the inner-tube heat transfer rate was used for all the calculations as it was the more accurate of the two. This was because the annulus flow rate was kept high such that its heat resistance was as low as possible. The consequences were

that the temperature difference between the inlet and outlet of the annulus were much smaller than those in the inner-tube, giving the heat transfer rate of the annulus a larger uncertainty than that of the inner-tube.

The log-mean temperature difference used in Equation (3.2) is given by

$$T_{lmtd} = \frac{\left(\bar{T}_{iin} - \bar{T}_{oout}\right) - \left(\bar{T}_{iout} - \bar{T}_{oin}\right)}{\ln\left(\frac{\bar{T}_{iin} - \bar{T}_{oout}}{\bar{T}_{iout} - \bar{T}_{oin}}\right)} \tag{3.6}$$

The wall resistance in Equation (3.1) is obtained by

$$R_w = \frac{\ln(D_o/D_i)}{2\pi k_{cu} L_{hx}} \tag{3.7}$$

The thermal conductivity of the copper was obtained from Abu-Eishah (2001) and is given by

$$k_{cu} = a\bar{T}_{Cu}^{b} e^{c\bar{T}_{Cu} + d/\bar{T}_{Cu}} \tag{3.8}$$

where the constants $a = 82.56648$, $b = 0.262301$, $c = -4.06701 \times 10^{-4}$ and $d = 59.72934$. $\bar{T}_{Cu}$ is the mean temperature of the copper tube in Kelvins.

As a first approximation, the wall temperature on the outer-surface of the inner-tube was used for T_{Cu} to calculate the tube's thermal conductivity. After this the temperature of the inner-wall of the inner-tube was calculated. The average of the outer-wall and the inner-wall temperature was then used to calculate a new thermal conductivity value, with the process being repeated until the solution converged. The influence of the wall resistance on the heat transfer coefficient in all cases, however, was found to be negligible.

Lastly, the annulus heat transfer coefficient was calculated by making use of the annulus outer-wall temperature and the temperature of the outer-wall of the inner-tube, all of which were measured. Thus,

$$\alpha_o = \frac{\dot{Q}_i}{A_o\left(\bar{T}_{wo} - \bar{T}_{woo}\right)} \tag{3.9}$$

Since the wall temperatures were measured along the length of the heat exchanger, an appropriate average value was used for all calculations. This average value was obtained by integrating the temperature as a function of the axial length position and dividing by the total length of the heat exchanger. The *trapezoidal rule* instead of a curve fit was used due to the relatively high uncertainty obtained when using a curve fit, as explained in Appendix B.

Alternative Methods

Two other methods were also used to calculate the average inner-tube heat transfer coefficient, namely the *Wilson Plot Technique* and the *Single-Stream Exchanger* method.

The method described by Shah (1990) was used for the Wilson Plot technique with the full analysis being given in Appendix C. This method is used to obtain an equation for the annulus heat transfer coefficient with which the average inner-tube heat transfer coefficient, Equation (3.1), is calculated. The resulting annulus heat transfer coefficient obtained from the Wilson Plot technique is given by

$$\alpha_o = 0.01983 Re_o^{0.8618} Pr_o^{0.4} \left(\frac{\mu_o}{\mu_w}\right)^{0.14} \frac{k_o}{D_{ho}} \tag{3.10}$$

For the single-stream exchanger method, the exchanger was modelled as a single-stream heat exchanger, as shown in Figure 3.8 and which is described in most heat transfer text books. Experimentally, this is accomplished by enforcing a constant wall temperature boundary condition on the inner-tube by means of a very high flow rate in the annulus. The temperature profile of the inner-fluid can then be derived (Mills, 1999) and is given by

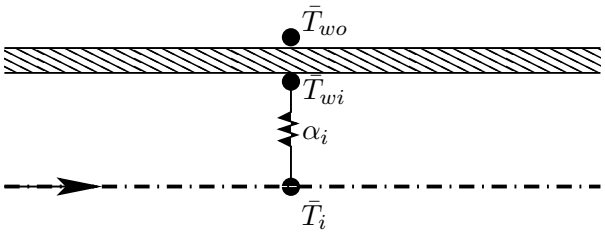

Figure 3.8 Schematic of the resistances inside an in-tube heat exchanger as modelled for a single-stream heat exchanger.

$$T_i(x) = \bar{T}_{wi} + \left(\bar{T}_{iin} - \bar{T}_{wi}\right) e^{\frac{-UP}{\dot{m}_i c_{pi}} x} \tag{3.11}$$

To obtain the average inner-fluid temperature, Equation (3.11) is integrated with respect to the axial distance, x, over the whole length of the tube, or

$$\begin{aligned} \bar{T}_i &= \frac{1}{L_{hx}} \int_0^{L_{hx}} T_i(x) \mathrm{d}x \\ &= \frac{1}{L_{hx}} \int_0^{L_{hx}} \left(\bar{T}_{wi} + \left(\bar{T}_{iin} - \bar{T}_{wi}\right) e^{\frac{-UP}{\dot{m}_i c_{pi}} x}\right) \mathrm{d}x \\ &= \frac{1}{L_{hx}} \left[\bar{T}_{wi} x - \frac{1}{UP} \left(\bar{T}_{iin} - T_{wii}\right) \dot{m}_i c_{pi} e^{\frac{-UP}{\dot{m}_i c_{pi}} x}\right]_0^{L_{hx}} \end{aligned} \tag{3.12}$$

Therefore, the average inner-fluid temperature is given by

$$\bar{T}_i = \bar{T}_{wi} - \frac{\left(\bar{T}_{iin} - \bar{T}_{wi}\right) \dot{m}_i c_{pi}}{UPL_{hx}} e^{\frac{-UPL_{hx}}{\dot{m}_i c_{pi}}} + \frac{\dot{m}_i c_{pi}}{UPL_{hx}} \left(\bar{T}_{iin} - \bar{T}_{wi}\right) \tag{3.13}$$

The average of the inlet and outlet temperatures of the inner-tube was used to obtain an initial value of the specific heat. A new value was determined after a new inner-fluid temperature was calculated, the process being repeated once the solution converged.

The inner-tube's heat transfer coefficient was then obtained by

$$\alpha_i = \frac{\dot{Q}_i}{A_i\left(\bar{T}_i - \bar{T}_{wi}\right)} \tag{3.14}$$

3.3.2 Friction Factor

The friction factors for a uniform-density, one-dimensional flow inside a smooth tube is defined as the ratio of the wall shear stress to the fluid kinetic energy, or

$$f = \frac{\tau_w}{1/2\rho u^2} \tag{3.15}$$

For a tube with length L and diameter D, the friction factor can be written in terms of the overall pressure drop, Δp, as

$$f = \frac{D_i \Delta p}{2\rho_i u_i^2 L_{\Delta p}} \tag{3.16}$$

Δp is obtained from the differential pressure transducers. The fluid properties were calculated at the average inner-tube fluid temperature which, in turn, was determined by the resulting heat transfer coefficient, Equation (3.1), as

$$\bar{T}_i = \frac{\dot{Q}_i}{\alpha_i A_i} + \bar{T}_{wi} \tag{3.17}$$

This temperature was also used to determine the Reynolds, Prandtl, Nusselt and other dimensionless groups with the fluid properties being obtained from Wagner and Pruß (2002).

3.4 Instruments

3.4.1 Thermocouples

T-type thermocouples with a wire diameter of 0.254 mm (30 American Wire Gauge) and an accuracy of 0.1°C were used for temperature measurements. All thermocouples were, however, calibrated in a constant temperature calibration bath with a Pt-100 temperature probe which itself was calibrated to 0.01°C. Calibration commenced at two different temperatures, one at 15°C and the other at 60°C, since the variation of thermocouple temperature with that of the Pt-100 was highly linear. One hundred points at each temperature for each thermocouple were captured and averaged. The standard deviation of each thermocouple was less than 0.01°C. A

first-order polynomial was then fitted through the two calibration points for each thermocouple. These linear equations were then saved into a file for use for the data-capturing program.

3.4.2 Pressure Drop

Pressure drops were measured with two differential pressure transducers. One of the transducers had an accuracy of 0.1% of full scale, full-scale being 7.1 kPa, while the other had an accuracy of 0.25% of full-scale. The difference with the latter transducer was that its full scale range could be varied by replacing the diaphragm. The two diaphragms used had a full scale range of 1.4 kPa and 14 kPa. Thus, the differential pressure accuracy at low Reynolds numbers was in the order of 3.5 Pa.

Each transducer was calibrated with a water manometer which had an uncertainty of 0.17%. Since the transducer's signal output varies linearly with pressure, only two points were required for a calibration. The two points chosen were the two extremities of the transducer's pressure range, namely zero and maximum differential pressure. This data was also saved into a file which was used by the data-capturing program.

3.4.3 Flow Meters

Coriolis mass flow meters were used to measure the flow rates inside the inner-tube and the annulus. The flow meters had a manufactured accuracy of 0.1% of the flow rate, but were factory-calibrated to within 0.03%. Three different models of flow meters were used. For the hot fluid loop through the inner-tube, a flow meter with a maximum flow rate of 144 kg/h was used for the low flow rate experiments, while for higher flow rates, a meter with a maximum flow rate of 2 415 kg/h was used. For the cold water loop through the annulus, two flow meters were also used; one with a maximum flow rate of 2 415 kg/h and the other with a maximum of 6 480 kg/h, although the larger of the two was mainly used.

3.5 Uncertainties

The method followed to calculate the uncertainties for the test section was that suggested by Kline and McClintock (1953), as well as Moffat (2000). All uncertainties were calculated within the 95% confidence interval. Table 3.2 lists these instruments with their respective range, bias, repeatability and total uncertainty. The range was determined by taking the standard deviation of each instrument from a sample containing 400 data points and multiplying it by two for the 95% confidence interval.

The full uncertainty analysis can be found in Appendix B with the final uncertainties listed in Table 3.3. The uncertainty of the heat transfer coefficients is between 0.6% and 4% for high and low Reynolds numbers, respectively. The friction factor uncertainty, however, is between 0.3% and 18% for high and low Reynolds numbers respectively. Using a pressure transducer

Table 3.2 Ranges and accuracies of instruments to be used.

Instrument	Range	Bias	Precision	Uncertainty
Thermocouple	$-200 - 350$ °C	0.1 °C[a]	0.023°C	0.103°C
Coriolis Flow Meter				
Inner-Tube High Re	$0 - 0.667$ kg/s	0.1%	0.06%	0.117%
Inner-Tube Low Re	$0 - 0.04$ kg/s	0.1%	0.08%	0.131%
Annulus	$0 - 1.8$ kg/s	0.1%	0.02%	0.102%
Pressure Transducers				
Transducer 1	Diaphragm Selection[b]	0.25%FS[c]	0.9%	0.93%
Transducer 2	0-7 kPa	0.1%FS	1.6%	1.6%

[a] Calibrated with a Pt-100, which had an uncertainty of 0.01°C.

[b] This pressure transducer has multiple diaphragms that can be changed for the desired pressure drop range.

[c] FS = Full Scale.

having a 0.25% accuracy with a full-scale pressure differential of 1.4 kPa, implies it will have an accuracy of approximately 3.5 Pa. Pressure drops at the lowest Reynolds numbers for a smooth tube is in the order of 20-25 Pa and hence uncertainties in the order of 18% are attainable. Lower available full-scale transducers would improve the uncertainty to approximately 11%, however, their usage is very impractical due to the limited range.

3.6 Experimental Procedure

After the start-up of the system, it was necessary to operate the system without changes to settle for at least an hour to reach steady-state conditions. This was due to the thermal inertia of the system being relatively slow before it got to steady-state temperatures and negligible changes in the mass flow rates. Once the system was stabilised small changes were made in the mass flow rates until the desired flow rates were set from where data would be captured.

Steady-state conditions were monitored by making use of the standard deviations of each measurement. For example, inlet temperatures were considered to be at steady state once its standard deviation for the last minute of measurement was less than 0.05°C. Mass flow rates were considered steady when the standard deviation was less that 0.1%, while that of the pressure drop less than 0.8%. Cases existed where these steady-state conditions could not be met and was normally due to the flow being in the transition region. In this region, pressure drops and temperature fluctuations were common.

After a change was made in the mass flow rate, it took approximately 2-4 minutes for steady-state conditions to be reachieved. The reason for such a short time was that the mass flow rate

Table 3.3 Uncertainties of the equations used to obtain heat transfer and friction factors at low Reynolds numbers (≈ 500) and high Reynolds numbers ($\approx 15\ 000$).

Property	Low Re	High Re
$\dot{m}_i$	0.28%	0.10%
$\dot{m}_o$	0.10%	0.11%
$\bar{T}_{iin/iout}$ & $\bar{T}_{oin/oout}$	0.073°C	0.058°C
$\bar{T}_{woo}$	0.047°C	0.047°C
$\bar{T}_{wo}$	0.017°C	0.021°C
$\bar{T}_{wi}$	0.017°C	0.021°C
$\bar{T}_i$	0.389°C	0.111°C
T_{lmtd}	0.383°C	0.070°C
$\dot{Q}_i$	0.32%	0.24%
UA	3.9%	0.41%
Re	1.04%	1.01%
Nu	4.21%	1.15%
Pr	1.97%	1.42%
Δp	18%	0.12%
α_i	4.09%	0.57%
f	18%	0.30%

increments from one measuring point to another were relatively small. Data were only captured once these conditions were met and an energy balance of less than 1% was achieved. This energy balance criterion was mostly achieved, and only at low Reynolds numbers (500 - 6 000) was it greater than 1%. This was due to the temperature difference between the annulus inlet and outlet being relatively small (less than 2°C) giving rise to high uncertainties in heat transfer rate. Energy balances of less than 1% were achieved, though, by substantially decreasing the annulus mass flow rate and hence decreasing the annulus heat transfer rate uncertainty. This was, however, only performed to show that good energy balances could be obtained at low Reynolds numbers and that the heat transfer in the inner-tube can be accurately measured.

A software program was written to monitor the steady state-conditions, energy balances, friction factors and heat transfer coefficients. The program was written in such a way that all this information could be used to capture the data automatically. This included the naming of the data files and the controlling of the mass flow rates. The flow rate increments were preset by the user for different Reynolds ranges. For example, fine increments were used where the flow was in or near the transition region while rougher or bigger increments were used in the fully laminar and turbulent regimes.

With regard to the capturing of data, one file for each mass flow rate (or Reynolds number)

was used. Each file consisted of 100 data points with each point being captured at a rate of approximately 0.5 Hz. These 100 data points were averaged to obtain a single value which was used in all the calculations. The data consisted of inlet and outlet temperatures of the inner-tube and annulus, pressure drops, the mass flow rates of the inner-tube and annulus and all the wall temperatures. These data were used in another, separate program for analysis purposes.

3.7 Validation

The validation of the methodologies of determining the heat transfer coefficients and friction factors was done by taking measurements for fully developed flow in the laminar and turbulent flow regimes inside a smooth tube and comparing it with established heat transfer and friction factor correlations. The validation friction factor measurements were taken for adiabatic flow only as this disregarded any influence of heat transfer on the properties of the fluid. Only the 15.88 mm smooth tube results will be shown for validation purposes as similar results were obtained with the 19.02 mm tube.

3.7.1 Heat Transfer Coefficients

Laminar flow heat transfer data obtained by means of the *LMTD* method, *Wilson Plot technique* and *Single-stream exchanger* method, is compared to mixed convection correlations from the literature. These are the correlations of Oliver (1962), Palen and Taborek (1985), and Shome and Jensen (1995), given in Table 3.4. The laminar correlation of Ghajar and Tam (1994) is also used for comparison purposes, however is not given in Table 3.4 as it was discussed in Chapter 2. The thermally developing forced convection correlation of Shah and London (1978) is also used for comparison.

Table 3.4 Laminar mixed convection heat transfer correlations.

Oliver (1962)

$$Nu = 1.75\left(Gz + 5.6\times10^{-4}\left(GrPrL/D\right)^{0.7}\right)^{1/3} \tag{3.18}$$

$$29 < Gr < 1.6\times10^{5},\ 7 < Gz < 187,\ 1.9 < Pr < 326$$

▶ Percentage deviation: -25%, + 110%

continued on next page...

...continued from previous page

Palen and Taborek (1985)

$$Nu = 2.5 + 4.55\left(Re^{*}D/L\right)^{0.37} Pr^{0.17}\left(\frac{\mu_b}{\mu_w}\right)^{0.14} \tag{3.19}$$

with

$$Re^{*} = Re + 0.8Gr^{0.5}exp\left(-42/Gr^{2}\right)$$

$$0 < L/D < \infty,\ 0 < Gr < 10^{7},\ 0.1 < Re < 2\ 000,\ 10^{-3} < \mu_b/\mu_w < 55,\ 20 < Pr < 10^{4}$$

► Percentage deviation: ± 30% (due to experimental database)

Shome and Jensen (1995)

For $\Delta \leq 1$

$$\frac{Nu}{Nu_{TD,CP}} = \begin{cases} \left(\frac{\nu_b}{\nu_w}\right)^{0.18} & \text{Thermally developing} \\ \left(\frac{\nu_b}{\nu_w}\right)^{0.22}\left[1 + 0.067\left(z^{+}Pr\right)^{-0.62}\right]^{0.27} & \text{Simultaneously dev.} \end{cases} \tag{3.20}$$

with

$$Nu_{TD,CP} = \begin{cases} -0.5632 + 1.57\left(z^{+}\right)^{-0.3351}, & 10^{-6} < z^{+} \leq 10^{-3} \\ 0.9828 + 1.129\left(z^{+}\right)^{-0.3686}, & 10^{-3} < z^{+} \leq 10^{-2} \\ 3.6568 + 0.1272\left(z^{+}\right)^{-0.7373} e^{\left(-3.1563z^{+}\right)}, & z^{+} > 10^{-2} \end{cases}$$

For $\Delta > 1$

$$Nu = 7.93Ra^{0.21}\Im^{-0.05}\ln\left(1 + 0.13\Delta\right)/\Delta \tag{3.21}$$

with

$$\Im = \frac{1 + \left(\frac{d\nu}{dT}\right)_b\left(\frac{T_w - T_b}{\nu_b}\right)}{\nu_b/\nu_w},\ \Delta = Ra^{1/4}\Im^{1/4}\left(z^{+}\right)^{1/2},\ z^{+} = \frac{z}{DRe_{in}Pr_{in}}$$

with Δ being a measure of the relative strengths of forced and natural convection.

► Percentage deviation: ± 15%

Figure 3.9 shows the correlations compared to the experimental data for 54 laminar data points. Comparing the different heat transfer techniques with each other, the Wilson Plot technique deviates from the LMTD method on average by 0.18% with a maximum deviation of 0.5%, while the single-stream exchanger method deviates on average by 1.2% with a maximum deviation of 3.9%. Hence, the three different methods of capturing laminar heat transfer coefficients are in excellent agreement, showing that making use of the LMTD method as a general method for capturing heat transfer data further on in this study (Chapter 4 onwards) would be acceptable.

These laminar results, however, are much higher than would be expected from fully developed laminar flow theory for a constant wall temperature boundary. These results are very

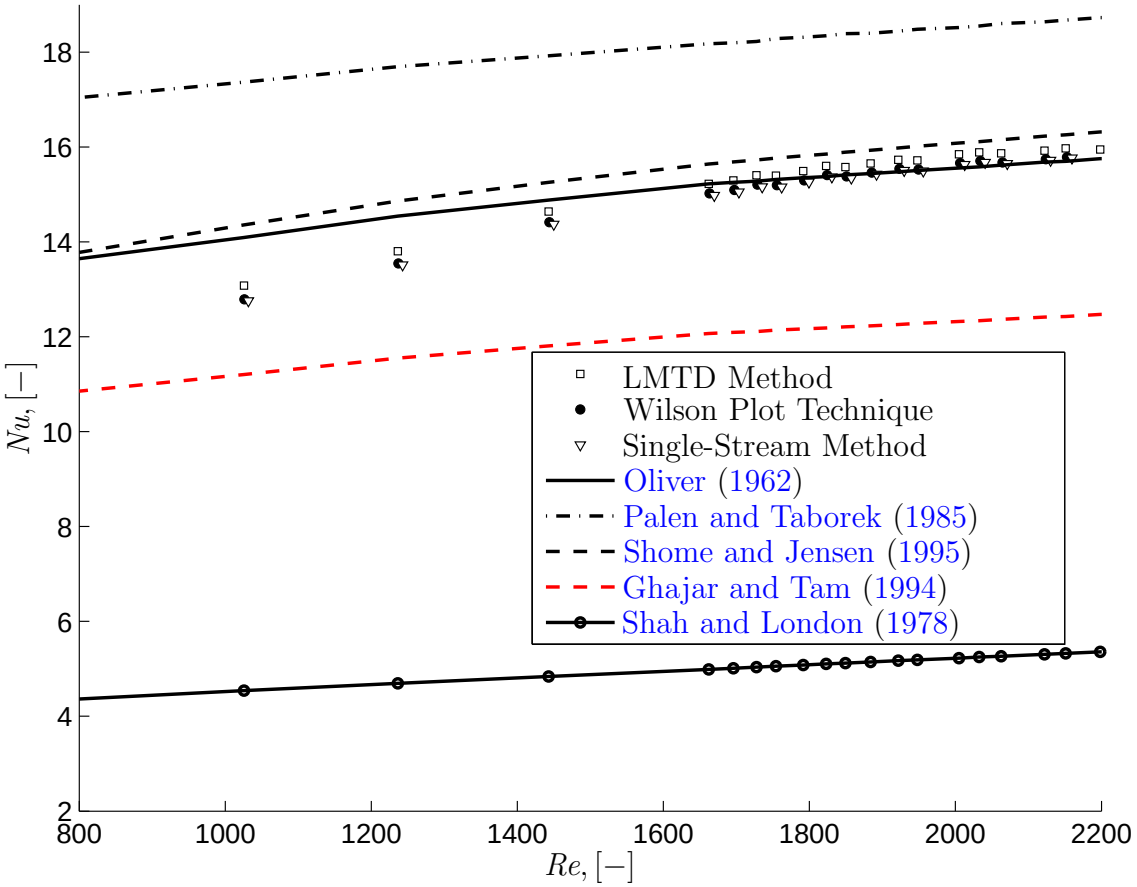

Figure 3.9 Laminar heat transfer results including correlations for natural convection effects and thermally developing flow.

similar to the results obtained by Oliver (1962), Depew and August (1971), Yousef and Tarasuk (1982), Palen and Taborek (1985) and Ghajar and Tam (1991) (to name but a few) who also reported higher laminar heat transfer results. This is mainly due to mixed convection due to the fluid property variation between the tube wall and centre. This variation brings about a secondary flow which in turn enhances the heat transfer. Metais and Eckert (1964) recommends the use of a flow regime map to distinguish between mixed and forced convection flow regimes. This map is based on the Reynolds number being a function of the product of the Grashof and Prandtl numbers, which is mainly the driving parameters for mixed convection. Such a graph is presented in Figure 3.10 which includes the current data. It is seen that the laminar flow data is well within the mixed convection boundary. It must be noted that this graph is based on the mean fluid temperature and all properties are calculated at the film temperature.

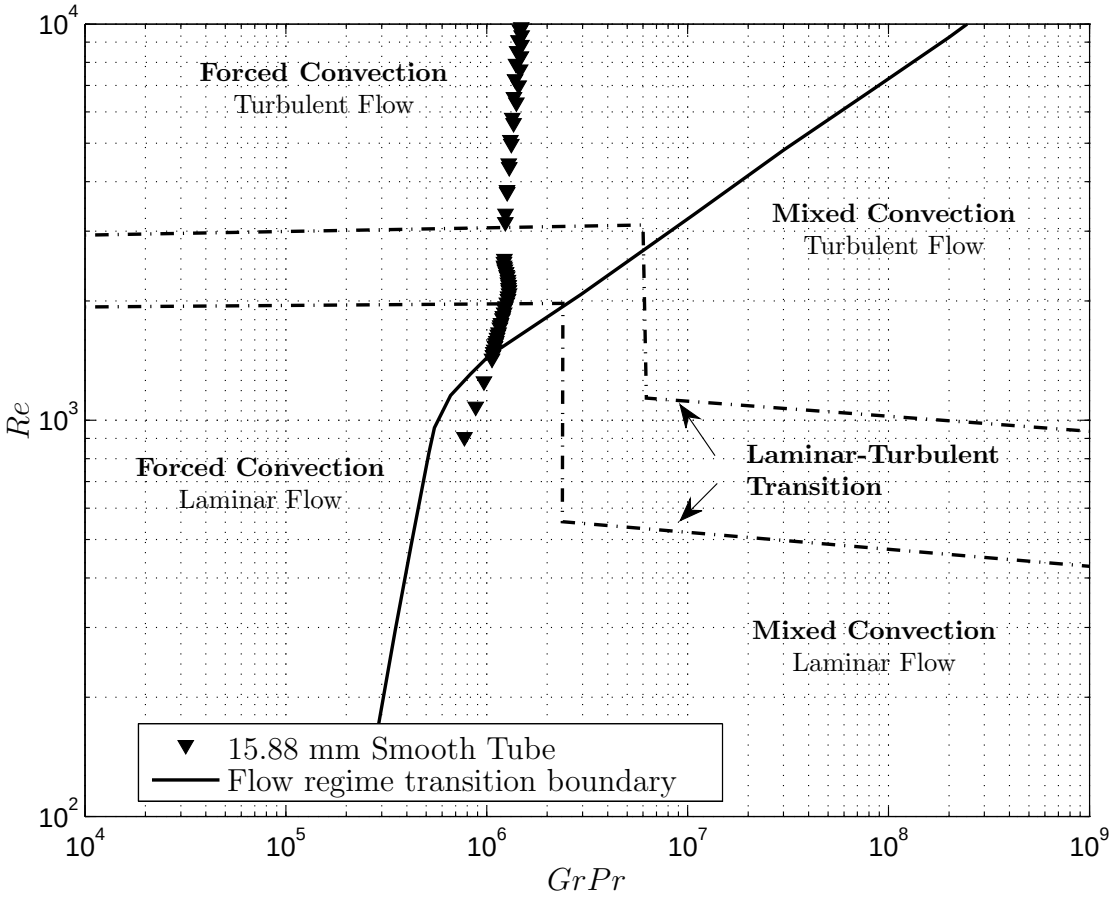

Figure 3.10 Laminar-turbulent heat transfer results on the flow regime map of Metais and Eckert (1964).

Comparing the correlations of Oliver (1962), Palen and Taborek (1985) and Shome and Jensen (1995) with the LMTD method (Figure 3.11), it was found that the correlation of Oliver underpredicts the data on average by 10% with a maximum deviation of 12%, Palen and Taborek overpredicts the data on average by 20% with a maximum of 34%, while the correlation of Shome and Jensen (1995) underpredicts the data on average by 7.4% with a maximum deviation of 8.9%. It should be mentioned, though, that Depew and August (1971) found Oliver (1962)'s correlation to represent their database to within -25% to +110%. Further, the use of the correlation of Palen and Taborek (1985) would be questionable as it falls outside the range of the experimental data ($Pr < 20$). The correlation of Ghajar and Tam (1994) underpredicts the data on average by 21% with a maximum deviation of 22%.

It should be mentioned that the correlation of Ghajar and Tam was developed for the heating of the fluid and is valid for much higher Prandtl numbers. The heating of the fluid

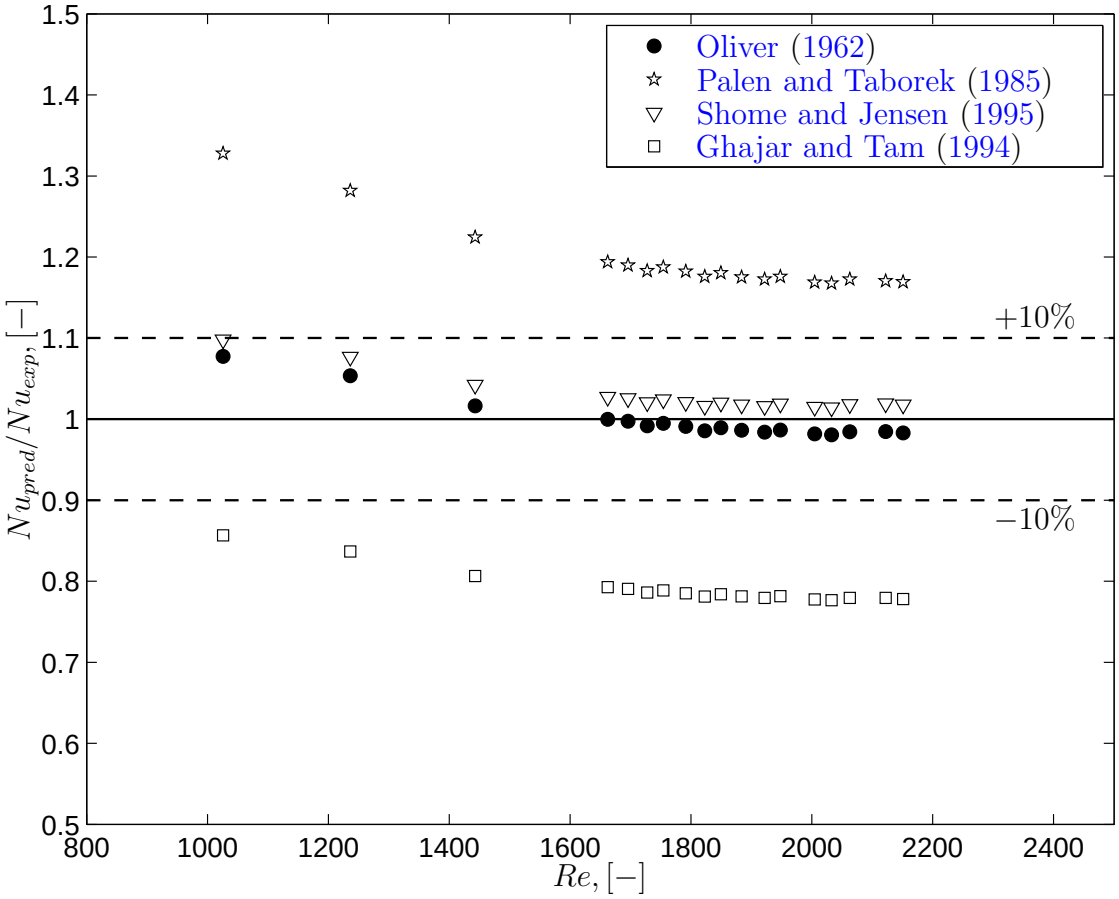

Figure 3.11 Ratio of predicted to measured Nusselt numbers as a function of the Reynolds number.

has a completely opposite effect regarding mixed convection when compared to the cooling of the fluid, as discussed by Shome and Jensen (1995). It must also be noted that the current experimental data and the correlations with which it is compared is for thermally developing flow. The correlation and data of Ghajar and Tam (1994) is for simultaneously developing flow. However, noting the overall trend of the heat transfer data of Ghajar and Tam when compared to the current data, it can be concluded that mixed convection combined with secondary flows to be the cause for the higher than expected heat transfer results.

Another effect which may explain the higher heat transfer coefficients measured than that of theory for a constant wall temperature and uniform heat flux is the developing thermal entrance region. For a uniform wall temperature, holding true for the current set-up, the thermal entrance length is defined by Shah and London (1978) as

$$L_{eh} = 0.0334654 Re \mathrm{Pr} D_i \tag{3.22}$$

The thermal entrance length at a Reynolds number of 2 300 will be in the order of 346 tube-diameters, or 5 m for the 15.88 mm tube and 6.1 m for the 19.02 mm tube. In this instance, the thermal entrance lengths are as long and even longer than the test sections themselves. The Nusselt number for thermally developing flow, given by Shah and London (1978), is also given in Figure 3.9. Although there is a thermal entrance effect it does not seem to be as substantial as the effect due to mixed convection. It can thus be concluded that the main mechanism to the laminar heat transfer is mixed convection and that measurements in the laminar flow regime have been validated.

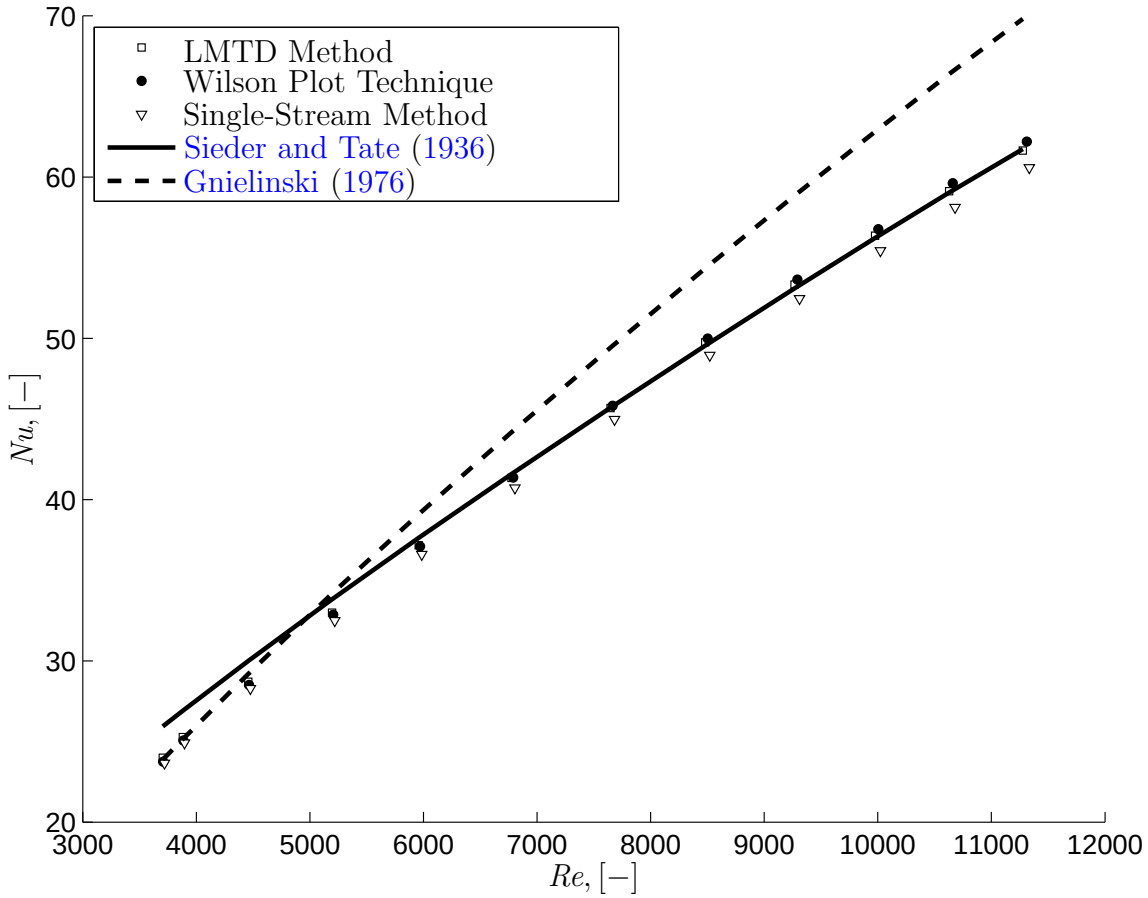

Figure 3.12 Validation of heat transfer results for turbulent flow inside a smooth tube.

Figure 3.12 shows the heat transfer results in the turbulent flow regime for a Reynolds number range of 3 000 - 12 000. The three different techniques as well as the Sieder and Tate (1936)[1] and Gnielinski (1976) equations are shown. These three methods compare very well with each other, with the Wilson Plot technique deviating from the LMTD method on average by 0.8% with a maximum deviation of 1.1%, while the single-stream exchanger method deviates on average by 3.7% with a maximum deviation of 4.3%. The single-stream exchanger results start to deviate from the other data points at high Reynolds numbers ($> 10\ 000$). This is due to the amount of heat transferred being high enough such that the tube wall no longer remains isothermal. The consequence is that Equations (3.11) to (3.13) are no longer valid.

There are two distinct trends regarding the prediction methods shown. The Sieder and Tate (1936) correlation predicts the turbulent results with very good accuracy at the upper end of the Reynolds number range tested ($> 5\ 000$) and over predicts the data at lower Reynolds numbers. The Gnielinski (1976) correlation, on the other hand, predicts the lower turbulent results quite well while over predicting the data at higher Reynolds numbers. The Sieder and Tate equation was only developed for Reynolds numbers greater than 10 000, hence its relatively poor performance at lower Reynolds numbers being understandable. The Gnielinski correlation, which is a more modern correlation, was initially developed by Petukhov and Popov (1963) for Reynolds numbers greater than 10 000. Gnielinski (1976) modified this correlation to predict heat transfer coefficients to Reynolds number values below 10 000 ($> 2\ 300$). The original correlation was, however, developed for fluids being heated and, as Petukhov and Popov (1963) stated, their correlation over-predicted their data for the cooling of fluids, thus explaining the current trend.

Comparing the LMTD method with the Sieder and Tate (1936) and Gnielinski (1976) equations, the LMTD method is underpredicted on average by less than 1% and 6%, respectively, with a maximum deviation of 8% and 11% respectively. Because of the good comparison of results and agreement with the turbulent correlations, it can be concluded that the system and procedure for calculating the heat transfer coefficient in the turbulent flow regime have been validated.

3.7.2 Friction Factor

The validation friction factor data consisted of a total of 317 data sets with 100 data points per set, giving a total of 317 000 data points. The data sets consisted of both increasing and decreasing increments of the Reynolds number which spanned from $Re = 500 - 12\ 000$, covering a good portion of the laminar and turbulent flow regimes. These measurements were made without any heat transfer to eliminate any varying density and viscosity effects. This also ensured that the results could be compared with the laminar flow Poiseuille relation as it is given for an isothermal fluid. A fully developed laminar velocity profile was enforced with

[1] It should be noted that any reference made to the Sieder and Tate equation is in fact the Colburn (1933) relation but with the viscosity correction proposed by Sieder and Tate (1936)

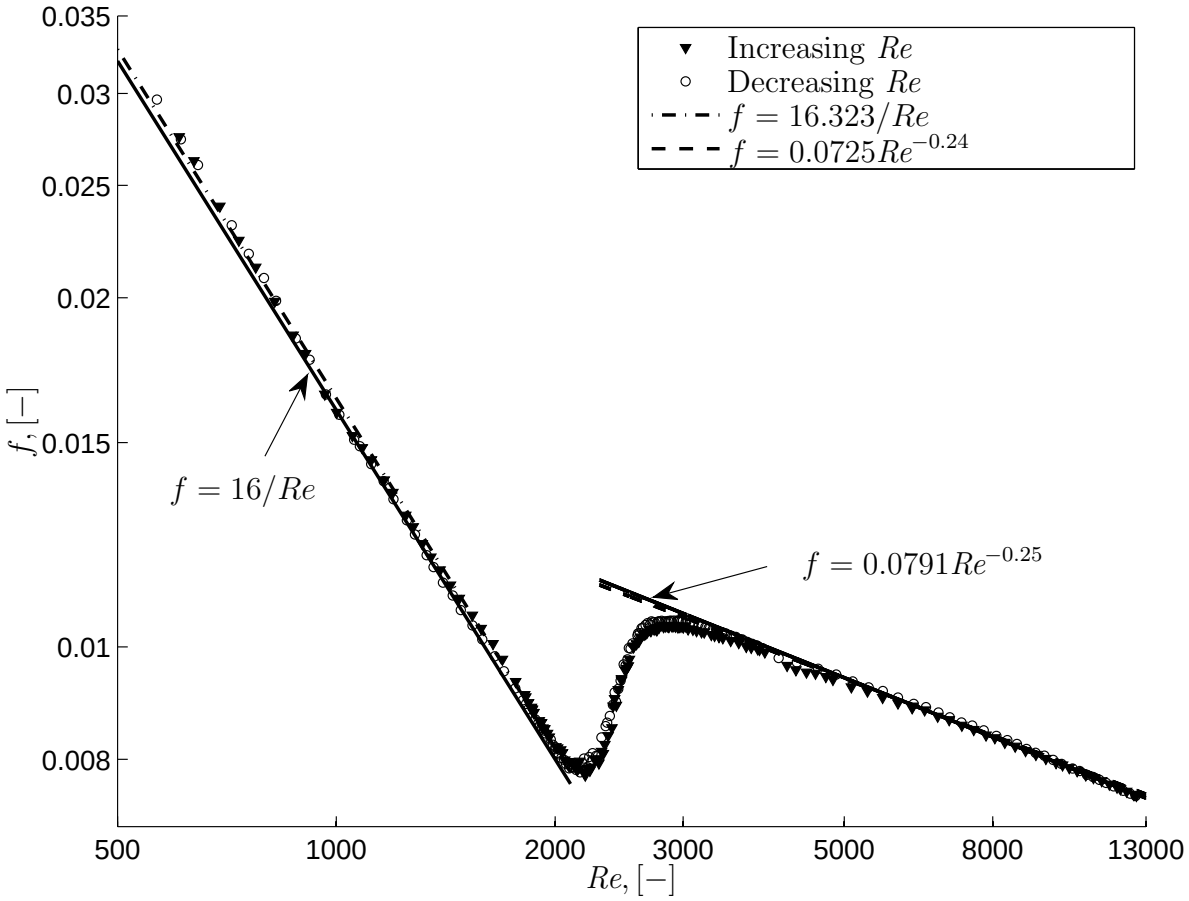

Figure 3.13 Validation of adiabatic friction factor results inside the 15.88 mm smooth tube with a fully developed inlet profile for increasing and decreasing Reynolds number increments.

the inlet length being long enough to ensure hydrodynamic fully developed flow.

Figure 3.13 shows the friction factor results for all the flow regimes, from laminar to turbulent, for increasing and decreasing Reynolds number increments. Also shown in the figure are the laminar, isothermal equation (Poiseuille flow), and the Blasius equation for turbulent flow.

Comparing the laminar results with the isothermal equation, the data is underpredicted on average by 1.5% with a maximum deviation of 4.5%. The constant of 16 in the Poiseuille relation is modified to a value of 16.373, which then predicts the data on average to within 0.5% with an average rms deviation of 1.4%. For the turbulent data, the correlation of Blasius on average overpredicts the data by 0.7% with a maximum deviation of 2.5%. The constants of the Blasius equation can also be modified to better predict the data, with the resulting equation

$$f = 0.0725Re^{-0.24} \tag{3.23}$$

predicting the turbulent data on average to within 0.5% with a mean rms deviation of less than 1%. Comparing the increasing and decreasing Reynolds number data, it was found that the two deviate from each other on average by 0.5% with a maximum deviation of 4.3%.

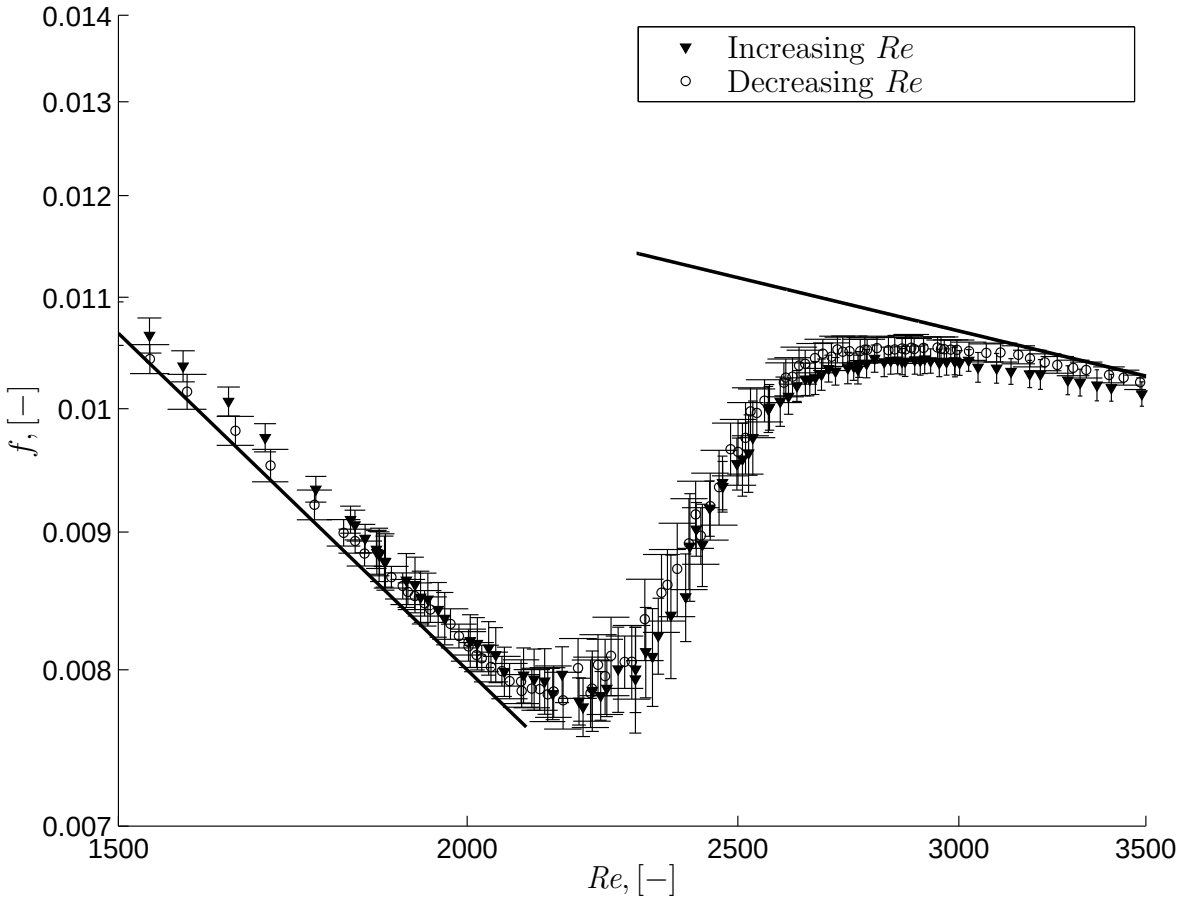

Figure 3.14 Validation of friction factor results inside smooth tube with a fully developed inlet profile for increasing and decreasing Reynolds number increments.

Figure 3.14 shows a close-up of the transition region. The uncertainties of the Reynolds number and friction factor are included. These uncertainties are higher in the transition region than in the laminar and turbulent region, showing the fluctuations which are encountered in this region. Looking at these uncertainties and the sudden change in friction factor values with increasing/decreasing Reynolds number, it can be concluded that the transition region lies between the Reynolds number values of 2 100 and 2 900. These are typical values being given

in most fluid mechanics textbooks. This also confirms the observation made by Binnie (1945), who visually observed transition to start at a Reynolds number of 1 970 and become fully turbulent at 2 900. It also seems from Figure 3.14 that no hysteresis occurs in the transition region. This result is also confirmed by the data of Patel and Head (1968), who studied reverse transition from turbulent to laminar flow.

Figure 3.15 includes data obtained from Senecal and Rothfus (1953), Nunner (1956), Koch (1960), Patel and Head (1969), Ghajar and Madon (1992) and García *et al.* (2005). Also included is the correlation of Churchill (1977) for fully developed flow. The data of Ghajar and Madon (1992) is highlighted in red since it is very closely related to this work. The data is based on the bellmouth inlet in the fully developed region of the tube. The current experimental data and the data of Ghajar and Madon (1992) are in excellent agreement with regard to transition. This is even further confirmed by the correlation of Churchill (1977) which is in excellent agreement with the data. This adds a great amount of confidence in the current measurement technique and further validates the experimental system. Hence, it can be concluded from all the comparisons of the measured data with theoretical data as well as data from other researchers in the laminar, transition and turbulent flow regimes that the friction factors are validated.

3.8 Conclusion

The experimental and test section set-ups were described in detail in this chapter. The test section was a tube-in-tube type, with hot fluid flowing in the inner-tube and cold fluid in the annulus. The main focus of the exchange process was inside the inner-tube. The set-up was developed so that tubes of different diameters, enhancements and inlet profiles could be tested.

For validation purposes, three different methods for calculating heat transfer coefficients were used. These methods were the *LMTD* method, the *Wilson Plot* technique and the *Single-Stream Exchanger* method.

For the friction factors, only adiabatic results were used for validation purposes. This was to eliminate any density and viscosity variations within the fluid which could bring about secondary flow, making comparison with the laminar flow theory very difficult.

An uncertainty analysis was performed based on the instruments used. Results showed that the uncertainties of the heat transfer coefficients were between 0.6% and 4%, while those of the friction factors were between 0.3% and 18%.

The experimental procedure followed was to ensure that steady-state conditions were always met. Initial start-up time as well as adequate time between data-capturing points was such to ensure these conditions were always met. Data was also only captured once an energy balance of less than 1% was achieved.

The three methods used for determining heat transfer coefficients were compared with each other with the results showing that a very close correlation existed between them all. It was concluded that the LMTD method could be used for representing the experimental heat transfer

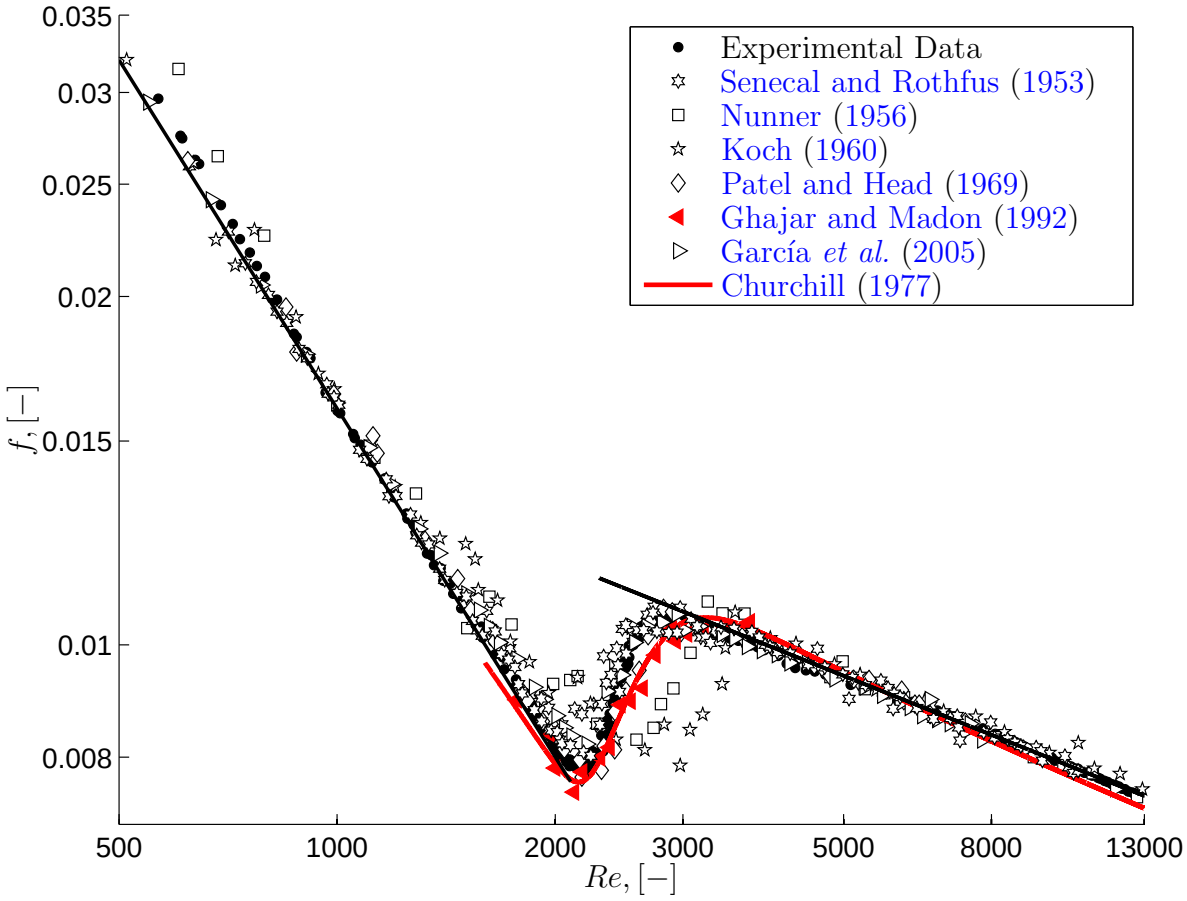

Figure 3.15 Experimental results compared with experimental data from other authors.

coefficients. This method was also closely predicted by the Sieder and Tate equation, predicting the data on average to within 1%.

Adiabatic friction factors were plotted against well-known isothermal equations. The experimental data was underpredicted by the laminar isothermal equation, on average, by 1.5%, while the turbulent results were overpredicted by the Blasius equation, on average, by 0.7%. Transition results showed that there was an increase in friction factor uncertainty when compared with the uncertainties in the laminar and turbulent regimes. This showed the typical chaotic characteristics encountered in this region. The increase in friction factor uncertainties as well as the sudden change in friction factor value showed that transition fell inside the Reynolds number region of 2 100 and 2 900. No hysteresis effects in the transition region could be noticed.

The comparison of heat transfer and pressure drop measurements with literature in the

laminar and turbulent flow regime shows that the experimental results compare well. It implies that the results generated and the procedures used to determine heat transfer coefficients and friction factors are accurate and can be used with confidence, especially with reference to the measurements taken in Chapters 4 to 7.

Chapter 4

Results: Fully Developed Smooth Tube

> For a successful technology, reality must take precedence over public relations, for Nature cannot be fooled.
>
> *Richard Feynman (1918 - 1988)*

4.1 Introduction

Since the field of study is relatively uncertain due to the transitional regime of flow this work is based on, it is of the utmost importance to lay a good foundation for comparison with other scenarios. For this reason, this section will be devoted to flow inside a smooth tube with a fully developed inlet. This implies that by the time the flow reaches the test section, it already has a fully developed velocity profile for both laminar and turbulent flow and hence momentum effects due to the growing boundary layer are negligible. For heat transfer, this implies that a thermally developing profile only need to be considered over the whole test section.

Since transition occurs in the growing boundary layer, a bellmouth inlet was inserted prior to the developing section to first, minimise the effect the inlet has on transition (as shown by Ghajar and Madon (1992)), and second to enforce a uniform velocity profile far upstream of the test section so that the flow would be fully developed by the time it reaches the test section and direct comparisons could be made to theoretical work.

Two smooth tubes with different diameters (15.88 mm and 19.02 mm outer-diameter) are investigated. These tubes are used as a reference for the different types of inlet profiles as well as the enhanced tubes, which are studied in Chapters 5, 6 and 7. The experimental results are divided into two parts, namely the adiabatic friction factor results and heat transfer results which also include diabatic friction factor results. After each section, a correlation is developed since the focus will be lost if done right at the end of the chapter.

4.2 Adiabatic Friction Factors

Figure 4.1 shows the experimental friction factor results for both diameter tubes. The data is comprised of a total of 427 data points with 317 data points being that for the 15.88 mm tube and 110 data points for the 19.02 mm tube. Note that throughout this document the 15.88 mm tube will have a solid marker (▼), while the 19.02 mm tube will have the same marker symbol for the same inlet profile but will be empty (▽). The results are plotted against the laminar flow Poiseuille theory, $f = 16/Re$, and the turbulent flow Blasius equation given by $f = 0.0791Re^{-0.25}$. Both tubes are in excellent agreement with the theoretical values, with all data being within 5% of the theoretical values. The two tubes are also in agreement with each other being within 3% of each other.

Zooming in on the transition region (Figure 4.2) shows that transition for the smooth tube

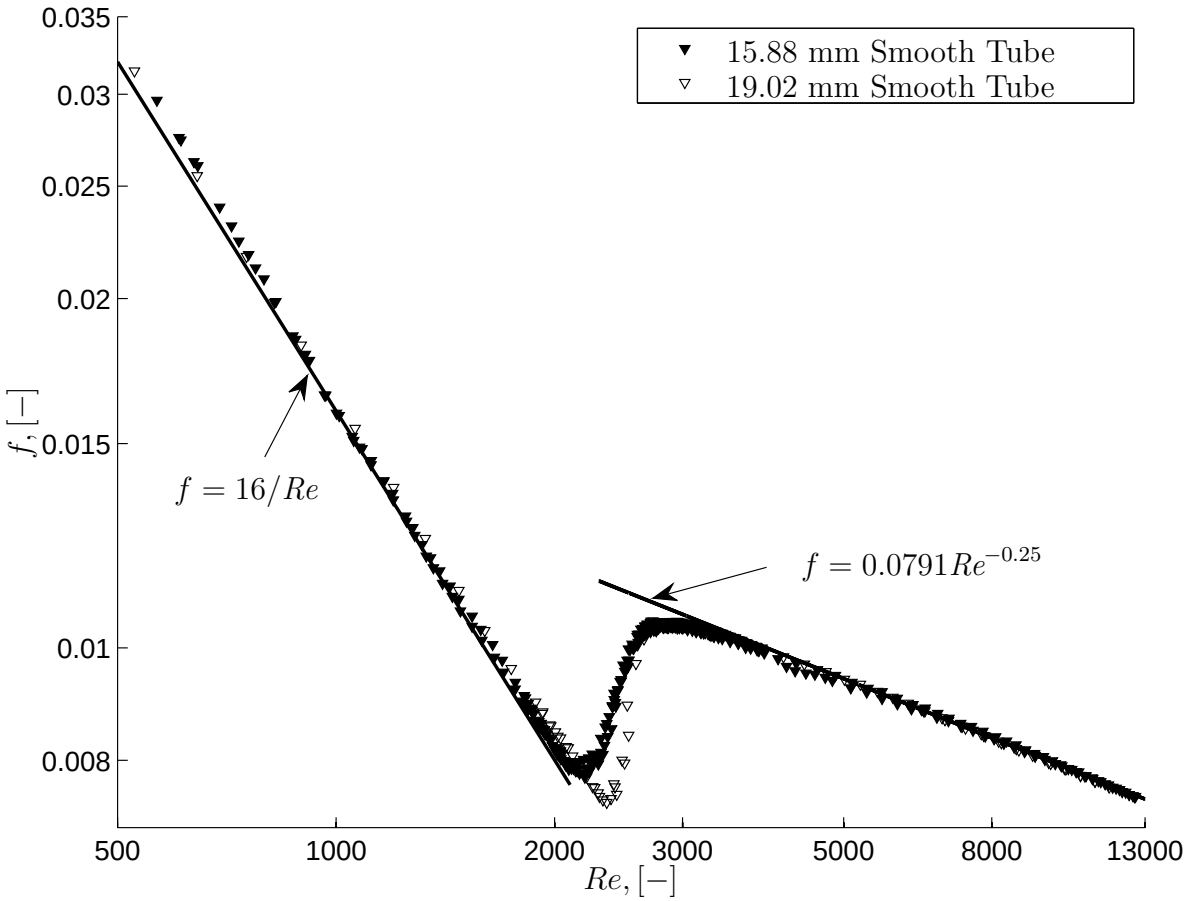

Figure 4.1 Fully developed adiabatic friction factors for the 15.88 mm and 19.02 mm smooth tubes.

starts at a Reynolds number of approximately 2 100 to 2 300 and ends at approximately 3 100. There is an increase in the size of the friction factor error bars in the transition region, starting smoothly prior to transition and becoming chaotic, yet semi-predictable, in the transition region and then smoothing out in the turbulent regime again. Further, this figure shows that there is no hysteresis in the transition region, as the data plotted in Figure 4.2 is for increasing and decreasing Reynolds numbers.

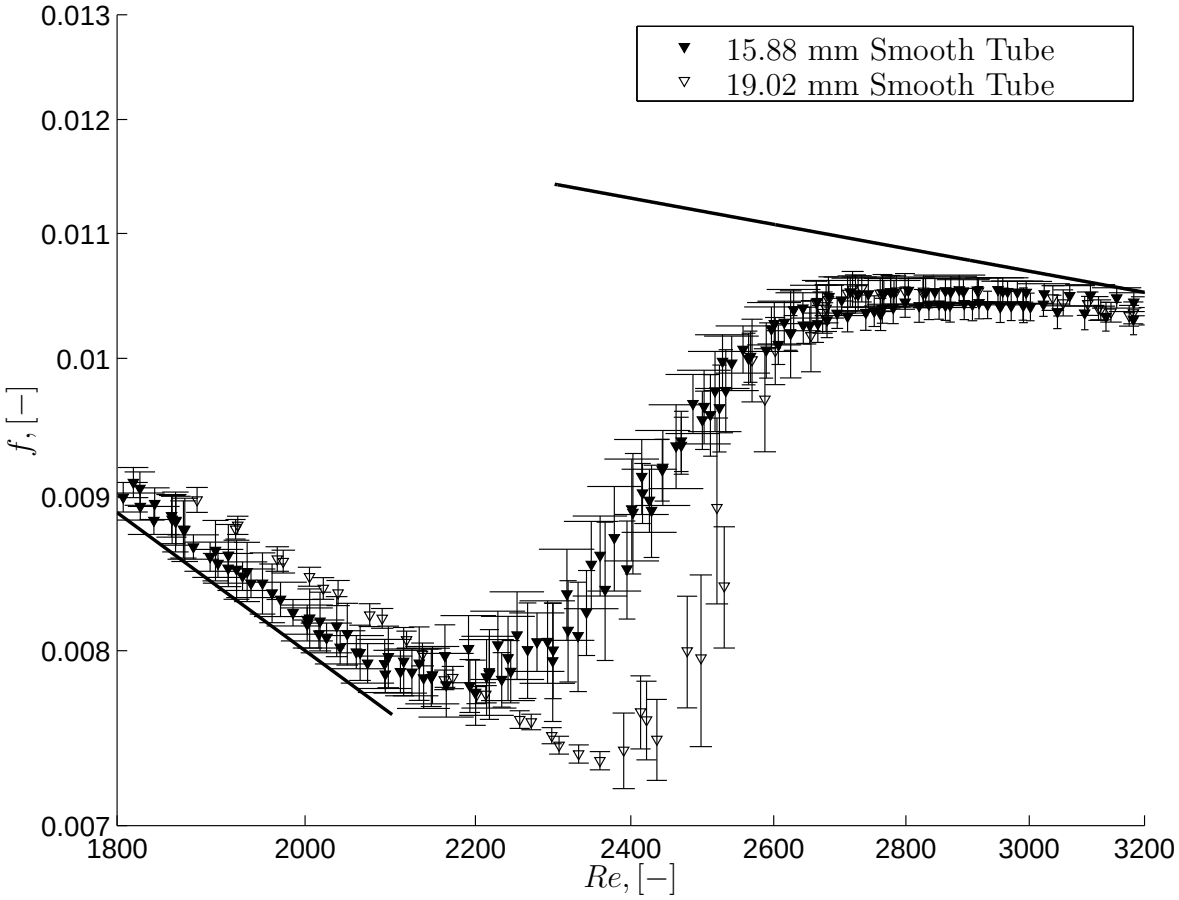

Figure 4.2 Experimental results zoomed in on the transition region.

This process is easier to visualise when plotting the relative friction factor standard deviation (σ_f/f) as a function of the Reynolds number. The standard deviation is obtained from the data point which is comprised of one hundred data entries. This is shown in Figure 4.3, showing the start and end of transition more clearly. For the 15.88 mm tube, transition starts at a Reynolds number of about 2 200 with an increase in fluctuations. The fluctuations peak at 2 400, after which there is a decrease and becomes constant after a Reynolds number of 2 600. The 19.02 mm tube starts with transition at a Reynolds number of 2 350 with fluctuations

peaking at 2 500. The fluctuations become stable again after a Reynolds number of 2 700. Both these profiles have a bell-shaped profile confirming that transition occurs gradually and does not happen instantaneously. The increase and decrease of fluctuations were also visually observed by Binnie (1945) and Lindgren (1953) as turbulent flashes which increase in number and intensity as the fluid velocity is increased until the flow is fully turbulent.

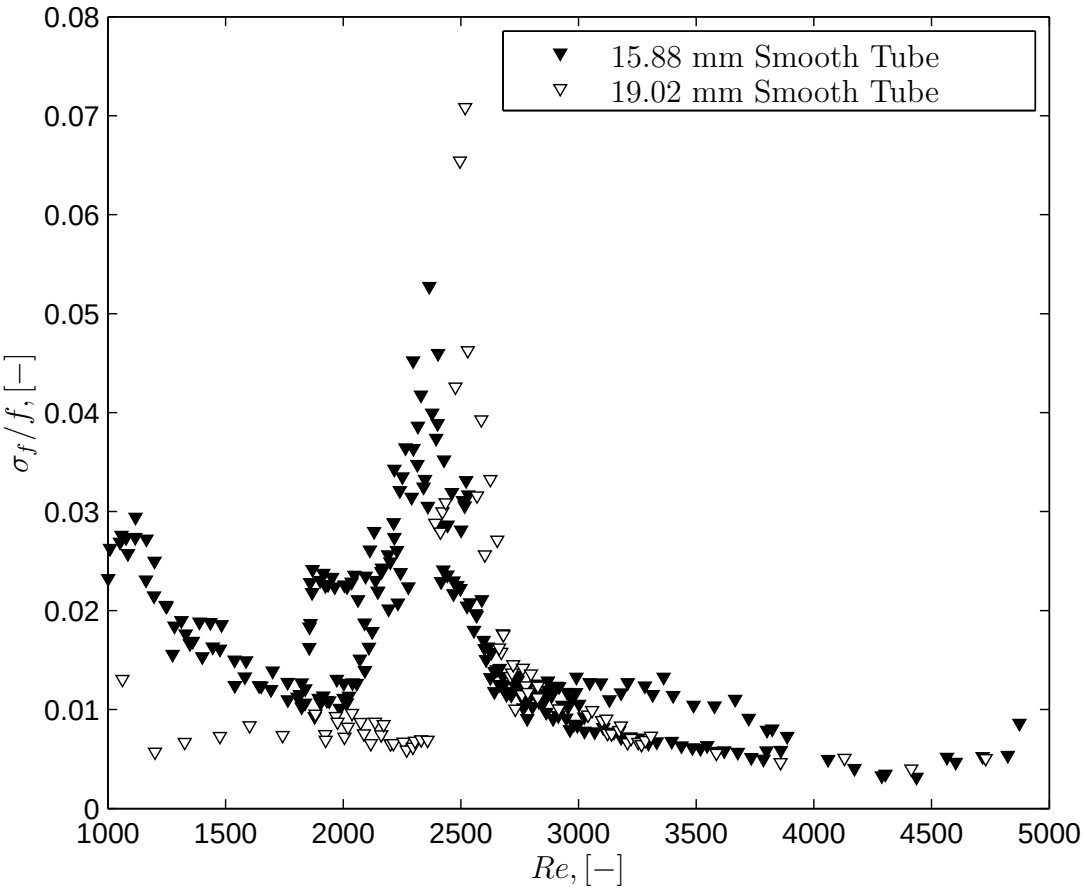

Figure 4.3 Relative standard deviation of the friction factor as a function of the Reynolds number.

The fact that there is a slight difference between the start of transition for the two diameter tubes is of interest. Figure 4.4 shows the experimental data combined with the data from other researchers. The tube diameters of the researchers varied between 6 mm and 50 mm. It would appear that most of the data agree well with the data for the 15.88 mm tube. Only the data of Nunner (1956) and Koch (1960) seem to disagree slightly since transition happens at a Reynolds number of approximately 2 900. These two authors used a tube with an inner-diameter of approximately 50 mm. Though it would seem as if transition is delayed with

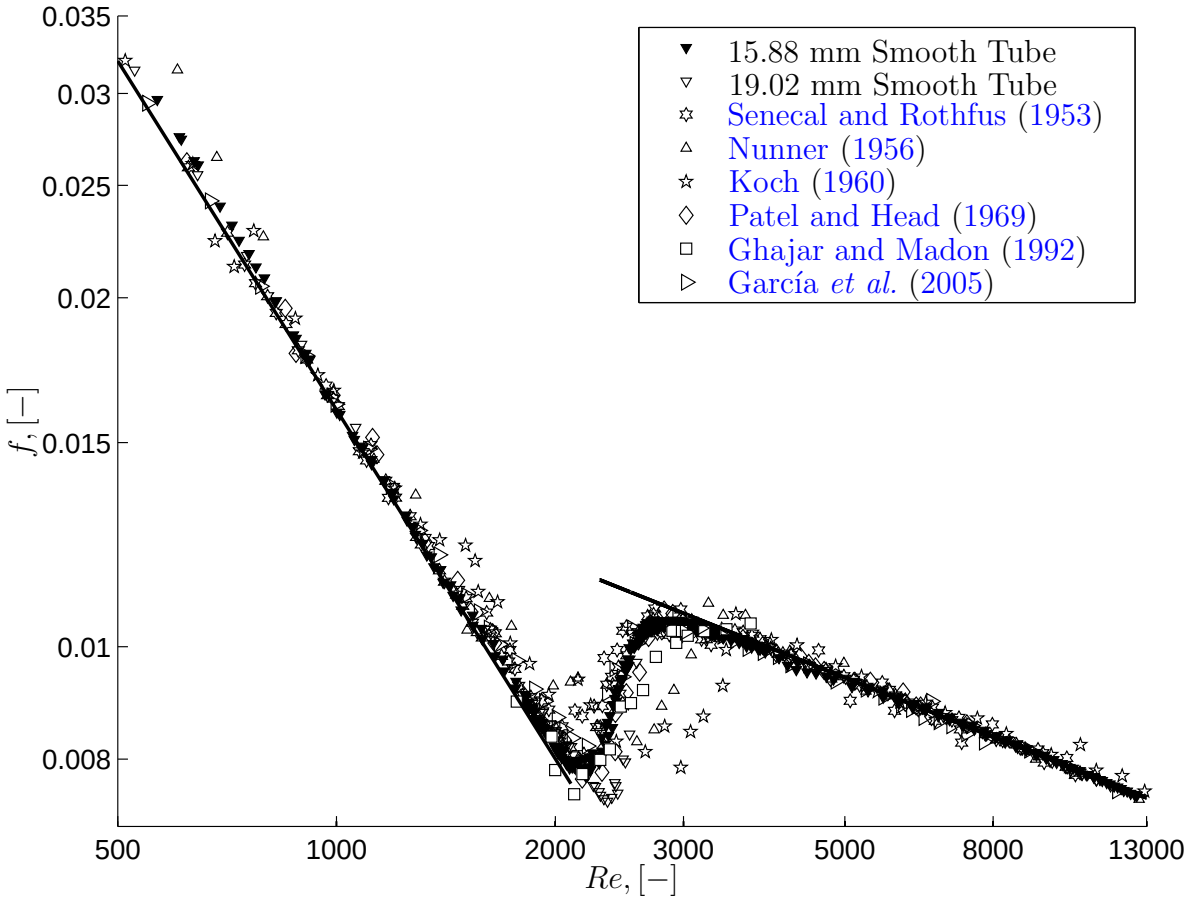

Figure 4.4 Friction factor data from other authors combined with the current experimental results.

respect to the larger-diameter tubes, this contradicts the observations of Lindgren (1953), who stated that the critical Reynolds number (where transition starts) decreased with increasing tube diameter. However, the nature of Lindgren's set-up shows that his results might have been influenced by inlet effects with the flow not being fully developed. One of the tubes in Senecal and Rothfus (1953)'s set-up had a square-edge entrance while the other was fully developed. The results of Nunner (1956) and Koch (1960) also show signs of entrance effects as their results, prior to transition, start to deviate from the Poiseuille relation. This is due to the effect of the centre core-region on the growing boundary layer, giving rise to an increase in pressure drop (Shah, 1978).

Ghajar and Madon (1992) also showed that inlet configurations have a major effect on fully developed flow where the inlet influences the growing boundary layer with regard to when it trips. This fact is supported more by the results obtained by Tam and Ghajar (1998) where

the same inlet was used, but different wire meshes with different roughness were installed prior to the inlet. It was found that the coarsest mesh caused transition to occur at a lower Reynolds number than for a finer mesh, due to the turbulence the coarse mesh generates being greater than for the finer one. Although this paper was based on heat transfer, the effect would be the same for adiabatic flows.

From the discussion above, it appears that differences in transition may appear. Since the flow for both diameter tubes were fully developed, the only cause for the different transitions would be due to inlet turbulence caused by the different bellmouth inlets far upstream of the test section.

4.2.1 Correlation

To develop a correlation which is valid for the whole Reynolds number range, the method of Churchill and Usagi (1972) was employed. To make the correlation more general, it would be best if the data from the previously mentioned authors was also used. However, since most of the other authors' data compares relatively well with the 15.88 mm experimental data, only this data would be used to develop the correlation. The other data will, however, be compared with the newly developed correlation.

Churchill (1977) developed a friction factor equation based on his own work having the form

$$f = f_L \left[1 + \left(\frac{f_{Tt}}{f_L} \right)^{c_1} \right]^{1/c_1} \tag{4.1}$$

where f_L is the laminar flow friction factor and f_{Tt} is the combined friction factor for the transition and turbulent flow regime. This is given by

$$f_{Tt} = f_T \left[1 + \left(\frac{f_T}{f_t} \right)^{-c_2} \right]^{1/c_2} \tag{4.2}$$

with f_T and f_t being the correlations for the turbulent and transition flow regimes, respectively. Since the experimental data compared so well with the laminar and turbulent theories, it was decided that they would remain unchanged. For the transition flow regime, the equation suggested by Churchill (1977), which was obtained from data of Patel and Head (1969), will be used, having the form

$$f_t = \left(\frac{16}{Re_{Cr_L}} \right) \left(\frac{Re}{Re_{Cr_L}} \right)^{c_3} \tag{4.3}$$

Here Re_{Cr_L} is the lower critical Reynolds number, i.e. where transition from laminar to turbulent flow starts. Figure 4.5 shows a plot of the experimental data and the correlations as given by the Poiseuille relation, Blasius equation and Equation (4.3), all shown as separate

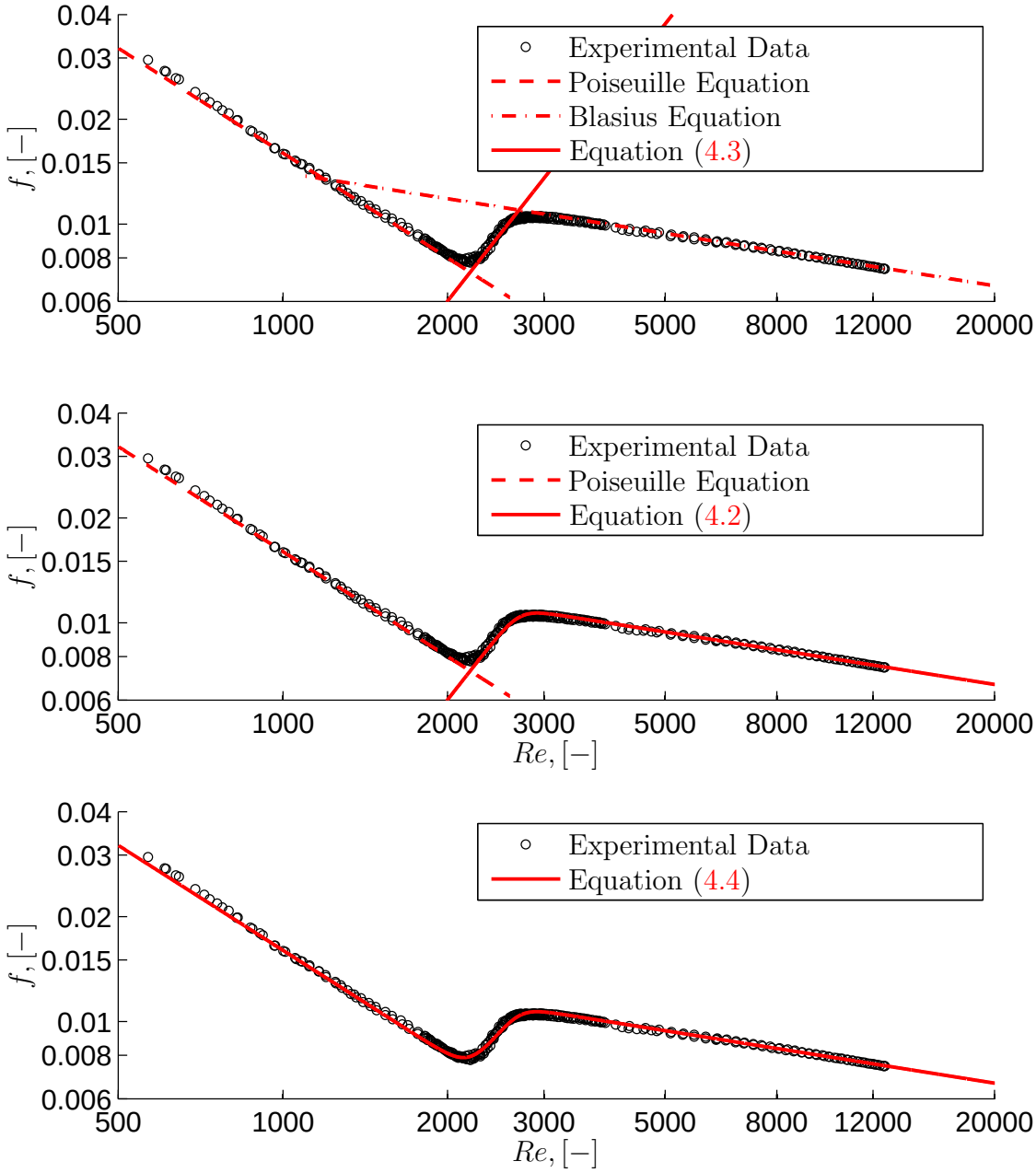

Figure 4.5 Experimental friction factors for the 15.88 mm tube with (top) Poiseuille, Blasius and transition equations, (middle) the Poiseuille equation and Equation (4.2) and (bottom) the complete adiabatic friction factor correlation, Equation (4.4).

lines. Figure 4.5 (middle) shows the effect of Equation (4.2) on the turbulent-transition equations, while Figure 4.5 (bottom) shows the final correlation as defined by Equation (4.1). The constants, c_1, c_2 and c_3, were chosen to be 8, -12 and 2, respectively.

Thus, the final fully developed smooth tube correlation can be given by

$$f = \frac{16}{Re}\left[1 + \left(0.0791Re^{-0.25}\left[1 + \left(\frac{\left(\frac{16}{2200}\right)\left(\frac{Re}{2200}\right)^2}{0.0791Re^{-0.25}}\right)^{-12}\right]^{-1/12}\frac{Re}{16}\right)^8\right]^{1/8} \tag{4.4}$$

This equation is valid for Reynolds numbers between 500 and 20 000, but would most

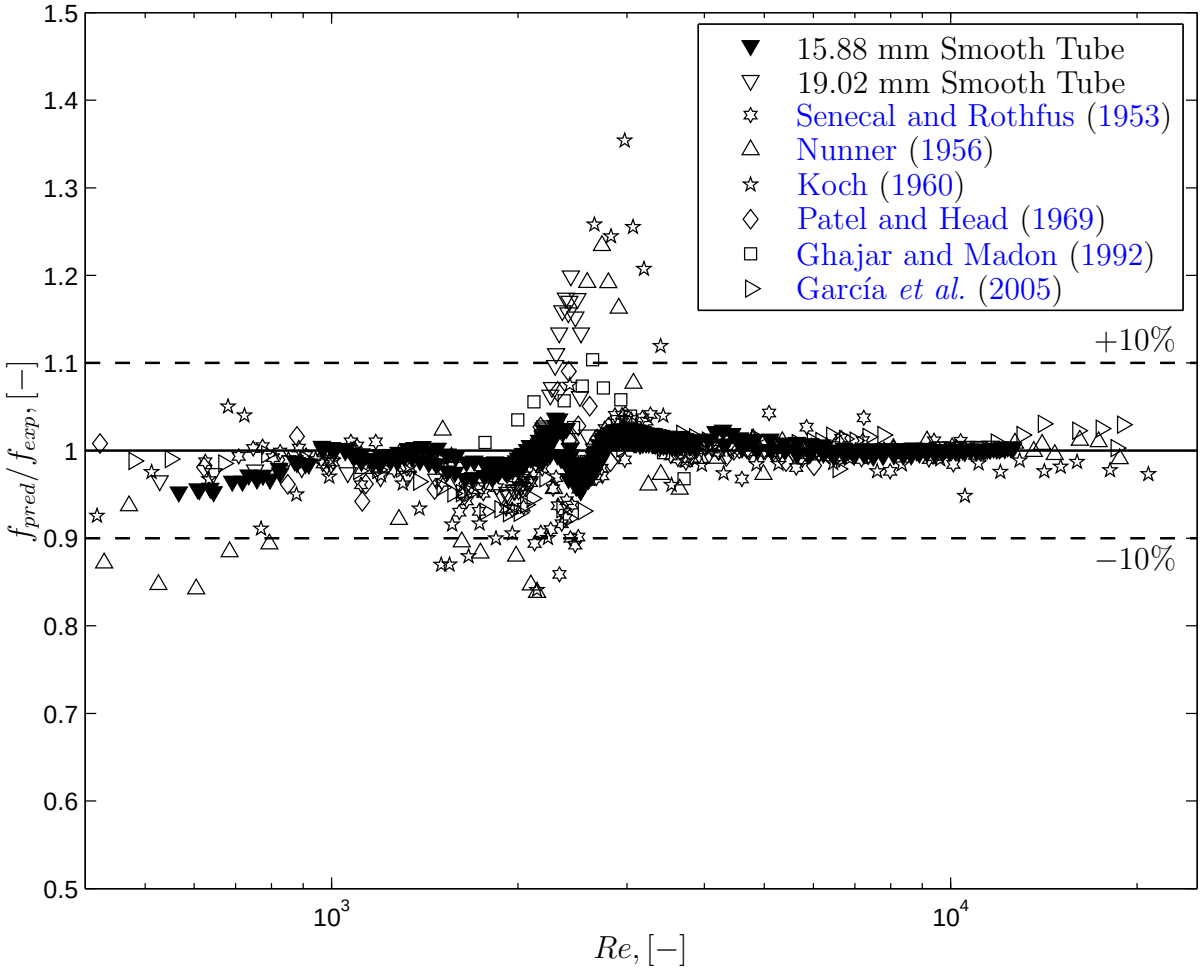

Figure 4.6 Ratio of predicted to measured friction factors as a function of the Reynolds number.

probably be valid for much higher values since the Blasius equation dominates this equation at high Reynolds numbers.

It seems, from Figure 4.5 (bottom), as if the correlation fits the data quite well. A more objective way in determining this would be to plot the ratio of predicted to experimental friction factors as a function of the Reynolds number. This is shown in Figure 4.6, which includes both the 15.88 mm and 19.02 mm fully developed smooth tube data and the data of Senecal and Rothfus (1953), Nunner (1956), Koch (1960), Patel and Head (1969), Ghajar and Madon (1992) and García *et al.* (2005).

The performance of this correlation is assessed in terms of the arithmetic mean deviation (amd) of relative residuals, and the root mean square deviation (rms) of relative residuals of friction factor, each defined respectively as

$$amd = \frac{1}{N}\sum \frac{f_{pred} - f_{exp}}{f_{exp}} 100\% \tag{4.5}$$

$$rms = \sqrt{\frac{1}{N}\sum \left(\frac{f_{pred} - f_{exp}}{f_{exp}}\right)^2} 100\% \tag{4.6}$$

Table 4.1 shows the arithmetic mean and rms values for all the current experimental data and that of the other authors when compared with the correlation.

Table 4.1 Performance of correlation of fully developed smooth tube friction factors.

Tube	Data	amd	rms	amd_{max}
15.88 mm	317	-0.2	1.8	-4.7
19.02 mm	110	1.3	5.6	20
15.88 & 19.02 mm	*427*	*0.1*	*3.1*	*20*
Senecal and Rothfus (1953)	131	-1.7	3.7	-14
Nunner (1956)	44	-1.7	9.0	23
Koch (1960)	55	-0.6	10.1	35
Patel and Head (1969)	54	-0.1	2.8	9
Ghajar and Madon (1992)	18	-3.4	4.7	10
García *et al.* (2005)	60	1.1	3.3	-8
All	**789**	**-0.4**	**4.6**	**35**

There is excellent agreement, especially with the 19.02 mm data as well as the data of Patel and Head (1969), Ghajar and Madon (1992) and García *et al.* (2005). The greatest deviation is in the transition zone, however, with the maximum value being in the order of 35% as shown

in Figure 4.6. This was for the data of Nunner (1956) and Koch (1960) as their transition points were at slightly higher Reynolds numbers than what the correlation was developed for. However, on average, all the data is predicted by the correlation to within 1% with a root mean square deviation of below 5%, which is reasonably good considering the database spans a time frame of over 50 years.

4.3 Heat Transfer

Figure 4.7 shows the heat transfer results in terms of the Nusselt number as a function of the Reynolds number. The results are for both the 15.88 mm and 19.02 mm tubes. A total of 198 data points represent the data; 50 data points for the 15.88 mm tube and 148 for the 19.02 mm tube.

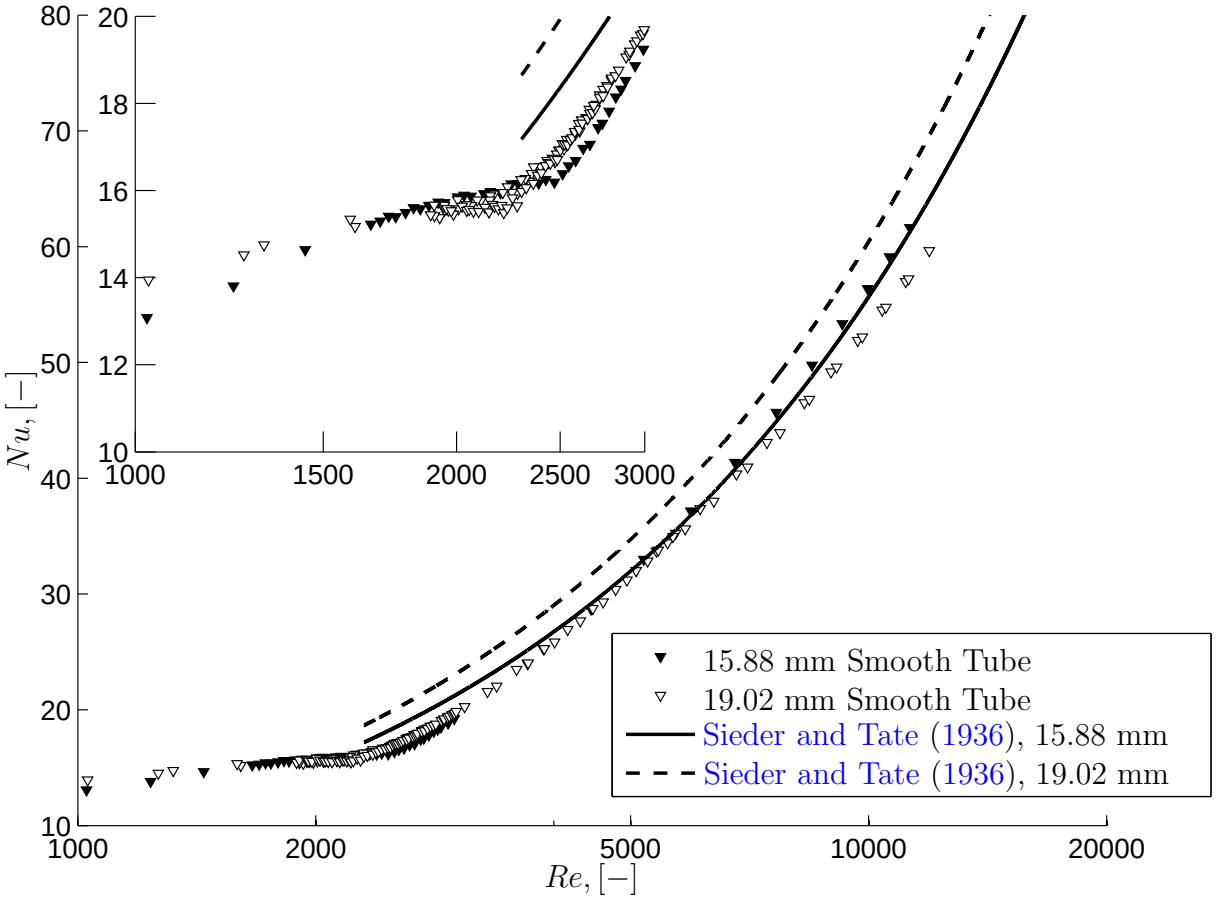

Figure 4.7 Fully developed smooth tube heat transfer results.

The two tubes are in excellent agreement with each other in the turbulent regime and the turbulent flow correlation of Sieder and Tate (1936), although the 19.02 mm data seem to be over predicted somewhat. The curves in the figure of Sieder and Tate (1936) are based on constant values for the Prandtl number and viscosity. On average, the Prandtl number for the 15.88 mm tube is 4.5, while for the 19.02 mm tube it is 5.1.

Since there is a slight difference in laminar Nusselt numbers, it would be better to plot the data in terms of the Colburn j-factor, defined as

$$j = NuPr^{-1/3}/Re \tag{4.7}$$

and takes into account the variation of the fluid Prandtl number. This is shown in Figure 4.8 with the Colburn j-factor as a function of the Reynolds number.

From the results of this figure and the previous figure shows that heat transfer in the

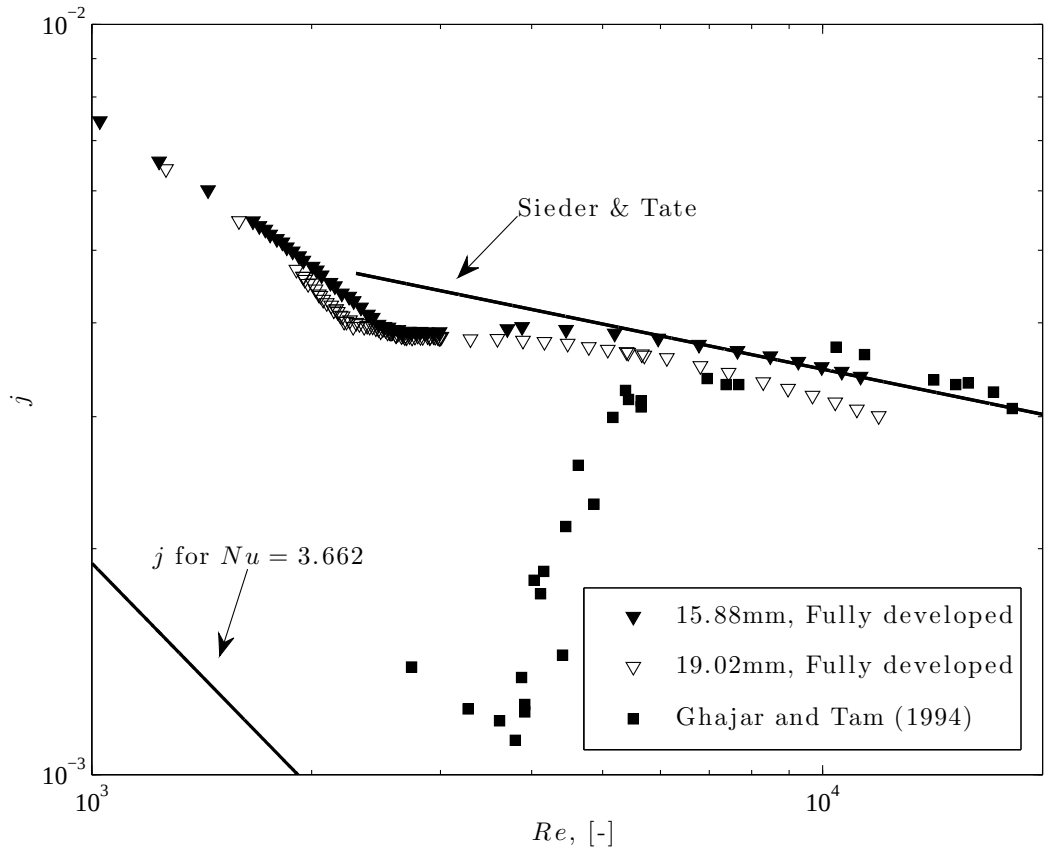

Figure 4.8 Fully developed smooth tube data in terms of the Colburn j-factor.

turbulent flow regime is very well predicted by the Sieder and Tate (1936) equation. Transition, unlike for the adiabatic results, is much less severe in changing from laminar to turbulent flow. The laminar results are much higher than predicted by laminar theory, which is due to the enhancements mixed convection bring about.

Also shown on the figure is the data of Ghajar and Tam (1994) for their bellmouth inlet. This data was taken approximately midway down the length of the tube. These values are local values and cannot really be compared to the averaged values presented. However, their data do show the effect of mixed convection in the laminar regime. Their Prandtl numbers ranged between 40 and 160 in this region.

On careful inspection of the laminar results, it is noticed that the 19.02 mm data are slightly lower than the results of the 15.88 mm tube. The data of both tubes are plotted on the flow regime map of Metais and Eckert (1964) in Figure 4.9, showing that the Grashof-Prandtl product for the 19.02 mm tube is less than that for the smaller diameter tube, indicating that mixed convection effects are more pronounced for the 15.88 mm tube.

Regarding transition, it appears from Figures 4.7 and 4.8 that the critical Reynolds number for transition occurs at a Reynolds number of about 2 000 to 3 000. A more objective way in determining this Reynolds number would be to plot the relative heat transfer coefficient standard deviations as a function of the Reynolds number. This is shown in Figure 4.10. It shows that the critical Reynolds numbers for both tubes are the same, and have a lower and upper value of 2 000 and 2 900 respectively.

To understand the origin of the heat transfer coefficient fluctuations in the transition regime (*viz.* Figure 4.10), it was undertaken to inspect the standard deviations of each data value pertaining to the calculation of the coefficient (mass flow rate and temperature measurements). Since over 52 thermocouples were used, only the thermocouples pertaining to the direct calculation of the heat transfer coefficient were investigated. These would be the inner-tube inlet, outlet and wall thermocouples. These thermocouples are represented by 11 stations along the length of the tube (nine stations for the wall thermocouples). It was found that the main fluctuations were caused by the temperature measurements. A three-dimensional plot was generated showing the standard deviations of all these thermocouples at each station as a function of the Reynolds number. This is shown in Figure 4.11. Similar results for the 19.02 mm tube were also obtained.

It is noticed that the outlet temperature is the cause of the increase in heat transfer coefficient fluctuation in the transition region. Although the second wall temperature error does seem relatively high when compared with the other wall temperatures, it seems to remain this way throughout the range of Reynolds numbers. However, it appears that the wall temperatures also fluctuate more in the transition region than anywhere else. The reason that they do not fluctuate as much as the outlet temperature is because of the annulus fluid damping most of these fluctuations. It is believed that the wall temperatures would fluctuate up the length of the tube as the Reynolds number increases. It is possible that this may be witnessed for a system consisting of a constant heat flux boundary condition.

4.3.1 Diabatic Friction Factors

Figure 4.12 show the experimental diabatic fully developed friction factors for the two smooth tubes (a total of 198 data points). Also included are the the laminar Poiseuille relation, the turbulent adiabatic Blasius equation and the Blasius equation with a viscosity ratio correction, $(\mu/\mu_w)^{-0.2}$, as suggested by Allen and Eckert (1964).

What is instantly noticed is the overall increase in friction factors compared to the adiabatic predictions. Turbulent results are correlated fairly well with the viscosity correction, predicting the data on average to within 3%. For the laminar region, friction factors were on average 35% higher than predicted by the Poiseuille relation. Even with a viscosity correction, the prediction only improves by 4%. This increase in friction factor can be attributed to the secondary flow effects, with data from Nunner (1956) showing similar results. Tam and Ghajar (1997) also attributed the increased fully developed friction factors they obtained to secondary flow. They

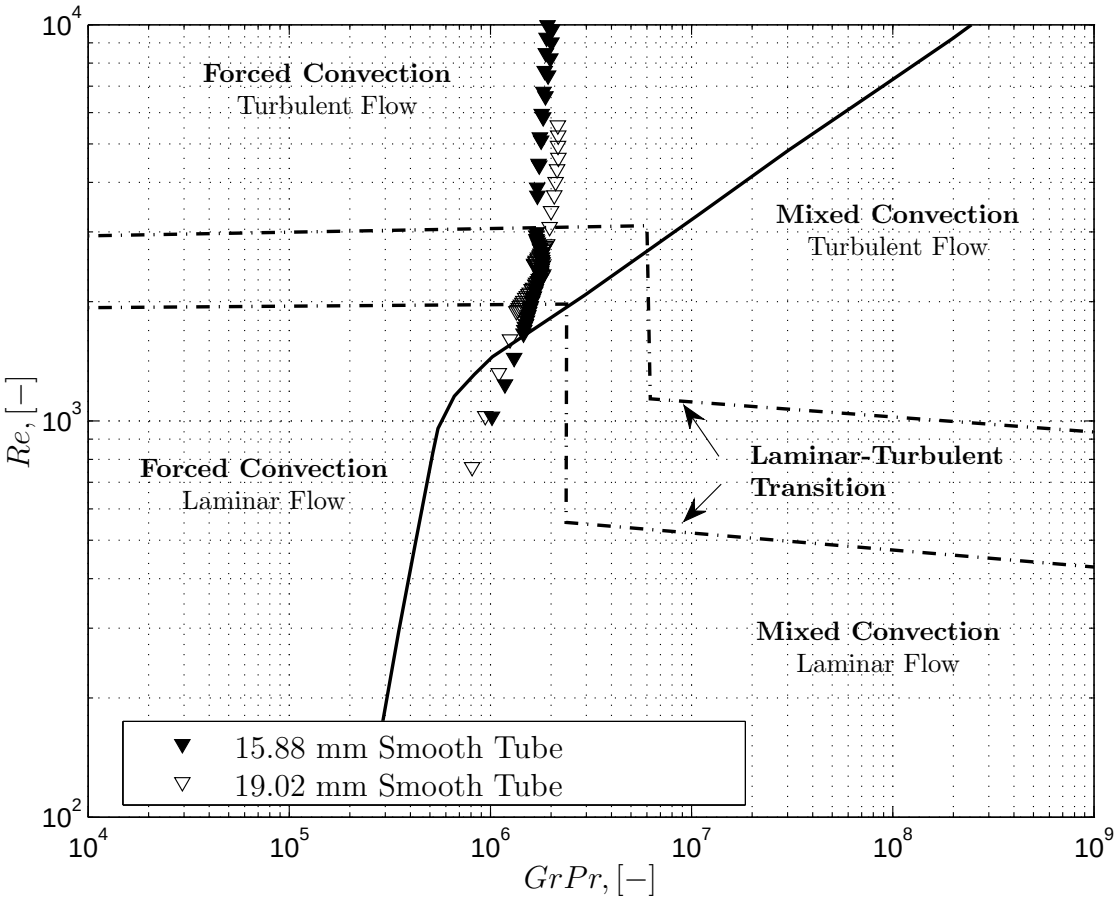

Figure 4.9 Experimental data in terms of the flow regime map.

further found that by increasing the overall heat flux, the laminar friction factors increased.

This implies that since the friction factor is proportional to the wall shear stress, which in turn is proportional to the velocity gradient at the wall, secondary flow distorts the velocity profile in such a way that the gradient near the wall is much steeper. This would then give rise to the higher friction factors. Many numerical and experimental studies have been performed showing this distortion. Mikesell (1963) suggested and observed that in certain cases back-flow might even occur. It would seem, though, that the friction factor will need to be written in terms of the factors describing secondary flow.

Looking at the transition from laminar to turbulent flow, it can be observed that the s-curve for the diabatic case is much smaller than that witnessed for the adiabatic case. This also confirms the heat transfer results with regard to transition being less severe in the sense that there is no sudden (or very little) increase in friction factor values in this region. This

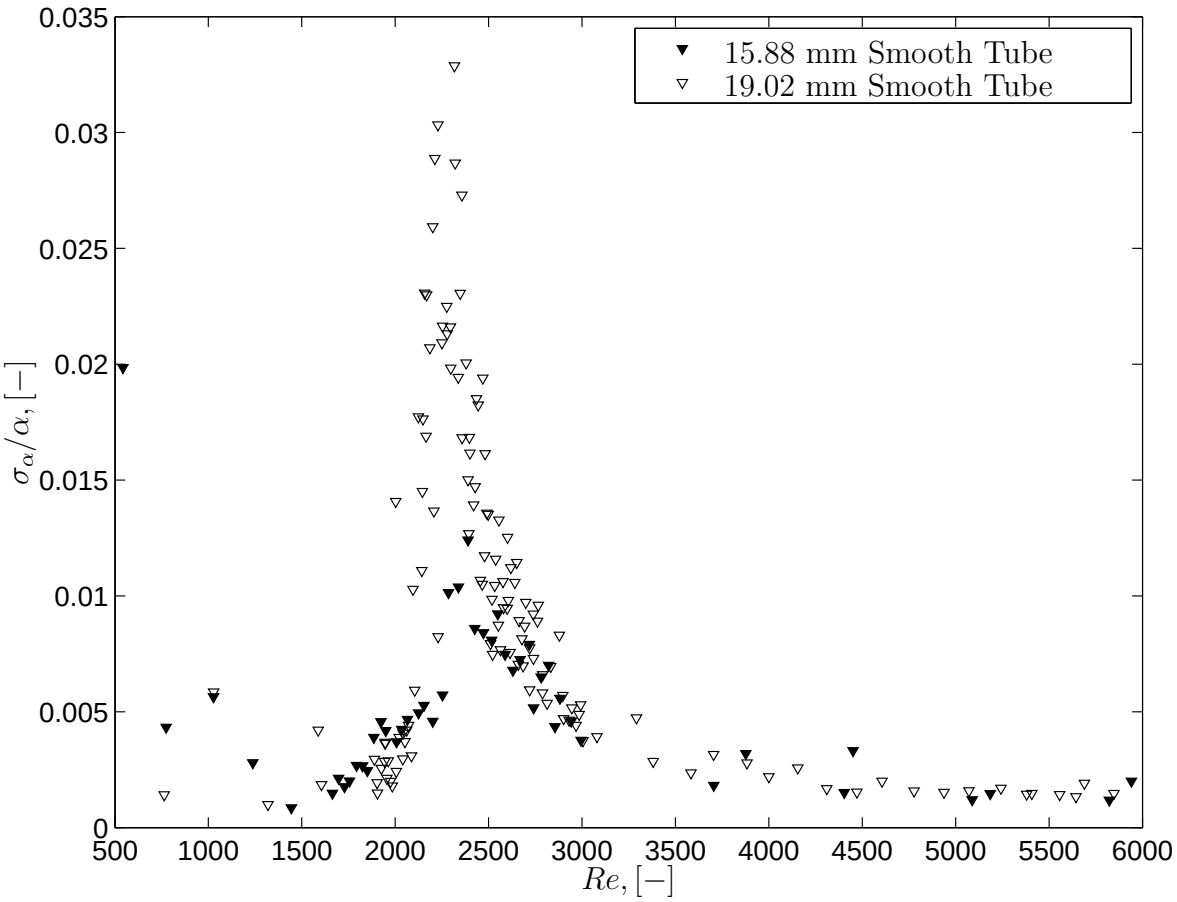

Figure 4.10 Relative heat transfer coefficient standard deviations.

effect is analogous to twisted tape inserts as discussed by Manglik and Bergles (1993) where the swirl induced by the tapes not only increase the friction factors, but also causes a smooth transition to turbulence. This is due to the secondary flow (swirl flow) having a competing effect on the onset of turbulence. This effect diminishes as flow rates are increased and full turbulence is reached.

4.3.2 Correlation

An interesting feature of the plot of the Colburn j-factor is that the friction factor plot can be inserted on the same graph. This graph then shows the parallel behaviour of j vs Re and f vs Re. This is shown in Figure 4.13 a) with the friction factors in the top part of the graph and the Colburn j-factors in the bottom part. The trends of the two graphs are striking. In fact,

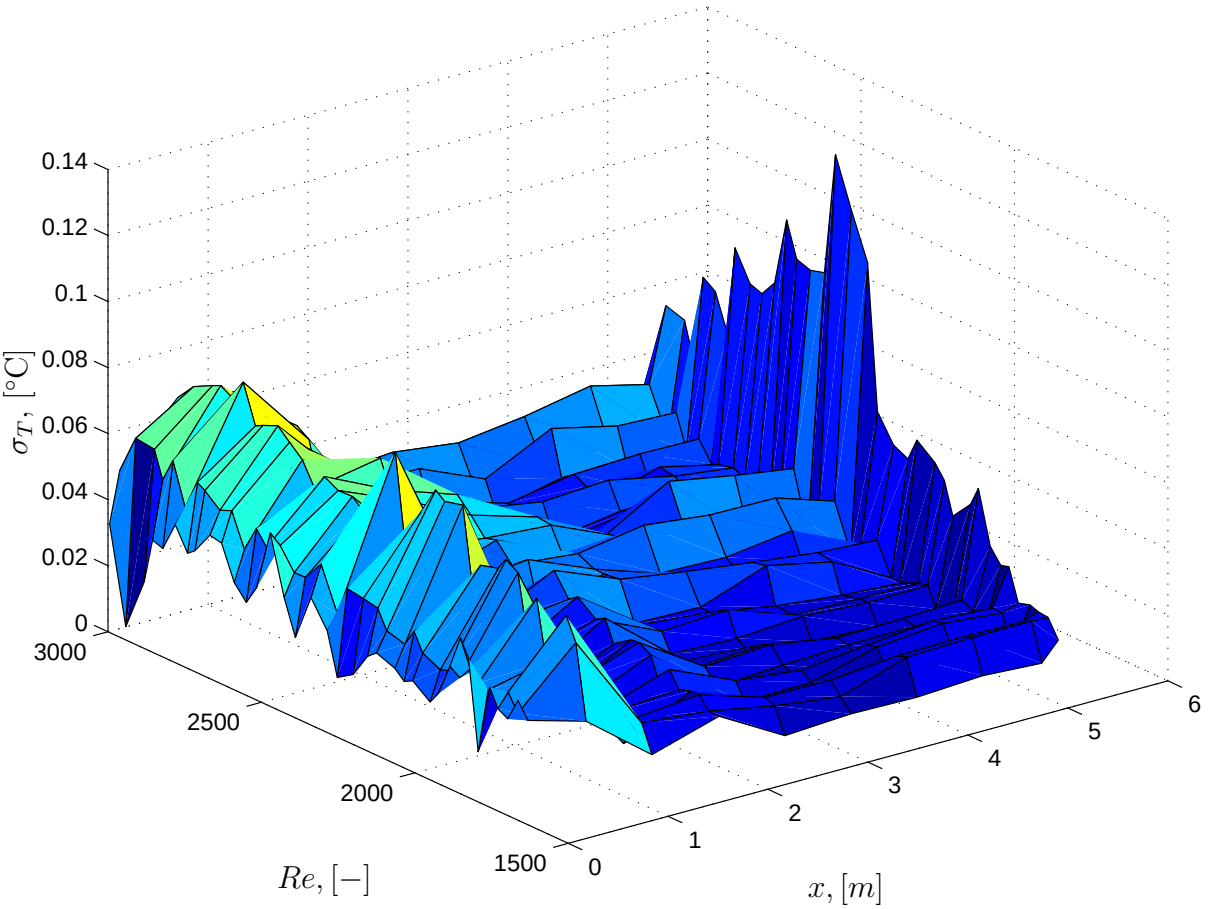

Figure 4.11 Standard deviation in thermocouple readings as a function of the Reynolds number at different measuring stations for the 15.88 mm tube.

by multiplying the j-factors by $Pr^{2/3}$ all the data collapse into one as shown in Figure 4.13 b). This is very similar to the Reynolds analogy for a flat plate and fully developed pipe flow, given respectively as

$$St = \frac{C_f}{2} Pr^{-2/3}, \quad St = \frac{f}{8} Pr^{-2/3} \tag{4.8}$$

where C_f is the skin friction coefficient. The extended Reynolds analogy, as given by Shah and Seculić (2003) , is given as

$$j = StPr^{2/3} = \frac{f}{2}\phi_w \tag{4.9}$$

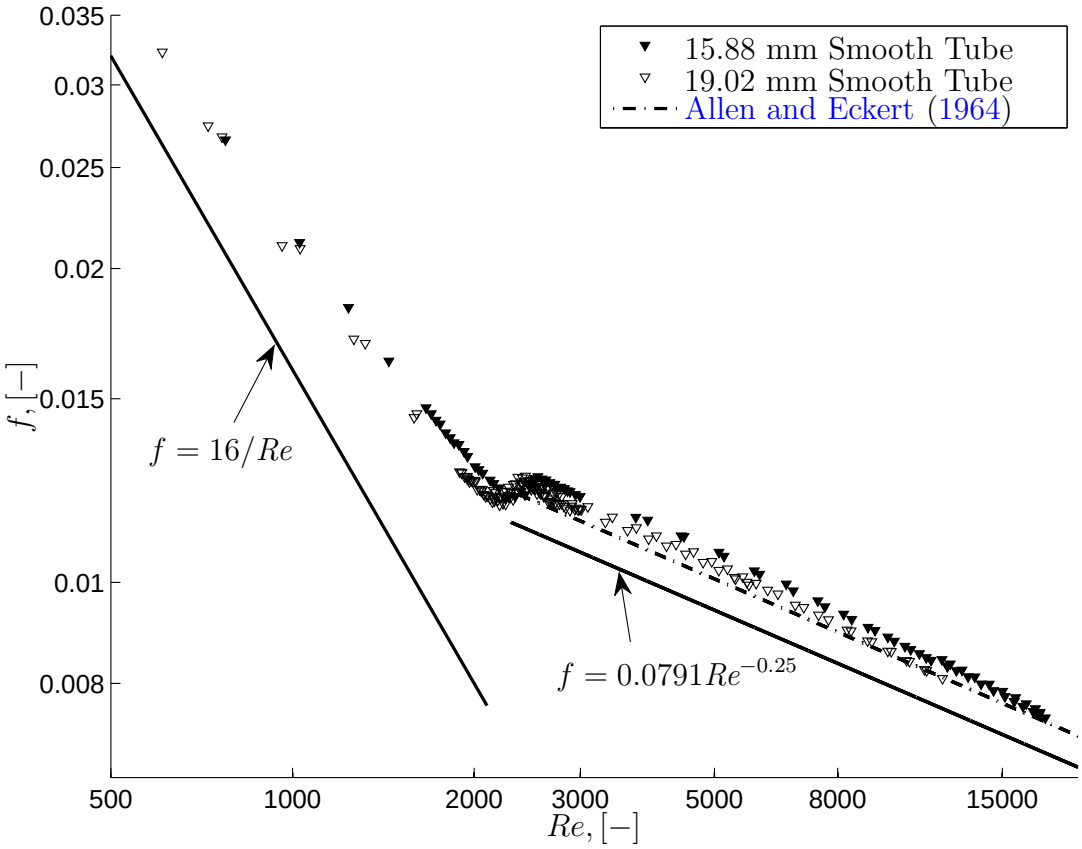

Figure 4.12 Experimental diabatic friction factors as a function of the Reynolds number.

where ϕ_w is a function of the tube/duct geometry, the flow type, boundary condition and the Prandtl number. It in effect modifies the Reynolds analogy relationship between j and f. Thus, from the current experimental data the value of ϕ would be $2Pr^{-2/3}$, or

$$StPr^{2/3} = fPr^{-2/3} \tag{4.10}$$

This, however, should be seen as a special case for water in smooth tubes only as it is bound to differ for higher Prandtl number fluids. One point that has to be mentioned is that this relation would never have been made if adiabatic friction factors were used.

Laminar Flow

Due to the uncertainty in friction factors at low Reynolds numbers, it was decided that a correlation for the Nusselt number should rather be developed (*viz* Table 3.3). For laminar flows, an equation similar to that developed by Martinelli and Boelter (1942) for flow in vertical pipes could be used, having the form

$$Nu_L = 1.75\left[RePr\frac{D}{L} + c_1\left(Gr_f Pr_f \frac{D}{L}\right)^{c_2}\right]^{1/3}\left(\frac{\mu}{\mu_w}\right)^{0.14} \tag{4.11}$$

What this equation shows is that as the velocity tends towards zero, the natural convection driving force still exists. What is cumbersome, though, is the fact that natural convection is a function of the ratio of the tube diameter to length. This was also mentioned by Oliver (1962), who suggested that this ratio should be removed, although he obtained better results by using the ratio L/D. He tried to determine the effect of the ratio on heat transfer, but due to the amount of scatter could not come to any conclusions. Depew and August (1971) had the same problem and could not come to any conclusion. Further, if the ratio D/L were to be used, it implies that the diameter would be to the fourth power when multiplied by the Grashof number, meaning that a small change in diameter would cause a large variation in $GrPrD/L$, which is not what was reflected in the change in heat transfer coefficients (Oliver, 1962). The correlation of Jackson *et al.* (1961) did not have the diameter-to-length ratio, suggesting that it should play no role in horizontal tubes. Brown and Thomas (1965) further suggested that the mass flow rate should play a more important role than the L/D. Brown and Thomas used relatively short tubes, however.

The tube length, however, does play a role in mixed convection since it needs a certain length for it to start, as shown experimentally by Ghajar and Tam (1991) and Ghajar and Tam (1994). For a uniform heat flux boundary condition the driving potential, after the required starting length, remains for the remainder of the length of the tube since the fluid and wall temperature increase together. For a uniform wall temperature boundary, however, this potential diminishes down the length since the fluid temperature slowly approaches the wall temperature. Thus, one could expect that mixed convection effects for a constant wall temperature boundary to be less than for a uniform heat flux boundary for the same heat input.

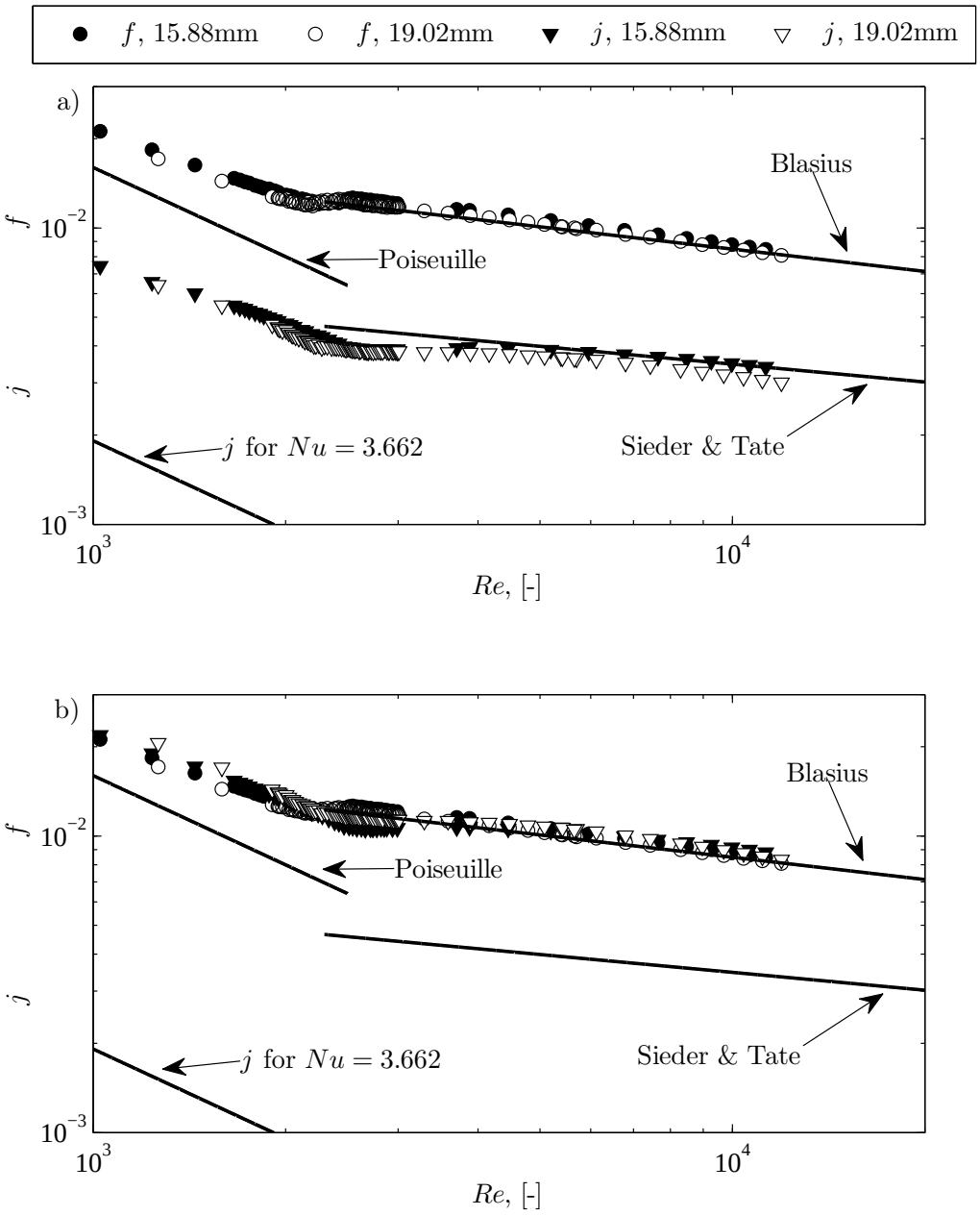

Figure 4.13 Plot of a) f and j vs Re and b) f and $jPr^{2/3}$ vs Re.

Further, secondary flow is negligible in the thermal entrance region as shown by Ghajar and Tam (1991) and from the numerical studies of Shome and Jensen (1995). This fact would be more pronounced for high Prandtl number fluids where the thermal entrance region is much

longer than for low Prandtl number fluids (Kakaç *et al.*, 1987). This was also observed from experiments by Marner and Bergles (1989), who reported that secondary flow effects were negligible, with their fluid having a Prandtl number in the order of 1 300 - 8 000. Thus, for relatively short tubes and high Prandtl number fluids, the effects of free/natural convection would be negligible.

Using Equation (4.11) as a base to work from, the best option would be to determine the exponents of each term since not each has an equal influence on heat transfer. Thus, Equation (4.11) is put in the form

$$Nu_L = c_1 \left[Re^{c_2} Pr^{c_3} \left(\frac{D}{L}\right)^{c_4} + c_5 \left(Gr_f^{c_6} Pr^{c_7} \left(\frac{D}{L}\right)^{c_8} \right)^{c_9} \right]^{c_{10}} \left(\frac{\mu}{\mu_w}\right)^{c_{11}} \tag{4.12}$$

By means of a non-linear least squares optimization method, the constants that fit the data the best were found to be

$$\begin{aligned} Nu_L = 2.686 \Bigg[& Re^{0.105} Pr^{1.133} \left(\frac{D}{L}\right)^{0.483} + \\ & 1.082 \left(Gr^{0.362} Pr^{-2.987} \left(\frac{L}{D}\right)^{0.202} \right)^{0.277} \Bigg]^{2.226} \left(\frac{\mu}{\mu_w}\right)^{0.152} \end{aligned} \tag{4.13}$$

What is of interest in this equation is the fact that heat transfer due to natural/mixed convection is inversely proportional to the Prandtl number, which correlates with the discussion from above. Further note that the natural convection is a function of L/D and not D/L, although a very weak function. This should, however, be seen as tentative since the range of Prandtl number and L/D ratio varies little, with more data being required to confirm these findings. This equation is valid for

$$\begin{aligned} 940 < & Re < 2\ 522 \\ 4.43 < & Pr < 5.72 \\ 1.5 \times 10^5 < & Gr < 4.3 \times 10^5 \\ 0.695 < & \mu/\mu_w < 0.85 \\ 289 < & L/D < 373 \end{aligned}$$

Equation (4.13) can now be used in conjunction with Equation (4.10) to determine the friction factor. The relative errors of the predicted to experimental Nusselt numbers and friction factors are given in Figure 4.14. The correlation predicts the heat transfer data on average to within 1% with an average rms deviation of less than 2.2%, while the friction factors are predicted on average to within 6.3% with an average rms deviation of less than 9%. Although

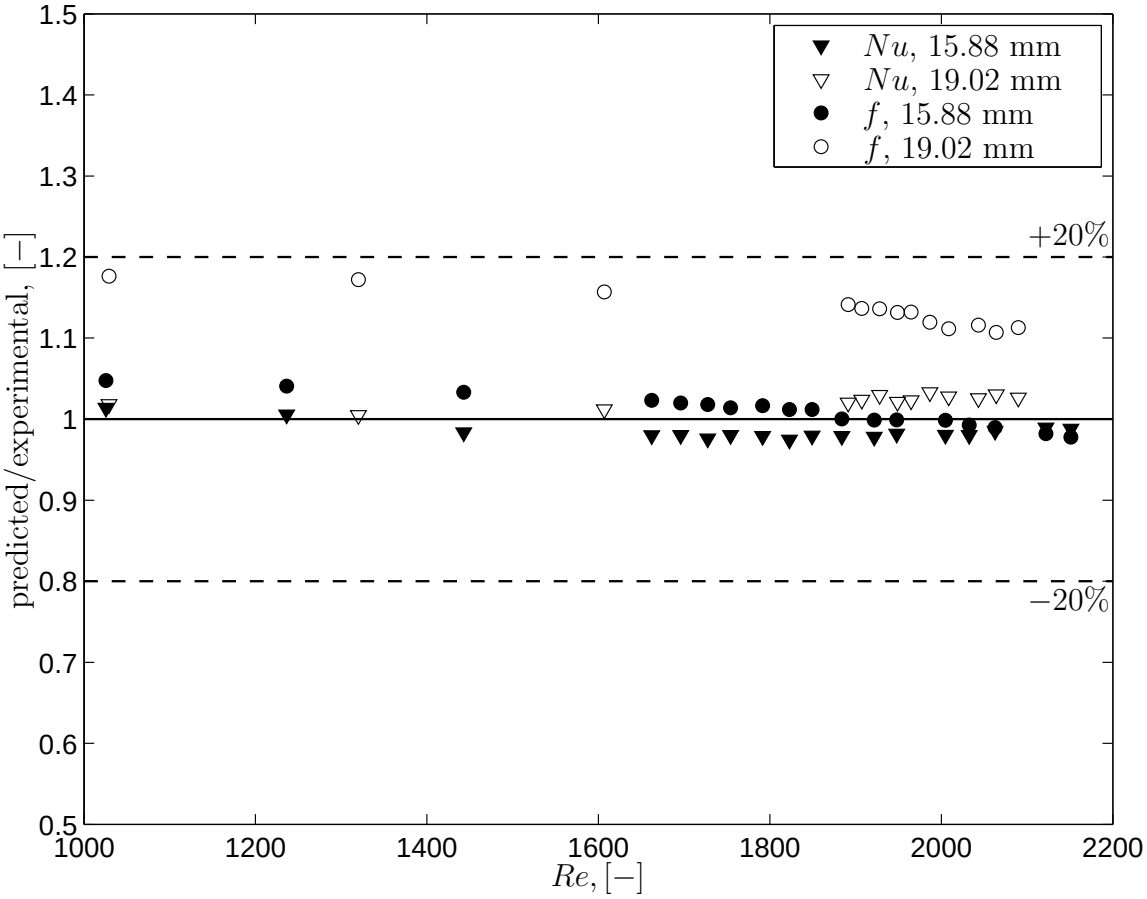

Figure 4.14 Ratio of predicted to measured laminar Nusselt numbers and friction factors as a function of the Reynolds number.

the friction factors seem to be predicted with less accuracy, it should be remembered that the uncertainties of the friction factors at low Reynolds numbers are in the order of 18%. Thus, Equation (4.10) predicts the data to within the uncertainties.

Turbulent Flow

The Sieder and Tate (1936) equation correlated the experimental data with reasonable accuracy. However, since this correlation is more than 70 years old and its validity is for Reynolds numbers greater than 10 000, it was updated with more accurate data from this study.

New constants for the Sieder and Tate equations were determined by, as was done for the laminar flow correlation, using a non linear least squares optimization program. The correlation obtained is

$$Nu_T = 0.032 Re^{0.802} Pr^{0.059} \left(\frac{\mu}{\mu_w}\right)^{0.14} \tag{4.14}$$

with its range of applicability being

$$\begin{aligned} 3\ 000 < &Re < 17\ 800 \\ 3.73 < &Pr < 5.06 \\ 0.678 < &\mu/\mu_w < 0.788 \end{aligned}$$

This correlation predicted the experimental data for the two diameter tubes on average to within 1.5% with an average rms deviation of less than 3%. With the analogy of Equation (4.10), the friction factors could also be determined. The correlation predicted the friction factors on average to within 1% with an average rms deviation of less than 4%. The relative errors of the correlation and the data are shown in Figure 4.15

Transition Regime

To correlate the transition region, it was decided to use an equation that is similar in form as that used by Ghajar and Tam (1994), which in turn is similar in form as that of Churchill (1977) . The correlation consists of a laminar, transition and turbulent part and is given as

$$Nu_t = \left[Nu_L + e^{(Re-c_1)/c_2} + Nu_T^{c_3}\right]^{c_3} \tag{4.15}$$

The data used to determine the constants, as was the case for Ghajar and Tam (1994), extended somewhat into the laminar and turbulent regimes. The constants were obtained by means of a least squares optimisation program, and the final equation is given as

$$Nu_t = \left[Nu_L + e^{(Re-2\ 717)/202} + Nu_T^{0.845}\right]^{0.845} \tag{4.16}$$

and is valid in the range

$$\begin{aligned} 2\ 000 < &Re < 3\ 000 \\ 4.47 < &Pr < 5.30 \\ 2.8 \times 10^5 < &Gr < 4.1 \times 10^5 \\ 0.702 < &\mu/\mu_w < 0.797 \\ 289 < &L/D < 373 \end{aligned}$$

Figure 4.16 shows the ratio of the predicted to the experimental values for the Nusselt number and friction factors in the transition regime. The Nusselt numbers are predicted on

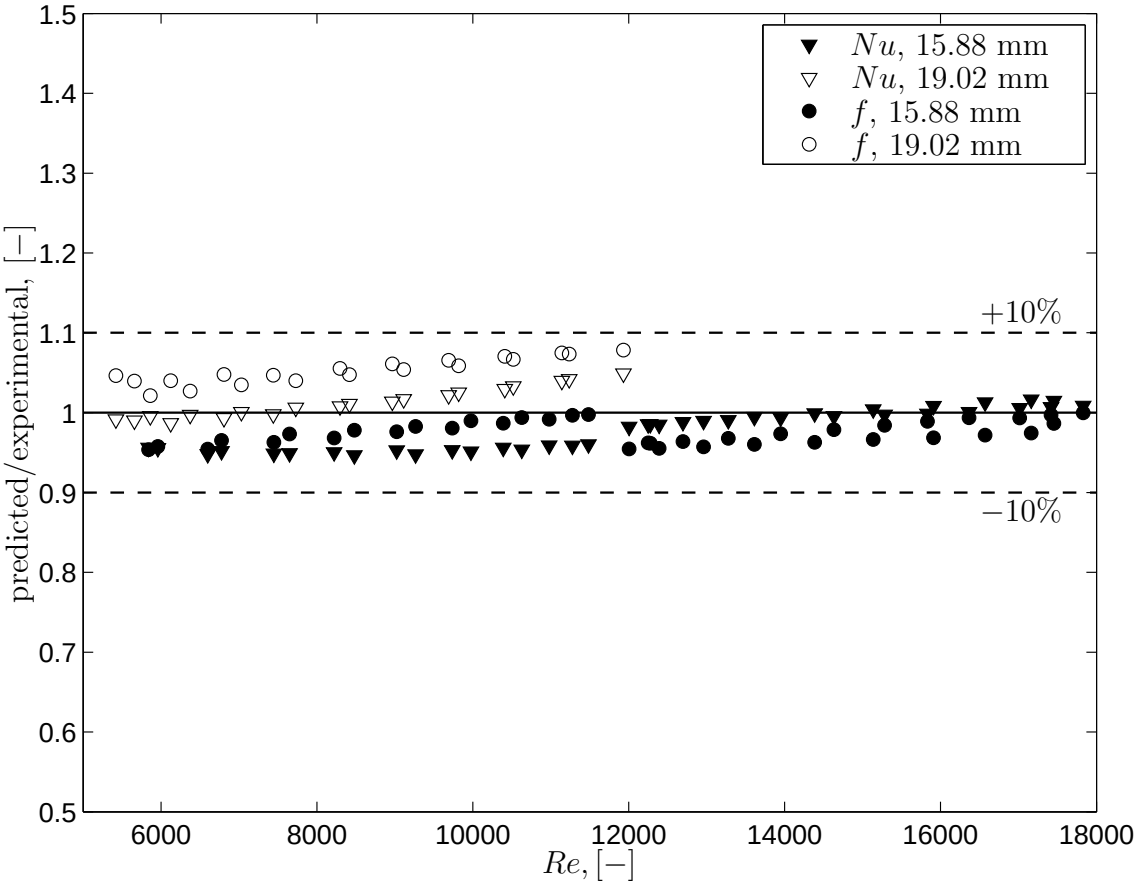

Figure 4.15 Ratio of predicted to measured turbulent Nusselt numbers and friction factors as a function of the Reynolds number.

average to within 1% with an average rms deviation of less than 2%. The friction factors, determined from Equation (4.10), is predicted on average to within 4% with an average rms deviation of less than 8%.

Complete Flow Regime

To aid in comparison with the enhanced tubes, it is better to combine the just-developed correlations into one correlations. By making use of the method of Churchill (1977), the complete correlation becomes of the form

$$Nu = \left[Nu_L^{c_1} + (Nu_t^{c_2} + Nu_T^{c_2})^{c_1/c_2} \right]^{1/c_1} \tag{4.17}$$

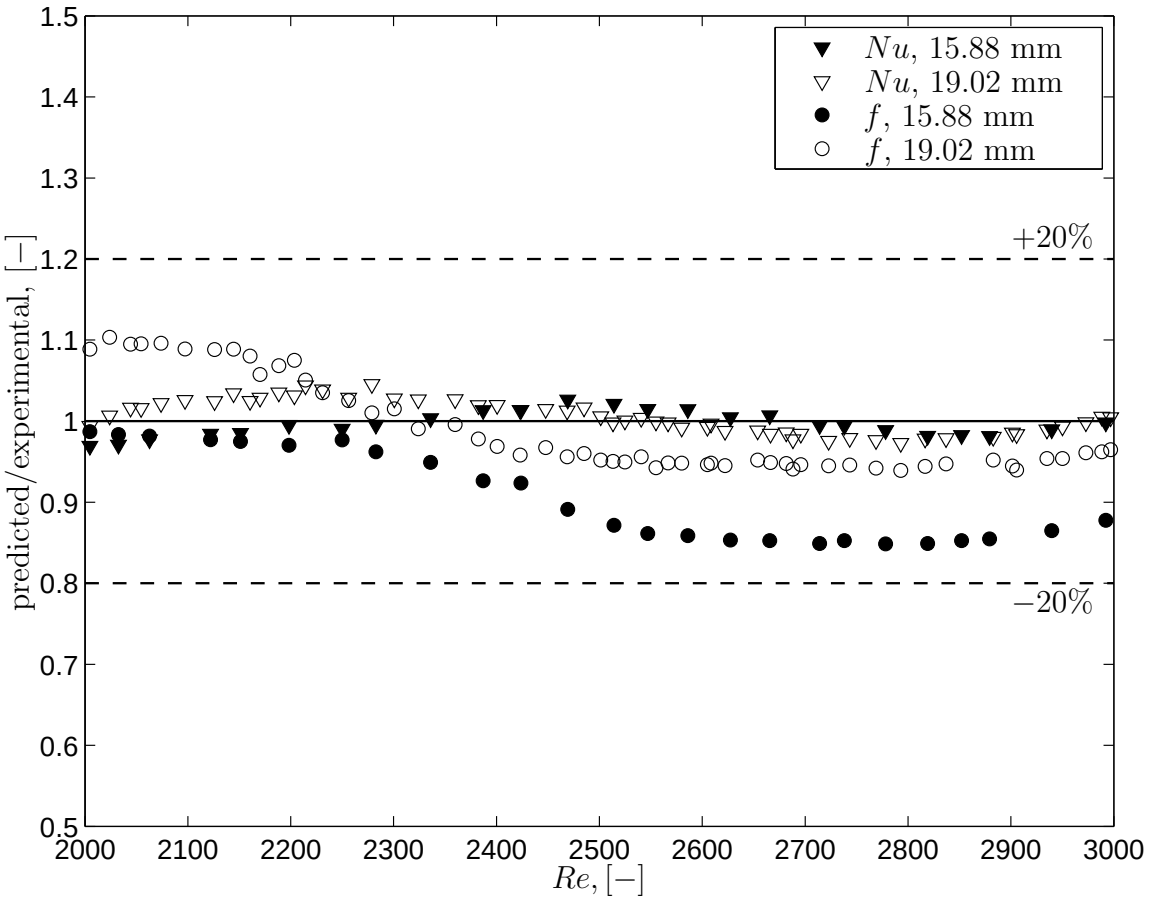

Figure 4.16 Ratio of predicted to measured transition Nusselt numbers and friction factors as a function of the Reynolds number.

The constants which best fit the correlation are $c_1 = 165$ and $c_2 = -23$. Thus, the correlation for the complete flow regime becomes

$$Nu = \left[Nu_L^{165} + \left(Nu_t^{-23} + Nu_T^{-23} \right)^{-165/23} \right]^{1/165} \tag{4.18}$$

$$\begin{aligned} 940 < &Re < 17\,800 \\ 3.73 < &Pr < 5.72 \\ 1.5 \times 10^5 < &Gr < 4.3 \times 10^5 \\ 0.678 < &\mu/\mu_w < 0.85 \\ 289 < &L/D < 373 \end{aligned}$$

These constants are very high, giving little tolerance for any variation in the variables other than those that it was developed for. Thus, for design purposes, it is better to use the separate correlations developed in the previous sections. Equation (4.18) is only useful to make a comparison of the current data. Table 4.2 lists the arithmetic mean deviations and root-mean-square deviations for each tube and each flow regime. Equation (4.18) predicts the heat transfer data on average to within 1% with an average rms deviation of less than 3%, while in combination with Equation (4.10) the friction factors are predicted on average to within 1% with an average rms deviation of less than 8%. The maximum deviation for the prediction of the friction factor is about 20%, occurring in the laminar flow regime. This is more or less the same as the experimental uncertainty for this region.

Table 4.2 Performance of Eq. (4.10) and (4.18) for fully developed smooth tube heat transfer and friction factor.

			Nu			f		
Regime	**Tube**	**Data**	amd	rms	amd_{max}	amd	rms	amd_{max}
Laminar								
	15.88 mm	18	-0.54	1.12	2.38	2.05	2.79	5.81
	19.02 mm	13	3.47	3.55	4.51	14.79	14.95	19.01
	15.88 & 19.02 mm	*31*	*1.14*	*2.45*	*4.51*	*7.39*	*9.91*	*19.01*
Turbulent								
	15.88 mm	39	-2.15	3.22	1.64	-2.48	2.86	-4.63
	19.02 mm	20	1.24	2.23	4.89	5.25	5.48	7.83
	15.88 & 19.02 mm	*50*	*-1.00*	*2.92*	*4.89*	*0.14*	*3.95*	*7.83*
Transition								
	15.88 mm	25	-0.29	1.20	2.09	-9.22	11.17	-15.50
	19.02 mm	54	0.95	3.07	5.74	-0.55	6.92	13.65
	15.88 & 19.02 mm	*79*	*0.56*	*2.63*	*5.74*	*3.30*	*8.50*	*-15.50*
Complete								
	15.88 mm	50	-1.61	2.45	-5.36	-5.20	8.35	-15.58
	19.02 mm	82	0.54	2.35	4.89	1.57	7.29	18.70
	15.88 & 19.02 mm	*132*	*-0.30*	*2.39*	*-15.58*	*-0.99*	*7.71*	*18.70*

4.4 Conclusion

Experimental friction factors for both adiabatic and diabatic flow, as well as heat transfer results were presented. The data was discussed and correlations were developed.

Adiabatic friction factors showed that transition from laminar to turbulent flow commenced at a Reynolds number of approximately 2 200 to 3 000. This was confirmed by a plot showing

the relative standard deviations of the friction factors. This showed that after a Reynolds number of 2 200, the fluctuations increased, peaking at approximately 2 400, after which it decreased, becoming more or less constant at a Reynolds number of 2 600. There was a slight difference regarding transition for the two tubes having different diameters, with the greater one of the two showing signs of delaying transition. This delay was only slight, though, and no conclusion could be made with regard to transition and tube diameter. Further, no hysteresis was noticed within the transition region when increasing and decreasing the Reynolds numbers.

A correlation for the adiabatic friction factors was developed for the entire laminar and turbulent regime. The correlation predicted all the experimental data, including data of six other authors, on average to within 1% with an average rms deviation of less than 5%. The maximum deviation was 35%, although this was due to data falling outside the transition range where the correlation was developed.

Heat transfer results showed that transition for both the tubes commence and ends at a Reynolds number of approximately 2 000 and 2 900. Heat transfer coefficient fluctuations were found to be more pronounced in this region. It was shown that these fluctuations are due to the outlet temperature measurements. Due to the nature of the experimental set-up, though, wall temperature fluctuations could not be detected.

Laminar heat transfer results were also substantially higher than predicted by theory. The heat transfer results, when eliminating the effect of Prandtl number, showed that the 15.88 mm tube showed higher values of heat transfer than the 19.02 mm tube. It was shown that this was due to the mixed convection in the 15.88 mm tube being higher than that of the 19.02 mm tube.

Diabatic friction factor results showed that mixed convection has a definite effect on the values, being on average 35% higher in the laminar region than predicted by the Poiseuille relation. These were similar to results obtained by previous authors for the heating of the fluid by means of a uniform heat flux . The secondary flow influences the velocity profile, making the gradient near the tube wall larger with the effect that the wall shear stress is higher. Turbulent results were also higher than its adiabatic counterpart, although this is shown by including the viscosity correction to the Blasius equation.

From the experimental data, it was further shown that there is a direct relation between heat transfer and friction factor, which is similar to the Reynolds-analogy. This had the implication that only one of the components, heat transfer or pressure drop, need to be determined to determine the other. Heat transfer correlations for the laminar, turbulent, transition and a combination of the three were developed. The correlation predicted the heat transfer results on average to within 1% with an average rms deviation of less than 3%. By using the analogy, the friction factors were also predicted on average to within 1% with an average rms deviation of less than 8%.

Chapter 5

Results: Entrance Effects for Smooth Tubes

> Nothing has such power to broaden the mind as the ability to investigate systematically and truly all that comes under thy observation in life.
>
> *Marcus Aurelius (121 - 180)*

5.1 Introduction

With the completion of the smooth tubes with fully developed results, the next logical step is to reveal the results of different inlet profiles for the same tubes. These profiles induce a hydrodynamically developing boundary layer for adiabatic flow and simultaneously developing boundary layer for diabatic flow, which includes the developing thermal boundary layer. These results are compared with the fully developed smooth tube results.

5.2 Adiabatic Friction Factors

The adiabatic friction factors for all the different inlets are shown in Figure 5.1. The fully developed friction factors are represented by Equation (4.4), which was developed in the previous section. This was to reduce the amount of clutter which otherwise would be experienced in the graphs.

For the different inlets, transition from laminar to turbulent flow commences at different Reynolds numbers. For the re-entrant inlet, transition appears to differ very little from the fully developed value, while the square-edged and bellmouth inlets delay transition quite considerably. The difference between the 15.88 mm and 19.02 mm tubes for the first two inlets is very subtle. However, for the bellmouth inlets, there is a definite difference between the two, with the 19.02 mm tube showing transition to only start at a Reynolds number of approximately

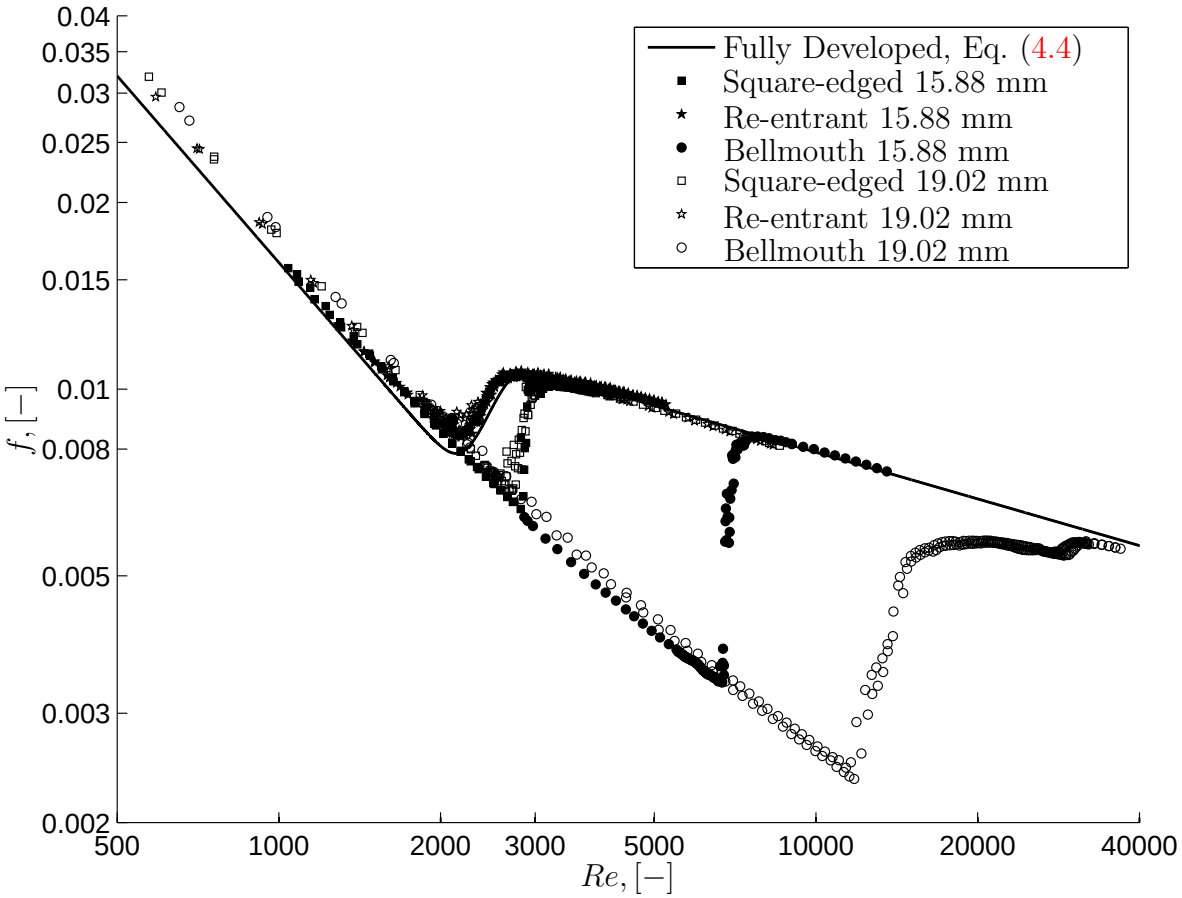

Figure 5.1 Adiabatic friction factors for different inlet configurations for the 15.88 mm and 19.02 mm tubes.

12 000. Transition for the 15.88 mm tube, only starts at approximately 7 000. As this difference was unexpected, the measurements were repeated for both tubes, although the same results were obtained. This difference in transition for the different inlets, as noted by Ghajar and co-workers, is due to the amount of turbulence the different inlets generate, with the re-entrant generating the most.

The difference between the 15.88 mm and 19.02 mm bellmouth entrances can be explained by the fact that the physical bellmouth entrance used for the two tubes are different in the sense that each has a different contraction ratio and that they were manufactured at different dates during the project. This could mean that their internal roughness might be different due to the manufacturing technique which might have differed. This difference in roughness will have an effect on the transition, as noted by Tam and Ghajar (1998), showing that the use of different mesh sizes prior to the inlet has an effect on transition, with the finer mesh delaying

transition the most. The fact is, though, that transition is severely influenced by the type of inlet used, with transition being the earliest for the inlet generating the most turbulence.

Turbulent results for all the different inlets are approximated very well by the Blasius equation. This shows, though, that as soon as the flow becomes turbulent for the different inlets, the hydrodynamic boundary layer is fully developed within the first few diameters of the tube and does not have a significant effect on the pressure drop over the length of the tube.

From Figure 5.1, it can almost be concluded that the laminar flow results follow the Poiseuille relation fairly well. However, on closer inspection, it follows that there is actually a slight increase in laminar friction factors. Similar results were obtained by Ghajar and Madon (1992). The main reason for this is the growing laminar hydrodynamic boundary layer from the inlet of the tube. Due to the flow being within a closure (the tube), the boundary layer grows on all sides at the same time. However, due to continuity requirements (White, 1991), a retardation near the tube wall causes the core at the centre of the flow to speed up, suppressing the boundary layer, causing it to become fully developed at distances much further than predicted by flat-plate theory. This suppression of the boundary layer and the acceleration of the centre core cause an increase in shear and hence an increase in friction. This increase in friction leads to an increase in friction factors, with this excess called the apparent friction factor.

Figure 5.2 shows the relative standard deviations of friction factors for all three different inlets. These graphs show that there is an increase in pressure fluctuation activity in the respective transition zones. This increase in activity for the square-edged inlet starts at a Reynolds number of approximately 2 600 and ends at 3 000. This delay in transition is an increase of approximately 600 Reynolds numbers when compared with the fully developed results. For the re-entrant inlet, transition is approximately the same as for the fully developed results, starting at a Reynolds number of approximately 2 000 and ending at 2 600.

For the 15.88 mm tube bellmouth inlet, transition starts at approximately 6 700 and ends at 7 400. The amount of friction factor fluctuation, though, is much greater than for the former two inlets with the pressure drop fluctuating by as much as 17%. It would seem that the more transition is delayed, the more chaotic the behaviour becomes within the transition zone. The 19.02 mm tube, on the other hand, shows a completely different pattern. Transition is delayed to a Reynolds number of approximately 10 400, but over a bandwidth of 4 500 Reynolds numbers, with the pressure fluctuations being relatively mediocre, peaking at approximately 7%.

Closer inspection of the transition results also showed that there was no difference between increasing Reynolds number data and decreasing data. This shows that, even with different inlet profiles, hysteresis is non existent in this region.

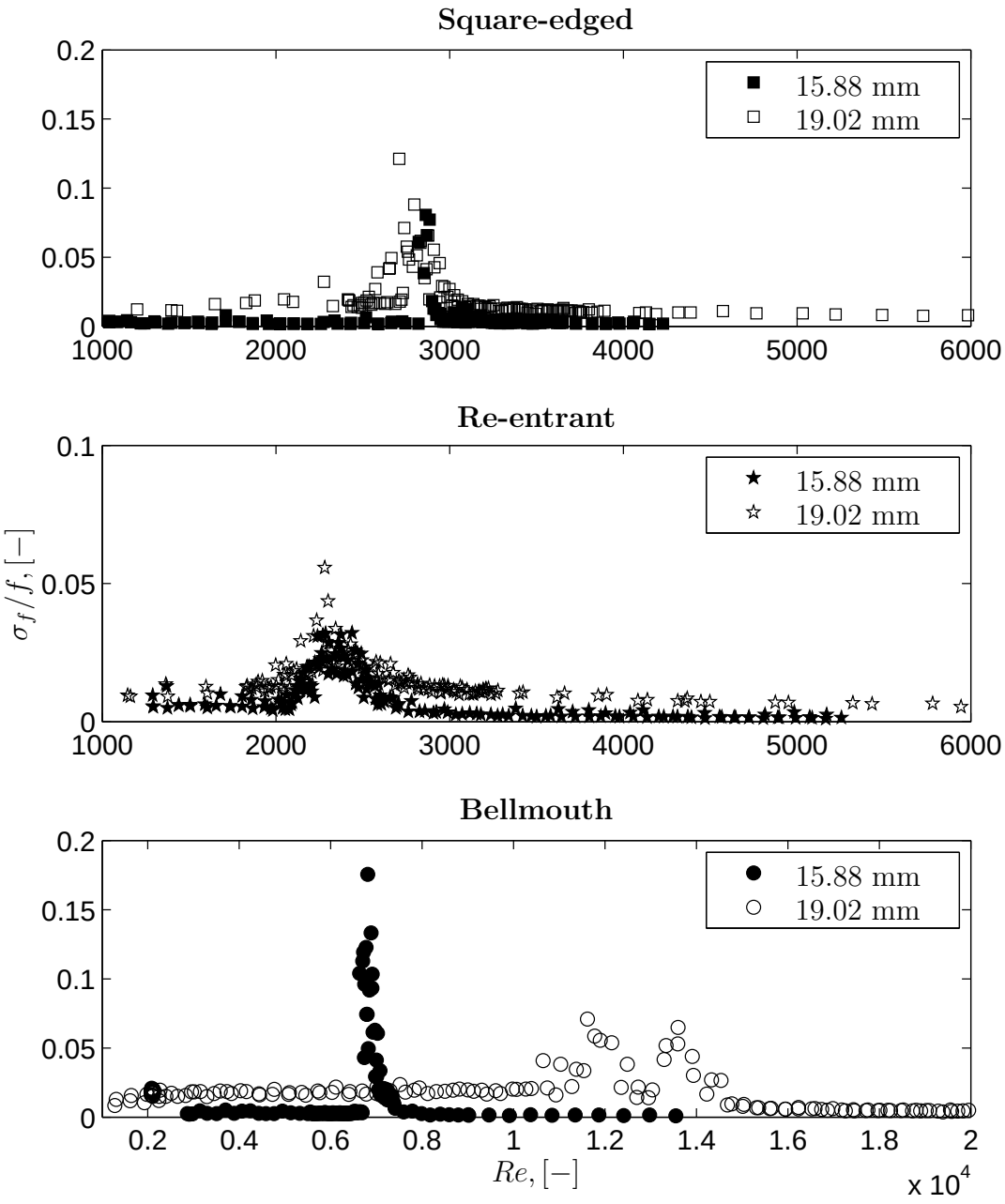

Figure 5.2 Ratio of friction factor standard deviation to friction factors for different inlet configurations.

5.2.1 Correlation

From the experimental results, it appears that the use of the Poiseuille relation for the laminar results would be inappropriate as it would underpredict the friction factors. To adjust for this increase in friction due to the boundary layer growth, Shah (1978) recommends the use of the following correlation for the apparent friction factor:

$$f_{app}Re = \frac{3.44}{\sqrt{\chi}} + \frac{f_pRe + K_\infty/4\chi - 3.44/\sqrt{\chi}}{1 + 0.000212/\chi^2} \tag{5.1}$$

where $\chi = (x/D)/Re$ and K_∞ is the excess pressure drop number in the hydrodynamic developed region, given by Shah and London (1978) as $K_\infty = 1.2 + 38/Re$. f_pRe is the constant value given by the Poiseuille relation, being 16 for a circular tube. Substituting Equation (5.1) for the Poiseuille relation, Equation (4.4) becomes

$$f = f_{app}\left[1 + \left(0.0791Re^{-0.25}\left[1 + \left(\frac{\left(\frac{16}{Re_{Cr_L}}\right)\left(\frac{Re}{Re_{Cr_L}}\right)^{c_3}}{0.0791Re^{-0.25}}\right)^{c_1}\right]^{1/c_1}\frac{1}{f_{app}}\right)^{c_2}\right]^{1/c_2} \tag{5.2}$$

The constants, c_1, c_2, c_3 and Re_{Cr_L}, are listed in Table 5.1 while Table 5.2 lists the respective arithmetic mean deviations and rms deviations for the correlation against the experimental data. The performance of the correlation for all the inlets is also given in Figure 5.3. Not shown is the 19.02 mm bellmouth data due to its unexpected behaviour. On average, Equation (5.2) predicts the data to within 1% with an average rms deviation of 4%. The maximum deviation is approximately 22%, being in the transition region for the bellmouth inlet. This is understandable, though, since the friction factor is an extremely strong function of the Reynolds number in this region. It should further be noted that the inlets which delay transition tend to have a larger deviation from the correlation due to this strong dependence.

It should be noted that Ghajar and Madon (1992) also compared their local friction factor data to the correlation of Shah (1978). It was found, unlike the current average data, that this correlation did not predict their square-edged and re-entrant data very well. The equation predicted their bellmouth data for Reynolds numbers greater than 1 500 very well.

The main question remaining now is: why is there a difference in transition Reynolds numbers for the different inlets? This can be answered by results obtained by Tam and Ghajar (1998) for a bellmouth inlet. It was shown that transition was dependent on the amount of disturbance induced at the inlet. The disturbance influences the growing laminar boundary layer that forms from the inlet of the tube. Down the length of the tube this boundary layer trips into transition and finally becomes turbulent far down stream. The region where the boundary layer trips moves towards the inlet of the tube as Reynolds numbers are increased. The greater the inlet disturbance, the earlier transition and the closer to the inlet it occurs. Thus, as pointed out by Ghajar and Madon (1992), the re-entrant causes the most disturbance,

with the square-edged inlet the second most, while the bellmouth exhibits the least amount of disturbance, and hence delays transition to much higher Reynolds numbers.

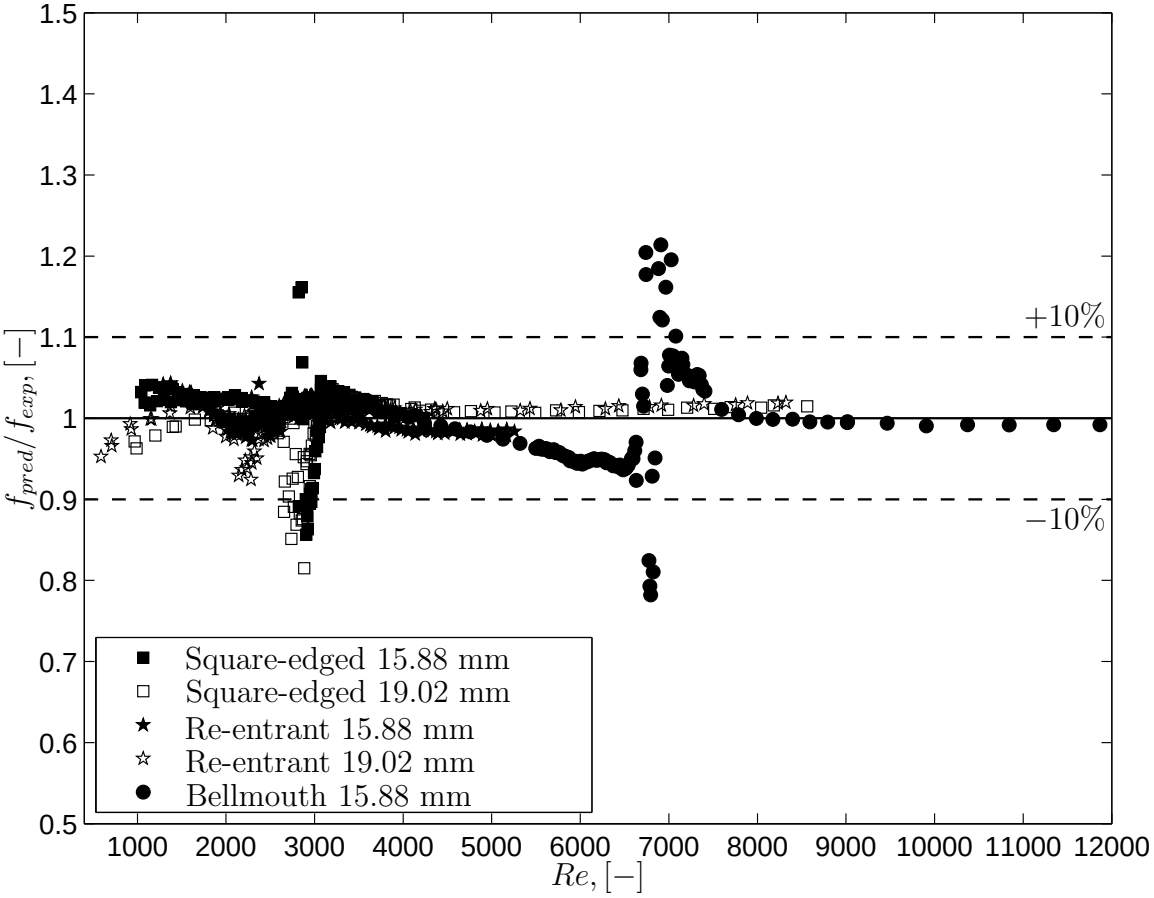

Figure 5.3 Performance of Equation (5.2) against the experimental friction factor data for all the inlets.

5.3 Heat Transfer

Figure 5.4 shows the heat transfer results in terms of the Colburn j-factor for all the inlets, including the fully developed inlet for both the 15.88 mm and 19.02 mm smooth tubes. This figure consists of a total of 581 data points. For the 15.88 mm smooth tube, the number of data points is 83 (fully developed), 59 (square-edged), 27 (re-entrant) and 72 (bellmouth), while for the 19.02 mm tube, the data points are 45 (fully developed), 57 (square-edged), 101 (re-entrant), and 137 (bellmouth). Also included on the graph are 811 data points (green)

Table 5.1 Values for the constants, c_1, c_2, c_3 and Re_{Cr_L}, in Eq. (5.2).

Inlet	c_1	c_2	c_3	Re_{Cr_L}
Square-edged	-12	18	5	2 700
Re-entrant	-9	15	2.2	2 140
Bellmouth	-6	7	25	6 600

Table 5.2 Performance of Eq. (5.2) against the adiabatic smooth tube friction factors for all the different inlets.

Inlet	Data	*amd*	*rms*	amd_{max}
15.88 mm				
Square-edged	150	0.9	4.2	16
Re-entrant	161	-0.2	1.6	4.3
Bellmouth	129	-0.9	7.1	-22
All 15.88 mm	*440*	*-0.03*	*4.7*	*-22*
19.02 mm				
Square-edged	149	-0.2	4	-19
Re-entrant	156	0.3	2.2	-7.6
Bellmouth	-	-	-	-
All 19.02 mm	*305*	*0.07*	*3.2*	-19
All	**745**	**0.01**	**4.1**	**-22**

from the same experimental facility for the 15.88 mm tube for the four inlets using a 50% v/v water-propylene glycol mixture. Further, data from Ghajar and Tam (1994) (red) are included.

The water-propylene glycol data were only added for comparison reasons and will not be analysed. Figure 5.4 shows that water has some special characteristics regarding laminar flow and transition. The laminar results are much higher than the other data while transition appears to start and end at the same Reynolds number. The water-propylene glycol data and the data of Ghajar and Tam (1994) compare fairly well with each other with regard to transition, although laminar results for the mixture are somewhat higher. The difference between the mixture and the data of Ghajar and Tam (1994) could be due to the fluid Prandtl numbers differing. The data for the mixture had an average Prandtl number of about 26 while that of Ghajar and Tam were between 40 and 160 in the laminar region. The Prandtl number

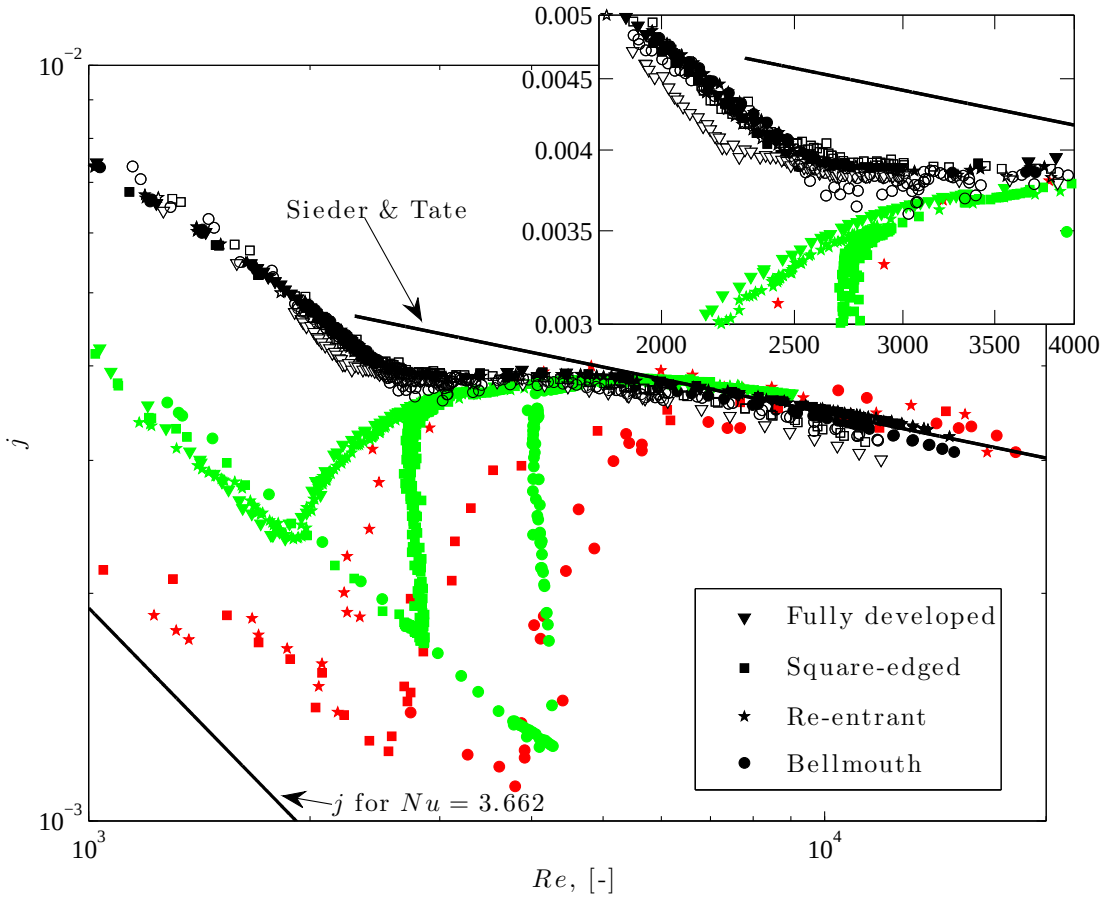

Figure 5.4 Smooth tube heat transfer results in terms of the Colburn j-factor for all the inlets. Solid markers represent the 15.88 mm tube, empty markers the 19.02 mm tube, the green markers water-propylene data and the red markers data from Ghajar and Tam (1994).

for the water results were in the order of 5-6, with the laminar results being the highest. This shows that the Prandtl number might actually have a negative effect on mixed convection and secondary flows as was discussed in Chapter 4. Comparing the results with the data of Ghajar and Tam (1994) is slightly cumbersome as their data are for local values at a distance halfway along the tube, while the current data are averaged values for the whole tube. Further, their data are for the heating of the fluid. Turbulent results, on the other hand, for all the inlets and for the different fluids are in excellent agreement with the correlation of Sieder and Tate (1936).

The fact that transition for the water data occur at the same Reynolds numbers shows that mixed convection and secondary flows have a huge influence on the growing laminar boundary

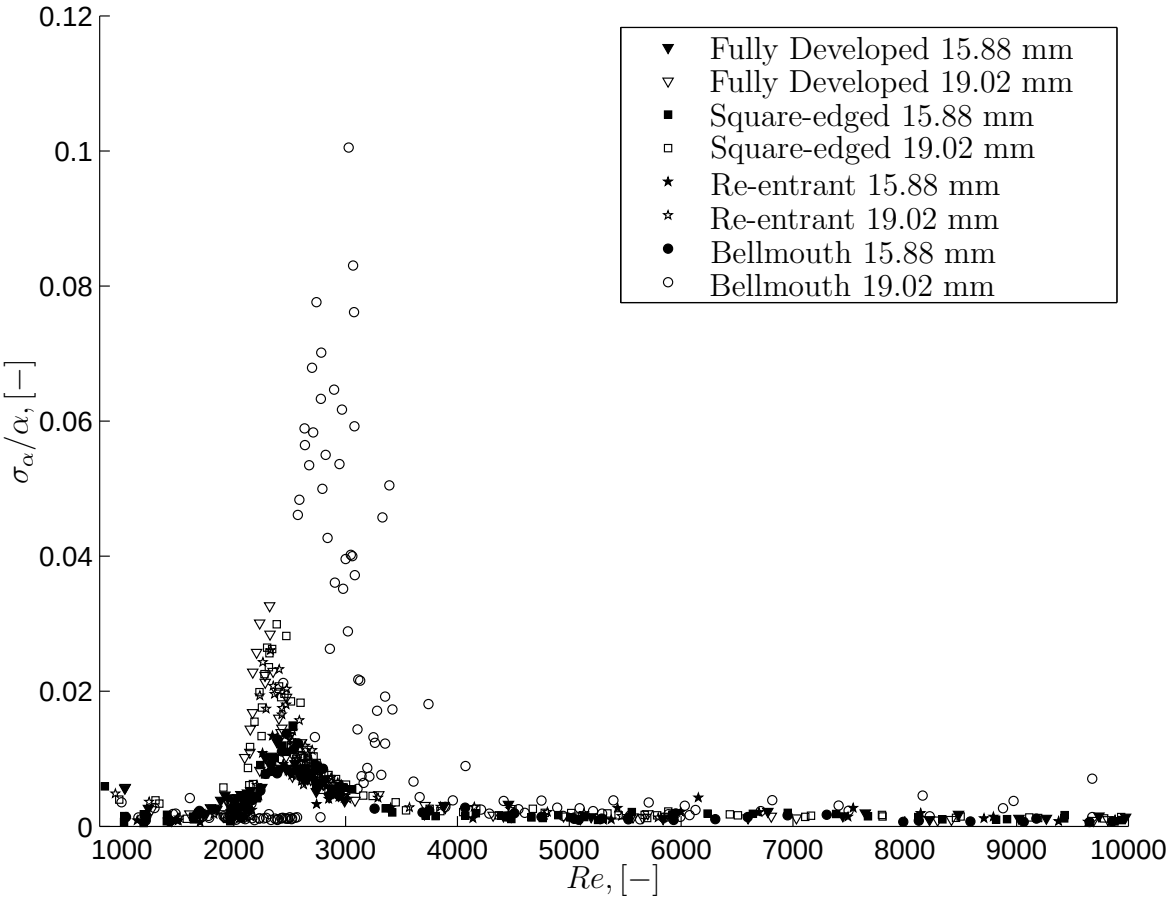

Figure 5.5 Relative heat transfer coefficient standard deviation as a function of the Reynolds number.

layer. From the adiabatic results it was confirmed that the transition was influence by the amount of turbulence generated by the inlet. This shows that, when the process of heat transfer is initiated, the secondary flows, due to mixed convection, influence the boundary layer to such a degree that it negates the effects of the inlet. It is only for the 19.02 mm bellmouth inlet where transition appears to be slightly delayed. This resembles the adiabatic results for which transition was delayed the most, showing that there is a balance between the inlet disturbance (or in this case, calming) and the disturbance from the secondary flows.

Figure 5.5, which is a plot of the relative heat transfer coefficient standard deviation for each inlet confirms that transition for all the inlets occur at the same Reynolds numbers, that is, between 2 000 and 3 000. It is only the 19.02 mm bellmouth which shows signs of delayed transition during heat transfer. Transition only starts at a Reynolds number of approximately 2 600 and ends at 3 900.

5.3.1 Diabatic Friction Factors

Figure 5.6 shows the diabatic friction factors for the square-edged, re-entrant and bellmouth inlets for both the 15.88 mm and 19.02 mm tubes for water. The solid lines are the respective Poiseuille and Blasius equations for the laminar and turbulent flow regime. This figure was comprised of the same amount of data points for each inlet as for the water heat transfer results in Figure 5.4.

Laminar results for all the inlets are very similar to the fully developed inlet results. Although there are some scatter of the data in this region, it all falls within the experimental uncertainty. The increased friction factor results, as discussed in the previous chapter, shows that mixed convection dominates the friction factors in the laminar region. The laminar diabatic friction factor results are approximately 35% higher than the Poiseuille relation.

Transition from laminar to turbulent flow also occur at the same Reynolds numbers, between 2 000 and 3 000. Only the 19.02 bellmouth inlet shows a slight delay. This is very similar to the heat transfer results.

A plot of the relative friction factor standard deviations are shown in Figure 5.7 for the 19.02 mm tube only. The reason why the 15.88 mm tube's data is not shown is that it's standard deviation data was corrupt. The results, however, should be similar. The relative heat transfer coefficient standard deviations (19.02 mm data from Figure 5.5) are included for comparison purposes, showing that there is excellent agreement between the two measuring methods. Thus, two independent methods of measurement confirm that transition during heat transfer for all the inlets occur between a Reynolds number of 2 000 and 3 000, while transition for the 19.02 mm bellmouth inlet occurs between 2 600 and 3 900.

Turbulent results for all the inlets are in excellent agreement with the Blasius equation with the viscosity correction of Allen and Eckert (1964). The data deviate the correlation on average by less than 5%.

5.3.2 Correlation

Since all the experimental data for each tube and inlet have the same results, it is unnecessary to develop a new correlation. It is thus concluded that, except for the 19.02 mm bellmouth, heat transfer is independent of the type of inlet used when using water. Thus, Equations (4.13) - (4.16) and Equation (4.18) from Chapter 4, which was developed for the fully developed inlet profile, can be used to correlate the data for the various inlets. Combining this with the Reynolds-type analogy of Equation (4.10), the diabatic friction factors are also known.

Table 5.3 gives a breakdown of the performance of Equation (4.18) and (4.10) against the experimental data for all the different inlets. On average, the correlation predicts the experimental heat transfer data for all the inlets and tubes to within 1%, deviating from the data by a maximum of 8.4%. The average rms deviation is in the order of 2.6%. For the friction factors, the correlation predicts the data on average to within 1% with a maximum deviation of 20%. The rms deviation is less than 8%

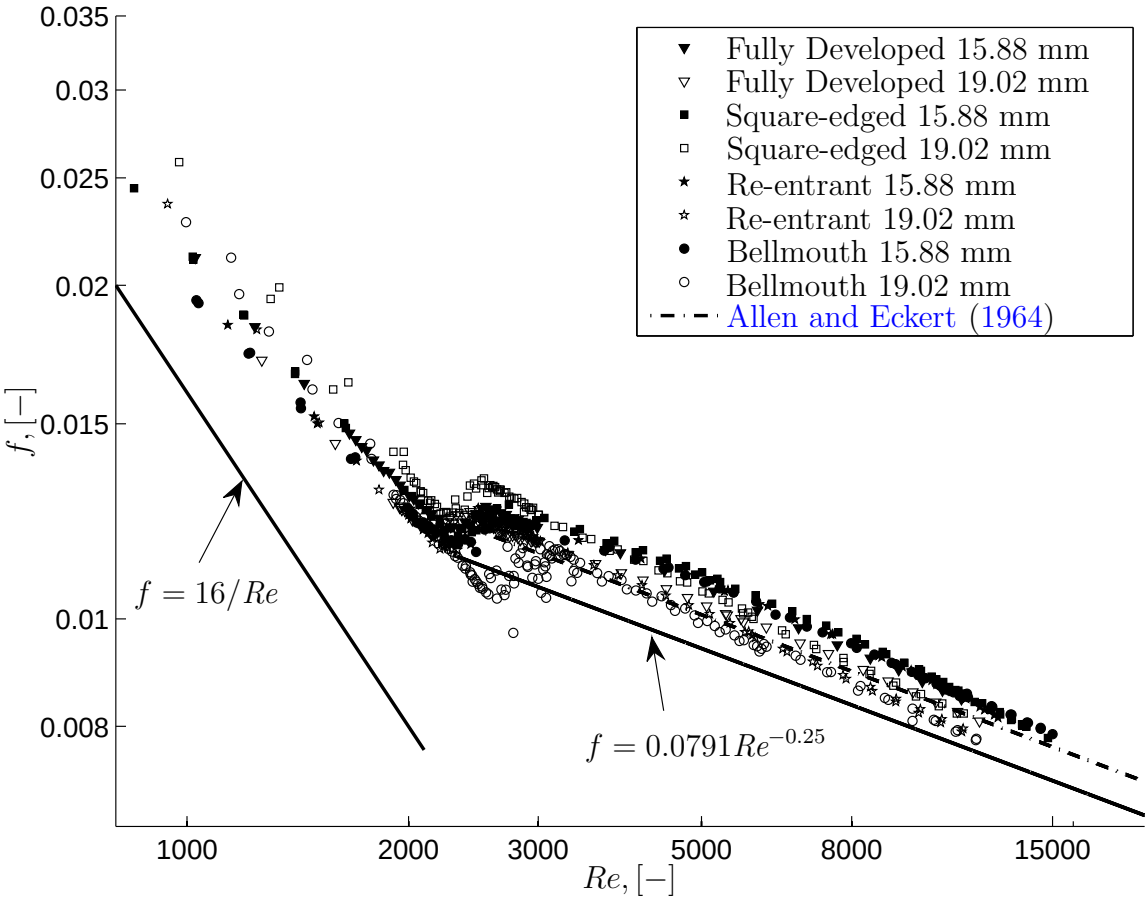

Figure 5.6 Smooth tube diabatic friction factor results for the square-edged, re-entrant and bellmouth inlets.

5.4 Conclusion

Results for the smooth tube with regard to three different types of inlets, namely the square-edged, re-entrant and bellmouth were obtained. These results were compared with the fully developed inlet results discussed in the previous chapter.

Turbulent adiabatic friction factors are hardly influenced by the different inlets with results being near identical to those of the fully developed inlet. Laminar results do, however, tend to be a bit higher than that given by the Poiseuille relation. This was due to the additional loss due to the growing boundary layer being suppressed by the centre core region.

Transition from laminar to turbulent flow is severely influenced by the inlet profile, with the bellmouth inlet showing transition to occur at a Reynolds number of approximately 7 000, much higher than the fully developed entrance case. The square-edged inlet showed the second-

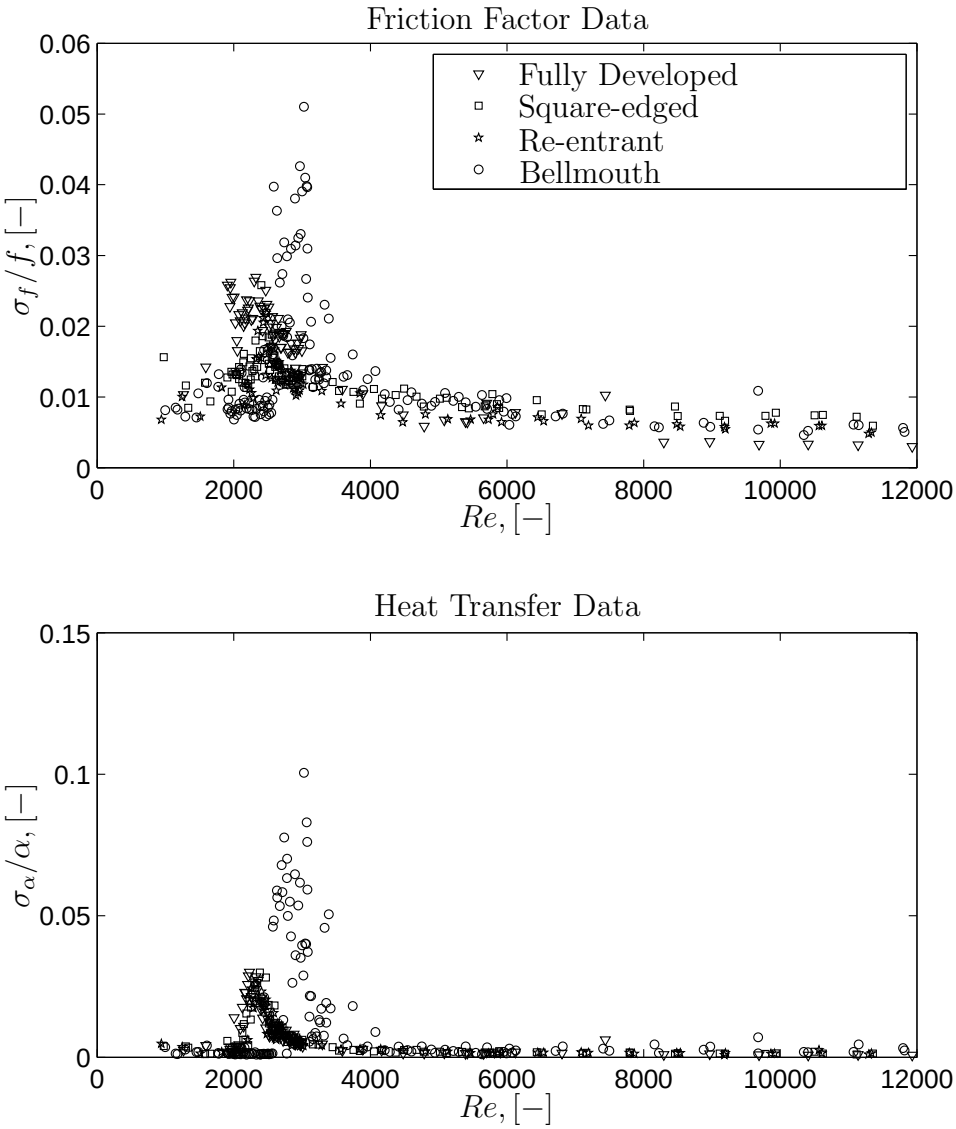

Figure 5.7 Diabatic friction factor and heat transfer coefficient fluctuations for the 19.02 mm smooth tube.

longest delay with transition occurring at a Reynolds number of approximately 2 600, while the re-entrant inlet showed little difference to the fully developed inlet. Further, no hysteresis was noted in the transition region for the different inlets. A correlation was developed to predict the friction factors for each inlet. The correlation predicted the data on average to within 1%.

Inlet profiles had little or no influence on heat transfer results, with transition for most of the inlets starting and ending at a Reynolds number of 2 000 and 3 000, respectively. This

Table 5.3 Performance of Eq. (4.10) and Eq. (4.18) for smooth tube heat transfer and friction factor for various inlets.

			Nu			f		
Tube	**inlet**	**Data**	amd	rms	amd_{max}	amd	rms	amd_{max}
15.88 mm								
	Fully developed	50	-1.67	2.45	-5.36	-5.12	8.35	-15.5
	Square-edged	59	-2.23	3.15	-4.96	-4.95	8.07	-14.8
	Re-entrant	79	-1.22	3.57	7.29	-4.62	7.42	-17.2
	Bellmouth	72	0.56	2.0	6.57	-3.69	7.75	14.7
19.02 mm								
	Fully developed	82	0.54	2.35	4.89	1.57	7.29	18.7
	Square-edged	101	-1.47	2.17	-4.7	-2.58	8.02	-14.0
	Re-entrant	57	-1.04	1.72	3.90	-1.16	7.27	16.5
	Bellmouth	137	0.02	2.50	7.68	6.45	7.68	14.4
15.88 & 19.02 mm		*637*	*-0.67*	*2.55*	*7.68*	*-0.78*	*7.72*	*18.7*

was due to the secondary flow effects encountered during heat transfer, which dominate the growing boundary layer to such an extent that the effect the inlets have are negligible. Only the bellmouth entrance for the 19.02 mm tube showed a slight delay in transition during heat transfer.

Diabatic friction factors remained relatively unchanged from the fully developed inlet results. These results did, however, confirm the heat transfer results with regard to the start and end of transition. This included the 19.02 mm bellmouth results with its slight delay in transition.

No new correlation was developed due to the results being near identical to those for the fully developed inlet. This correlation was thus used to compare the results for the different inlets. The correlation predicted all the heat transfer data (including the 19.02 mm bellmouth inlet) to within 1%. By means of the Reynolds-type analogy shown in the previous chapter, the heat transfer correlation predicted all the experimental smooth tube friction factor data for all the various inlets to within 1%.

Chapter 6

Results: Fully Developed Enhanced Tubes

> Science is wonderfully equipped to answer the question "How?" but it gets terribly confused when you ask the question "Why?"
>
> *Erwin Chargaff (1905 - 2002)*

6.1 Introduction

With the analysis of the smooth tube complete, a next step would be to determine the effects enhanced tubes have. This chapter is dedicated to friction factor and heat transfer results for four different enhanced tubes. The chapter will start with adiabatic friction factors followed by heat transfer results and then by diabatic friction factor results. In each of these sections, a correlation will be developed. The main objective for the use of enhanced tubes, though, is to determine whether it is viable for them to replace smooth tubes. For this reason, a performance evaluation of the enhanced tubes is also conducted at the end of this chapter.

6.2 Adiabatic Friction Factors

The fully developed adiabatic friction factor results for the 18° and 27° enhanced tubes are given in Figure 6.1, for both the 15.88 mm and 19.02 mm tubes. This data consists of a total of 767 data points. The friction factors are given in terms of the effective friction factor,

$$f_e = \frac{D\Delta p}{2\rho u^2 L_{\Delta p}} \tag{6.1}$$

which is based on the root diameter of the tube, while the actual cross-sectional flow area of the enhanced tube was used in calculating the mean velocity.

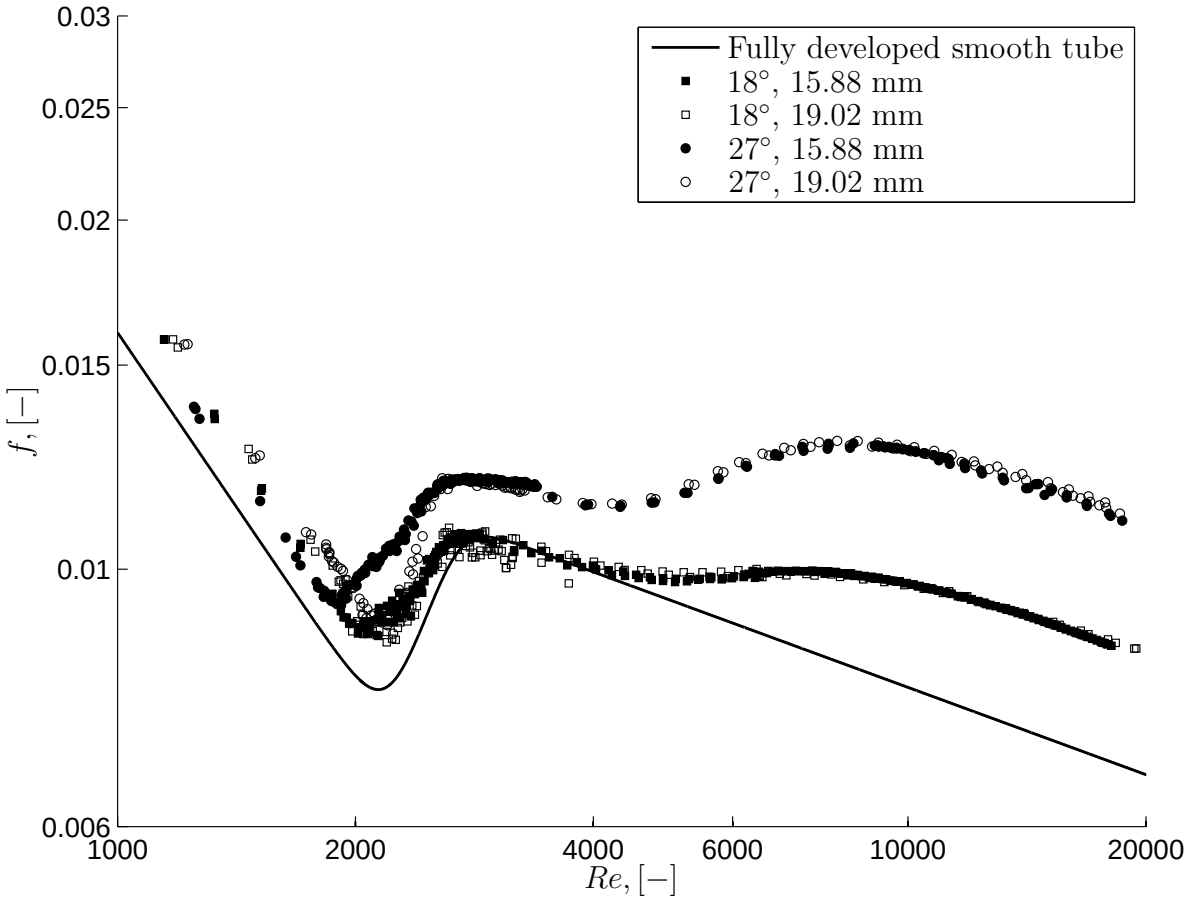

Figure 6.1 Experimental fully developed adiabatic friction factor data for the 18° and 27°, 15.88 mm and 19.02 mm, enhanced tubes.

A few things can immediately be noticed from this figure. Firstly, there is a definite upwards shift in friction factor values in the turbulent as well as the laminar flow regimes compared with the smooth tube results. Secondly, transition occurs earlier than for the smooth tube. Thirdly, there appears to be a 'secondary transition' between Reynolds numbers of 3 000 and 10 000.

The upward shift in friction factor is understandable. This is due to the increase in roughness the fins exhibit which in turn increases the amount of resistance to flow. These results are in conjunction with those of other authors, for example, Vicente *et al.* (2002b) and García *et al.* (2005), who looked at laminar-to-turbulent flow inside dimpled tubes and tubes with wire-inserts. The earlier transition can also be attributed to this increase in roughness. The secondary transition, however, would most probably be due to the rotation the fins bring about the fluid. Results where different roughness for tubes were compared, did not show this secondary effect, where these roughness were in the form of ring inserts or dimples tubes

(Koch, 1960; Nunner, 1956; Vicente *et al.*, 2002b). This shape of the curve in this region can be explained by means of the effectiveness the fins have in rotating the fluid. At the lower Reynolds numbers, the fins are ineffective in rotating the fluid and only as the velocity is increased, do they become more effective. Similar effects are seen in the results of Brognaux *et al.* (1997) and Jensen and Vlakancic (1999), with micro-fin and high-fin tubes. The penalty of this rotation, however, is an increased cost in energy, and hence the increase in friction factor is observed. Only after a Reynolds number of approximately 10 000 does this secondary transition stop and the friction factors continue along the standard roughness-height-to-diameter ratio lines depicted in the Moody chart. It should be noted that the relative roughness of the two diameter tubes for both the 18° and 27° enhanced tubes are the same. Thus, the higher friction factor values of the 27° tubes are then purely due to the helix angle.

Figure 6.2 depicts the relative friction factor standard deviation for both the 18° and 27° en-

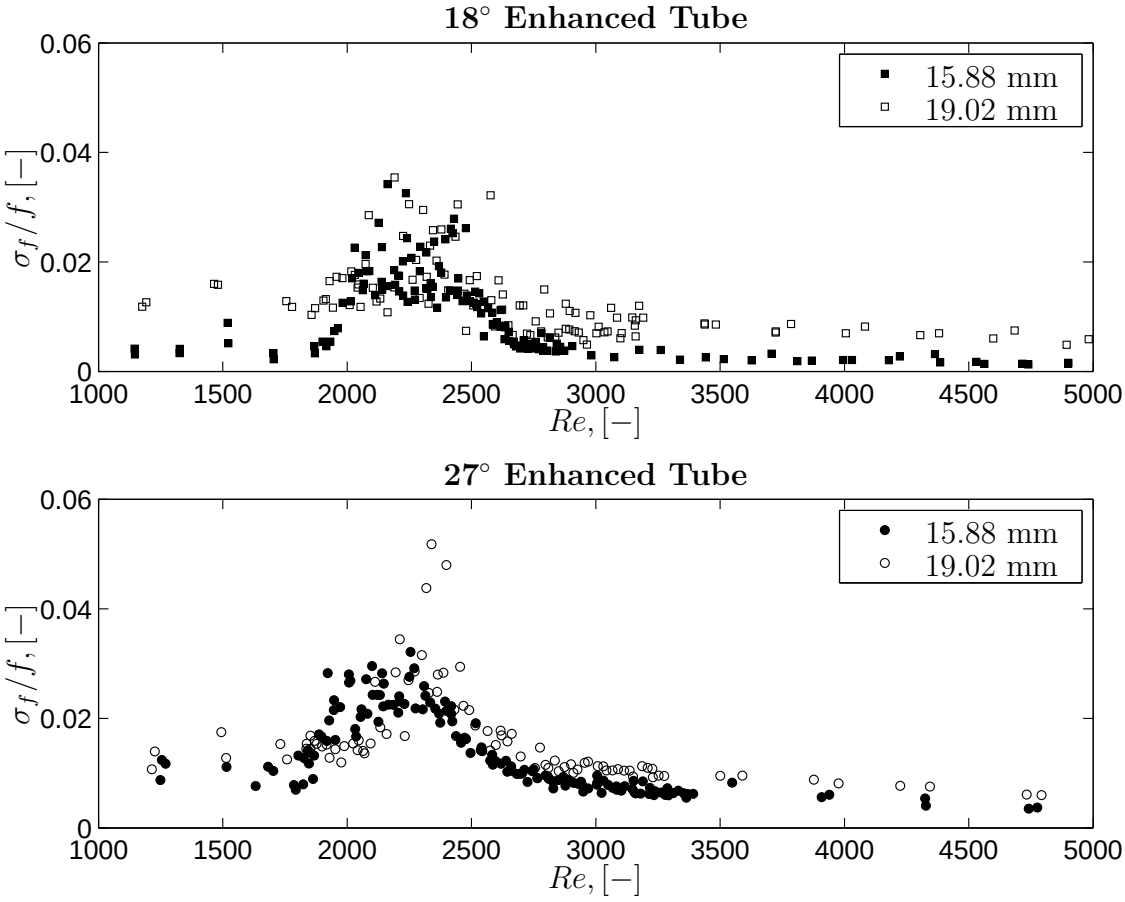

Figure 6.2 Relative friction factor standard deviations for the 18° and 27° enhanced tubes.

hanced tubes. Transition for the two different helix angles appears to commence at approximately the same Reynolds number. However, only the 27°, 19.02 mm tube, shows a slight delay in transition. Transition for this tube occurs at a Reynolds number of about 2 070, while for the other tubes it occurs at 1 870. This slight delay in transition is not due to inlet disturbances, as the same inlet was used for all the tubes. Further, the fin pitch-diameter ratios have values of 0.39 and 0.18 for the 18° and 27° enhanced tubes, respectively, showing that their effect is also negligible. The same can be said regarding the helix angle. Thus, the only geometrical aspect that would have an influence on transition is the fin height-diameter ratio. Three of the tubes have a ratio of 0.027 with transition occurring at a Reynolds number of 1 870, while the fourth tube, being the 27° 19.02 mm tube, has a ratio of 0.022. Thus, it is clear that only the roughness height has an influence on transition.

Similar conclusions were made by Vicente *et al.* (2002b) and Vicente *et al.* (2004), who performed tests on corrugated and dimpled tubes. Their correlations predicting the critical Reynolds numbers, given in Section 2 as Equations (2.23) and (2.24), is only in terms of the roughness-height-to-diameter ratio.

The friction factor fluctuations peak at a Reynolds number of approximately 2 200 and drop down again at approximately 2 600 with increasing Reynolds numbers. It should be noted, though, that in the Reynolds number region of 3 000 to 10 000 where the secondary transition commences, the fluctuations are stable. This shows that this region is not at all chaotic and is, from repeated experiments, predictable. It can further be stated that fully turbulent flow for these enhanced tubes is only reached at Reynolds numbers above 10 000.

For the enhanced tubes, as with the smooth tubes, no hysteresis was noted. All the data presented in Figure 6.1 are for increasing and decreasing Reynolds numbers.

6.2.1 Correlation comparison

Since there is a definite increase in laminar and turbulent friction factors, it will be of interest to compare these results with correlations from the literature. For laminar flow, the increase in friction factor would mainly be due to the roughness height of the fins and not the fin helix angle or number of fins. This was observed by Vicente *et al.* (2002b), examining helical dimpled tubes. They found that it was only the dimple height that affects the friction factor, and not the density of the dimples. They propose the following correlation for laminar flow:

$$f_{Le} = \frac{16}{Re}\left[1 + 123.2\,(e/D)^{2.2}\,Re^{0.2}\right] \tag{6.2}$$

This correlation predicted the laminar friction factor data for all four enhanced tubes with an average mean deviation of 6% and an average rms deviation of 10%. This is improved, though, by changing the constant, 123.2, to 88, predicting the data with an average mean deviation of 1.3% and an average rms deviation of 7.3%. It is thus proposed that Equation (6.2) become

$$f_{Le} = \frac{16}{Re}\left[1 + 88\,(e/D)^{2.2}\,Re^{0.2}\right] \tag{6.3}$$

Table 6.1 Adiabatic friction factor correlations for enhanced tubes

Carnavos (1980)[a]

$$f_e = 0.046 Re^{-0.2} \left(D/D_h\right)^{1.2} \left(A_c/A_{cn}\right)^{0.5} \left(\sec\beta\right)^{0.75} \tag{6.4}$$

$$0 < \beta < 30^\circ,\ 10\ 000 < Re < 100\ 000,\ 0.7 < Pr < 30$$

Ravigururajan and Bergles (1996)

$$f_e/f_s = \left\{1 + \left[29.1 Re^{a1} \left(e/D\right)^{a2} \left(p_f/D\right)^{a3} \left(\beta/90\right)^{a4} \left(1 + 2.94\cos\left(\gamma/2n\right)\right)\right]^{15/16}\right\}^{16/15} \tag{6.5}$$

$$0.01 < e/D < 0.2,\ 0.1 < p_f/D < 7.0,\ 0.3 < \beta/90 < 1.0,$$
$$5\ 000 < Re < 250\ 000,\ 0.66 < Pr < 37.6$$

$a1 = 0.67 - 0.06 p_f/D - 0.49\beta/90$
$a2 = 1.37 - 0.157 p_f/D$
$a3 = -1.66e - 6Re - 0.33\beta/90$
$a4 = 4.59 + 4.11e - 6Re - 0.15 p_f/D$

Jensen and Vlakancic (1999)

$$f_e/f_s = \left(l_{csw}/D\right)^{-1.25} \left(A_{cn}/A_c\right)^{1.75} - 0.0151/f_s \left[\left(l_{csw}/D\right)^{-1.25} \left(A_{cn}/A_c\right)^{1.75} - 1\right] e^{-Re/6780} \tag{6.6}$$

$$2\ 000 < Re < 80\ 000,\ Pr \approx 7,\ 0 < \beta < 45^\circ,\ 0.0075 < e/D < 0.05$$

$l_{csw}/D = \left[1 - 0.994 \left(n \sin\beta/\pi\right)^{0.89} \left(2e/D\right)^{0.44} \times \left\{\left(\pi/n - s/D\right)\cos\beta\right\}^{0.41}\right]$
$s = 4/3e \tan\left(\gamma/2\right) =$ average width of triangular fin

[a] Appears to be incorrectly given in his original paper, with this correlation being taken from Wang and Rose (2004)

For turbulent flow, the correlations of Carnavos (1980), Ravigururajan and Bergles (1996) and Jensen and Vlakancic (1999) are compared with the experimental data. Table 6.1 lists the authors and their respective correlations as well as their limits of use. The reason the correlations of these three were chosen was the fact that these are the most recent correlations developed for low-fin enhanced tubes.

Figure 6.3 shows the performance of these correlations against the experimental data for the four enhanced tubes, spanning a Reynolds number range of 3 000 to 19 000. The Carnavos (1980) correlation, developed from a wide range of enhanced tubes, predicts the data on average to within 7% with an rms deviation of 12.5%.

The data deviates from the correlation by a maximum of 32%, although this is in the region where the secondary transition is situated. For a Reynolds number above 10 000 (from where this correlation is valid), the data is predicted to within 1% with an rms deviation of 7% and a maximum deviation of 11.5%.

The correlation of Ravigururajan and Bergles (1996) predicts the data on average to within 2.3% with an rms deviation of 7%, deviating from the data by a maximum of 21%. This deviation is also in the lower turbulent region, Reynolds numbers lower than 5 000. This is also below the applicable range of this correlation. The correlation of Jensen and Vlakancic (1999) predicts the data on average to within 1.7% with an rms deviation of 5.4% and a maximum deviation of 11.5%. This is the only correlation that predicts the data for the whole turbulent regime while noting that it is applicable for Reynolds numbers greater than 2 000. This excellent agreement between data and correlations also further validates the experimental system.

6.2.2 Adiabatic Friction Factor Correlation

Since the laminar and turbulent correlations mentioned in the previous section predicted the data so well, a new correlation will only be developed for the transition regime. It is further necessary to develop a prediction method for the critical Reynolds numbers for enhanced tubes.

Critical Reynolds Numbers

Since very few data regarding these values for enhanced tubes exist (including the present data), it was decided to utilise the data of Vicente *et al.* (2004) in the development of the correlations. The choice for using the helical corrugated tube data was due to these tubes having the closest resemblance to the current enhanced tubes for the available data. Other data for wire coil inserts (García *et al.*, 2007a) in the transition region were found. However, the wire heights were much greater than the current study with their results showing not only very early transitions, but also a very gradual change of laminar to turbulent flow with no distinct critical value. This was due to the wires inducing a swirl flow in the laminar regime, with the trends being very similar to the twisted tape inserts investigated by Manglik and Bergles (1993).

Data of fin height-to-diameter ratio and critical Reynolds numbers are given in Figure 6.4. Since pressure fluctuation data was not available, the critical Reynolds numbers were taken as the minimum friction factor at transition.

From the data it was found that the curve that predicts the critical Reynolds the best is

$$Re_{cr} = 262 \left(\frac{e}{D}\right)^{-0.526} \tag{6.10}$$

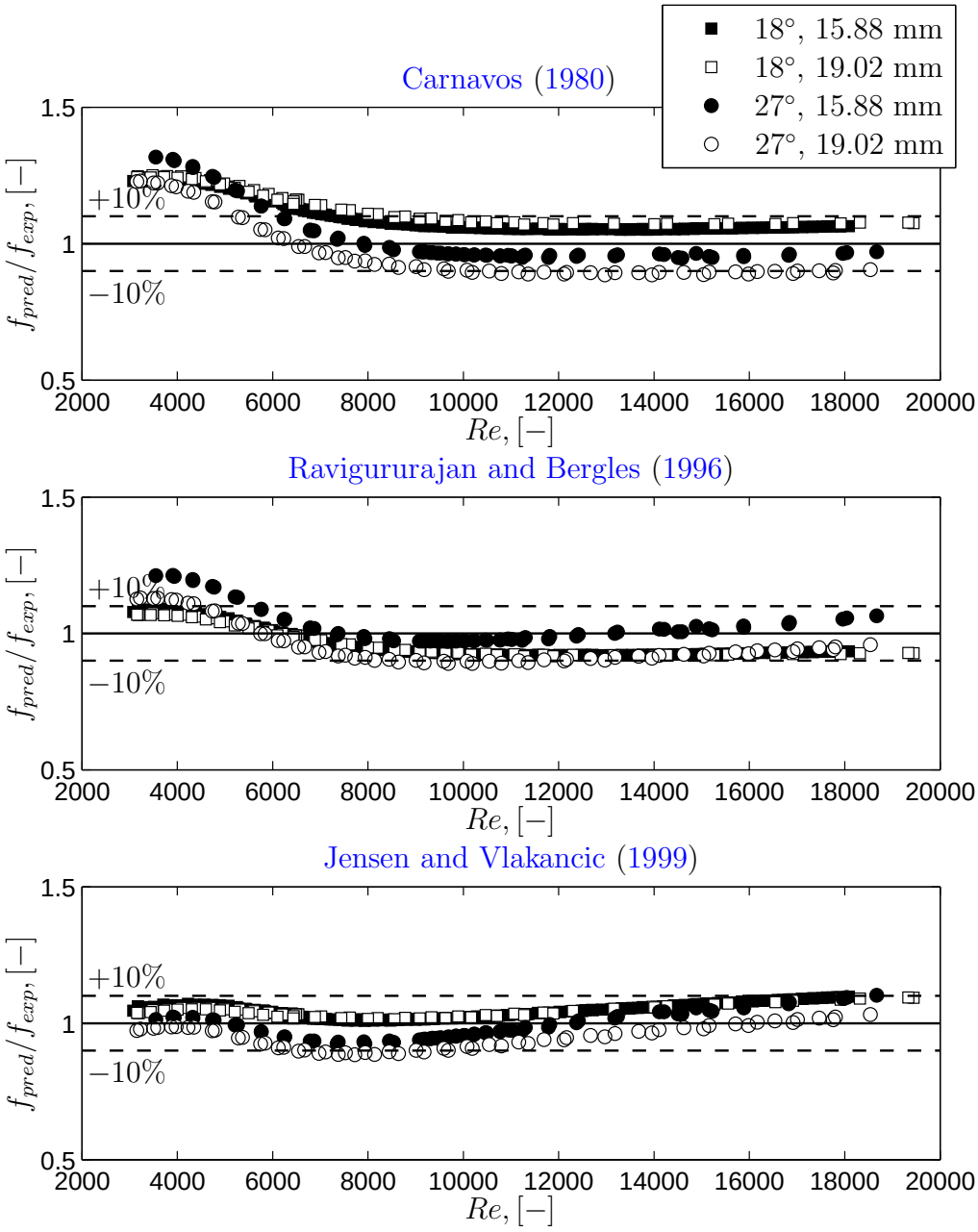

Figure 6.3 Performance of the correlations listed in Table 6.1 against the experimental adiabatic friction factor data for the four enhanced tubes.

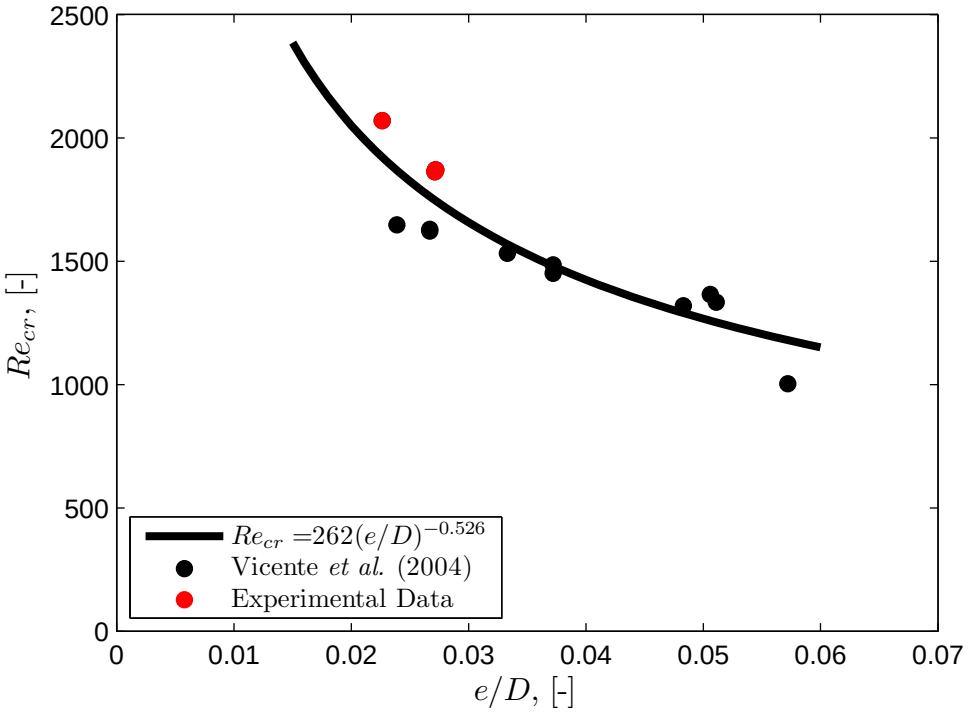

Figure 6.4 Critical Reynolds numbers for varying fin height-to-diameter ratios.

which is valid for $0.022 \leq (e/D) \leq 0.057$. To extend its range of validity to include the critical Reynolds number of the smooth tube with a fully developed inlet profile ($Re_{cr} = 2\ 200$), the method of Churchill and Usagi (1972) was incorporated. Thus, the limiting form for a fully developed smooth tube is

$$Re_{cr} = 2\ 200 \left(\frac{e}{D}\right)^{0} \tag{6.11}$$

Writing Equations (6.10) and (6.11) in the form of an nth-order asymptotic solution and re-arranging gives

$$Re_{cr}/2\ 200 = \left[1 + \left(\frac{262\,(e/D)^{-0.526}}{2\ 200}\right)^{-n}\right]^{-1/n} \tag{6.12}$$

which also has the form

$$Y = \left[1 + Z^{-n}\right]^{-1/n} \tag{6.13}$$

The constant n can be evaluated for $Z = 1$ which gives the central value of e/D, which in this case has a value of 0.0175. Thus, the value of n could be computed for $Z = 1$ if the value

of $Y(1)$ were known, which unfortunately it is not. Thus, by loosely fitting Equation (6.12) for different values of n to the data, a value of $n = 10$ was chosen. Thus, the final correlation predicting the critical Reynolds number is given as

$$Re_{cr} = 2\ 200 \left[1 + 9.13 \times 10^{9} \left(\frac{e}{D}\right)^{5.8}\right]^{-1/10} \tag{6.14}$$

This correlation predicts the current set of data on average to within 1% with an rms deviation of 8% and a maximum deviation of less than 18%.

Transition Region

Since the transition region is characterised as being between the laminar and turbulent flow regime, it would only be fitting if this region were described by the same parameters used to predict these regimes. Thus, as with turbulent flow for enhanced tubes, the main parameters having an influence in this region will be similar. It is thus suggested that the correlation should have the form

$$f_{te} = f\left(Re,\ Re_{Cr},\ e,\ D,\ p,\ \beta\right) \tag{6.15}$$

By re-arranging the parameters, the best form of the correlation was found to be

$$f_{te} = \left(\frac{16}{Re_{Cr}}\right)^{c_1} exp\left(c_2 \frac{Re}{Re_{Cr}}\right) \left(\frac{\beta}{90}\right)^{c_3} \left(\frac{e^2}{pD}\right)^{c_4} \left(\frac{p}{D}\right)^{c_5} \left(\frac{e}{D}\right)^{c_6} \tag{6.16}$$

The constants were found by means of a non-linear least squares optimisation method with the correlation becoming

$$f_{te} = \left(\frac{16}{Re_{Cr}}\right)^{0.94} exp\left(0.57 \frac{Re}{Re_{Cr}}\right) \left(\frac{\beta}{90}\right)^{0.37} \left(\frac{e^2}{pD}\right)^{0.028} \left(\frac{p}{D}\right)^{-0.009} \left(\frac{e}{D}\right)^{0.06} \tag{6.17}$$

This correlation is valid for

$$\begin{aligned} Re_{Cr} \leq & Re \\ 18^\circ \leq & \beta \leq 79^\circ \\ 6.14 \times 10^{-4} \leq & e^2/pD \leq 0.004 \\ 6.48 \times 10^{-4} \leq & p/D \leq 1.23 \\ 0.022 \leq & e/D \leq 0.057 \end{aligned}$$

Note that the upper limit for the Reynolds number has not been defined. This limit can be set as the intersect of Equation (6.17) and an appropriate turbulent correlation. For the current

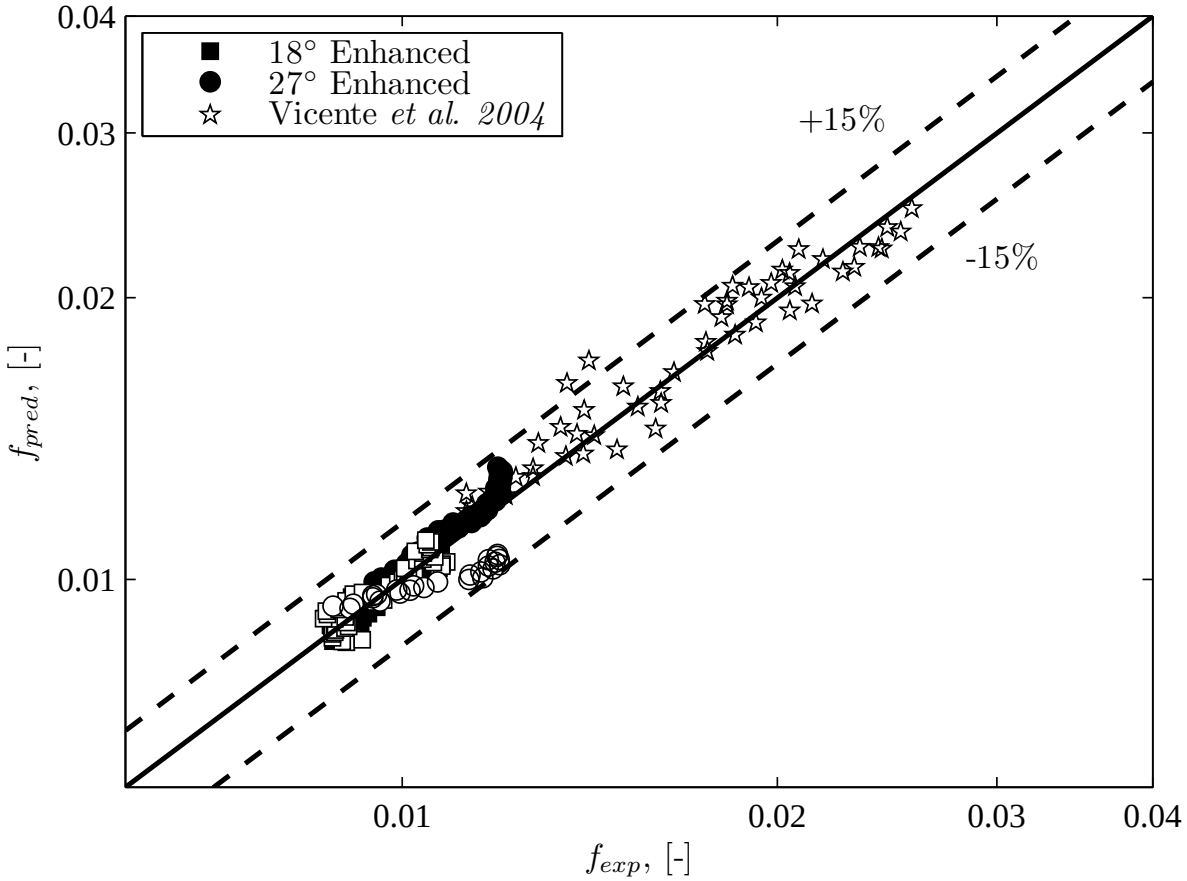

Figure 6.5 Experimental vs. predicted adiabatic enhanced tube friction factors. Solid markers represent the 15.88 mm tubes while the empty markers the 19.02 mm tubes.

experimental data, the model of Jensen and Vlakancic (1999) should be used. A comparison of the experimental data with Equation (6.17) is shown in Figure 6.5. The correlation predicts the data on average to within 1% with an rms deviation of 4.8%.

6.3 Heat Transfer

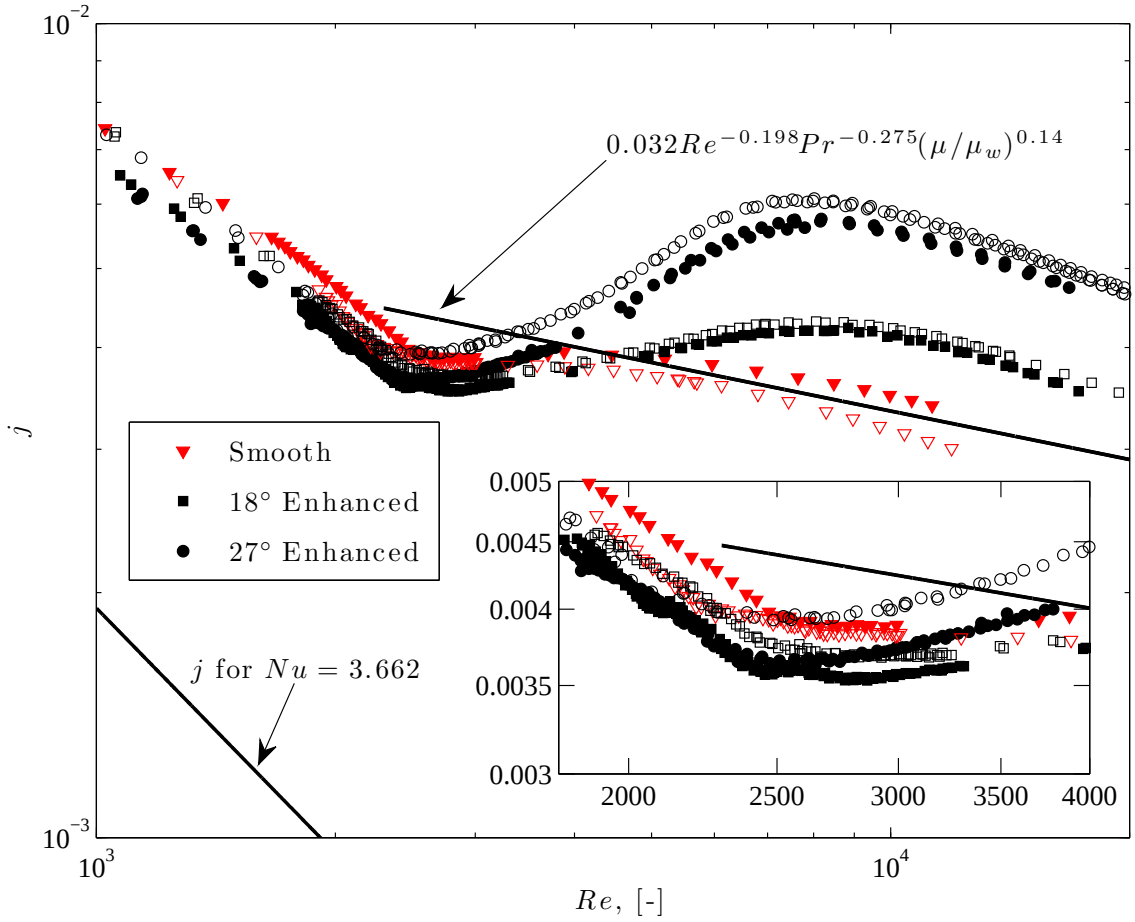

Figure 6.6 Fully developed heat transfer results in terms of the Colburn j-factor for the smooth and enhanced tubes. Solid markers: 15.88 mm. Empty markers: 19.02 mm.

The heat transfer coefficients for the enhanced tubes were calculated in terms of the nominal surface area which is based in terms of the nominal or root diameter. This approach is suggested by Marner *et al.* (1983) and facilitates in the direct comparison of enhanced and smooth tube performance.

Figure 6.6 shows the fully developed heat transfer results for the smooth tubes as well as for the four enhanced tubes. The enhanced tubes consisted of a total of 664 data points. The revised turbulent heat transfer correlation of Sieder and Tate (1936), Equation (4.14),

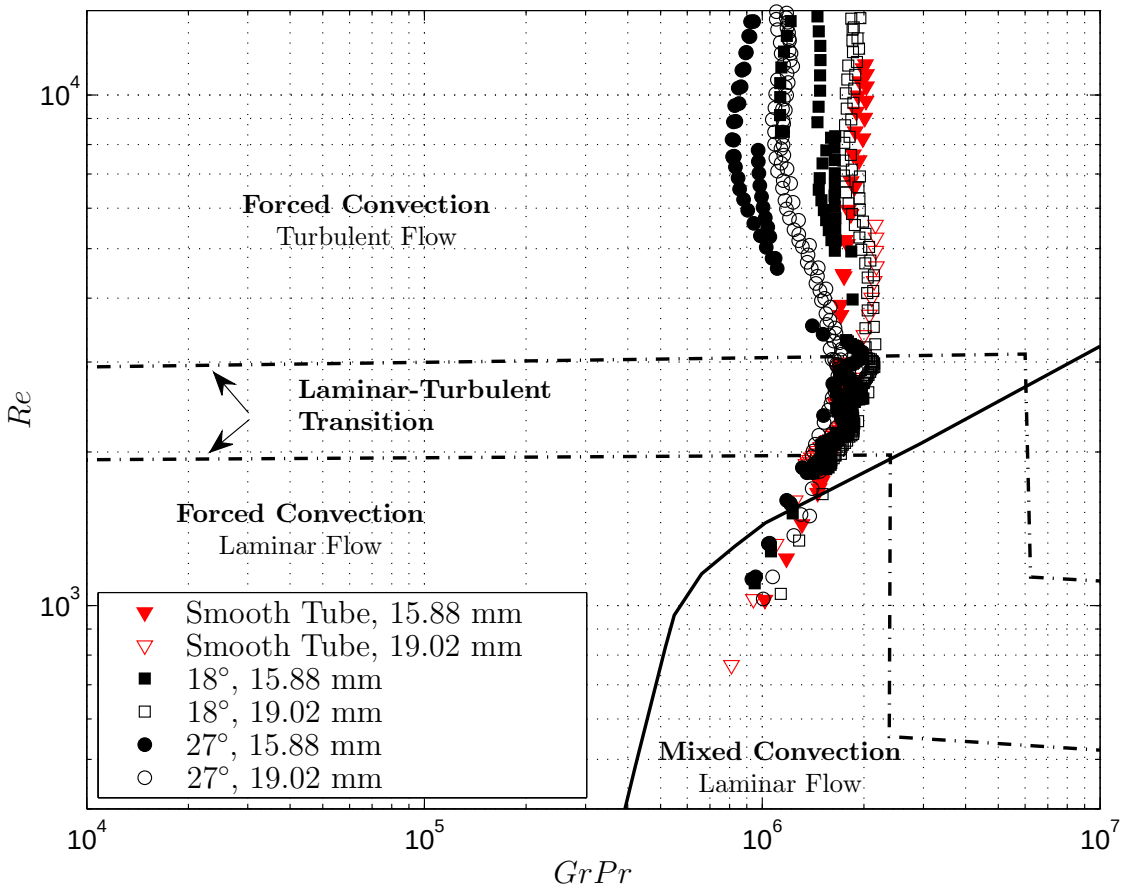

Figure 6.7 Experimental heat transfer data for the smooth and enhanced tubes on the flow regime map of Metais and Eckert (1964).

is also included and is presented in the form of the Colburn j-factor. The transition region ($Re = 1\,800 - 4\,000$) is enlarged and included as an insert in the figure. The smooth tube data are shown as red markers to aid in the discussion.

Turbulent results show that there is a definite increase in heat transfer with the use of the enhanced tubes, with the 27° tube showing the highest enhancement. It is further noted that the 19.02 mm enhanced tubes have slightly higher values compared with the equivalent 15.88 mm tube. This is due to the Prandtl numbers of the 19.02 mm tube being slightly higher than their 15.88 mm counterparts.

Between Reynolds numbers of 3 000 and 8 000, the j-factors are actually increasing with Reynolds number, unlike the smooth tube results that vary little. The increase is due to the fins breaking up the laminar viscous sublayer which can accounts for 60% of a liquid's temperature drop during turbulent flow (Shah and Seculić, 2003). Since the fin-height to diameter ratios

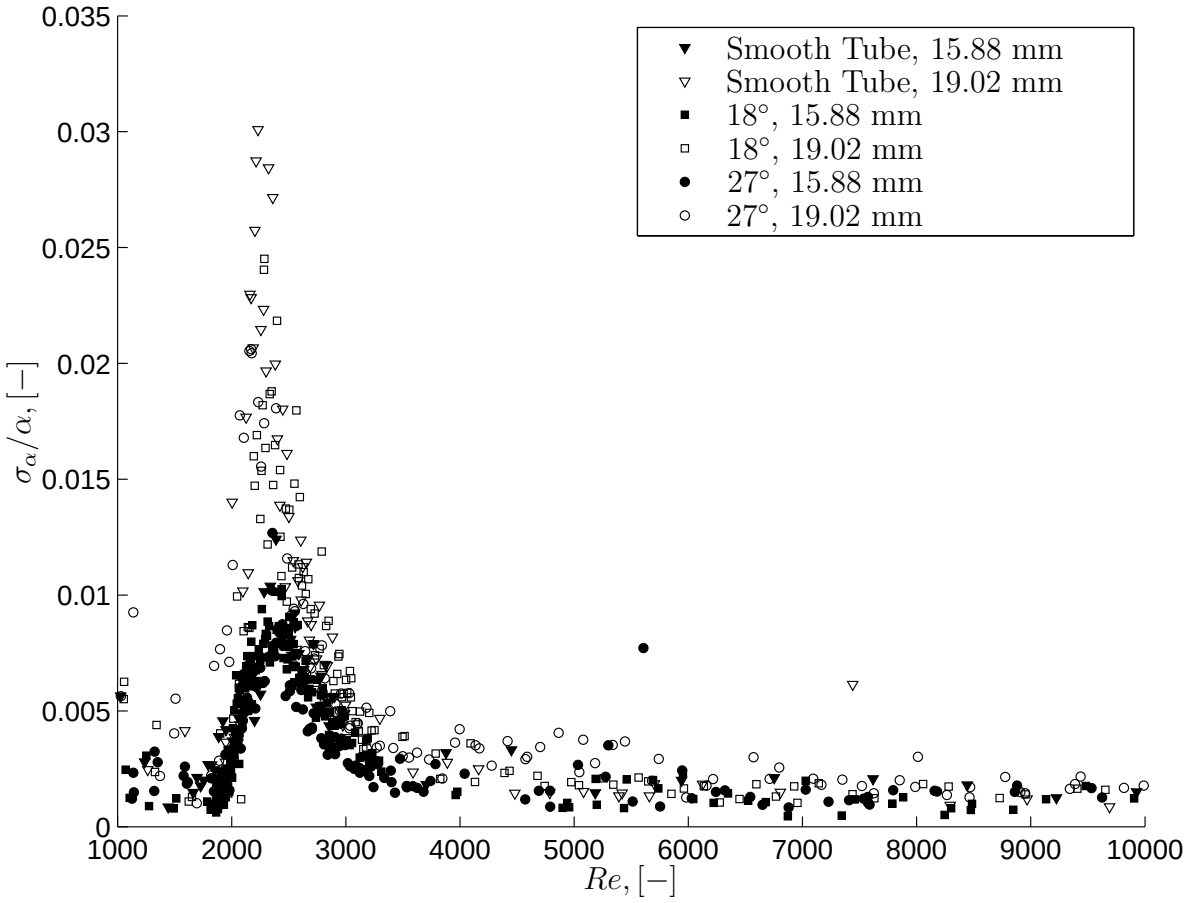

Figure 6.8 Heat transfer coefficient fluctuations for the fully developed smooth and enhanced tubes.

for all the enhanced tubes are the same, the further increase would then be due to the helix angle, which in turn spins the fluid. This is seen for Reynolds numbers greater than 2 600 and 2 500 for the 15.88 mm and 19.02 mm enhanced tubes, respectively, where the 27° tubes start to deviate from the 18° tubes as the Reynolds number increases. This deviation would be due to the fins with the greater helix angle spinning the fluid more effectively, and hence aids in the mixing thereof. Only after a Reynolds number of approximately 9 000 do the enhanced tubes reach a maximum and they stop to deviate from the smooth tube. The j-factors then start to decrease with increasing Reynolds number, following a parallel path with the smooth tube.

For the laminar regime, it appears as if the enhanced tube heat transfer results are slightly lower than for the smooth tubes. Further, on closer inspection, it also appears that heat transfer for the 15.88 mm enhanced tubes are lower than for the 19.02 mm tubes. The helix angle, however, has no noticeable effect in the laminar regime.

Thus, it seems that the fins have a negative influence on heat transfer in the laminar regime, although heat transfer values are still higher than the theoretical values for uniform wall temperature boundaries. Since the enhancement of the laminar region is due to mixed convection, as observed in the previous chapters, the fins could act as a restriction to secondary flows. Similar effects were observed by Vicente *et al.* (2002b) with the helical dimpled tubes at relatively low Rayleigh numbers ($10^4 - 10^6$). The Rayleigh numbers for the current experimental results were in the order of 10^5.

Figure 6.7 shows the flow regime map of Metais and Eckert (1964) with the enhanced tube and smooth tube data. This figure shows that the potential for mixed convection for the enhanced tubes are roughly the same as the smooth tubes. Thus, the only explanation for the lower performance is that the fins partially obstruct the flow path for secondary flows. Note, though, that the mixed convection potential for the 19.02 mm tubes are greater than for the 15.88 mm tubes. This is reflected in the laminar heat transfer results.

What is further noted from this graph is the lower values of $GrPr$ for the enhanced tubes in the turbulent region. This shows that the fins aid in the mixing of the fluid, and subsequently the breaking of the laminar viscous sub-layer. This is especially true after transition, as the mixed convection potential decreases for Reynolds numbers greater than the transition Reynolds numbers.

Transition from laminar to turbulent flow for the enhanced tubes appear to occur at the same Reynolds numbers as for the smooth tube. This is odd as transition for adiabatic flow was clearly at lower Reynolds numbers. Figure 6.8, however, shows the fluctuations in heat transfer coefficients for the fully developed smooth and enhanced tubes. As was the case for the smooth tubes and all its different inlets tested, the enhanced tubes do not seem to differ with regard to the start and end of transition. Transition starts and ends at a Reynolds number of 2 000 and 3 000, respectively. It appears that roughness during heat transfer has little or no effect on the transition region. The only noticeable difference is in the percentage of fluctuation, although this difference is between the two diameter tubes and not between the smooth and enhanced tubes.

6.3.1 Diabatic Friction Factors

The diabatic friction factors for the fully developed enhanced tubes are given in Figure 6.9. Included are the friction factors for the fully developed diabatic smooth tubes. For reference purposes, the laminar Poiseuille relation is included as well as the turbulent flow correlation of Allen and Eckert (1964).

These results show that there is an overall increase in friction factor for the enhanced tubes compared with the smooth tubes. The turbulent results are very similar to those of the adiabatic friction factors, also having the same secondary transition region between a Reynolds number of 3 000 and 10 000. These trends are also similar to the heat transfer results.

Enhanced tube diabatic friction factors in the laminar regime show that there is an increase in friction factors when compared with their adiabatic counterparts. These results are in line

with the smooth tube results, with this increase being attributed to the secondary flow effects. The diabatic friction factors for the enhanced tubes, though, appear to be even-higher than those found for the smooth tubes. Since the cause for the increase in friction factor for the smooth tubes was due to the secondary flow, it can be concluded that for the enhanced tubes the fins add to the extra increase. However, there appears to be a difference between the different helix angles, as well, with the 27° tubes showing the greatest increase.

A reason for this increase could be related to the secondary flows and the fins. From the heat transfer results it was shown that the fins act negatively towards the heat transfer process in the laminar regime. It could be further argued that the fins act as a barrier for secondary flow, preventing the bulk of the fluid to mix with fluid at the tube wall. This could have the effect that the relatively unmixed liquid between the fins to be at a cooler temperature than the rest of the fluid, thus having a higher viscosity and hence greater shear stress.

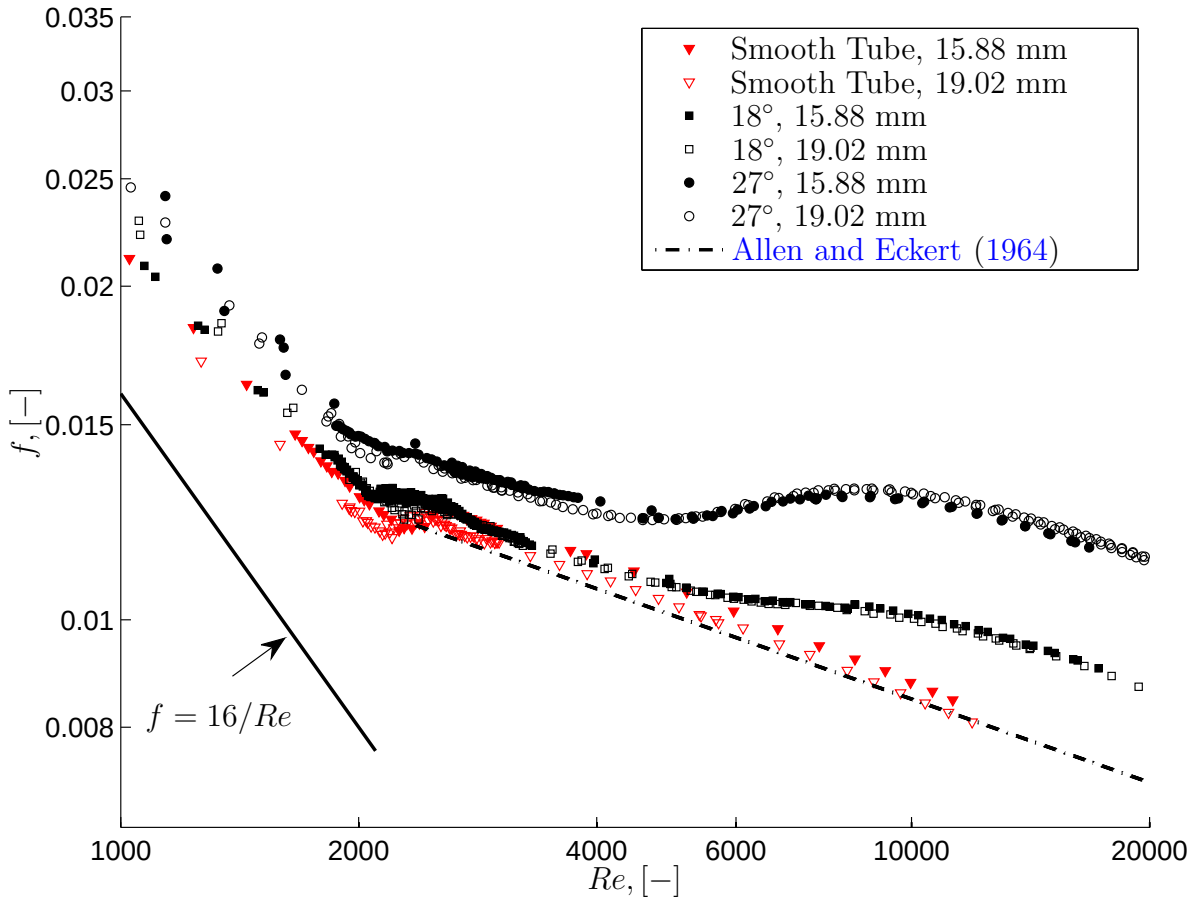

Figure 6.9 Fully developed diabatic friction factors for the smooth and enhanced tubes.

Transition for the enhanced tubes is also in the same region as those for their smooth tube counterparts, being between Reynolds numbers of 2 000 and 3 000. Figure 6.10 shows the fluctuations of the friction factors and heat transfer coefficient as a function of the Reynolds number. This figure shows that the fluctuations regarding friction and heat transfer are coupled. Thus, by means of two independent measuring techniques, transition occurs between a Reynolds number of 2 000 and 3 000, unlike the adiabatic results where transition for the enhanced tubes occurred at a lower Reynolds number of approximately 1 800.

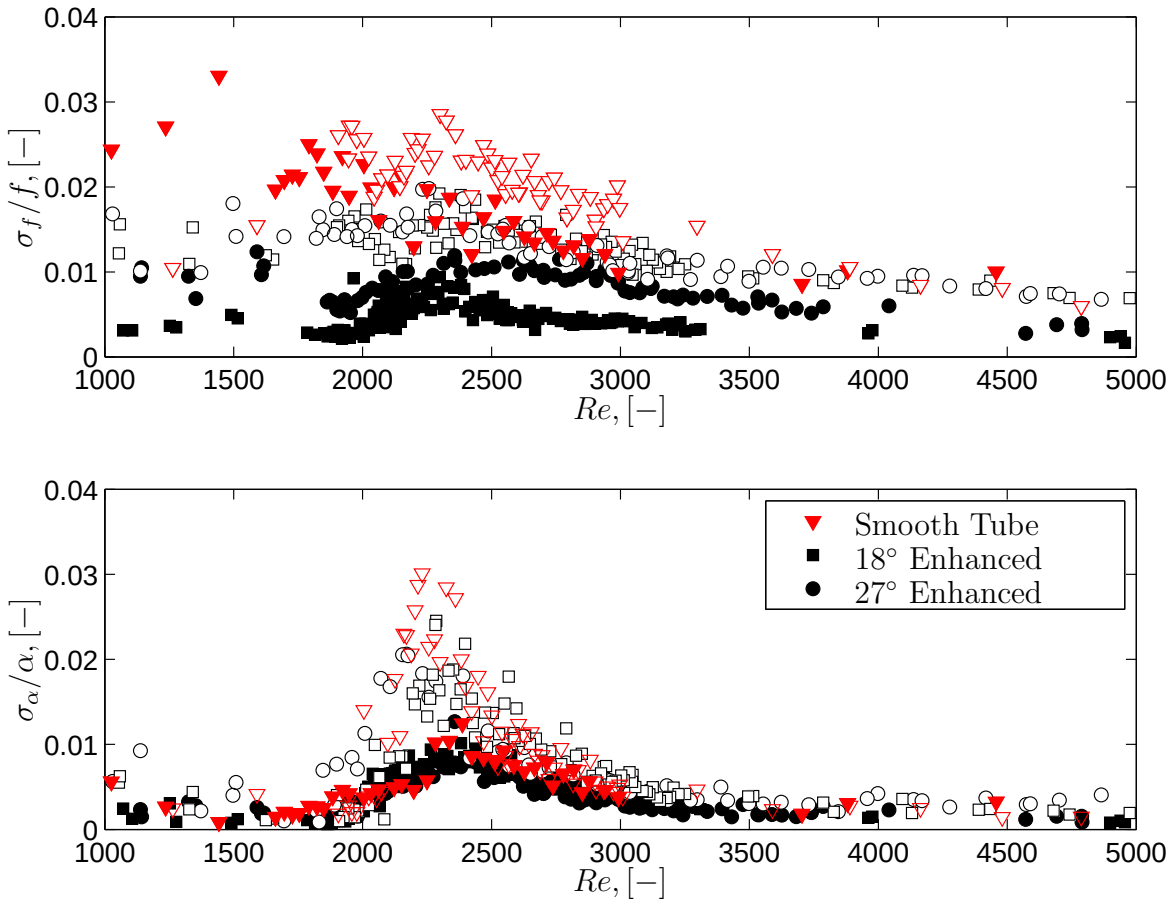

Figure 6.10 Fully developed diabatic friction factor and heat transfer coefficient fluctuations for the enhanced tubes. Solid markers are for the 15.88 mm tubes while the empty markers are for the 19.02 mm tubes.

6.3.2 Correlation comparison

Three turbulent heat transfer correlations relating to enhanced tubes are compared and are listed in Table 6.2. Figure 6.11 shows the performance of these correlations against the experimental heat transfer data.

Table 6.2 Heat transfer correlations for enhanced tubes.

Carnavos (1980)

$$Nu_e = 0.023 Re^{0.8} Pr^{0.4} \left(A_c/A_{cn}\right)^{0.1} \left(A_n/A_i\right)^{0.5} \left(\sec\beta\right)^3 \tag{6.18}$$

$$0 < \beta < 30°,\ 10\ 000 < Re < 100\ 000,\ 0.7 < Pr < 30$$

Ravigururajan and Bergles (1996)

$$Nu_e = Nu_s \left\{1 + \left[2.64 Re^{0.036} \left(e/D\right)^{0.212} \left(p_f/D\right)^{-0.21} \left(\beta/90\right)^{0.29} Pr^{0.024}\right]^7\right\}^{1/7} \tag{6.19}$$

$$0.01 < e/D < 0.2,\ 0.1 < p_f/D < 7.0$$
$$0.3 < \beta/90 < 1.0,\ 5\ 000 < Re < 250\ 000$$
$$0.66 < Pr < 37.6$$

Jensen and Vlakancic (1999)

$$Nu_e = Nu_s \left(l_c/D\right)^{-0.5} \left(A_{cn}/A_c\right)^{0.8} F \tag{6.20}$$

$$F = \left(A_i/A_n\right)^{0.29} \left[1 - 1.792 \left(n \sin\left(\beta/\pi\right)\right)^{0.64} \left(2e/D\right)^{2.76} Re^{0.27}\right]$$
$$l_c/D = A_{core}/A_c \left(1 - 2e/D\right) + A_{fin}/A_c \left[\pi/n \left(1 - 2e/D\right) - s/D\right]$$
$$s = 4/3e \tan\left(\gamma/2\right) = \text{ average width of triangular fin}$$

$$2\ 000 < Re < 80\ 000,\ \ Pr \approx 7$$
$$0 < \beta < 45°,\ \ 0.0075 < e/D < 0.05$$

The figure shows that the data deviates from all the correlations at a Reynolds number below approximately 8 000. Above a Reynolds number of 8 000, the Carnavos (1980) correlation predicts the 18° tubes with good accuracy, while underpredicting the 27° tubes. The Ravigururajan and Bergles (1996) correlation overpredicts all the data although it seems to predict the 18° and 27° tubes with the same accuracy. The Jensen and Vlakancic (1999) correlation underpredicts all the data with the prediction of the 27° tubes being the worst.

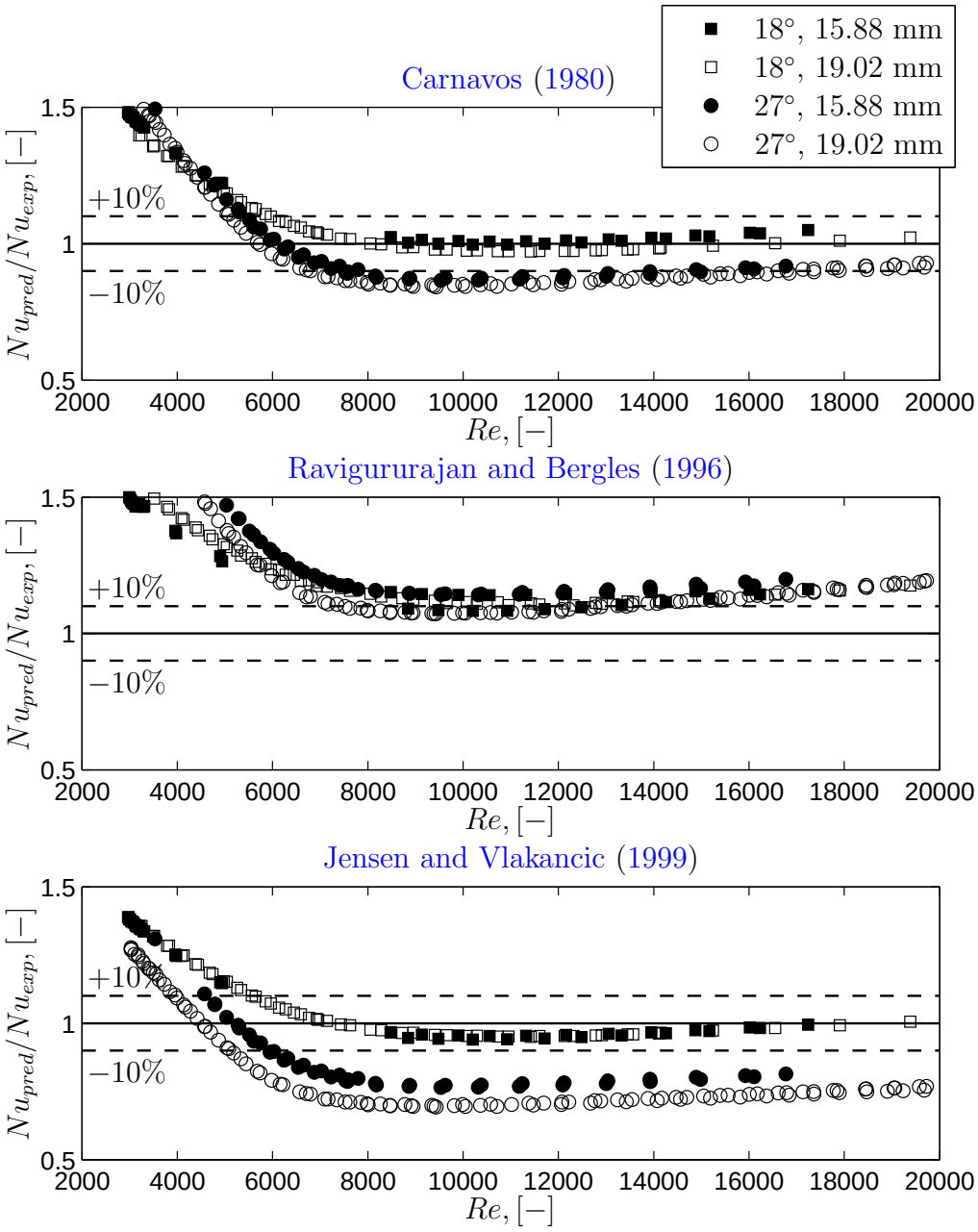

Figure 6.11 Performance of the correlations listed in Table 6.2 against the experimental heat transfer data for the four enhanced tubes.

The Carnavos (1980) correlation predicts the data on average to within 3.5% with an rms deviation of 21% and a maximum deviation of 55%. The Ravigururajan and Bergles (1996) correlation predicts the data on average to within 23% with an rms deviation of 30% and a maximum of 85%, while the correlation of Jensen and Vlakancic (1999) predicts the data on average to within 8% with an rms deviation of 23% and a maximum of 39%.

This is a pessimistic review of the results, since all the data deviate from the correlations at a Reynolds number below 8 000. By only considering data above a Reynolds number of 8 000, the correlation of Carnavos (1980) predicts the data on average to within 8% with an rms deviation of 11%, deviating from the data at a maximum by 18%. The corresponding values for the Ravigururajan and Bergles (1996) correlation are 11%, 12% and 19%, while those of the Jensen and Vlakancic (1999) correlation are 18%, 22% and 32%.

6.3.3 Heat Transfer Correlation Development

From the above comparison it is clear that a new correlation would need to be developed to satisfactorily predict the entire Reynolds number range. Unfortunately, unlike for the smooth tube, there does not seem to be an easy relationship between heat transfer and friction factor in the sense of a Reynolds analogy-type prediction. It was therefore decided that separate correlations for heat transfer and friction factor need to be developed. Heat transfer correlations will first be developed followed by the friction factor correlations.

Laminar regime

From the results reported, it was postulated that the degradation in laminar heat transfer was due to the fins preventing/obstructing much of the secondary flow, which normally aids in the better mixing of the fluid. This can be graphically explained by looking at Figure 6.12, which is a depiction (exaggerated) of the secondary flow patterns inside a smooth tube and an enhanced tube having similar root diameters.

Since only the fin height would obstruct the secondary flow (no difference in results for different helix angles), the correlation developed for laminar flow inside smooth tubes, Equation (4.13), could be used to predict the enhanced tube data. This correlation predicts the enhanced tube data on average to within 3.7% with an average rms deviation of less than 4%. This is improved, though, by including the fin height-to-diameter ratio in the mixed convection term. The correlation for enhanced tube laminar heat transfer then becomes

$$Nu_{Le} = 2.686 \left[Re^{0.105} Pr^{1.133} \left(\frac{D}{L}\right)^{0.483} + 1.082 \left(Gr^{0.362} Pr^{-2.987} \left(\frac{L}{D}\right)^{0.202} \left(\frac{e}{D}\right)^{0.0612} \right)^{0.277} \right]^{2.226} \left(\frac{\mu}{\mu_w}\right)^{0.152} \tag{6.24}$$

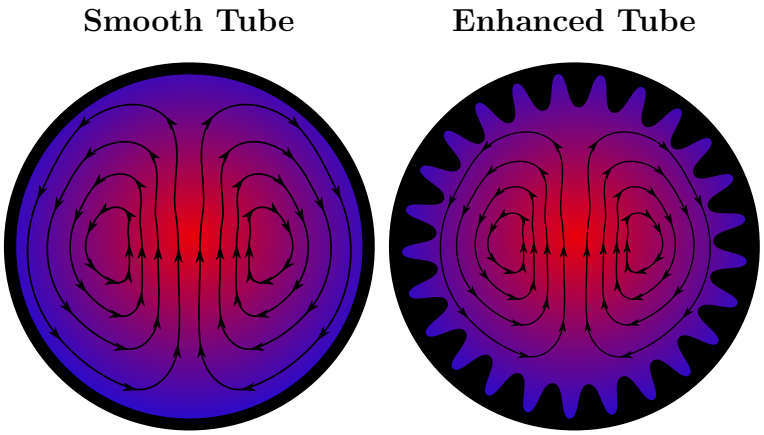

Figure 6.12 Illustration of secondary flow patterns inside a smooth tube and an enhanced tube of equivalent root diameters.

The addition of this ratio improves the correlation to predict the data on average to within 1% with an average rms deviation of 1.8%. This is shown graphically in Figure 6.13. This correlation is valid for

$$\begin{aligned} 1\ 030 < &Re < 2\ 198 \\ 4.58 < &Pr < 5.67 \\ 1.4 \times 10^5 < &Gr < 2.5 \times 10^5 \\ 0.7 < &\mu/\mu_w < 0.847 \\ 0.023 < &e/D < 0.027 \\ 286 < &L/D < 349 \end{aligned}$$

Turbulent regime

It was seen from Section 6.3.2 that the correlation of Carnavos (1980) and Ravigururajan and Bergles (1996) predict the data with fair accuracy at Reynolds numbers greater than 8 000. It will thus be attempted to develop a correlation for Reynolds numbers 3 500 to 8 000.

Some of the parameters that will have an influence in this region will be the helix angle, fin pitch and roughness height. Thus, the correlation would be a function of fluid properties and tube geometrical properties,

$$Nu_{Te38} = f\left(Re,\ Pr,\ e,\ D,\ p,\ \beta\right) \tag{6.25}$$

It is proposed that the correlation have the form

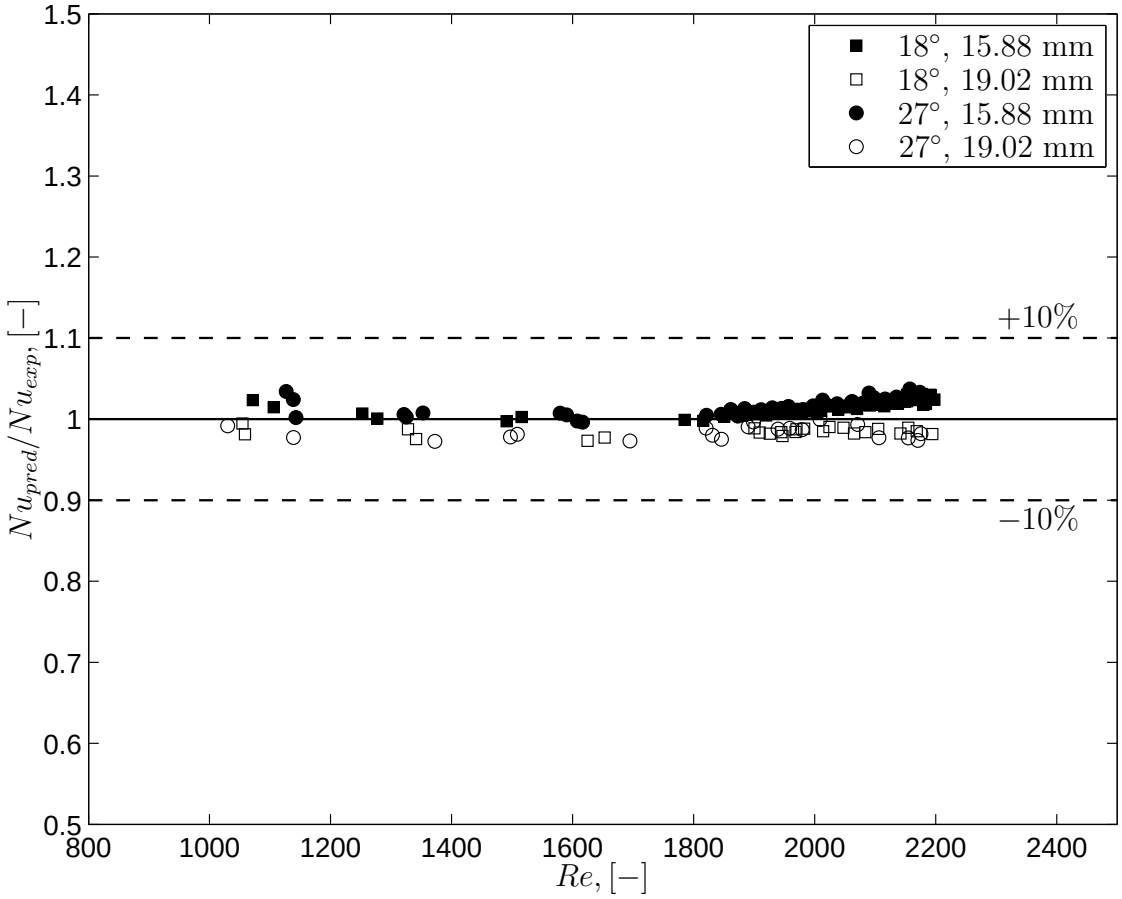

Figure 6.13 Performance of Equation (6.24) against the enhanced tube experimental laminar heat transfer data.

$$Nu_{Te_{38}} = c_1 Re^{c_2} Pr^{c_3} \left(\frac{e}{D}\right)^{c_4} \left(\frac{p}{D}\right)^{c_5} \left(\frac{\beta}{90}\right)^{c_6} \tag{6.26}$$

By using a least squares optimisation, the constants were found with the final correlation being

$$Nu_{Te_{38}} = 0.35 Re^{1.33} Pr^{1.19} \left(\frac{e}{D}\right)^{-0.11} \left(\frac{p}{D}\right)^{2} \left(\frac{\beta}{90}\right)^{4.4} \tag{6.27}$$

for

$$\begin{aligned} 3\ 500 \leq & Re \leq 8\ 000 \\ 4.5 \leq & Pr \leq 5.4 \\ 18^\circ \leq & \beta \leq 27^\circ \\ 0.176 \leq & p/D \leq 0.387 \\ 0.023 \leq & e/D \leq 0.027 \end{aligned}$$

It should be noted that the relative roughness for the current tubes varied very little and that the value of it's constant should be seen as tentative. This correlation predicted all the data on average to within 3% with an rms deviation of 4.4%.

Transition regime

Since it was shown that transition follows a smooth path between laminar and turbulent flow with increasing Reynolds numbers, it would be best to combine the newly developed laminar and turbulent correlations to form a new, transition correlation. This is done by following the approach of Churchill and Usagi (1972). The transition Reynolds number will then have the form

$$Nu_{te} = \left[Nu_{Le}^a + Nu_{Te_{38}}^a\right]^{1/a} \tag{6.28}$$

Since transition during the heat transfer process occurred between Reynolds numbers of 2 000 and 3 000, to extend the range of validity for this correlation, it was decided to use data for Reynolds numbers between 1 900 and 4 000. The best value for the constant to fit all the data was 7. Thus, the enhanced tube transition region heat transfer correlation is given as

$$Nu_{te} = \left[Nu_{Le}^7 + Nu_{Te_{38}}^7\right]^{1/7} \tag{6.29}$$

for

$$\begin{aligned} 1\ 900 \leq & Re \leq 4\ 000 \\ 4.5 \leq & Pr \leq 5.4 \\ 2.62 \times 10^5 \leq & Gr \leq 4.45 \times 10^5 \\ 0.686 \leq & \mu/\mu_w \leq 0.804 \\ 286 \leq & L/D \leq 349 \\ 18^\circ \leq & \beta \leq 27^\circ \\ 0.176 \leq & p/D \leq 0.387 \\ 0.023 \leq & e/D \leq 0.027 \end{aligned}$$

This correlation predicted the transition data on average to within 1% with an rms deviation of less than 3.5%. A comparison between the correlation and experimental data is shown in Figure 6.14.

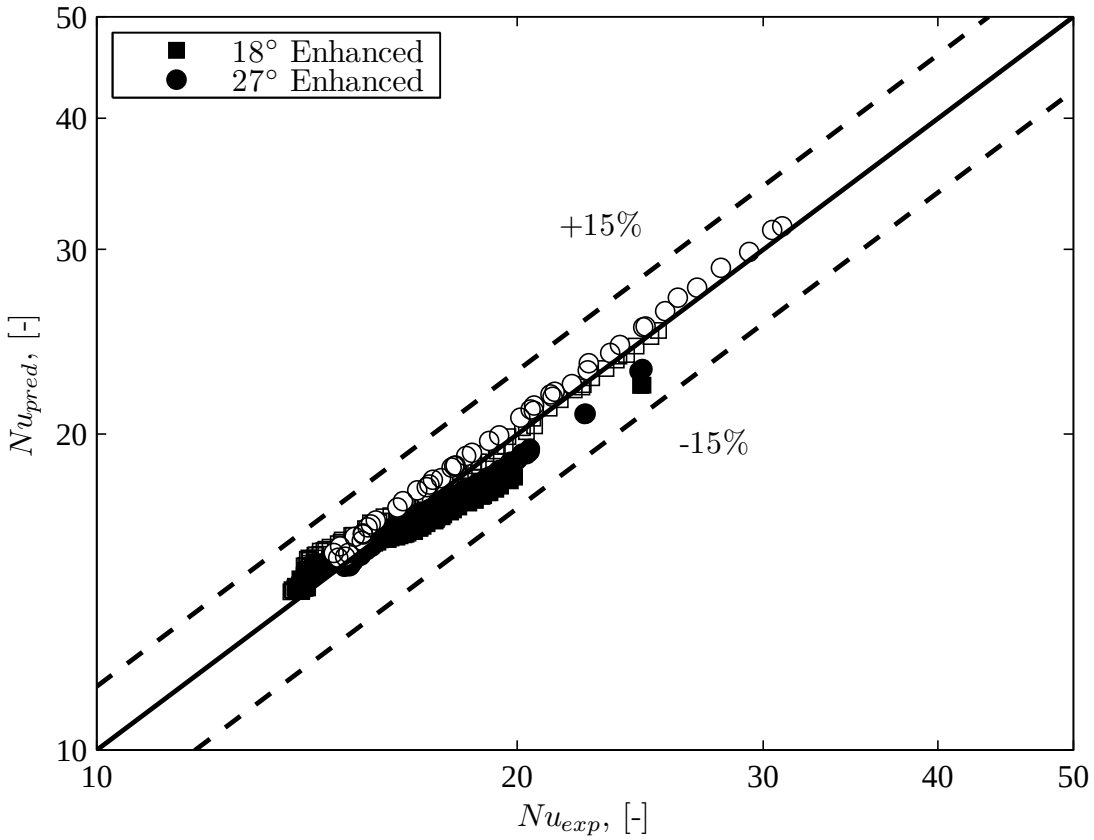

Figure 6.14 Comparison of experimental enhanced tube Nusselt numbers in the transition flow regime against Equation (6.29). Solid markers: 15.88 mm tubes, empty markers: 19.02 mm tubes.

6.3.4 Diabatic Friction Factor Correlation Development

Although it appears that transition from laminar to turbulent flow occurs smoothly, on closer inspection it can actually be seen that the slope in this region almost becomes independent of Reynolds number (*viz* Figure 6.15). Further, laminar results are also slightly higher than their smooth tube counterparts. For turbulent flow, it should be noticed that the correlation of Jensen and Vlakancic (1999) was developed for isothermal flow. It was found that this correlation, by including the viscosity ratio, predicted the data with fair accuracy above a Reynolds number of 7 000. Below this value, however, the correlation deviates from the data. It is thus necessary to modify this correlation to incorporate the effects of heat transfer at the lower turbulent Reynolds numbers.

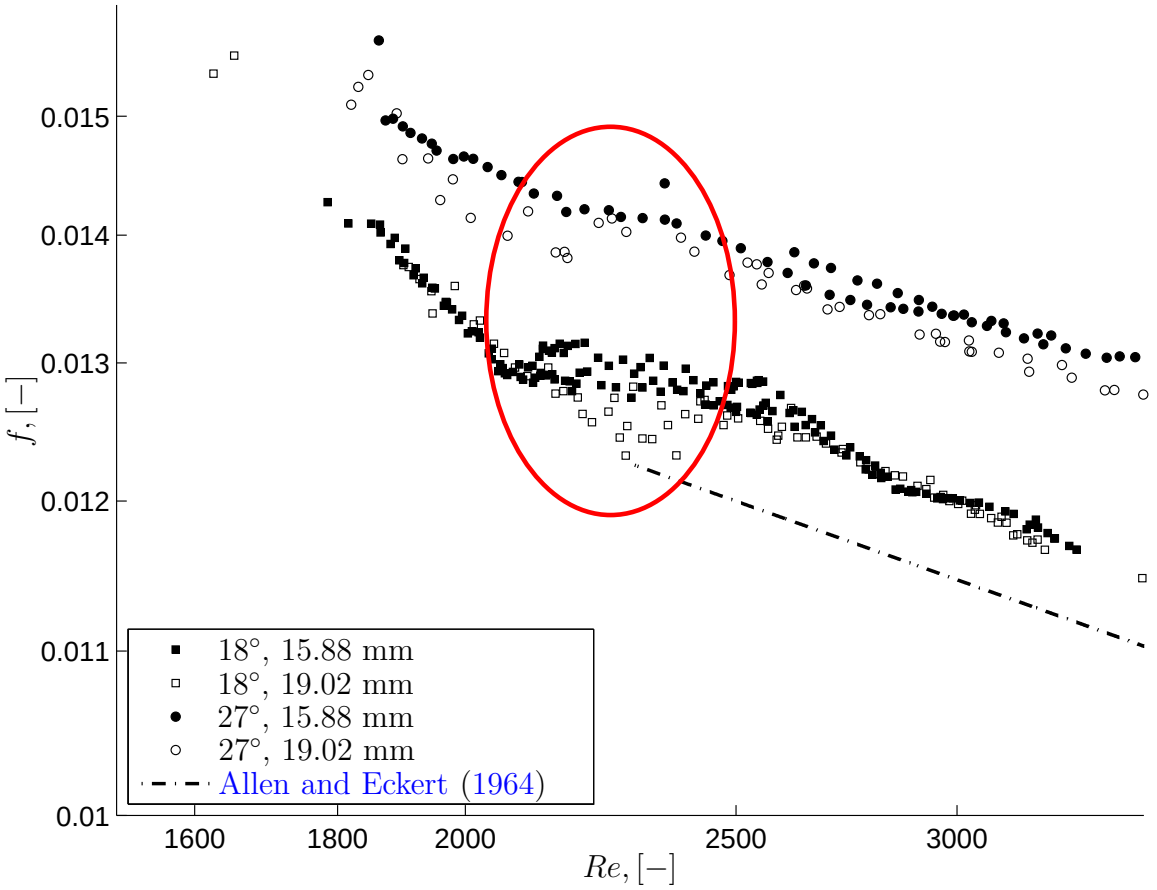

Figure 6.15 Transition diabatic friction factors.

Laminar regime

From the diabatic smooth tube results in Chapter 4, it was concluded that the increase in laminar friction factors was due to the secondary flow effects. It was shown that for enhanced tubes, however, additional friction is generated due to the helix angle. From Section 6.2, it was shown that the adiabatic friction factor increase was only due to the fin height, and Equation (6.3) was developed. For the diabatic situation, however, additional terms would need to be added to incorporate the effect of mixed convection and secondary flows.

A proposed correlation would be to make use of the enhanced tube adiabatic correlation, Equation (6.3), and to add the necessary terms describing mixed convection. Included in this mixed convection term, however, the effects of the tube enhancement would need to be added. From the results, the only geometrical aspect of the enhanced tubes which had an effect on the friction factor was the helix angle. Thus, the form of the correlation would be

$$f_{Le} = \frac{16}{Re}\left[1 + 88\,(e/D)^{2.2}\,Re^{0.2} + Gr^{c1}Pr^{c2}\left(\frac{D}{L}\right)^{c3}(\sin\beta)^{c4}\right] \tag{6.30}$$

Using the method of least squares, the constants, c_1, c_2, c_3 and c_4, were determined to be 0.49, -0.98, 0.71 and 1.04, respectively. These constants were obtained with a least squares coefficient of 0.987. Thus, the final diabatic laminar friction factor correlation for enhanced tubes is given by

$$f_{Le} = \frac{16}{Re}\left[1 + 88\,(e/D)^{2.2}\,Re^{0.2} + Gr^{0.49}Pr^{-0.98}\left(\frac{D}{L}\right)^{0.71}(\sin\beta)^{1.04}\right] \tag{6.31}$$

$$\begin{aligned} 1\,030 < &Re < 2\,198 \\ 4.58 < &Pr < 5.67 \\ 1.4 \times 10^5 < &Gr < 2.5 \times 10^5 \\ 0.7 < &\mu/\mu_w < 0.847 \\ 0.023 < &e/D < 0.027 \\ 18^\circ < &\beta < 27^\circ \\ 286 < &L/D < 349 \end{aligned}$$

This correlation predicts the laminar data, consisting of 86 data points, on average to within 2% with an average rms deviation of 2.8%. The correlation deviated from the data by a maximum of 6.7%.

Lower turbulent regime

The lower turbulent regime will be defined as Reynolds numbers between 2 500 and 7 000. Since the correlation of Jensen and Vlakancic (1999) predicted the adiabatic friction factors very well, it was decided to make use of this correlation and add the necessary terms describing heat transfer. At the lower Reynolds numbers, one of the parameters which might still have an effect is the Grashof number. This is due to the secondary flow which might still be present in this region. A second parameter pertaining to fluid properties which has an influence in heat transfer is the Prandtl number. Further, to incorporate the effects between the wall and the bulk of the fluid, the viscosity ratio will also be included.

By making use of Equation 6.6 the main basis of the correlation would become

$$\begin{aligned} f_e/f_s = &\left[(l_{csw}/D)^{c_1}\,(A_{cn}/A_c)^{c_2} - 0.0151/f_s\left[(l_{csw}/D)^{c_1}\,(A_{cn}/A_c)^{c_2} - 1\right]e^{-Re/c_3}\right] \times \\ &Pr^{c_4}Gr^{c_5}\left(\frac{\mu}{\mu_w}\right)^{c_6} \end{aligned} \tag{6.32}$$

The definition of the characteristic length scale and nominal cross-sectional area will remain unchanged, and is given in Table 6.1. By a method of least squares the constants were determined such that the new correlation becomes

$$f_{Tle}/f_s = \left[(l_{csw}/D)^{-2.2}\,(A_{cn}/A_c)^{-46} - 0.0151/f_s\left[(l_{csw}/D)^{-2.2}\,(A_{cn}/A_c)^{-46} - 1\right]e^{-Re/5428}\right] \times Pr^{0.55}Gr^{-0.09}\left(\frac{\mu}{\mu_w}\right)^{-1.2} \tag{6.33}$$

being valid for

$$\begin{aligned} 2\ 500 < &Re < 6\ 956 \\ 4.47 < &Pr < 5.39 \\ 1.63 \times 10^5 < &Gr < 4.45 \times 10^5 \\ 0.69 < &\mu/\mu_w < 0.84 \\ 0.023 < &e/D < 0.027 \\ 18^\circ < &\beta < 27^\circ \\ 286 < &L/D < 349 \end{aligned}$$

This correlation predicted the data, on average to within 1% with an average rms deviation of less than 2%.

Transition regime

From the discussion in the introduction to this section, it was shown that the friction factors in the transition region were nearly independent of the Reynolds number. The fact that the slope in the transition changes would justify for a correlation to be developed in this region. Since the adiabatic enhanced tube friction factor has already been developed, this correlation can be modified for diabatic flow. Thus, the correlation will have the form

$$f_{te} = \left(\frac{16}{Re_{Cr}}\right)^{c_1} exp\left(c_2\frac{Re}{Re_{Cr}}\right)\left(\frac{\beta}{90}\right)^{c_3}\left(\frac{e^2}{pD}\right)^{c_4}\left(\frac{p}{D}\right)^{c_5}\left(\frac{e}{D}\right)^{c_6} Pr.^{c_7}Gr^{c_8}\left(\frac{\mu}{\mu_w}\right)^{c_9} \tag{6.34}$$

In this case, the critical Reynolds number was the same for all the tubes, having a value determined by Equation (6.14). Data were taken for Reynolds numbers greater than 2 100 and less than 2 600. The constants were determined by a least squares optimisation method. The correlation predicted the transition data on average to within 0.5% with an rms deviation of 1%. The final correlation is given as

$$f_{te} = \left(\frac{16}{Re_{Cr}}\right)^{-0.131} exp\left(-0.111\frac{Re}{Re_{Cr}}\right)\left(\frac{\beta}{90}\right)^{2.363}\left(\frac{e^2}{pD}\right)^{-0.313}\left(\frac{p}{D}\right)^{0.766}\times \left(\frac{e}{D}\right)^{0.786} Pr.^{0.081} Gr^{0.028}\left(\frac{\mu}{\mu_w}\right)^{-0.289} \tag{6.35}$$

valid for

$$\begin{aligned} 2\ 105 < &Re < 2\ 596 \\ 4.47 < &Pr < 5.33 \\ 2.8 \times 10^5 < &Gr < 4.5 \times 10^5 \\ 0.69 < &\mu/\mu_w < 0.8 \\ 0.023 < &e/D < 0.027 \\ 18^\circ < &\beta < 27^\circ \\ 286 < &L/D < 349 \end{aligned}$$

To summarise, Equations (6.31), (6.33) and (6.35) are compared to the experimental values and are shown in Figure 6.16. For all the values, the correlations predict the data on average to within 1% with an rms of less than 2%.

6.4 Performance Evaluation

The discussion of enhanced tubes would be incomplete if performance comparisons were not made. These comparisons relate to the amount of enhancement gained (if any) by employing an enhanced tube instead of a regular smooth tube. Bergles *et al.* (1974) and Webb (1981) list the different criteria which can be used for comparison. Although many such criteria have been done, none were performed to include the transition flow regime.

Four of these criteria will be investigated. The first two are concerned with the increase in heat duty, the third with reduction in pumping power, while the fourth looks at the reduction in exchanger size. Information pertaining to these four criteria should give the designer an idea of the performance of these tubes.

The first criterion is to determine the amount of heat transfer enhancement gained by using an enhanced tube instead of a smooth tube if the geometry of the exchanger were to remain fixed (i.e. tube length and diameter are the same) and the pressure drop remains the same. This is the criterion, $R_2 = \alpha_e/\alpha_s$, as defined by Bergles *et al.* (1974). This ratio can only be obtained if the correct smooth tube Reynolds number is used, which will give the same amount of pressure drop as the enhanced tube. Since the pressure drops between the two tubes are to be equal, the following holds:

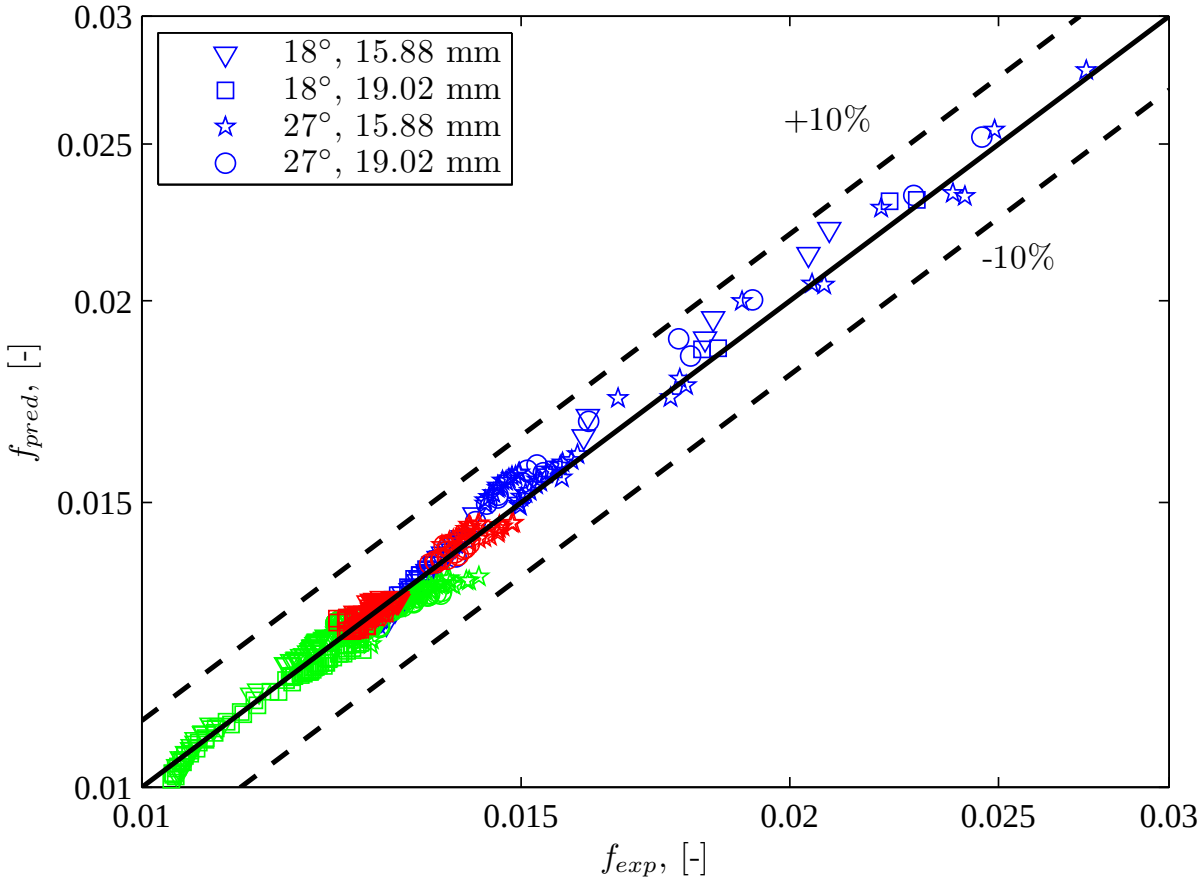

Figure 6.16 Comparison of the newly developed correlations for the (blue) laminar regime, (red) transition regime and (green) turbulent regime.

$$\Delta p = f\frac{\rho u^2 L_{\Delta p}}{2D} = \text{const} \tag{6.36}$$

Since the geometry is fixed and it is assumed that the fluid properties will remain more or less the same for the two tubes, the equation becomes

$$f_e u_e^2 = f_s u_s^2 \tag{6.37}$$

$$f_e Re_e^2 = f_s Re_s^2 \tag{6.38}$$

$$\therefore Re_s = \left(\frac{f_e}{f_s} Re_e^2\right)^{0.5} \tag{6.39}$$

This shows that for a given enhanced tube Reynolds number (and hence an enhanced tube friction factor), the equivalent smooth tube Reynolds number that will give the same amount

of pressure drop can be obtained if an appropriate smooth tube friction factor correlation is used. The obvious choice for a smooth tube friction factor would be that developed in Chapter 4, Equation (4.10) and (4.18). Since the performance criterion is in terms of the heat transfer process, it would be incorrect to use the adiabatic friction factors for comparison.

The problem with using the friction factor correlation is that Equation (6.39) becomes implicit. By using an iterative process, though, a solution can be obtained. With the enhanced tube and equivalent smooth tube Reynolds numbers known, the corresponding heat transfer coefficients (or Nusselt numbers) can be obtained, from which the performance criterion can be made.

Figure 6.17 gives the performance of all the enhanced tubes for a fixed geometry and constant pressure drop. According to these results, enhanced tubes only become viable above a smooth tube Reynolds number of approximately 4 500, if the requirement of constant pressure drop were enforced. The maximum performance will be gained at a smooth tube Reynolds number of approximately 9 500. Above this value the performance starts to deteriorate.

Further, the 27° enhanced tubes give the greatest performance increase, with maximums ranging from 54% to 64% heat transfer increase above that of smooth tubes. The 18° tubes only have a maximum of 23 - 28% increase in heat transfer coefficient. It appears, though, that the better performance is obtained for the greater of the two diameter tubes. It is also further noted that no advantage is gained in the transition and laminar region.

The next performance criterion would be used if the pumping power and basic geometry were to remain the same. This is often the case where heat transfer enhancement is required without the penalty of having to replace a pump currently being used for a smooth tube exchanger. This criterion is given by Bergles *et al.* (1974) as $R_3 = \alpha_e/\alpha_s$, and for constant pumping power

$$P_p = N_t u A f \frac{\rho u^2 L_{\Delta p}}{2D} = \text{const} \tag{6.40}$$

Once again, to make a direct comparison between enhanced and smooth tubes using this criterion, an appropriate smooth tube Reynolds number needs to be determined. Thus, from the equation for pumping power above, it can be shown that

$$Re_s = \left(\frac{A_{ce} f_e Re_e^3}{A_{cs} f_s} \right)^{1/3} \tag{6.41}$$

Using Equation (4.10) and (4.18) for the smooth tube friction factor, the equivalent smooth tube Reynolds number can be obtained in an iterative manner. This equivalent Reynolds number is then to be used to obtain the corresponding heat transfer coefficient and criterion R_3 can be determined. The performance of the four enhanced tubes is shown in Figure 6.18.

For the same pumping power and geometry, enhanced tubes only become viable above a smooth tube Reynolds number of about 4 000. With this criterion, though, the maximum increase in heat transfer coefficient is 25 - 29% for the 18° tubes and 62% - 69% for the 27° tubes. This maximum increase also only occurs if the smooth tube which is going to be replaced were

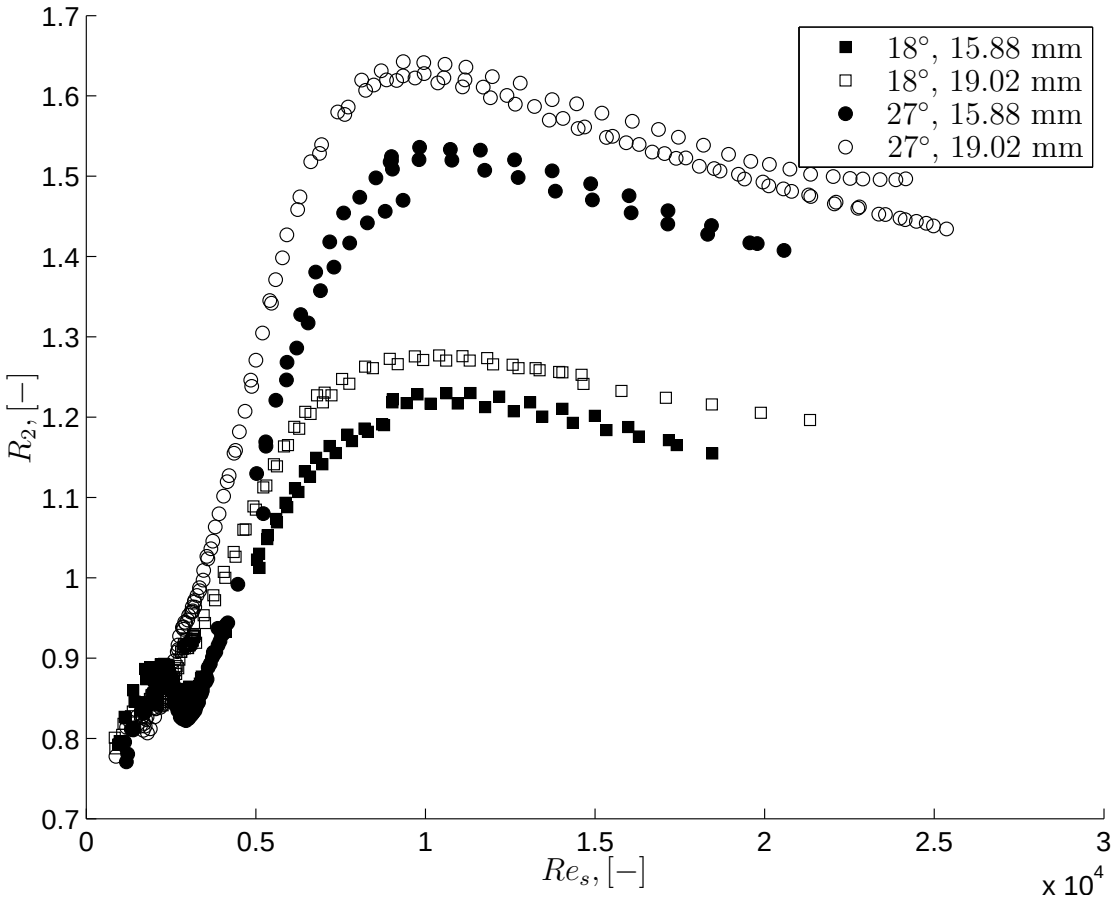

Figure 6.17 Performance of the enhanced tubes compared with the smooth tube according to criteria R_2.

operating at a Reynolds number of approximately 10 000 for the 18° tubes and 9 000 for the 27° tubes. Performance slowly starts to decrease for higher Reynolds numbers. Once again, no advantage can be taken in the laminar and transition region.

The next criterion can be used if the requirements were to reduce the pumping power by maintaining the amount of heat being transferred and keeping the geometry fixed. This criterion is given by Bergles *et al.* (1974) as $R_4 = P_{pe}/P_{ps}$. Thus, the smaller R_4, the less pumping power is required. This requires, though, that for a given enhanced tube heat transfer coefficient, the equivalent smooth tube Reynolds number having the same heat transfer coefficient be determined. With the equivalent smooth tube Reynolds number obtained, the corresponding smooth tube friction factor can be determined. Criterion R_4 can be written as

$$R_4 = \frac{P_{pe}}{P_{ps}} = \frac{f_e Re_e^3 A_{ce}}{f_s Re_s^3 A_{cs}} \tag{6.42}$$

Figure 6.19 shows the reduction in pumping power for a fixed heat transfer rate and geometry. The greatest reduction is achieved for the 27° enhanced tubes at a Reynolds number of approximately 9 000. This reduction is in the order of 85%. The 18° enhanced tube has a reduction of approximately 59% at a Reynolds number of 10 000. The reason for the large increase in R_4 in the laminar regime is that the enhanced tube heat transfer results being lower than those of the smooth tube.

The final criterion is concerned with the reduction in exchanger size with regard to its length (the diameter remains unchanged) if it is required that the heat duty as well as the pumping power remain the same. This criterion is given as $R_5 = A_e/A_s$, as defined by Bergles *et al.*

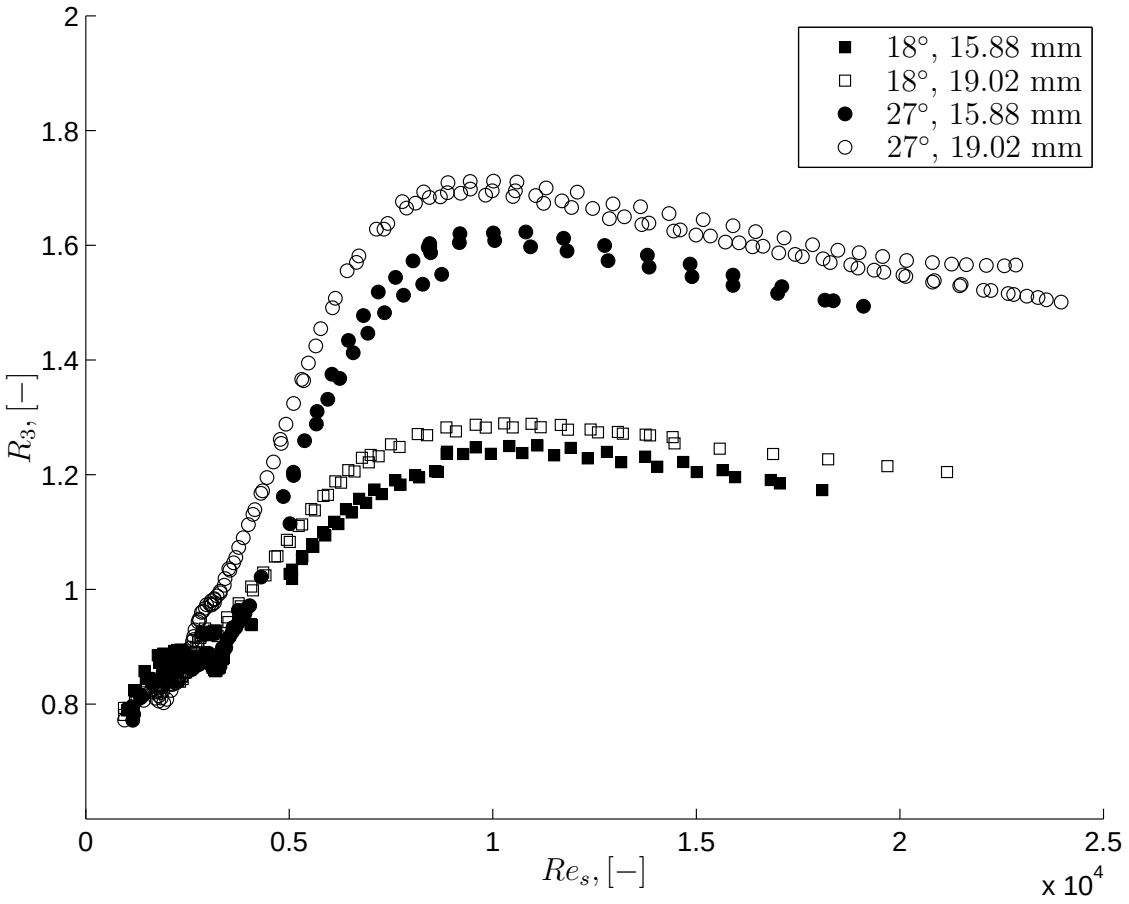

Figure 6.18 Performance of the enhanced tubes compared with the smooth tube according to criteria R_3.

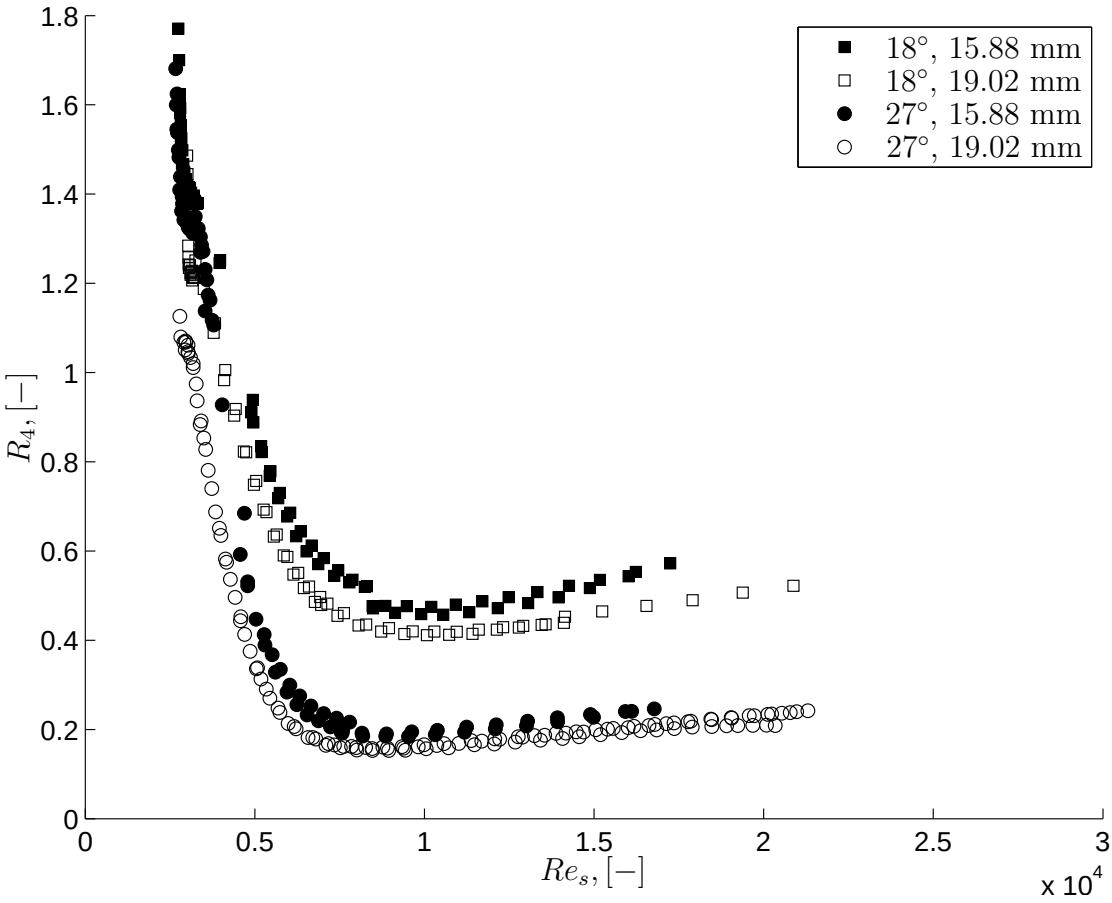

Figure 6.19 Performance of the enhanced tubes compared with the smooth tube according to criteria R_4.

(1974). With constant pumping power and constant heat duty, it can be shown that

$$\frac{A_e}{A_s} = \frac{f_s Re_s^3}{f_e Re_e^3} = \frac{Nu_s}{Nu_e} \tag{6.43}$$

Thus, the equivalent smooth tube Reynolds number can then be obtained by

$$Re_s = \left(\frac{f_e Nu_s Re_e^3}{f_s Nu_e} \right)^{1/3} \tag{6.44}$$

Figure 6.20 shows the results for the area reduction when using an enhanced tube instead of a smooth tube. The maximum with which the surface area, and hence length of the tubes, can be reduced is in the order of 30% for the 18° tubes and 53% for the 27° tubes. This is also obtained at a Reynolds number of approximately 9 000 and 7 500, respectively.

One thing that follows from all the above criteria is that the maximum performance for all the enhanced tubes is in more or less the same smooth tube Reynolds number region. From the transition region up to the Reynolds numbers where these maximum values are, a sharp increase in performance is observed. This increase is in the region where the secondary transition resides. Further increases in Reynolds number show a steady decrease in performance, although higher Reynolds number data is required to make any conclusions regarding this trend.

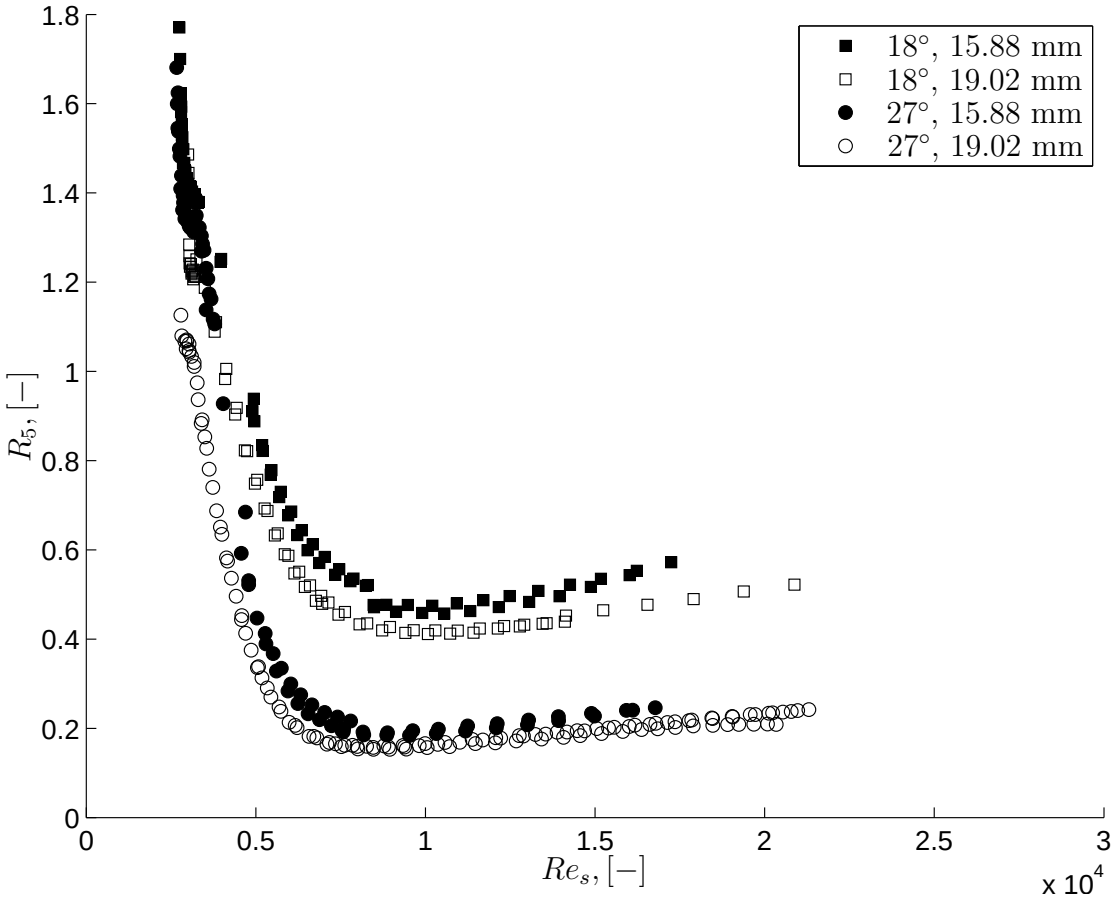

Figure 6.20 Performance of the enhanced tubes compared with the smooth tube according to criteria R_5.

6.5 Conclusion

Adiabatic friction factor and heat transfer results were presented for four enhanced tubes with a fully developed inlet profile. All four tubes exhibited an increase in turbulent friction factors

as well as heat transfer coefficients. In the laminar regime, however, heat transfer coefficients were lower than those of their smooth tube counterparts. The reason is that the fins obstruct or even diminish the secondary flow, which increases the mixing of the fluid, inside the tube. Laminar friction factors were, on the other hand, slightly higher than obtained for the smooth tubes due to the increase in surface roughness. Transition for the enhanced tubes commenced at a slightly lower Reynolds number. It was shown, though, that transition was only influenced by the roughness height (fin height), while the helix angle had little or no effect. No hysteresis was found for increasing and decreasing Reynolds numbers.

Turbulent adiabatic friction factors were compared with generally used enhanced tube correlations obtained from the literature. Most of these correlations were, however, only valid for Reynolds numbers greater than 10 000. One correlation with its validity being as low as a Reynolds number of 2 300, predicted the data with excellent accuracy. On average, the correlation predicted the data to within 1.7%, deviating the data by a maximum of 11.5%.

Two adiabatic friction factor correlations were developed. The first for predicting the critical Reynolds number, while the second was for predicting friction factors in the transition region of flow. The correlation for critical Reynolds numbers were developed by using the current data as well as data obtained for helical corrugated tubes. The correlation predicted critical Reynolds numbers on average to within 1%, deviating the data by a maximum of 18%. The transition friction factor correlation predicted the data on average to within 1% with an rms deviation of less than 5%.

A 'secondary transition' region was identified between a Reynolds number of approximately 3 000 and 10 000. This secondary transition was characterised by an increase in friction factor (instead of the normal decrease observed with the smooth tube) as the Reynolds number increased, after which it followed a decreasing trend for Reynolds numbers greater than 10 000. After transition from laminar to turbulent flow, at approximately a Reynolds number of 3 000, does the helix angle of the fins start to have an effect on the fluid. As the Reynolds numbers increase the fluid starts to rotate, giving rise to an increase in wall shear stress, and hence increase in friction factor. The tube with the greater helix angle had the greatest effect on friction factors.

Heat transfer results in this region also showed the effect of this rotation of the fluid with the Colburn j-factors showing an increase in value when compared with the smooth tube. Only after a Reynolds number of 10 000, did it start to decrease at more or less the same rate as that of the smooth tube. This was due to the fluid's rotation increasing with Reynolds number, improving the amount of mixing.

The heat transfer results were also compared with enhanced tube correlations. These correlations also predicted the data with fair accuracy for Reynolds numbers greater than 8 000. Therefore an new correlation, having a similar form as the Dittus-Boelter equation, was developed for the Reynolds number range of 3 000 to 8 000. This correlation included the geometrical aspects of the tube and predicted the data on average to within 3% with an rms deviation of less than 4.5%.

The smooth tube laminar correlation was used to predict the laminar region for enhanced

tubes. This was due to the fact that the main driving mechanism for heat transfer was the secondary flow due to mixed convection, with the driving potential for the enhanced tubes being lower than for the smooth tubes. This was reflected in the Grashof number that appears in the correlation. This correlation predicted the data on average to within 1% with an rms deviation of less than 2%.

A correlation for the transition region was also developed. This correlation, valid for Reynolds numbers between 1 900 and 4 000, predicted the data on average to within 1% with an rms deviation of less than 3.5%.

Enhanced tube diabatic friction factors were also investigated. These friction factors followed a similar trend as those for the adiabatic case, except that the laminar friction factors were considerably higher than those encountered in adiabatic flow. These friction factors were, however, very similar to those obtained for the laminar smooth tube diabatic case since the secondary flows increase the overall wall shear stress. A correlation for the laminar friction factors was developed, predicting the data on average to within 1% with an average rms deviation of approximately 2.7%. Correlations for the transition regime as well as the region between a Reynolds number of 2 500 and 7 000 was developed, each of which predicted the data on average to within 1% with an rms deviation of 1% and 2%, respectively.

An evaluation of the performance of the enhanced tubes was done to determine if it would be viable to replace the smooth tubes with the enhanced tubes. A number of criteria were set and the performance determined. In all the cases, the enhanced tubes only became a viable option when the to-be-replaced smooth tubes were operating at a Reynolds number greater than approximately 4 500. Peak performance for all the enhanced tubes was obtained for smooth tubes operating at a Reynolds numbers of approximately 9 000 - 10 000. The greater helix angle tube had the best performance increase. A decrease in performance was observed for smooth tubes operating at Reynolds numbers greater than the above values, although more data would be needed to confirm this trend. No advantage in the laminar and transition region is gained if smooth tubes were replaced with the enhanced tubes.

Chapter 7

Results: Entrance Effects for Enhanced Tubes

> If an elderly but distinguished scientist says that something is possible, he is almost certainly right; but if he says that it is impossible, he is very probably wrong.
>
> *Arthur C. Clarke (1917 - 2008)*

7.1 Introduction

Inlet profiles for smooth tubes with adiabatic flow had a significant influence on the transition from laminar to turbulent flow. Transition was either slightly accelerated or, in most cases, delayed to Reynolds numbers greater than expected from current literature. This influence, though, was nullified when the flow was diabatic, with transition occurring at the same Reynolds numbers for all the different inlets. Fully developed adiabatic flow inside enhanced tubes show that transition occurred at slightly lower Reynolds numbers than those of their smooth tube counterparts. This delay was, however, attributed to the height of the fins or the tube roughness, with the helix angle having no effect whatsoever.

This chapter will investigate the influence these inlet profiles have when used with enhanced tubes. Adiabatic flow will first be investigated, which will be followed by results from the heat transfer process.

7.2 Adiabatic Friction Factors

Figure 7.1 shows the adiabatic friction factor results for the 18° (top) and 27° (bottom) enhanced tubes. The solid markers are results for the 15.88 mm tube, while the empty ones are for the 19.02 mm tube. Also shown in the figure are the smooth tube fully developed correlation,

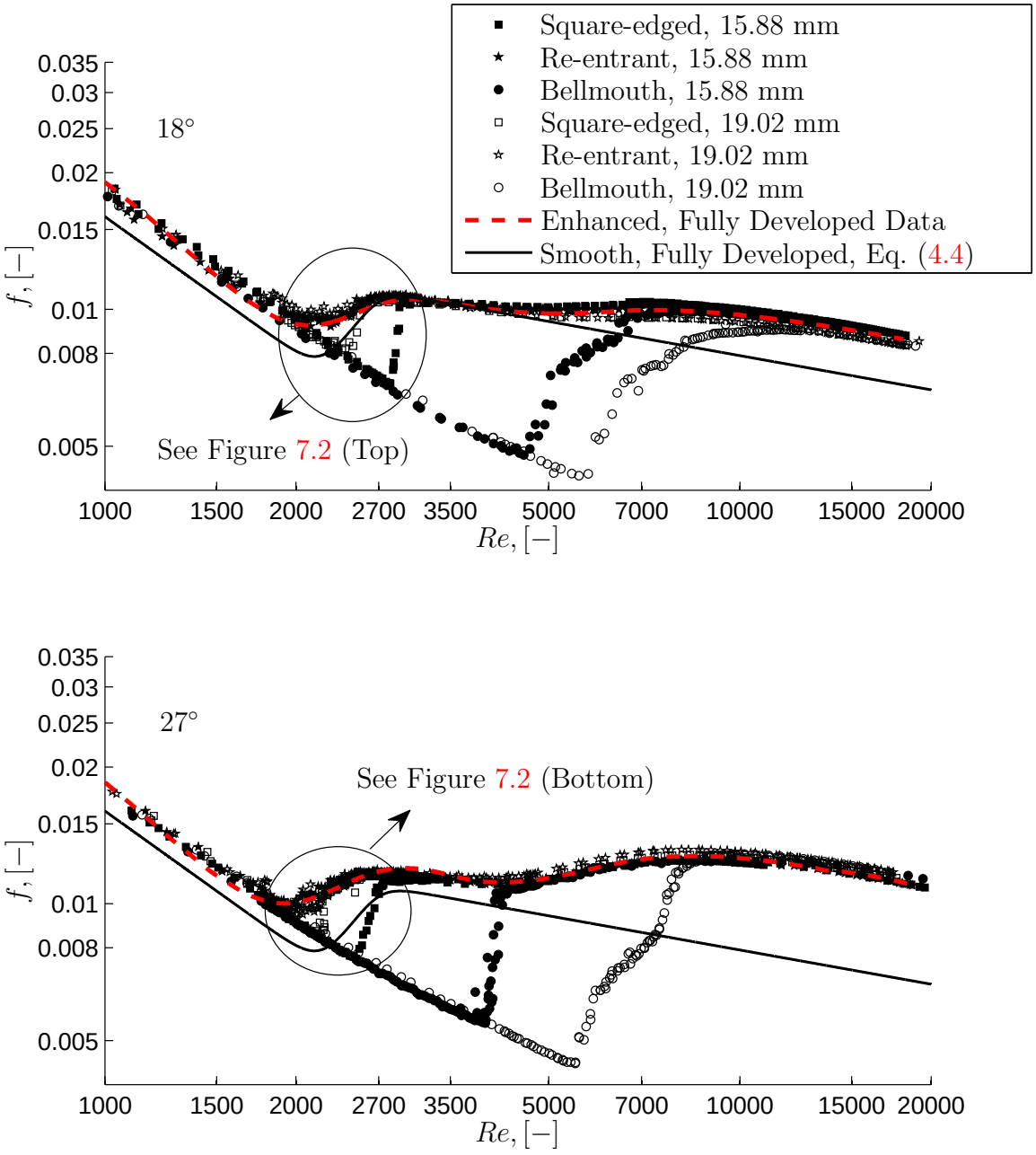

Figure 7.1 Adiabatic friction factors for the 18° (top) and 27° (bottom) enhanced tubes for different inlet configurations for the 15.88 mm (solid markers) and 19.02 mm (empty markers) enhanced tubes.

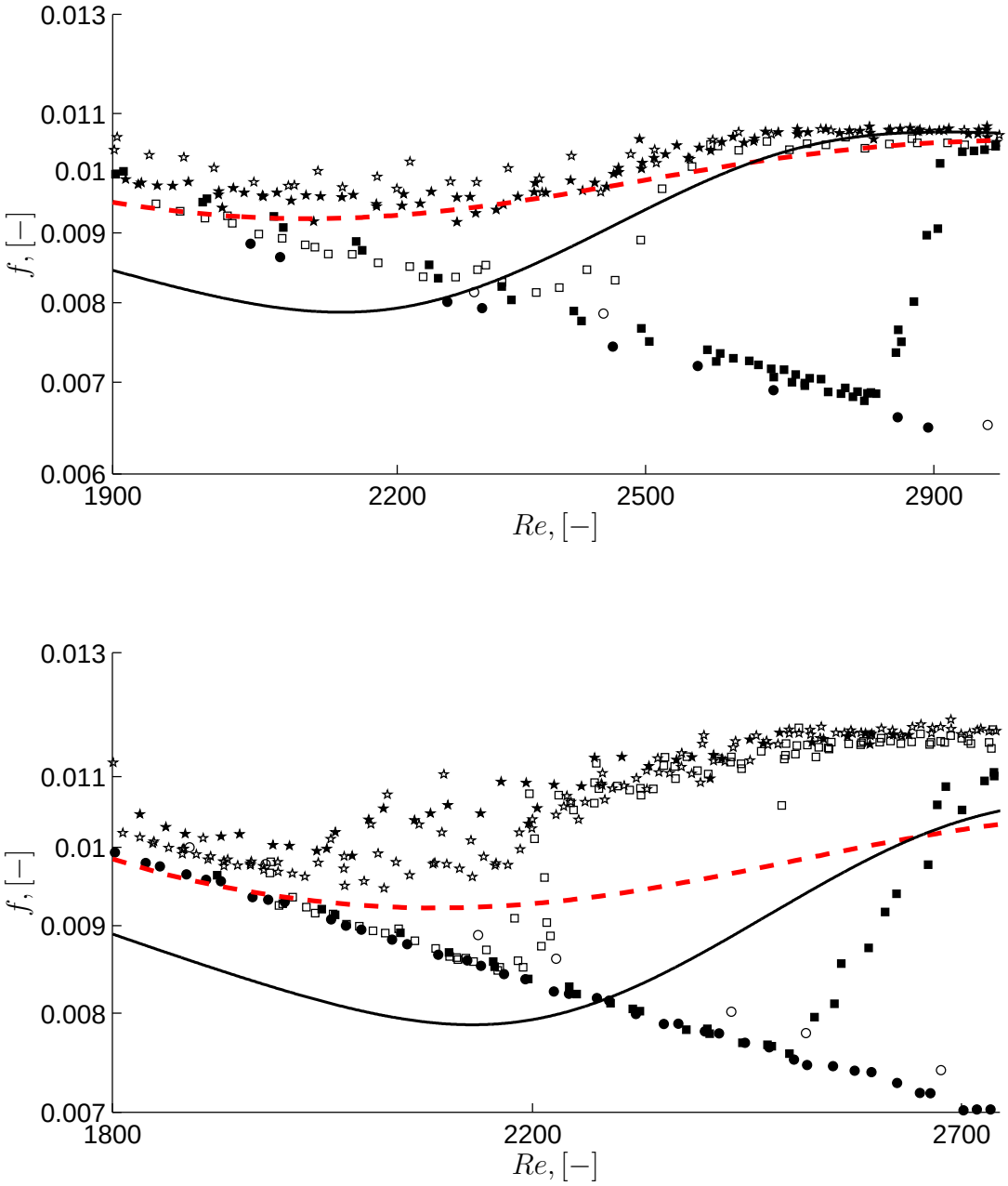

Figure 7.2 Adiabatic friction factors: close-up view of the region of transition.

Equation (4.4), and 15.88 mm enhanced tube fully developed data. This figure consists of a total of 2 074 data points; 941 for the 18° enhanced tube and 1 133 for the 27° enhanced tube. A zoomed region of the transition area is shown in Figure 7.2 for clarity.

From the figures, transition for the 15.88 mm tubes is positioned at different Reynolds numbers, depending on the type of inlet used. The bellmouth inlet delays transition to Reynolds numbers higher than those for the square-edged and re-entrant inlets, while the square-edged inlet delays transition to Reynolds numbers higher than that for the re-entrant inlet. These trends are similar to those obtained for the smooth tube. For the 19.02 mm tube, these delays in transition are less pronounced, with only the bellmouth inlet showing significant delays. The delay in transition for the 19.02 mm square-edged inlet is much less than obtained for its 15.88 mm counterpart. The 19.02 mm bellmouth inlet does, however, show a greater delay in transition when compared with the 15.88 mm bellmouth inlet, with the effect being very similar to the delay in transition between the 15.88 mm and 19.02 mm smooth tube with the bellmouth inlet. For all these results there was no noticeable hysteresis.

Turbulent flow results are unaffected by inlet profile as shown by the current data and the fully developed enhanced tube data Chapter 6 . Laminar results are also the same, both being slightly higher than the Poiseuille relation. This is also attributed to the fin height/surface roughness, with the helix angles having no effect. Although there is a boundary layer growth due to the inlet profiles, this is not evident in the laminar friction results. In Chapter 5, it was shown that this developing boundary layer was responsible for the increase in friction factors for the smooth tubes with various inlets when compared with the fully developed inlet. This is not evident for the enhanced tubes, implying that the tube roughness has a greater effect on the wall shear stress than the effect of the boundary layer. Only the bellmouth inlets near the transition region are slightly affected by the boundary layer growth. It is also evident from the results that the helix angle has no effect on this increase in friction factor, as was found for the fully developed case in Chapter 6.

Figure 7.3 shows the fluctuation in friction factors for all the inlets and enhanced tubes. This confirms the results from Figure 7.1 with regard to where transition starts and ends. For the re-entrant inlet, the start of transition varies between 1 985 and 2 080 for the different tubes, showing that it is unaffected by the tube diameter and fin helix angle. Only the end of transition appears to be affected by the helix angle, with transition ending at approximately 3 000 for the 18° tubes and 2 500 for the 27° tubes. This shows that the turbulence is higher for the greater of the two helix angles as Reynolds numbers increase.

For the square-edged inlet, transition for the 15.88 mm starts at a Reynolds number of approximately 2 800 for the 18° tube, and 2 500 for the 27° tube. For the 19.02 mm tube, transition starts at 2 200 and 2 050 for the respective helix angles. It would appear that in this instance, the helix angle and tube diameter have an effect on the delay of transition. The transition from laminar to turbulent flow for the square-edged inlet is very abrupt, spanning a relatively small range of Reynolds numbers.

The bellmouth inlet shows the greatest delay in transition, being in the Reynolds number range of 3 900 to 4 600 for the 15.88 mm enhanced tubes, and 5 500 to 5 800 for the 19.02 mm

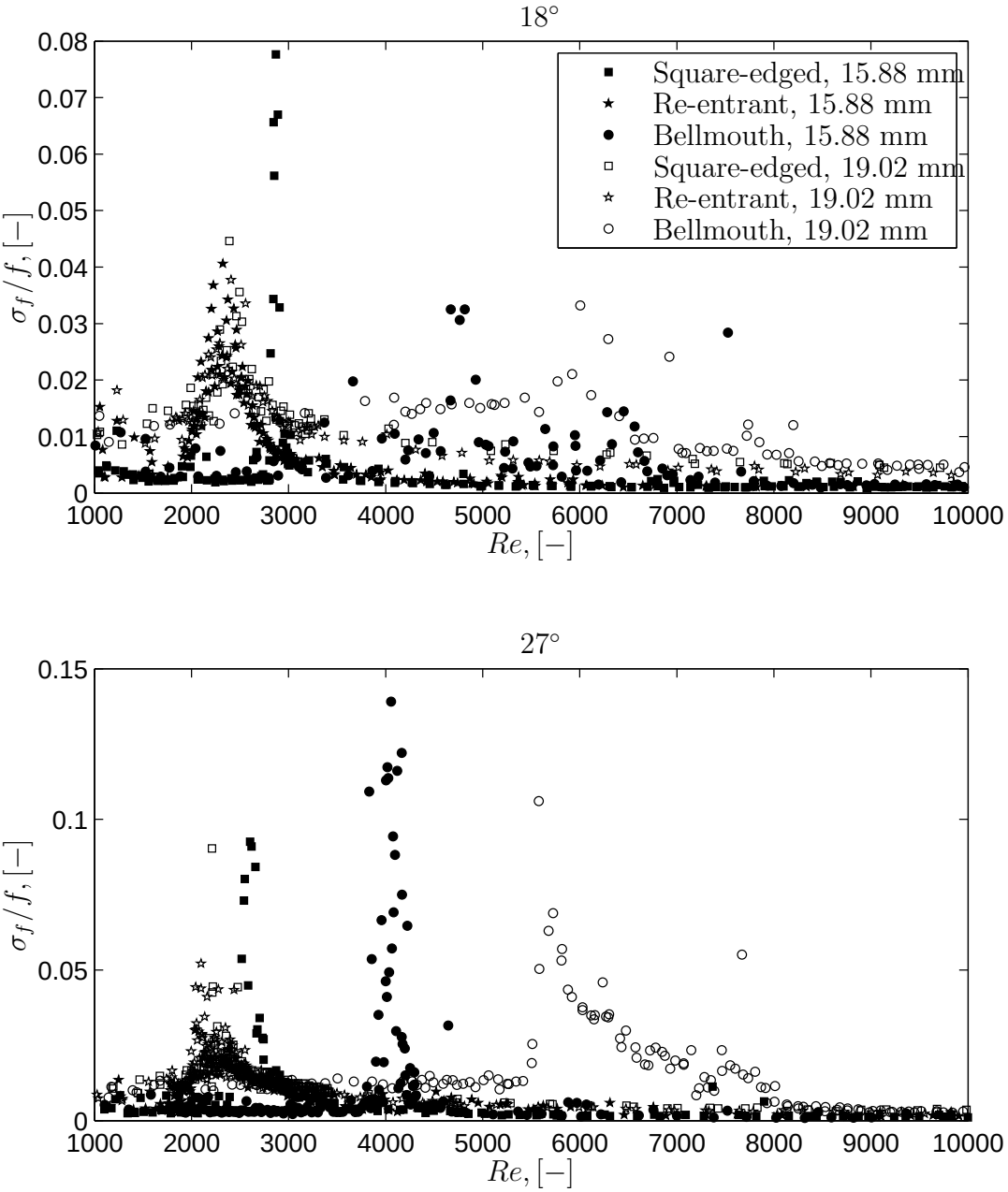

Figure 7.3 Fluctuations in adiabatic friction factors for the 18° (top) and 27° (bottom) enhanced tubes for different inlet configurations for the 15.88 mm (solid markers) and 19.02 mm (empty markers) enhanced tubes.

tubes. The transition for the bellmouth, though, occurs at lower Reynolds numbers than its smooth tube counterparts (7 000 and 12 000 for the 15.88 mm and 19.02 mm smooth tubes, respectively). This shows that the roughness of the fins influences the stability of the boundary layer, and hence its ability in maintaining laminar flow at high Reynolds numbers.

7.2.1 Correlation

Although each inlet profile has its own specific transition region, the rest of the results are very similar to the fully developed inlet for the enhanced tubes outside this region (*viz.* Figure 7.1 with regard to the fully developed data). Thus, the main focus of this section will be to develop the correlation for the transition region of flow for each inlet. For this the adiabatic correlation developed in Chapter 6, Equation (6.17), will be used. It is given in its raw form as

$$f_t = \left(\frac{16}{Re_{Cr}}\right)^{c_1} exp\left(c_2\frac{Re}{Re_{Cr}}\right)\left(\frac{\beta}{90}\right)^{c_3}\left(\frac{e^2}{pD}\right)^{c_4}\left(\frac{p}{D}\right)^{c_5}\left(\frac{e}{D}\right)^{c_6} \tag{7.1}$$

Since no real trend regarding the critical Reynolds numbers could be found, it was decided that these values would be used as constants in the above equation. By using only the transition data for all the tubes and inlets (consisting of 393 data points), the constants, found by least squares optimisation, were determined for each set of inlets. These values are given in Table 7.1. These correlations predict the data on average to within 1% with an rms deviation of less than 10%. The correlations are compared to the experimental data in Figure 7.4. The correlations are valid for

$$\begin{aligned} Re_{cr} &\leq Re \\ 18^\circ &\leq \beta \leq 79^\circ \\ 6.14\times10^{-4} &\leq e^2/pD \leq 0.004 \\ 6.48\times10^{-4} &\leq p/D \leq 1.23 \\ 0.022 &\leq e/D \leq 0.057 \end{aligned}$$

This correlation can thus be used in combination with an appropriate laminar and turbulent correlation by adopting the method of Churchill and Usagi (1972). Since the laminar and turbulent data do not differ significantly from the fully developed data, the correlations suggested in Chapter 6 should be used.

7.3 Heat Transfer

The heat transfer results for the different inlets consisted of a total of 1 458 data points; 959 for the 15.88 mm enhanced tubes, and 499 for the 19.02 mm enhanced tubes. The Colburn j-factors as a function of the Reynolds number are given in Figure 7.5. Included in the figure

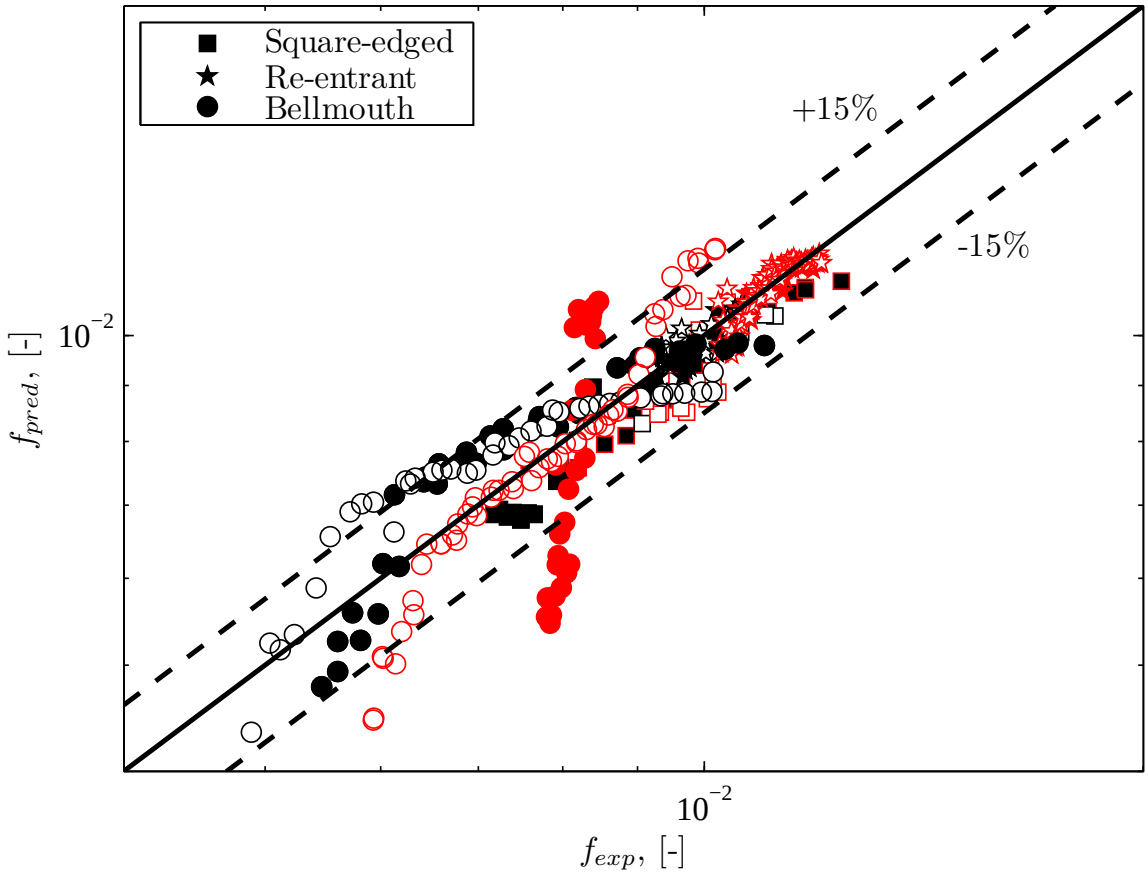

Figure 7.4 Performance of Equation (7.1) against the adiabatic friction factor data of the 15.88 mm (solid markers) and the 19.02 mm (empty markers) enhanced tubes for the various inlets. The black markers represent the 18° tubes while the red markers the 27° tubes.

Table 7.1 Values for the constants, c_1 to c_6 and Re_{Cr}, in Eq. (7.1).

							Re_{Cr}, 15.88 mm		Re_{Cr}, 19.02 mm	
Inlet	c_1	c_2	c_3	c_4	c_5	c_6	**18°**	**27°**	**18°**	**27°**
Square-edged	-0.76	3.49	6.72	-0.21	3.03	-0.02	2 800	2 487	2 230	2 050
Re-entrant	0.30	0.50	1.67	-0.07	0.68	0.23	2 080	1 986	2 050	1 985
Bellmouth	0.47	1.13	0.82	-0.07	-0.01	0.78	4 568	3 950	5 772	5 507

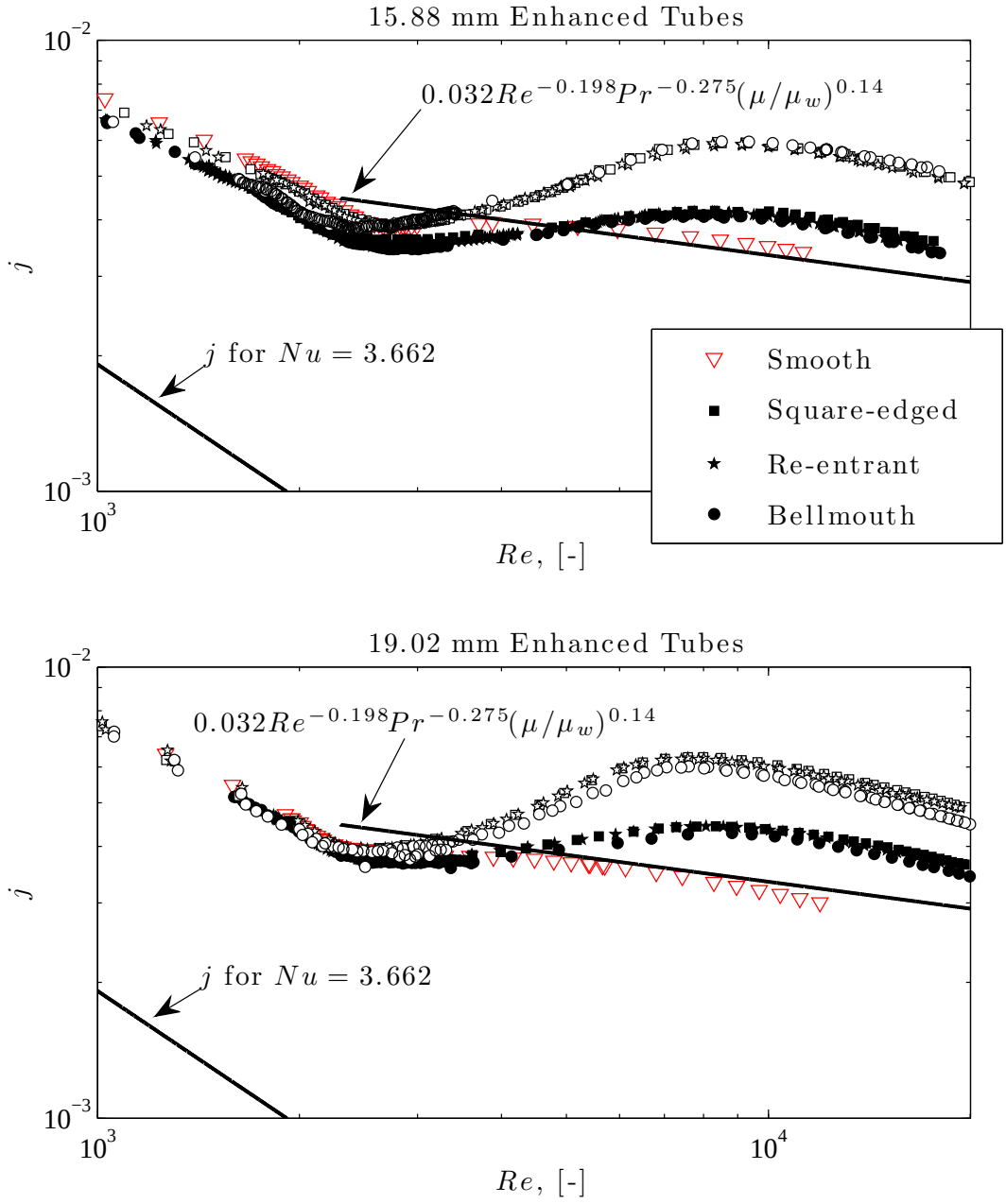

Figure 7.5 Enhanced tube heat transfer results for the 15.88 mm (top) and 19.02 mm (bottom) enhanced tubes for different inlet configurations.

is the fully developed smooth tube results from Chapter 4. Unlike the previous section where the solid symbols represented the 15.88 mm tube and the empty ones the 19.02 mm tube, they

now represent the 18° and 27° tubes, respectively. This was done to make the reading of the graph easier.

The figure shows the increase in turbulent heat transfer above that of the smooth tube. This increase is very similar to the fully developed enhanced tubes discussed in Chapter 6, with the 27° tube showing the greatest increase.

The laminar Nusselt numbers for the 15.88 mm, 27° enhanced tubes are higher than those for the 15.88 mm, 18° tube due to these experiments having a greater secondary flow component. Specifically, it is the square-edged and re-entrant data of the 27° tubes that are higher than the other data, while the bellmouth data are similar to the 18° tubes. This is shown in Figure 7.6, which indicates the experimental data for the 15.88 mm, 18° and 27° enhanced tubes for the different inlets. To ease the complexity of the graph, all the results for the 18°, 15.88 mm tube with all the various inlets were consolidated and are represented by a the red × symbols.

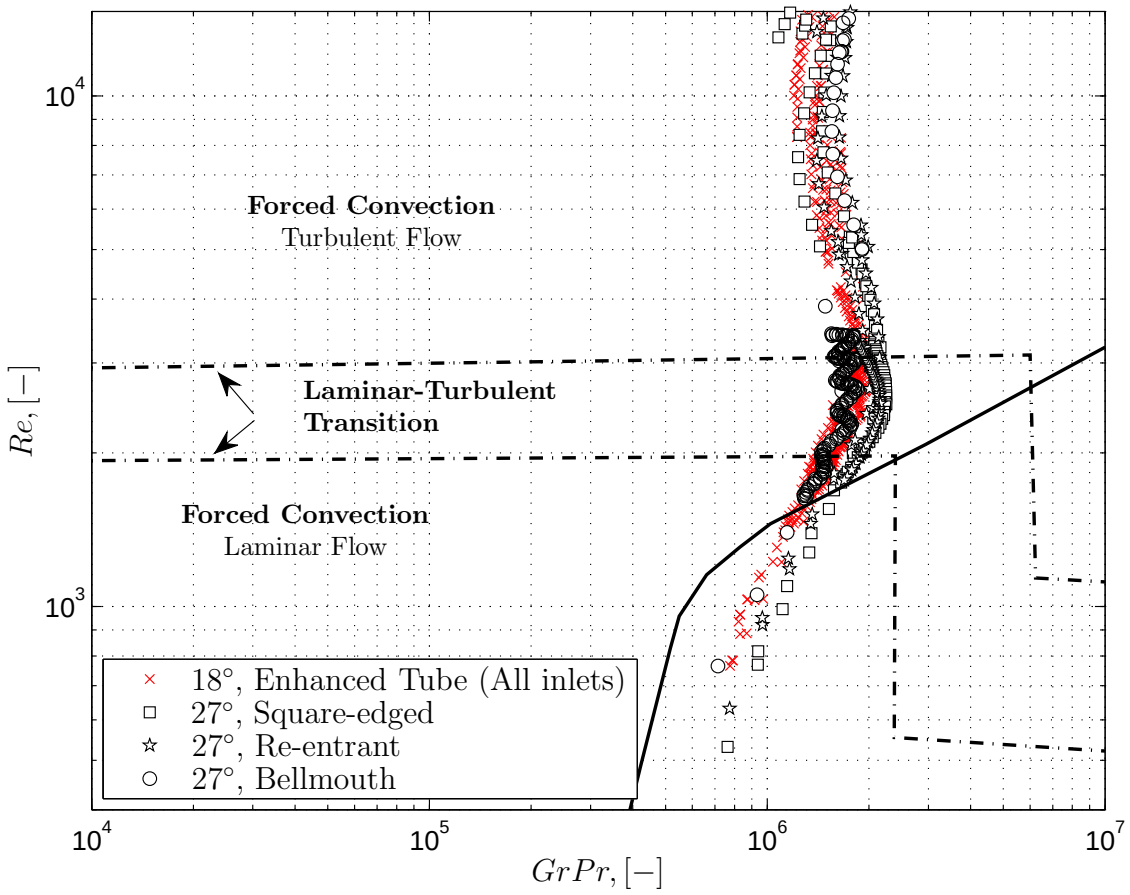

Figure 7.6 Experimental data for the 15.88 mm enhanced tubes in terms of the flow regime map of Metais and Eckert (1964).

These results show that higher values of $GrPr$ for the 15.88 mm, 27° tube are obtained when compared with its 18° counterpart. Only the bellmouth inlet appears to be unchanged, which is also reflected in the results given in Figure 7.5.

Figure 7.7 shows the heat transfer coefficient fluctuations as a function of the Reynolds number. These results show that irrespective of the inlet type, transition starts at a Reynolds number of approximately 1 900 and ends at 3 500. The results are near identical to the smooth tube results with regard to transition for the different inlets. The smooth tube data in Chapter 5 showed that transition from laminar to turbulent flow was independent of the inlet. Only the bellmouth entrance for the 19.02 mm smooth tube showed some variance, with transition being slightly delayed. This is also observed for the 19.02 mm enhanced tubes (18° and 27°) where transition commences at a Reynolds number of approximately 1 900 and ends at 3 500, but with its peak occurring at a Reynolds number of approximately 2 500, unlike the other inlets

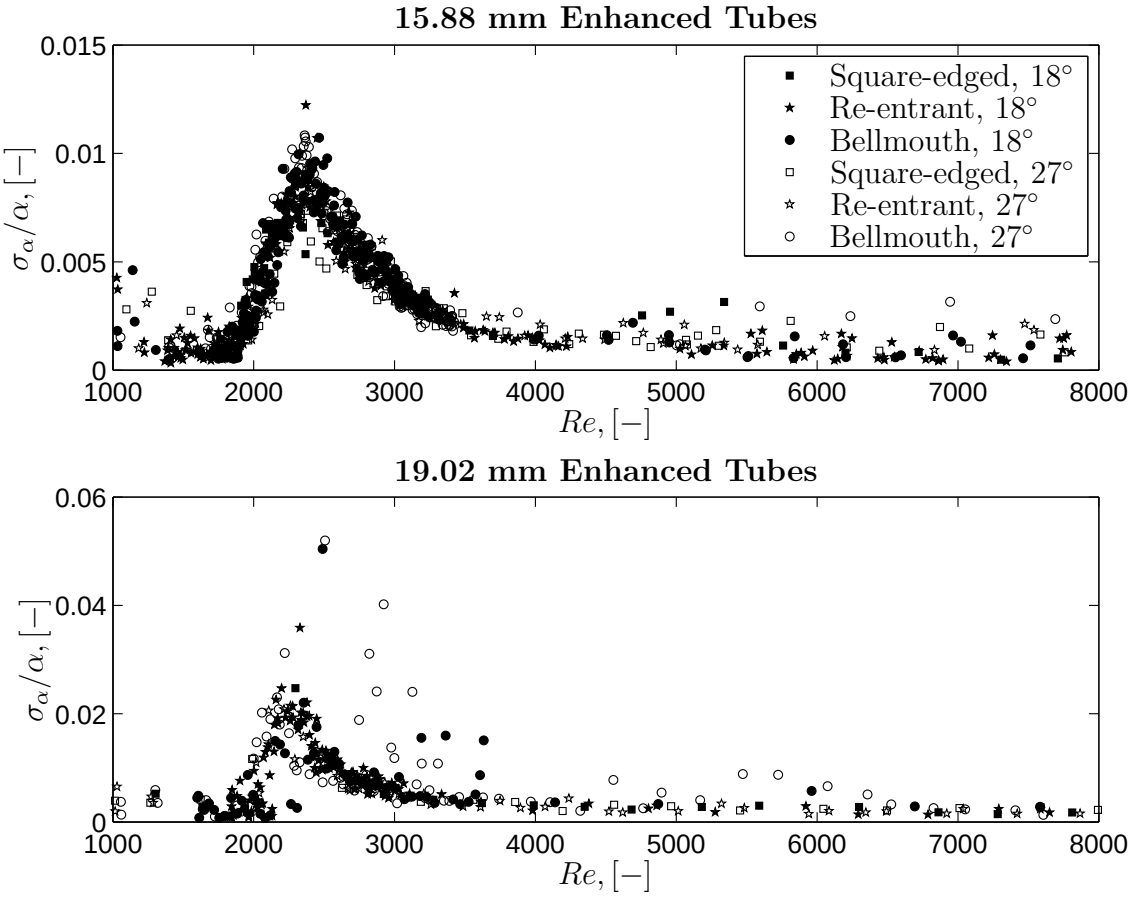

Figure 7.7 Heat transfer fluctuations for the 15.88 mm (top) and 19.02 mm (bottom) enhanced tubes with different inlet configurations.

where it occurs at a Reynolds number of approximately 2 200. This is also observed only for the 19.02 mm tubes. Further, the figure shows that the intensity of the fluctuations is greater for the 19.02 mm tube, although no explanation can be given for this behaviour.

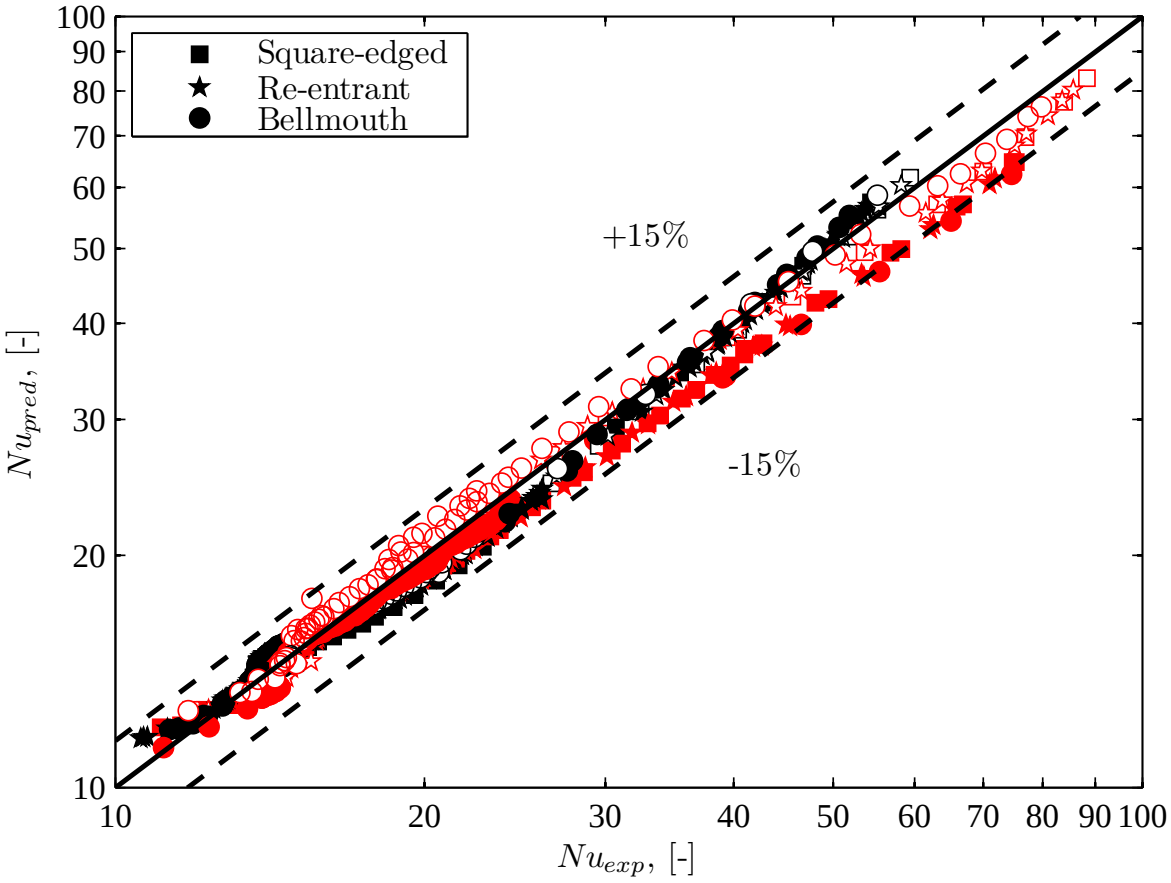

Figure 7.8 Performance of Equations (6.24), (6.27) and (6.29) against the heat transfer data for the various inlets for the 15.88 mm (solid markers) and 19.02 mm (empty markers) enhanced tubes. The black markers represent the 18° tubes while the red markers the 27° tubes.

In light of the results obtained for the enhanced tubes with the various inlets, developing a new correlation would be unnecessary. Hence Equations (6.24), (6.27) and (6.29) could be used in determining enhanced tube heat transfer characteristics, irrespective of the inlet profile.

The performance of these equations against the experimental data is shown in Figure 7.8. The correlations predict the data, on average, to within 1.5% with an average rms deviation of less than 5%. The equation deviates from the data by a maximum of less than 20%.

7.4 Diabatic Friction Factors

The diabatic friction factors are shown in Figures 7.9 and 7.10 for all the enhanced tubes and their respective inlets. The figure is comprised of 1 458 data points. Shown are the solid lines depicting the Poiseuille equation for laminar flow and the Blasius equation with viscosity correction for turbulent flow.

The results show the same trends as for the fully developed results, with an increase in laminar friction factors (approximately 30%), not due to the fins, but rather due to the secondary flow effects. The transition region is also seen to be in the region of a Reynolds number of between 1 900 and 3 000, as was found for the heat transfer data. The turbulent friction factors show the 'secondary transition' region, which is due to the fluid spinning as the Reynolds number is increased. This region and the fully turbulent region are a strong function of the helix angle, as was shown for the fully developed case.

All the data shown in Figures 7.9 and 7.10, indicates that the effect of the inlet disturbance are negligible for diabatic flows. This is purely due to the secondary flow induced by buoyancy forces within the fluid. This was also discussed in the previous chapters and will not be repeated here. This just shows, though, that inlet geometries combined with enhanced tubes also do not differ from their fully developed counterparts, as was found with the smooth tube results.

In support of the heat transfer data, Figure 7.11 shows the diabatic friction factor fluctuations as a function of the Reynolds number. This figure shows that transition is in the same region as depicted by the heat transfer results. This is significant since the measurement of heat transfer and friction factor are totally independently from each other.

Since the diabatic friction factor results are also very similar to the fully developed enhanced tube results, these were compared with the correlations developed for the fully developed enhanced tube in Chapter 6, Equations (6.31), (6.33) and (6.35).

Figure 7.12 shows the performance of these correlations against the experimental data. On average, the correlations predict the data to within 2% with an average rms deviation of less than 7%. The data deviates from the correlation by a maximum of 27%. This deviation is in the laminar regime for the square-edged and re-entrant data of the 27° enhanced tubes, which, from the results, showed a slight deviation from the other data.

7.5 Conclusion

Heat transfer and friction factor data for enhanced tubes with various inlets were presented. Adiabatic friction factor data showed that the inlet type had an influence on where transition commences. The transition from laminar to turbulent flow for the enhanced tubes were, however, commencing at lower Reynolds numbers than obtained for the smooth tube counterparts. This was mainly due to the increase in roughness the fins pose on the fluid. A correlation developed for the fully developed enhanced tube transition adiabatic friction factors was slightly modified to incorporate the effects of the different inlets. This correlation predicted the data

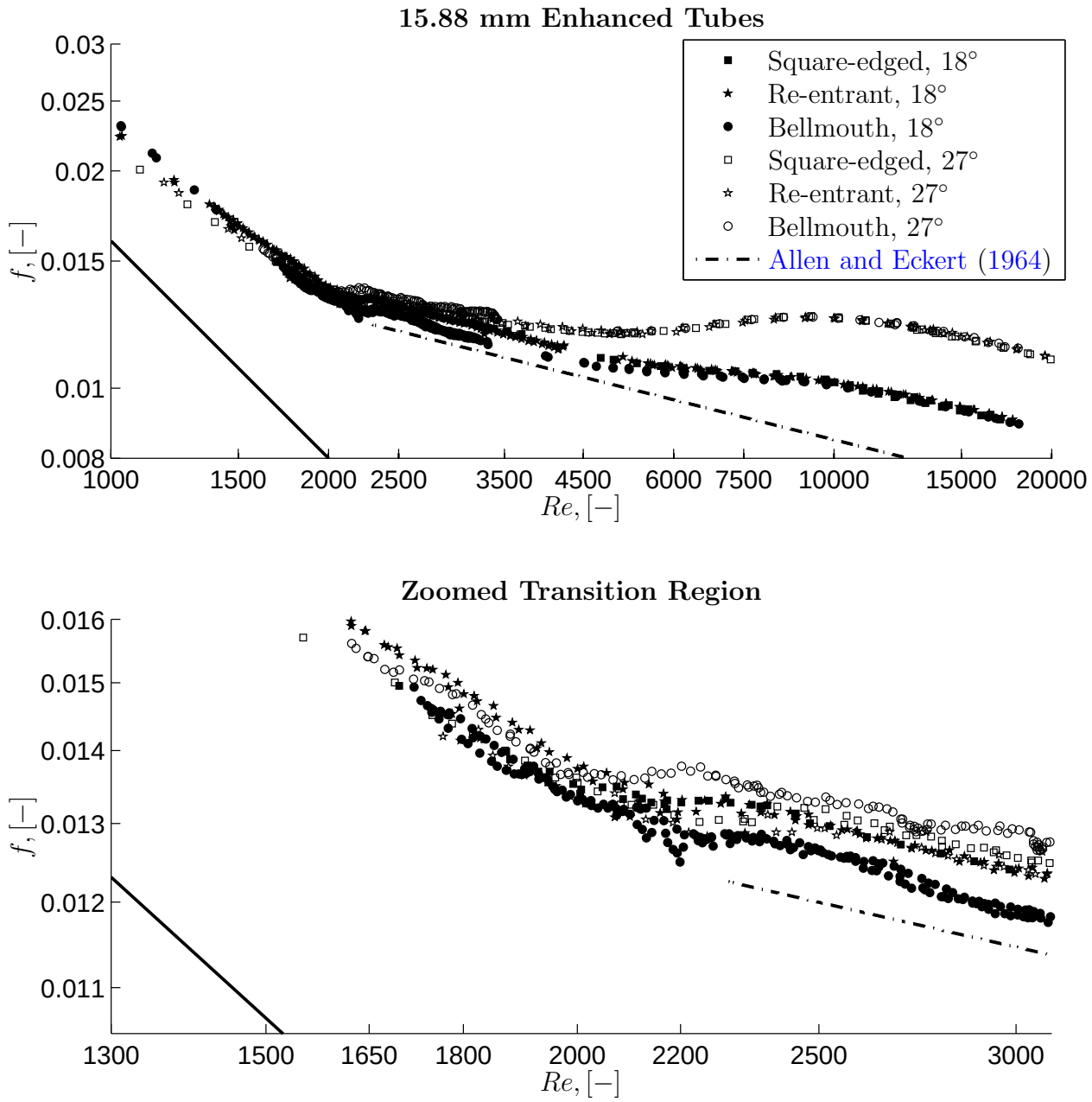

Figure 7.9 Diabatic friction factor results for the 15.88 mm enhanced tubes for different inlet configurations with the bottom figure being zoomed into the transition region. The solid line represents the Poiseuille relation for laminar flow.

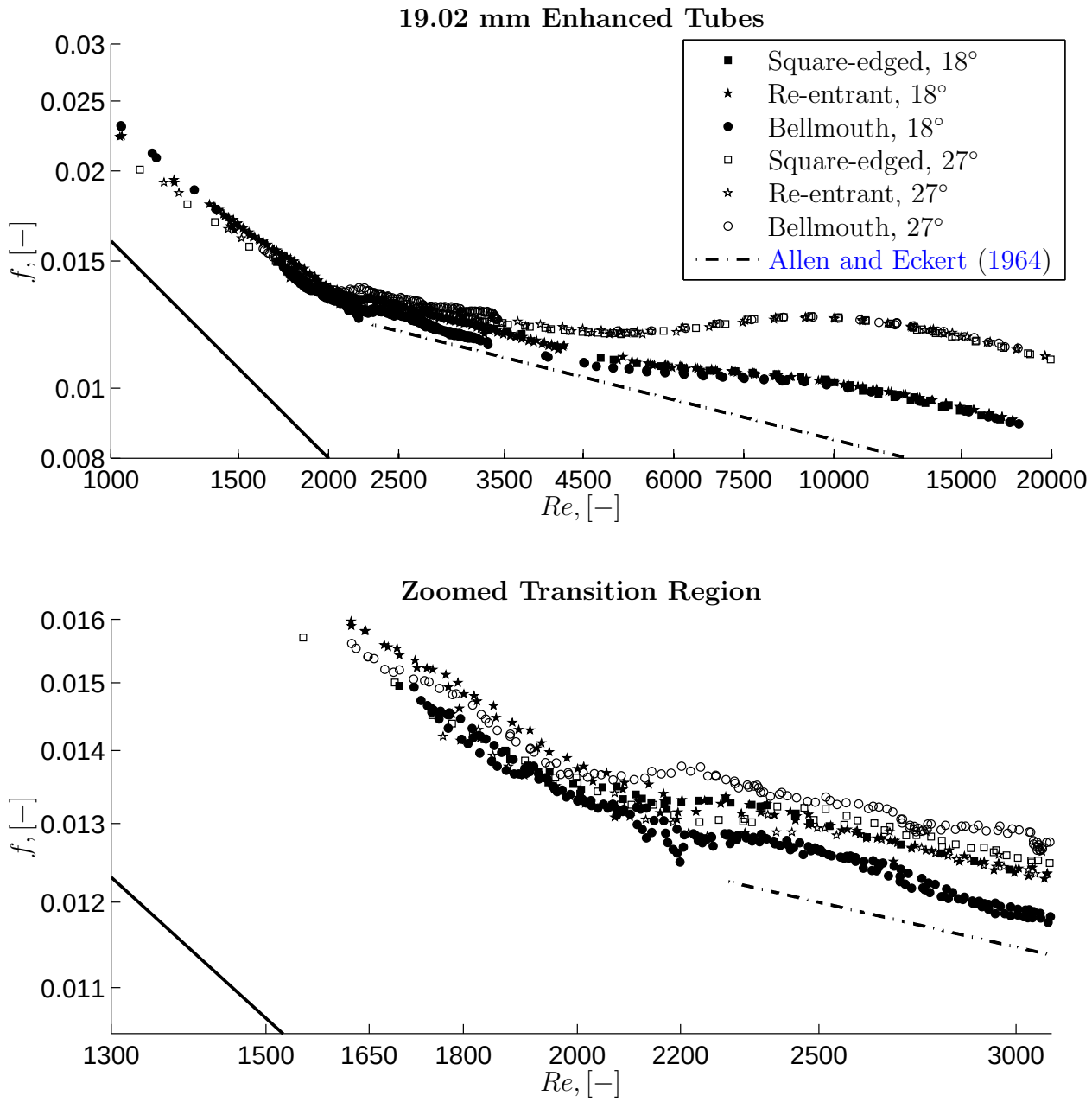

Figure 7.10 Diabatic friction factor results for the 19.02 mm enhanced tubes for different inlet configurations with the bottom figure being zoomed into the transition region. The solid line represents the Poiseuille relation for laminar flow.

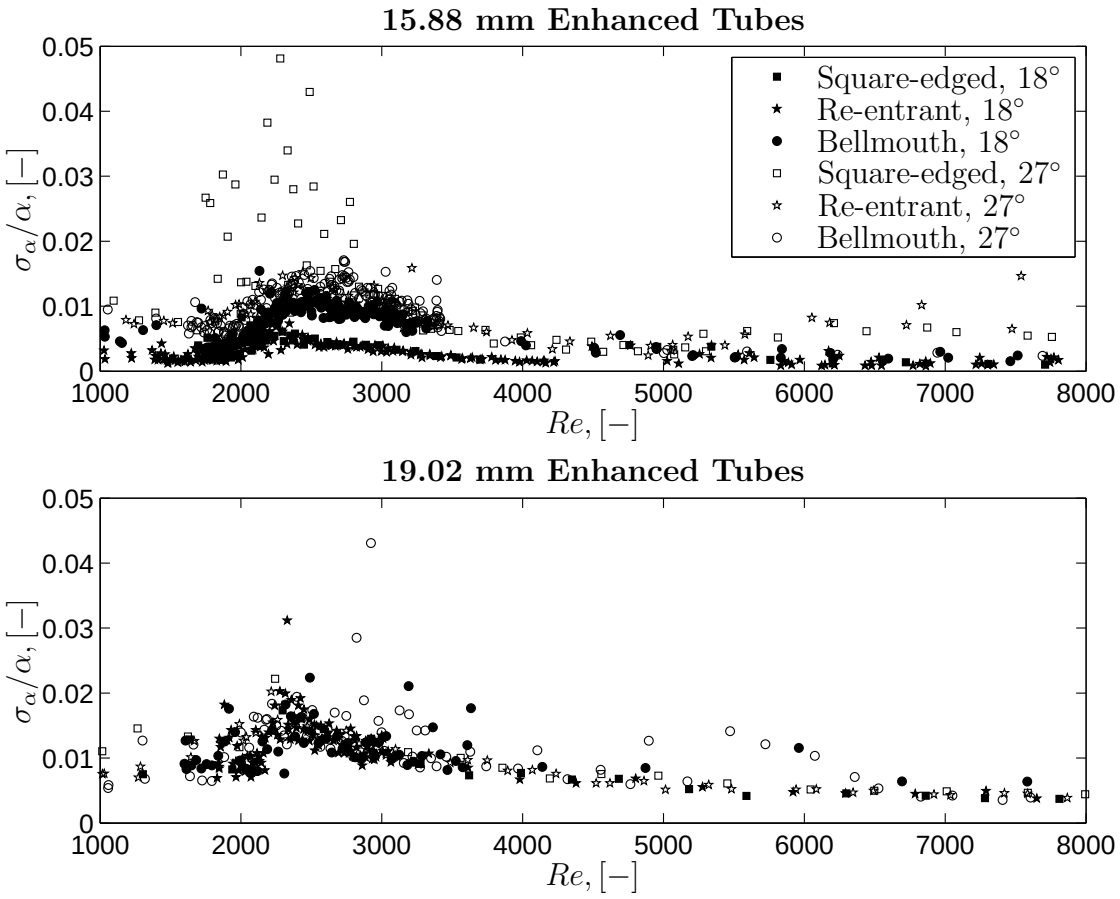

Figure 7.11 Diabatic friction factor fluctuations for the enhanced tubes with different inlet configurations.

on average to within 1%, deviating from the data by 30% at most. However, the rms deviation was below 10%.

Heat transfer results for the different inlets of the enhanced tubes showed very similar results to those found for the fully developed case. Transition from laminar to turbulent flow was between 1 900 and 3 500. This was due to the secondary flow effects dominating the hydrodynamic effects, causing the effect of the inlet disturbance to have little influence on transition.

The equations describing heat transfer inside the fully developed enhanced tube were used to predict the enhanced tubes with different inlets since the results differed little. The correlation predicted the data to within 1.5% with an average rms deviation of less than 5%.

Diabatic friction factors also showed similar results to those for the fully developed enhanced tube. Once again transition was found to be within a Reynolds number range of 1 900 to 3 500,

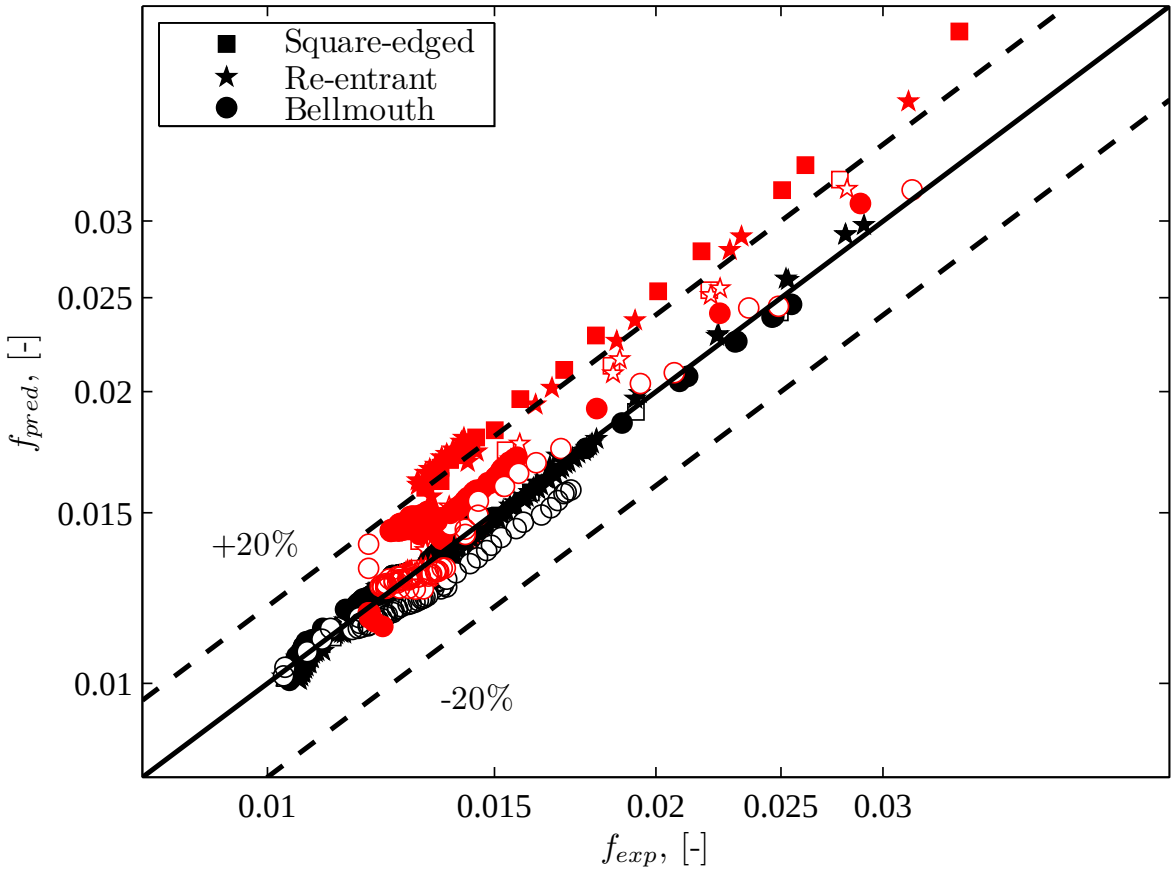

Figure 7.12 Performance of Equations (6.31), (6.33) and (6.35) for the 15.88 mm (solid markers) and 19.02 mm (empty markers) diabatic enhanced tube friction factor data with different inlets. The black markers represent the 18° tubes while the red markers the 27° tubes.

confirming the heat transfer results. The diabatic friction factor correlations developed for fully developed enhanced tubes were used for the different inlets. These correlations deviated from the data by less than 2% with an average rms deviation of less than 7%.

Chapter 8

Conclusion

Nothing shocks me. I'm a scientist.

Harrison Ford, as Indiana Jones (1942 -)

8.1 Summary

Heat exchangers in general are designed to either operate in the fully turbulent or fully laminar regime. These requirements are only laid down due to the relatively good understanding designers have of these regions, and due to the existing prediction methods working with fair accuracy. The transition region, however, is still an area with many unknowns, making predictions very difficult.

Some research into transitional flow has been performed inside smooth tubes over the years. Some important conclusions were made with regard to the transition Reynolds numbers being dependent on the inlet geometry or disturbance of the tube. The smoother the inlet, the more the transition is delayed. The transition region is also seen to have a chaotic behaviour, although the process is smooth when moving from the laminar to the turbulent flow regime, and does not change abruptly as previously thought.

A few prediction methods for heat transfer and friction factor do exist in the literature, although, these are only for smooth tubes with the fluid being heated. The aim of this study was to obtain heat transfer and friction data in the transition regime inside smooth and enhanced tubes. Different inlet profiles were also investigated to determine their effect on transition, especially for enhanced tubes. The investigation was also based on the cooling of the fluid, unlike previous research, as this is more applicable to chiller units.

An experimental system was developed to determine the effects of different inlet types, tube diameters and tube enhancements on the heat transfer and pressure drop performance in the transition region of flow. This investigation was based on the fact that heat exchangers are starting to operate in this region due to efficiency requirements, prompting the use of enhanced tubes for which little or no information is available to aid designers. Therefore, it was proposed that new heat transfer and pressure drop correlations be developed to cover the transition region of flow.

The experimental system consisted of an in-tube heat exchanger with a hot fluid flowing in the inner tube and a cold fluid in the opposite direction in the annulus, resulting in the inner fluid being cooled as found in chiller units. Six different tubes were investigated, namely two smooth tubes and four enhanced tubes. The enhanced tubes were helical low-fin tubes with fin heights of 0.4 mm and helix angles of 18° and 27°. Two different diameters were investigated, namely 15.88 mm (5/8″) and 19.02 mm (3/4″). To investigate the influence of inlet geometries, a calming section was designed to house different inlets. The inlets investigated were the square-edged, re-entrant and bellmouth inlets.

The number of data points captured was in the order of 6 946. These data points delivered 346 graphs from which a total of 19 equations were generated. In this section, only the most original data are summarised (graphs and equations) as there is just too much for a short summary. The results are summarised in three parts; adiabatic friction factors followed by heat transfer results and ending with diabatic friction factors.

8.2 Results

8.2.1 Adiabatic Friction Factors

Experimental test results have shown that transition from laminar to turbulent flow can vary between a Reynolds number of 1 800 and 10 000, depending on the inlet geometry. Very smooth inlets tend to delay transition, with the rougher inlets expediting it. This is shown in Figure 8.1 (top) which shows the adiabatic friction factor results for a smooth tube (diameter 15.88 mm) as a function of the Reynolds number.

Similar results were obtained for enhanced tubes, except that the transition friction factors occurred at lower Reynolds numbers than their smooth tube counterparts. Transition for enhanced tubes, however, was only a function of the tube roughness or fin height, with the helix angle in this case not having any effect. After transition, though, a ‘secondary transition’ region exists, which is due to the helix angle of the fins causing the fluid to spin, increasing its friction factor to higher values than those of a smooth tube until fully turbulent flow is reached. This region occurs for Reynolds numbers from 3 000 to 10 000. Turbulent friction factors are up to 38% higher for a 27° enhanced tube than those for the smooth tube. The greater the fin helix angle, the higher the turbulent friction factors are. These effects are seen in Figure 8.1 (bottom) for an 18° enhanced tube with various inlets.

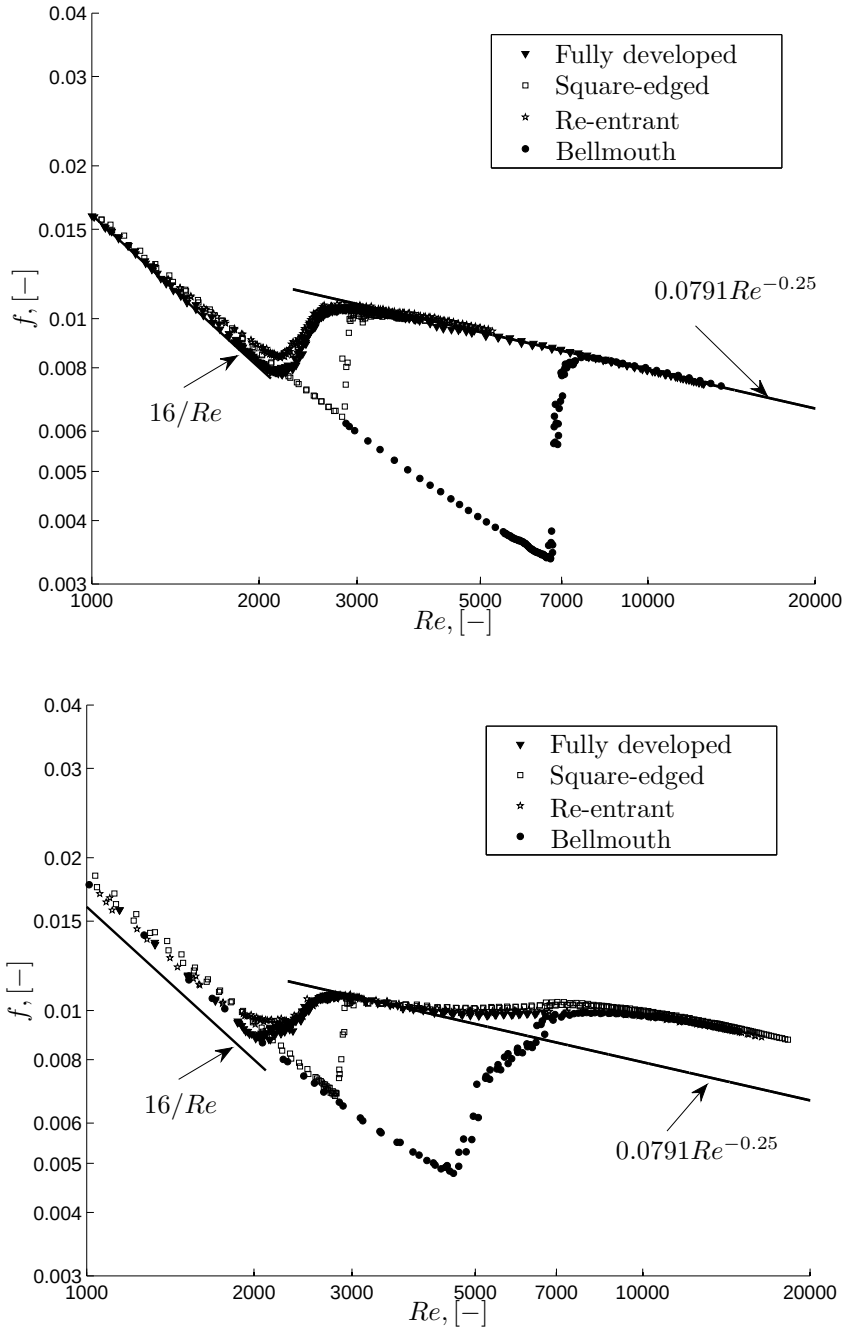

Figure 8.1 Adiabatic friction factors inside a smooth (top) and an 18° enhanced tube (bottom) for different inlets (tube diameter of 15.88 mm).

8.2.2 Heat Transfer

With the specific fluid being used, which in this case was water, transition between laminar and turbulent flow occurred at the same Reynolds number, with neither the inlet geometry nor tube enhancement having any effect. This is shown in Figure 8.2, which is a plot of all the tubes, smooth and enhanced, with all of the inlets. Transition occurs at a Reynolds number of approximately 2 100. The reason for this is the secondary flow forces, induced by the differences in density at the centre of the tube and the tube wall, which disturb the growing boundary layer. This, however, is valid for water (or a low Prandtl number fluid), as results for higher Prandtl number fluids show that inlet disturbances still influence transition. Laminar results are also much higher than predicted values for a constant wall temperature boundary, also being due to the secondary flows which enhance the amount of mixing in the fluid.

Similar results regarding transition were obtained for the diabatic friction factors, with transition also occurring for all the tubes and their inlets at the same Reynolds numbers. This confirms the heat transfer results. The diabatic friction factors for all the tubes are shown in Figure 8.3. This graph also shows the effect heat transfer has on the laminar friction factors. These are in the order of 40% higher than the friction factors for adiabatic flow. This is also attributed to the secondary flow inside the tube, increasing the wall shear stress and hence increasing the overall pressure drop.

8.2.3 Correlations

As mentioned in the summary, 19 correlations were developed from this work. To summarise it all, the correlations are presented in Table 8.1, which gives the type of configuration, the correlation and some comments relating to the correlation. Each item in Table 8.1 will briefly be discussed.

1. The adiabatic smooth tube friction factor consists of a combination of three correlation, each predicting the friction factor in their region of applicability. This correlation can be used for fully developed or developing flow by making use of the appropriate constants. This correlation is valid for Reynolds numbers greater than 500 and less than 20 000, although it would probably be valid for a wider range. This correlation predicts the data on average to within 1% with an rms deviation of less than 5%.

2. The laminar smooth tube heat transfer correlation was developed to account for the increase in heat transfer found in this region. It is of similar form as developed by previous authors, except that the $GrPr$-term makes use of a negative power to the Prandtl number. This was due to high Prandtl number fluids that tend to resist secondary flow motion due to their high viscosity.

   The diabatic friction factors can also be determined with this correlation due to the Reynolds-type analogy that could be made. This analogy was found to be valid for

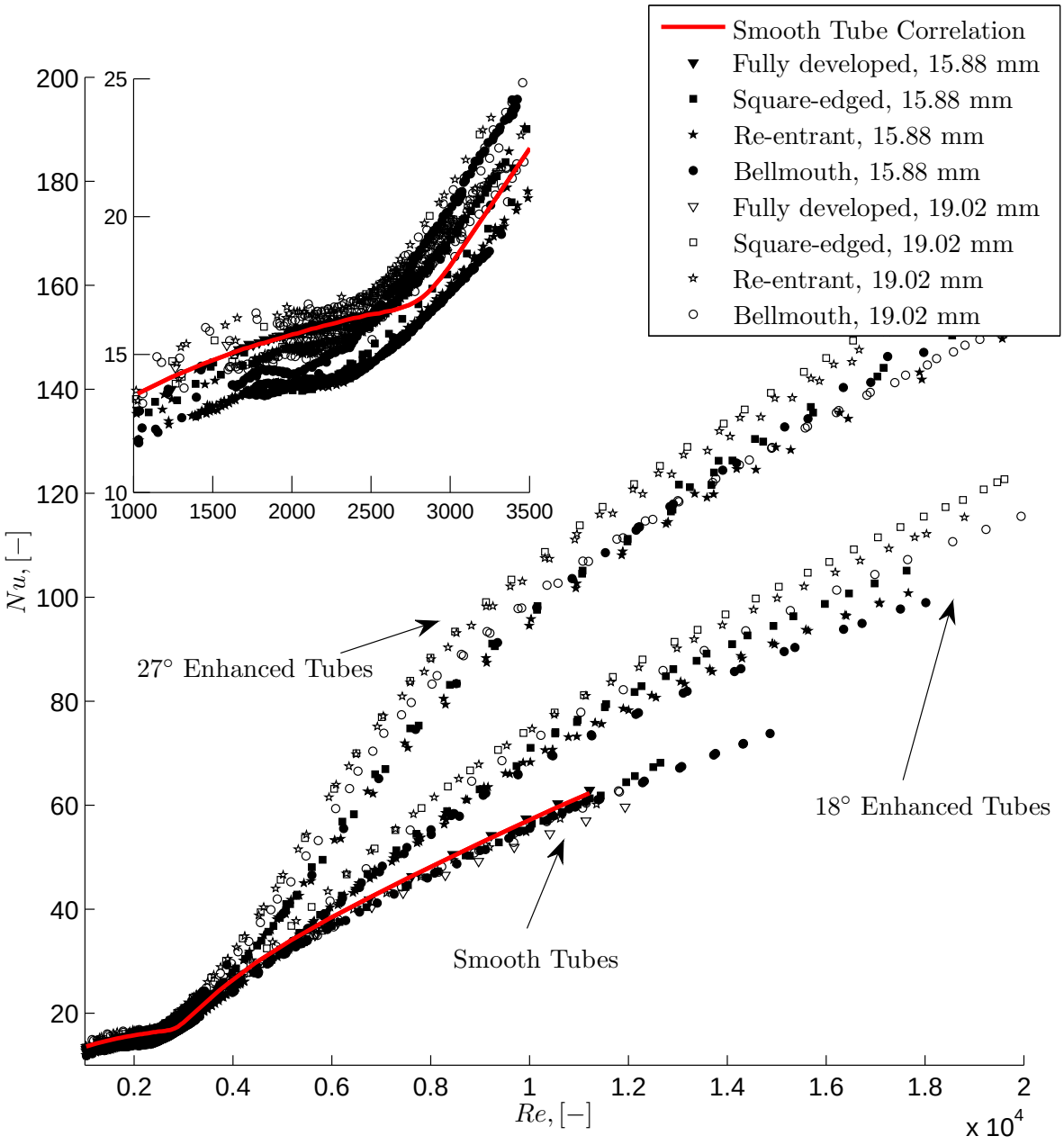

Figure 8.2 Heat transfer results for all the smooth and enhanced tubes with various inlets.

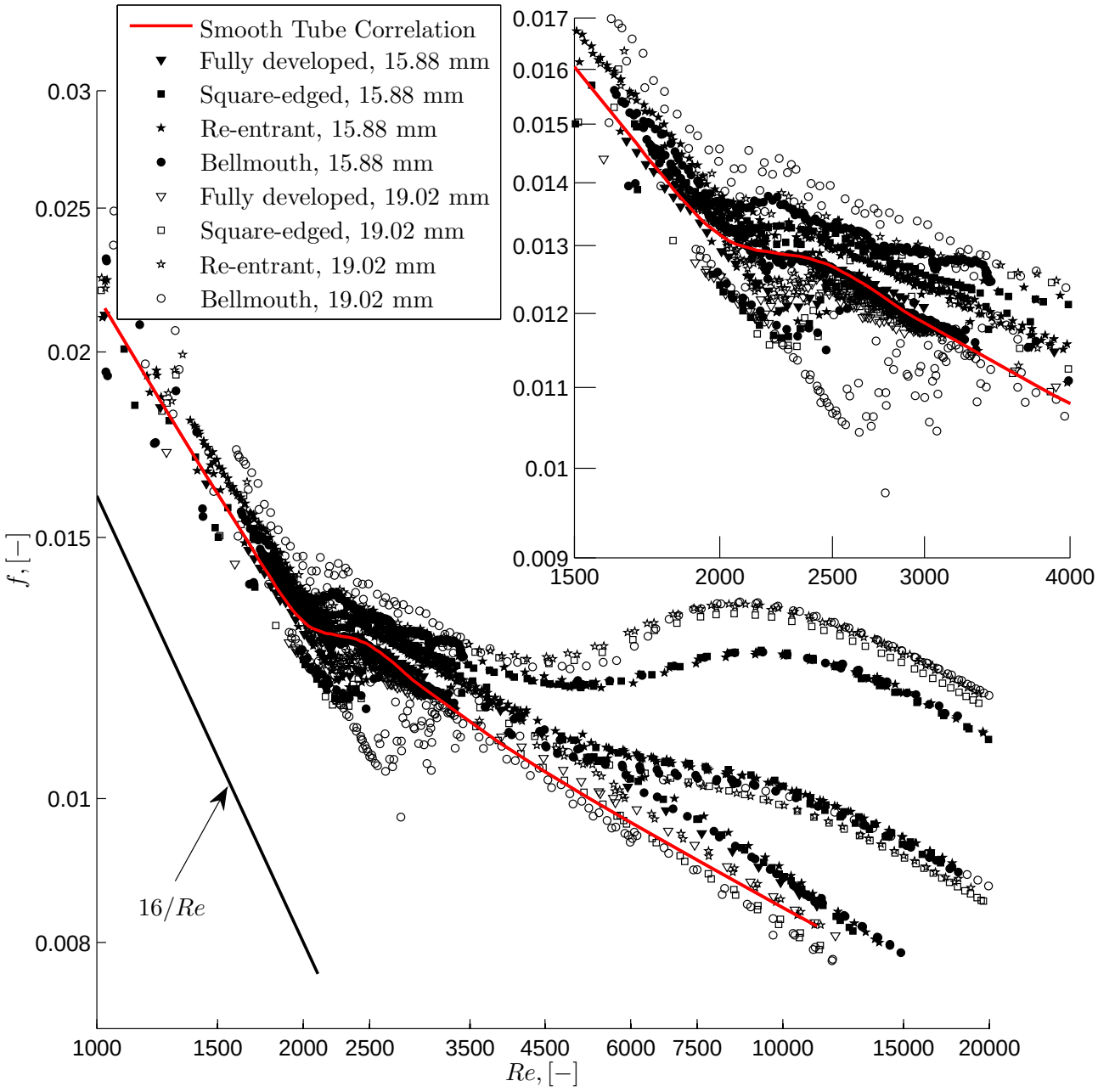

Figure 8.3 Diabatic friction factor results for all the smooth and enhanced tubes with various inlets.

use with water, although it might be valid for other low Prandtl number fluids. The correlation predicts the heat transfer data on average to within 1% with an rms deviation of less than 3%, while it predicts the diabatic friction factors on average to within 7% with an rms deviation of less than 9%. This correlation is valid fully developed or developing flow for smooth tubes.

3. The turbulent heat transfer correlation is in the form of the Dittus-Boelter equation, except it is valid for Reynolds numbers below 10 000. This correlation predicts the data on average to within 1.5% with an rms deviation of less than 3%. The correlation also predicts the friction factors to within 1% with an rms deviation of less than 4%.

4. The transitional heat transfer correlation for smooth tubes is a combination of the laminar and turbulent correlation, with its range of applicability being between Reynolds numbers of 2 000 and 3 000. It is independent of the type of inlet used. The correlation predicts the data on average to within 1% with an rms deviation of less than 2%, while for friction factors it predicts the data to within 4% with an rms deviation of less than 8%.

5. Adiabatic friction factors for enhanced tubes was found to be a function of the critical Reynold number as well as the enhancement geometry. This correlation is valid for fully developed and developing flow with entrance disturbance when used with the appropriate constants given. The correlation predicts the data on average to within 1% with an rms deviation of less than 5%. This correlation could be combined with the laminar correlation to extend its applicability to Reynolds numbers lower than the critical value.

6. Enhanced tube adiabatic friction factors in the laminar flow regime was found from previous authors to be only a function of the roughness height, or the fin height. The correlation is valid for roughness height ratios of 0.022 to 0.057 and predicts the data on average to within 1.3% with an rms deviation of less than 8%.

7. For fully developed flow it was found that the critical Reynolds number is only a function of the enhancement roughness height. A correlation was developed from the current database and one other source to predict this value. It predicted all the data on average to within 1% with an rms deviation of less than 8% and is valid for roughness height ratios of 0.022 to 0.057.

8. Laminar heat transfer inside enhanced tubes was found to be more or less the same as in smooth tubes. Therefore, the smooth tube correlation was used with the roughness height ratio added. This correlation is valid for fully developed and developing flow and is independent of the type of inlet disturbance. It predicts the data on average to within 2% with an rms deviation of less than 5%.

9. It was found that the lower turbulent region ($3\ 500 \leq Re \leq 8\ 000$) was poorly predicted by correlations found in the literature for heat transfer within enhanced tubes. It was

found that the heat transfer is a function of the enhancement geometry, which includes the fin pitch and helix angle. The correlation predicts the data on average to within 3% with an average rms deviation of less than 5% and is valid for fin helix angles between 18° and 27°.

10. The enhanced tube transition heat transfer correlation was developed by combining the laminar and lower turbulent correlations. This was done since transition occurred in a smooth manner from laminar to turbulent flow, unlike found for the adiabatic friction factors. Inlet profiles had no influence in this region due to the secondary flows. The correlation is valid for Reynolds numbers between 1 900 and 4 000 and predicts the data on average to within 1% with an rms deviation of less than 4%.

11. Since no Reynolds analogy between friction and heat transfer could be found for the enhanced tubes, separate correlation for the diabatic friction factors were developed. By making use of the laminar enhanced tube friction factor and adding natural convection terms, which also was found to be influenced by the helix angle, the correlation was developed being valid for Reynolds numbers up to 2 200. The correlation predicts the data on average to within 2% with an rms deviation of less than 3%. This correlation is also valid for fully developed as well as developing flow.

12. Turbulent adiabatic friction factors were found to predict the adiabatic friction factors very well. However, with heat transfer, the lower Reynolds number region was poorly predicted due to the influence natural convection can still has in this region. The adiabatic correlation was modified to include these terms, which predicted the diabatic data on average to within 1% with an rms deviation of less than 2%.

13. As was done for the lower turbulent region, the adiabatic transition correlation for enhanced tubes was modified to incorporate the effect of natural convection. Since transition occurred at the same Reynolds number for all the different types of inlets, only one correlation is required. The transition diabatic correlation predicts the data on average to within 0.5% with an rms deviation of 1%.

Table 8.1 Summary of the correlations developed.

No.	Configuration	Correlations	Comments
1	Laminar, transitional and turbulent adiabatic friction factors for smooth tubes	$f = f_L\left[1 + \left(0.0791Re^{-0.25}\right.\right.$ $\left.\left.\left[1 + \left(\frac{\left(\frac{16}{Re_{Cr_L}}\right)\left(\frac{Re}{Re_{Cr_L}}\right)^{c_3}}{0.0791Re^{-0.25}}\right)^{c_1}\right]^{1/c_1} \frac{1}{f_L}\right)^{c_2}\right]^{1/c_2}$	Constants for different inlet profiles: Inlet | c_1 | c_2 | c_3 | Re_{Cr} | f_L Fully developed | -12 | 8 | 2 | 2 200 | $16/Re$ Square-edged | -12 | 18 | 5 | 2 700 | f_{app} Re-entrant | -9 | 15 | 2.2 | 2 140 | f_{app} Bellmouth | -6 | 7 | 25 | 6 600 | f_{app} $f_{app}Re = \frac{3.44}{\sqrt{\chi}} + \frac{f_pRe + K_\infty/4\chi - 3.44/\sqrt{\chi}}{1 + 0.000212/\chi^2}$ $500 \leq Re \leq 20\ 000$
2	Laminar heat transfer and diabatic friction factors for smooth tubes	$f_L = \frac{Nu_L}{Re}Pr^{1/3}$ $Nu_L = 2.686\left[Re^{0.105}Pr^{1.133}\left(\frac{D}{L}\right)^{0.483} + 1.082\left(Gr^{0.362}Pr^{-2.987}\left(\frac{L}{D}\right)^{0.202}\right)^{0.277}\right]^{2.226}\left(\frac{\mu}{\mu_w}\right)^{0.152}$	Valid for all inlets. $940 < Re < 2\ 522$ $4.43 < Pr < 5.72$ $1.5 \times 10^5 < Gr < 4.3 \times 10^5$ $0.695 < \mu/\mu_w < 0.85$ $289 < L/D < 373$
3	Turbulent heat transfer and diabatic friction factors for smooth tubes	$f_T = \frac{Nu_T}{Re}Pr^{1/3}$ $Nu_T = 0.032Re^{0.802}Pr^{0.059}\left(\frac{\mu}{\mu_w}\right)^{0.14}$	Valid for all inlets. $3\ 000 < Re < 17\ 800$ $3.73 < Pr < 5.06$ $0.678 < \mu/\mu_w < 0.788$

continued on next page

continued from previous page

No.	Configuration	Correlations	Comments
4	Transitional heat transfer and diabatic friction factors for smooth tubes	$f_t = \frac{Nu_t}{Re} Pr^{1/3}$ $Nu_t = \left[Nu_L + e^{(Re-2\ 717)/202} + Nu_T^{0.845}\right]^{0.845}$	Valid for all inlets. $2\ 000 < Re < 3\ 000$ $4.47 < Pr < 5.30$ $2.8 \times 10^5 < Gr < 4.1 \times 10^5$ $0.702 < \mu/\mu_w < 0.797$ $289 < L/D < 373$
5	Transition adiabatic friction factor for enhanced tubes	$f_{te} = \left(\frac{16}{Re_{Cr}}\right)^{c_1} exp\left(c_2 \frac{Re}{Re_{Cr}}\right)\left(\frac{\beta}{90}\right)^{c_3} \times \left(\frac{e^2}{pD}\right)^{c_4}\left(\frac{p}{D}\right)^{c_5}\left(\frac{e}{D}\right)^{c_6}$	See the table below for the constants for different inlets. $Re_{Cr} \leq Re$ $18° \leq \beta \leq 79°$ $6.14 \times 10^{-4} \leq e^2/pD \leq 0.004$ $6.48 \times 10^{-4} \leq p/D \leq 1.23$ $0.022 \leq e/D \leq 0.057$
6	Laminar adiabatic friction factor for enhanced tubes	$f_L = \frac{16}{Re}\left[1 + 88\,(e/D)^{2.2}\,Re^{0.2}\right]$	Valid for all inlets $0.022 \leq e/D \leq 0.057$
7	Critical Reynolds numbers for enhanced tubes during adiabatic flow	$Re_{cr} = 2\ 200\left[1 + 9.13 \times 10^9 \left(\frac{e}{D}\right)^{5.8}\right]^{-1/10}$	Valid for fully developed flow only. $0.022 \leq (e/D) \leq 0.057$

Inlet	c_1	c_2	c_3	c_4	c_5	c_6	Re_{Cr}, 15.88 *mm* 18°	Re_{Cr}, 15.88 *mm* 27°	Re_{Cr}, 19.02 *mm* 18°	Re_{Cr}, 19.02 *mm* 27°
Fully developed	0.94	0.57	0.37	0.028	-0.009	0.06	See 7			
Square-edged	-0.76	3.49	6.72	-0.21	3.03	-0.02	2 800	2 487	2 230	2 050
Re-entrant	0.30	0.50	1.67	-0.07	0.68	0.23	2 080	1 986	2 050	1 985
Bellmouth	0.47	1.13	0.82	-0.07	-0.01	0.78	4 568	3 950	5 772	5 507

continued on next page

continued from previous page

No.	Configuration	Correlations	Comments
8	Laminar heat transfer inside enhanced tubes	$Nu_{Le} = 2.686 \left[Re^{0.105} Pr^{1.133} \left(\frac{D}{L}\right)^{0.483} + 1.082 \left(Gr^{0.362} Pr^{-2.987} \left(\frac{L}{D}\right)^{0.202} \times \left(\frac{e}{D}\right)^{0.0612} \right)^{0.277} \right]^{2.226} \left(\frac{\mu}{\mu_w}\right)^{0.152}$	Valid for all inlets $1\ 030 < Re < 2\ 198$ $4.58 < Pr < 5.67$ $1.4 \times 10^5 < Gr < 2.5 \times 10^5$ $0.7 < \mu/\mu_w < 0.847$ $0.023 < e/D < 0.027$ $286 < L/D < 349$
9	Lower turbulent heat transfer inside enhanced tubes	$Nu_{Te_{38}} = 0.35 Re^{1.33} Pr^{1.19} \left(\frac{e}{D}\right)^{-0.11} \left(\frac{p}{D}\right)^{2} \left(\frac{\beta}{90}\right)^{4.4}$	Valid for all inlets $3\ 500 \leq Re \leq 8\ 000$ $4.5 \leq Pr \leq 5.4$ $18^\circ \leq \beta \leq 27^\circ$ $0.176 \leq p/D \leq 0.387$ $0.023 \leq e/D \leq 0.027$
10	Transition heat transfer inside enhanced tubes	$Nu_{te} = \left[Nu_{Le}^7 + Nu_{Te_{38}}^7 \right]^{1/7}$	Valid for all inlets $1\ 900 \leq Re \leq 4\ 000$ $4.5 \leq Pr \leq 5.4$ $2.62 \times 10^5 \leq Gr \leq 4.45 \times 10^5$ $0.686 \leq \mu/\mu_w \leq 0.804$ $286 \leq L/D \leq 349$ $18^\circ \leq \beta \leq 27^\circ$ $0.176 \leq p/D \leq 0.387$ $0.023 \leq e/D \leq 0.027$

continued on next page

continued from previous page

No.	Configuration	Correlations	Comments
11	Laminar diabatic friction factors for enhanced tubes	$f_{Le} = \frac{16}{Re}\left[1 + 88\,(e/D)^{2.2}\,Re^{0.2} + Gr^{0.49}\,Pr^{-0.98}\left(\frac{D}{L}\right)^{0.71}(\sin\beta)^{1.04}\right]$	Valid for all inlets $1\,030 < Re < 2\,198$ $4.58 < Pr < 5.67$ $1.4 \times 10^5 < Gr < 2.5 \times 10^5$ $0.7 < \mu/\mu_w < 0.847$ $0.023 < e/D < 0.027$ $18^\circ < \beta < 27^\circ$ $286 < L/D < 349$
12	Lower turbulent diabatic friction factors for enhanced tubes	$f_{Tle}/f_s = \left[(l_{csw}/D)^{-2.2}\,(A_{cn}/A_c)^{-46} - 0.0151/f_s\left[(l_{csw}/D)^{-2.2}\,(A_{cn}/A_c)^{-46} - 1\right]e^{-Re/5428}\right] \times Pr^{0.55}\,Gr^{-0.09}\left(\frac{\mu}{\mu_w}\right)^{-1.2}$	Valid for all inlets $2\,500 < Re < 6\,956$ $4.47 < Pr < 5.39$ $1.63 \times 10^5 < Gr < 4.45 \times 10^5$ $0.69 < \mu/\mu_w < 0.84$ $0.023 < e/D < 0.027$ $18^\circ < \beta < 27^\circ$ $286 < L/D < 349$

continued on next page

continued from previous page

No.	Configuration	Correlations	Comments
13	Transitional diabatic friction factors for enhanced tubes	$f_{te} = \left(\frac{16}{Re_{Cr}}\right)^{-0.131} exp\left(-0.111\frac{Re}{Re_{Cr}}\right)\left(\frac{\beta}{90}\right)^{2.363} \times \left(\frac{e^2}{pD}\right)^{-0.313}\left(\frac{p}{D}\right)^{0.766}\left(\frac{e}{D}\right)^{0.786} \times Pr.^{0.081} Gr^{0.028}\left(\frac{\mu}{\mu_w}\right)^{-0.289}$	Valid for all inlets $2\ 105 < Re < 2\ 596$ $4.47 < Pr < 5.33$ $2.8 \times 10^5 < Gr < 4.5 \times 10^5$ $0.69 < \mu/\mu_w < 0.8$ $0.023 < e/D < 0.027$ $18^\circ < \beta < 27^\circ$ $286 < L/D < 349$

8.3 Conclusion

Smooth tube adiabatic friction factors showed that transition from laminar to turbulent flow commenced at a Reynolds number of approximately 2 200 and ended at 3 000. The different inlets, however, showed delay in transition, except for the re-entrant inlet. Transition for the square-edged inlet only occurred at a Reynolds number of approximately 2 600 and ended at 3 000, while the bellmouth inlet showed the largest delay in transition. Transition for the bellmouth, however, was dependent on the tube diameter as the larger of the two tubes tested showed a greater delay. Transition for the smaller tube started at a Reynolds number of approximately 6 700 and ended at 7 400, while for the larger tube it only started at a Reynolds number of approximately 10 400 and ended at about 15 000. The difference between these values was attributed to the construction of the bellmouth inlet and since they both had different contraction ratios, which could influence the flow at the entrance. These results are, however, in agreement with results from other researchers showing that the less the inlet disturbance, the more transition is delayed.

The transition from laminar to turbulent flow showed an increase in chaotic behaviour. This was observed from pressure fluctuations that increase in this region. These fluctuations were also dependent on the type of inlet used. Square-edged and bellmouth inlets showed the greatest amount of fluctuations when compared with the fully developed and re-entrant inlets. It was also found that the more transition was delayed, the shorter the critical region was and the greater the fluctuations were. Some bellmouth results, however, did not show this type of behaviour.

Results for the enhanced tubes showed similar trends as those for the smooth tubes regarding the different delays in transition for the different inlets. Transition, however, occurred at slightly lower Reynolds numbers than those for the smooth tubes. This was attributed to the tube roughness with the helix angle having no effect whatsoever. The enhanced tubes did show an overall increase in friction factor; laminar friction factors were higher than those for the smooth tube attributed to the increase in roughness the fins impose. The helix angle had no effect in this increase.

The turbulent results, after transition, had the shape of an elongated s-curve with respect to the Reynolds number, deviating away from the smooth tube results with ever-increasing values. This was termed the 'secondary transition', although, unlike the flow in the critical region, the secondary transition did not have a chaotic behaviour. In fact, it was very smooth, as if the flow were in the fully turbulent regime. This secondary transition was attributed to the velocity of the fluid being high enough such that the helical fins of the tube start to become effective in spinning the fluid. This spinning becomes more intense as the fluid velocity is increased. For all the enhanced tubes, this secondary transition stopped around a Reynolds number of 10 000, for which a constant decrease in friction factor was observed for ever-increasing Reynolds numbers. The secondary transition friction factors as well as the fully turbulent friction factors were strongly dependent on the helix angle, with the greater helix angle giving higher values.

Heat transfer results were different with regard to transition. For all the inlets, tube geome-

tries and tube enhancements, transition commenced at a Reynolds number of approximately 2 000 and ended at 3 000. Only the bellmouth inlet of the bigger diameter tube showed a slight delay in transition, but it was not substantial. This phenomenon is attributed to the buoyancy-induced secondary flow which occurred inside the tube. Tubes with relatively low Prandtl numbers, such as water, are susceptible to these secondary flow patterns with regard to the transition region.

The secondary flow effects were also noticed in the laminar region, with results being substantially higher than those for pure forced convection. This is due to the mixing the secondary flow induces inside the tube, enhancing the heat transfer process. The laminar region also looks like an extension of the turbulent results with transition simply being a slight change in the slope with regard to the Reynolds number.

Fluctuations of the heat transfer coefficient in the critical region were also observed. This confirmed the start and end of transition being the same for all the inlets and tubes. The origin of these fluctuation, however, arose from the outlet fluid temperature. On closer inspection, it was found that all the wall temperatures fluctuated, although to a lesser degree. These fluctuations were smaller than the outlet fluid temperature due to them being suppressed by the annulus fluid. Uniform heat flux experiments should expose these wall temperature fluctuations.

Heat transfer results for the enhanced tubes also showed higher values than their smooth tube counterparts. For Reynolds numbers greater than 3 000, but less than 10 000, the Nusselt numbers increase at a much greater rate than for those of the smooth tube. Only after a Reynolds number of 10 000 does this rate decrease to rates similar to that of the smooth tube. The region between a Reynolds number of 3 000 and 10 000 is due to the secondary transition which was initially observed in the adiabatic friction factor results. The increase in Nusselt numbers in this region is thus attributed to the amount of spin the fins induce on the fluid, which is a function of the velocity of the fluid.

Enhanced tube laminar results, however, show a slight decrease in value when compared with the smooth tube results. This was due to the fins disrupting the path of the secondary flow patterns, which in turn reduced the amount of mixing. This was also reflected in the $GrPr$ product, which had lower values than its smooth tube counterparts. The helix angle in the laminar flow region has no effect on the spin of the fluid due to the fluid velocities being too low and hence having no enhancement effect.

Diabatic friction factor results confirmed all the heat transfer results with regard to the start and end of the transition region. This confirmation was obtained from the friction factor fluctuations, corresponding to the heat transfer coefficient fluctuations. These results also confirmed the fact that transition commenced at the same Reynolds number irrespective of the inlet type or tube enhancement. Laminar diabatic friction factors were, however, much higher than their adiabatic counterparts. These diabatic values were up to 40% higher than the adiabatic ones, being attributed to the secondary flow effects. Turbulent flow friction factors were unaffected by the secondary flow effect. The only influence on the turbulent friction factors was the difference in bulk-to-wall viscosity, which was corrected. This correction is a well-known

means in better predicting turbulent diabatic friction factors with adiabatic correlations.

The enhanced tube diabatic friction factors showed similar results with regard to the secondary transition region of their adiabatic counterparts. The turbulent friction factors were also a strong function of the helix angle, with the greater helix angle giving the highest friction factor values. Tube diameters had no effect on the friction factor values in the turbulent regime since the relative roughness of both diameter tubes were the same.

Throughout all the test data were captured in increments of increasing and decreasing Reynolds numbers. This was to investigate hysteresis. Since no difference between the two sets were observed in the transition region concludes that there is no hysteresis.

Lastly, a performance evaluation of the enhanced tubes was performed. By selecting a numerous number of criteria, it was found that enhanced tubes only became viable when smooth tube Reynolds numbers were higher than 6 000. The performance of all the criteria peaked at a smooth tube Reynolds number of around 10 000, after which it started to deteriorate. No performance enhancement was found in the transition region. This was mainly due to the fact that the diabatic instead of the adiabatic friction factors were used for the evaluation. It was further found that the tube with the greatest helix angle gave the best performance.

8.4 Future Work

Although an extensive amount of work was covered within this document, some questions are still unanswered. Thus, future recommended work should include the following:

- Heat transfer results showed that within the critical region, the wall and fluid outlet temperatures fluctuate. This should be investigated more closely as this could give an indication of where transition occurs within the length of the tube. One way of observing this would be to make use of a uniform heat flux boundary layer by means of a heating blanket. This should then eliminate the annulus fluid, which suppresses the wall temperature fluctuations.

- Only one fluid, namely water, was investigated. To fully understand the transition effects, other fluids, or rather different Prandtl numbers, should be investigated. These results could possibly show that, for other fluids, transition during heat transfer for different inlet profiles does actually vary, unlike for water. It would also be more useful for designers as the correlations would be valid for a greater range of fluids.

- A greater range of diameters should be investigated within the laminar regime as secondary flow effects are stronger for larger-diameter tubes.

- A wider range of enhanced tubes should also be investigated as this would add valuable information to the database for researchers to use.

References

Abu-Eishah, S.I. 2001. Correlations for the Thermal Conductivity of Metals as a Function of Temperature. *International Journal of Thermophysics*, **22**(6), 1855–1868.

Al-Fahed, S.F., Ayub, Z.H., Al-Marafie, A.M., and Soliman, B.M. 1993. Heat Transfer and Pressure Drop in a Tube with Internal Microfins under Turbulent Water Flow Conditions. *Experimental Thermal and Fluid Science*, **7**, 249–253.

Al-Fahed, S.F., Chamra, L.M., and Chakroun, W. 1999. Pressure Drop and Heat Transfer Comparison for both Microfin Tube and Twisted-Tape Inserts in Laminar Flow. *Experimental Thermal and Fluid Science*, **18**, 323–333.

Allen, R.W., and Eckert, E.R.G. 1964. Friction and Heat-Transfer Measurements to Turbulent Pipe Flow of Water (Pr=7 and 8) at Uniform Wall Heat Flux. *Journal of Heat Transfer*, **86**, 301–310.

Bandyopadhyay, P.S., Gaitonde, U.N., and Sukhatme, S.P. 1991. Influence of Free Convection on Heat Transfer during Laminar Flow in Tubes with Twisted Tapes. *Experimental Thermal and Fluid Science*, **4**, 577–586.

Bergles, A.E., Blumenkrantz, A.R., and Taborek, J. 1974. Performance Evaluation Criteria for Enhanced Heat Transfer Surfaces. *Pages 239–243 of: Proceedings of the International Centre for Heat and Mass Transfer*, vol. 2.

Binnie, A.M. 1945. A Double-Refraction Method of Detecting Turbulence in Liquids. *Proceedings of the Physical Society*, **57**(5), 390–402.

Briggs, D.E., and Young, E.H. 1969. Modified Wilson Plot Techniques for Obtaining Heat Transfer Correlations for Shell and Tube Heat Exchangers. *Chemical Engineering Progress Symposium Series*, **65**(92).

Brognaux, L.J., Webb, R.L., Chamra, L.M., and Chung, B.Y. 1997. Single-phase Heat Transfer in Micro-fin Tubes. *International Journal of Heat and Mass Transfer*, **40**(18), 4345–4357.

Brown, A.R., and Thomas, M.A. 1965. Combined Free and Forced Convection Heat Transfer for Laminar Flow in Horizontal Tubes. *Journal of Mechanical Engineering Science*, **7**, 440–448.

Carnavos, T.C. 1980. Heat Transfer Performance of Internally Finned Tubes in Turbulent Flow. *Heat Transfer Engineering*, **1**(4), 32–37.

Chiou, C.B., Wang, C.C., and Lu, D.C. 1995. Single-phase Heat Transfer and Pressure Drop Characteristics of Microfin Tubes. *ASHRAE Transactions: Symposia*, **11**(1), 1041–1048.

Churchill, S.W. 1977. Comprehensive Correlating Equations for Heat, Mass and Momentum Transfer in Fully Developed Flow in Smooth Tubes. *Industrial and Engineering Chemistry Fundamentals*, **16**, 109–116.

Churchill, S.W., and Usagi, R. 1972. A General Expression for the Correlation of Rates of Transfer and other Phenomena. *Journal of the American Institute for Chemical Engineers*, **18**, 1121–1128.

Colburn, A.P. 1933. A Method of Correlating Forced Convection Heat Transfer Data and a Comparison with Fluid Friction. *Transactions of the American Institute for Chemical Engineers*, **29**, 174–210.

Copetti, J.B., Macagnan, M.H., De Souza, D., and De Césaro Oliveski, R. 2004. Experiments with Micro-fin Tube in Single Phase. *International Journal of Refrigeration*, **27**(8), 876–883.

Depew, C.A., and August, S.E. 1971. Heat Transfer due to Combined Free and Forced Convection in a Horizontal and Isothermal Tube. *Journal of Heat Transfer*, **93**, 380–384.

Dittus, F.W., and Boelter, L.M.K. 1985. Heat Transfer in Automobile Radiators of the Tubular Type. *International Communication in Heat and Mass Transfer*, **12**(1), 3–22. Reprint of Dittus, F.W. and Boelter, L.M.K., 1930, University of California Publications in Engineering, **2**(13), 443–461.

Dobson, M.K. 1994. *Heat Transfer and Flow Regimes During Condensation in Horizontal Tubes*. Ph.D. thesis, University of Illinois at Urbana-Champaign.

Durst, F., Ray, S., Ünsal, B., and Bayoumi, O.A. 2005. The Development Lengths of Laminar Pipe and Channel Flows. *Journal of Fluids Engineering*, **127**, 1154–1160.

Ede, A.J. 1961. The Heat Transfer Coefficient for Flow in a Pipe. *International Journal of Heat and Mass Transfer*, **4**, 105–110.

Eiamsa-ard, S., and Promvonge, P. 2006. Experimental Investigation of Heat Transfer and Friction Characteristics in a Circular Tube Fitted with V-Nozzle Turbulators. *International Communication in Heat and Mass Transfer*, **33**, 591–600.

ESDU. 1993. *Forced Convection Heat Transfer in Straight Tubes Part 2: Laminar and Transitional Flow*. Tech. rept. 93018. Engineering Sciences Data Unit.

Galaktionov, O.S., Anderson, P.D., Peters, G.W.M., and Meijer, H.E.H. 2003. Analysis and Optimization of Kenics Mixers. *International Polymer Processing*, **2**, 138–150.

García, A., Vicente, P.G., and Viedma, A. 2005. Experimental Study of Heat Transfer Enhancement with Wire Coil Inserts in Laminar-Transition-Turbulent Regimes at Different Prandtl Numbers. *International Journal of Heat and Mass Transfer*, **48**, 4640–4651.

García, A., Solana, J.P., Vicente, P.G., and Viedma, A. 2007a. Enhancement of Laminar and Transitional Flow Heat Transfer in Tubes by Means of Wire Coil Inserts. *International Journal of Heat and Mass Transfer*, **50**, 3176–3189.

García, A., Solana, J.P., Vicente, P.G., and Viedma, A. 2007b. Flow Pattern Assessment in Tubes with Wire Coil Inserts in Laminar and Transition Regimes. *International Journal of Heat and Fluid Flow*, **28**, 516–525.

Ghajar, A.J., and Madon, K.F. 1992. Pressure Drop Measurements in the Transition Region for a Circular Tube with Three Different Inlet Configurations. *Experimental Thermal and Fluid Science*, **5**, 129–135.

Ghajar, A.J., and Tam, L. 1994. Heat Transfer Measurements and Correlations in the Transition Region for a Circular Tube with Three Different Inlet Configurations. *Experimental Thermal and Fluid Science*, **8**, 79–90.

Ghajar, A.J., and Tam, L. 1995. Flow Regime Map for a Horizontal Pipe with Uniform Wall Heat Flux and Three Inlet Configurations. *Experimental Thermal and Fluid Science*, **10**, 287–297.

Ghajar, A.J., and Tam, L.M. 1991. Laminar-Transition-Turbulent Forced and Mixed Convective Heat Transfer Correlations for Pipe Flows with Different Inlet Configurations. *HTD, Fundamentals of Forced Convective Heat Transfer, ASME*, **181**, 15–23.

Ghajar, A.J., and Zurigat, Y.H. 1990. Microcomputer-Assisted Heat Transfer Measurement/Analysis in a Circular Tube. *International Journal of Applied Engineering Education*, **7**(2), 125–134.

Ghajar, A.J., Tam, L., and Tam, S.C. 2004. Improved Heat Transfer Correlation in the Transition Region for a Circular Tube with Three Inlet Configurations Using Artificial Neural Networks. *Heat Transfer Engineering*, **2**(25), 30–40.

Gnielinski, V. 1976. New Equation for Heat and Mass Transfer in Turbulent Pipe and Channel Flow. *International Chemical Engineering*, **16**, 359–368.

Han, D.H., and Lee, K. 2005. Single-phase Heat Transfer and Flow Characteristics of Micro-fin Tubes. *Applied Thermal Engineering*, **25**, 1657–1669.

Hrycak, P., and Andrushkiw, R. 1974. Calculation of Critical Reynolds numbers in Round Pipes and Infinite Channels and Heat Transfer in Transition Region. *Pages 183–187 of: Heat Transfer 1974; Proceedings of the Fifth International Conference, Tokyo, Japan, September 3-7, 1974*, vol. 2.

IAPWS. 2003. *Uncertainties in Enthalpy for the IAPWS Formulation 1995 for the Thermodynamic Properties of Ordinary Water Substance for General and Scientific Use (IAPWS-95) and the IAPWS Industrial Formulation 1997 for the Thermodynamic Properties of Water and Steam (IAPWS-IF97), Advisory Note No 1.* Tech. rept. International Association for the Properties of Water and Steam.

Jackson, T.W., Spurlock, J.M., and Purdy, K.R. 1961. Combined Free and Forced Convection in a Constant Temperature Horizontal Tube. *Journal of the American Institute for Chemical Engineers*, **7**(1), 61–41.

Jensen, M.K., and Vlakancic, A. 1999. Experimental Investigation of Turbulent Heat Transfer and Fluid Flow in Internally Finned Tubes. *International Journal of Heat and Mass Transfer*, **42**, 1343–1351.

Kakaç, S., Shah, R.K., and Aung, W. 1987. *Handbook of Single-Phase Convective Heat Transfer*. New York: Wiley. Chap. 16.

Kalinin, E.K., and Yarkho, S.A. 1966. Flow Pulsations and Heat Transfer in the Transition Region between the Laminar and Turbulent Regimes in a Tube. *International Chemical Engineering*, **6**(4), 571–574.

Kern, D.Q., and Othmer, D.F. 1943. Effect of Free Convection on Viscous Heat Transfer in Horizontal Tubes. *Transactions of the Journal of the American Institute for Chemical Engineers*, **39**, 517–555.

Kline, S.J., and McClintock, F.A. 1953. Describing Uncertainties in Single-Sample Experiments. *Mechanical Engineering*, **75**, 3–8.

Koch, R. 1960. Pressure Loss and Heat Transfer for Turbulent Flow. *Atomic Energy Commission Translation Series*, **3875**, 1–135.

Lambrechts, A. 2003. *Heat Transfer Performance during In-tube Condensation in Horizontal Smooth, Micro-fin and Herringbone Tubes*. M.Eng. dissertation, University of Johannesburg.

Lienhard, J.H., and Lienhard, J.H. 2003. *A Heat Transfer Text Book*. Third edn. Cambridge: Phlogiston Press.

Lindgren, E.R. 1953. Some Aspects of the Change between Laminar and Turbulent Flow of Liquids in Cylindrical Tubes. *Arkiv för Fysik*, **7**(23), 293–308.

Manglik, R.M., and Bergles, A.E. 1993. Heat Transfer and Pressure Drop Correlations for Twisted-Tape Inserts in Isothermal Tubes: Part 1 - Laminar Flows. *Journal of Heat Transfer*, **115**, 881–889.

Marner, W.J., and Bergles, A.E. 1989. Augmentation of Highly Viscous Laminar Heat Transfer Inside Tubes with Constant Wall Temperature. *Experimental Thermal and Fluid Science*, **2**, 252–267.

Marner, W.J., Bergles, A.E., and Chenoweth, J.M. 1983. On the Presentation of Performance Data for Enhanced Tubes used in Shell-and-Tube Heat Exchangers. *Journal of Heat Transfer*, **105**, 358–365.

Martinelli, R.C., and Boelter, L.M.K. 1942. The Analytical Prediciton of Superposed Free and Forced Viscous Convection in a Vertical Pipe. *University of California Publications in Engineering*, **5**(2), 23.

Metais, B., and Eckert, E.R.G. 1964. Forced, Mixed and Free Convection Regimes. *Transactions of the ASME Journal of Heat Transfer*, **10**, 295–296.

Mikesell, R.D. 1963. *The Effects of Heat Transfer on the Flow in a Horizontal Pipe*. Ph.D. thesis, Chemical Engineering Department, University of Illinois.

Mills, A.F. 1999. *Heat Transfer*. Second edn. New Jersey: Prentice-Hall.

Moffat, R.J. 1988. Describing the Uncertainties in Experimental Results. *Experimental Thermal and Fluid Science*, **1**, 3–17.

Moffat, R.J. 2000. *Experimental Methods in Heat Transfer*. June 2000 edn. California: Moffat Thermosciences, Inc.

Morel, T. 1975. Comprehensive Design of Axisymmetric Wind Tunnel Contractions. *Journal of Fluids Engineering*, **97**(2), 225–233.

Mori, Y., Futagami, K., Tokuda, S., and Nakamura, M. 1966. Forced Convective Heat Transfer in Uniformly Heated Horizontal Tubes. *International Journal of Heat and Mass Transfer*, **9**, 453–463.

Mullin, T., and Peixinho, J. 2006. Recent Observations of the Transition to Turbulence in a Pipe. *Pages 45–55 of: Sixth IUTAM Symposium on Laminar-Turbulent Transition*. Fluid Mechanics and its Applications, vol. 78Springer, for IUTAM.

Nagendra, H.R. 1973. Interaction of Free and Forced Convection in Horizontal Tubes in the Transition Regime. *Journal of Fluid Mechanics*, **57**, 269–288.

Nicholas, J.V., and White, D.R. 1982. *Traceable Temperatures*. Wellington: Science Information Division.

Nunner, W. 1956. Heat Transfer and Pressure Drop in Rough Tubes. *VDI-Forschungsheft*, **455-B**, 5–39.

Obot, N.T., Esen, E.B., and Rabas, T.J. 1990. The role of Transition in Determining Friction and Heat Transfer in Smooth and Rough Passages. *International Journal of Heat and Mass Transfer*, **33**(10), 2133–2143.

Oliver, D.R. 1962. The Effect of Natural Convection on Viscous-flow Heat Transfer in Horizontal Tubes. *Chemical Engineering Science*, **17**, 335–350.

Palen, J.W., and Taborek, J. 1985. An Improved Heat Transfer Correlation for Laminar Flow of High Prandtl Number Liquids in Horizontal Tubes. *AIChE Symposium Series*, **81**(245), 90–96.

Patel, V.C., and Head, M.R. 1968. Reversion of Turbulent to Laminar Flow. *Journal of Fluid Mechanics*, **34**, 371–392.

Patel, V.C., and Head, M.R. 1969. Some Observations on Skin Friction and Velocity Profiles in Fully Developed Pipe and Channel Flows. *Journal of Fluid Mechanics*, **38**, 181–201.

Petersen, A.W., and Christiansen, E.B. 1966. Heat Transfer to Non-Newtonian Fluids in Transitional and Turbulent Flow. *Journal of the American Institute for Chemical Engineers*, **12**(2), 221–232.

Petukhov, B.S., and Popov, V.N. 1963. Theoretical Calculation of Heat Exchange and Frictional Resistance in Turbulent Flow in Tubes of an Incompressible Fluid with Variable Physical Properties. *Teplofizika Vysokikh Temperatur*, **1**(1), 85–101.

Petukhov, B.S., Polyakov, A.F., and Strigin, B.K. 1969. Heat Transfer in Tubes with Viscous-Gravity Flow. *Heat Transfer - Soviet Research*, **1**(1), 24–31.

Ravigururajan, T.S., and Bergles, A.E. 1996. Development and Verification of General Correlations for Pressure Drop and Heat Transfer in Single-Phase Turbulent Flow in Enhanced Tubes. *Experimental Thermal and Fluid Sciences*, **13**, 55–70.

Rayle, R.E. 1959. Influence of Orifice Geometry on Static Pressure Measurements. *ASME Paper No. 59-A-234*.

Reynolds, O. 1883. On the Experimental Investigation of the Circumstances which Determine whether the Motion of Water shall be Direct or Sinuous, and the Law of Resistance in Parallel Channels. *Philosophical Transactions of the Royal Society of London Series A–Mathematical and Physical Sciences*, **174**, 935–982.

Saha, S.K., Dutta, A., and Dhal, S.K. 2001. Friction and Heat Transfer Characteristics of Laminar Swirl Flow through a Circular Tube Fitted with Regularly Spaced Twisted-tape Elements. *International Journal of Heat and Mass Transfer*, **44**, 4211–4223.

Said, M.N.A., and Trupp, A.C. 1984. Predictions of Turbulent Flow and Heat Transfer in Internally Finned Tubes. *Chemical Engineering Communications*, **31**, 65–99.

Senecal, V.E., and Rothfus, R.R. 1953. Transition Flow of Fluids in Smooth Tubes. *Chemical Engineering Progress*, **49**, 533–538.

Sethumadhavan, R., and Raja Rao, M. 1986. Turbulent Flow Friction and Heat Transfer Characteristics of Single- and Multistart Spirally Enhanced Tubes. *Journal of Heat Transfer*, **108**, 55–61.

Shah, R.K. 1978. A Correlation for Laminar Hydrodynamic Entry Length Solutions for Circular and Noncircular Ducts. *Journal of Fluids Engineering*, **100**, 177–179.

Shah, R.K. 1990. Assessment of Modified Wilson Plot Techniques for Obtaining Heat Exchanger Design Data. *Pages 51–56 of: 9th International Heat Transfer Conference.*

Shah, R.K., and London, A.L. 1978. *Laminar Flow Forced Convection in Ducts.* New York: Academic Press.

Shah, R.K., and Seculić, D.P. 2003. *Fundamentals of Heat Exchanger Design.* New Jersey: John Wiley and Sons Inc.

Shannon, R.L., and Depew, C.A. 1969. Forced Laminar Flow Convection in a Horizontal Tube with Variable Viscosity and Free-Convection Effects. *Journal of Heat Transfer*, **91**, 251–258.

Shome, B., and Jensen, M.K. 1995. Mixed Convection Laminar Flow and Heat Transfer of Liquids in Isothermal Horizontal Circular Ducts. *International Journal of Heat and Mass Transfer*, **38**(11), 1945–1956.

Sieder, E.N., and Tate, G.E. 1936. Heat Transfer and Pressure Drop in Liquids in Tubes. *Industrial and Engineering Chemistry*, **28**(12), 1429–1435.

Sivashanmugam, P., and Nagarajan, P.K. 2007. Studies on Heat Transfer and Friction Factor Characteristics of Laminar Flow through a Circular Tube Fitted with Right and Left Helical Screw-tape Inserts. *Experimental Thermal and Fluid Science*, **32**(1), 192–197.

Sivashanmugam, P., and Suresh, S. 2006. Experimental Studies on Heat Transfer and Friction Factor Characteristics of Laminar Flow through a Circular Tube Fitted with Helical Screw-tape Inserts. *Applied Thermal Engineering*, **26**, 1990–1997.

Smith, A.M.O. 1960. Remarks on Transition in a Round Tube. *Journal of Fluid Mechanics*, **7**(4), 565–576.

Takahashi, K., Nakayama, W., and Kuwahara, H. 1988. Enhancement of Forced Convective Heat Transfer in Tubes having Three-Dimensional Spiral Ribs. *Heat Transfer - Japanese Research*, **17**(4), 12–28.

Tam, L., and Ghajar, A.J. 1997. Effect of Inlet Geometry and Heating on the Fully Developed Friction Factor in the Transition Region of a Horizontal Tube. *Experimental Thermal and Fluid Science*, **15**, 52–64.

Tam, L., and Ghajar, A.J. 1998. The Unusual Behavior of Local Heat Transfer Coefficient in a Circular Tube with a Bell-Mouth Inlet. *Experimental Thermal and Fluid Science*, **16**, 187–194.

Tam, L., and Ghajar, A.J. 2006. Transitional Heat Transfer in Plain Horizontal Tubes. *Heat Transfer Engineering*, **5**(27), 23–38.

Tam, L., Ghajar, A.J., and Tam, H. 2008. Contribution Analysis of Dimensionless Variables for Laminar and Turbulent Flow Convection Heat Transfer in a Horizontal Tube using Artificial Neural Networks. *Heat Transfer Engineering*, **9**(29), 793–804.

Tatsumi, T. 1952. Stability of the Laminar Inlet-flow priorto the Formation of Poiseuille Regime, II. *Journal of the Physical Society of Japan*, **7**(5), 495–502.

Tijing, L.D., Pak, B.C., Baek, B.J., and Lee, D.H. 2006. A Study on Heat Transfer Enhancement using Straight and Twisted Internal Fin Inserts. *International Communication in Heat and Mass Transfer*, **33**, 719–726.

Vicente, P.G., García, A., and Viedma, A. 2002a. Experimental Study of Mixed Convection and Pressure Drop in Helically Dimpled Tubes for Laminar and Transition Flow. *International Journal of Heat and Mass Transfer*, **45**, 5091–5105.

Vicente, P.G., García, A., and Viedma, A. 2002b. Heat Transfer and Pressure Drop for Low Reynolds Turbulent Flow in Helically Dimpled Tubes. *International Journal of Heat and Mass Transfer*, **45**, 543–553.

Vicente, P.G., García, A., and Viedma, A. 2004. Mixed Convection Heat Transfer and Isothermal Pressure Drop in Corrugated Tubes for Laminar and Transition Flow. *International Communication in Heat and Mass Transfer*, **31**(5), 651–662.

Wagner, W., and Pruß, A. 2002. The IAPWS Formulation 1995 for the Thermodynamic Properties of Ordinary Water Substance for General and Scientific Use. *Journal of Physical and Chemical Reference Data*, **31**(2), 387–535.

Wang, C.C., C.B., Chiou., and Lu, D.C. 1996. Single-phase Heat Transfer and Flow Friction Correlations for Microfin Tubes. *International Journal of Heat and Fluid Flow*, **17**, 500–508.

Wang, H.S., and Rose, J.W. 2004. Prediction of Effective Friction Factors for Single-phase Flow in Horizontal Microfin Tubes. *International Journal of Refrigeration*, **27**, 904–913.

Watkinson, A.P., Miletti, D.L., and Tarassoff, P. 1972. Turbulent Heat Transfer and Pressure Drop in Internally Finned Tubes. *AIChE Symposium*, **69**(131), 94–103.

Webb, R.L. 1981. Performance Evaluation Criteria for use of Enhanced Heat Transfer Surfaces in Heat Exchanger Design. *International Journal of Heat and Mass Transfer*, **24**(4), 715–726.

Webb, R.L. 1994. *Principles of Enhanced Heat Transfer*. New York: John Wiley & Sons, Inc.

White, F.M. 1991. *Viscous Fluid Flow*. Second edn. Singapore: McGraw-Hill, Inc.

Wilson, E.E. 1915. A Basis for Rational Design of Heat Transfer Apparatus. *Transaction of the ASME*, **37**, 47–70.

Withers, J.G. 1980a. Tube-Side Heat Transfer and Pressure Drop for Tubes having Helical Internal Ridging with Turbulent/Transitional Flow of Single-Phase Fluid. Part 1. Single-Helix Ridging. *Heat Transfer Engineering*, **2**(1), 48–58.

Withers, J.G. 1980b. Tube-Side Heat Transfer and Pressure Drop for Tubes having Helical Internal Ridging with Turbulent/Transitional Flow of Single-Phase Fluid. Part 2. Multiple-Helix Ridging. *Heat Transfer Engineering*, **2**(2), 43–50.

Yousef, W.W., and Tarasuk, J.D. 1982. Free Convection Effects on Laminar Forced Convective Heat Transfer in a Horizontal Isothermal Tube. *Journal of Heat Transfer*, **104**, 145–152.

Appendix A

Calculation of Enhanced Tube Areas

A.1 Introduction

For calculation purposes it is of interest to know what the cross-sectional and heat transfer surface areas inside an enhanced tube are. This appendix contains the details taken from Lambrechts (2003) explaining the method used in determining these two parameters.

A.2 Cross-Sectional and Heat Transfer Surface Areas

A section of the actual cross-sectional area of the enhanced tube is shown in Figure A.1.a) with a simplified version in Figure A.1.b). Thus, the original trapezoidal fin is simplified to a triangular fin by assuming that the area lost at the top of the fin (marked as A_1 and A_2) is equal to the area gained at the base of the fin.

Thus, from Figure A.1.c), the heat transfer surface area of the enhanced tube with a heat transfer length of L is calculated by taking the contact area of the maximum inside diameter A_x of the enhanced tube, subtracting the contact area of the base thickness of the fins A_y and adding the contact areas from the sides of the fin A_z. The heat transfer surface area of the enhanced tube is then given as

$$A_e = A_x - A_y + A_z \tag{A.1}$$

where

$$A_x = \pi d_r L \tag{A.2}$$

and

$$\begin{aligned} A_y &= 2nyl \\ &= 2neL\tan(\gamma/2) \end{aligned} \tag{A.3}$$

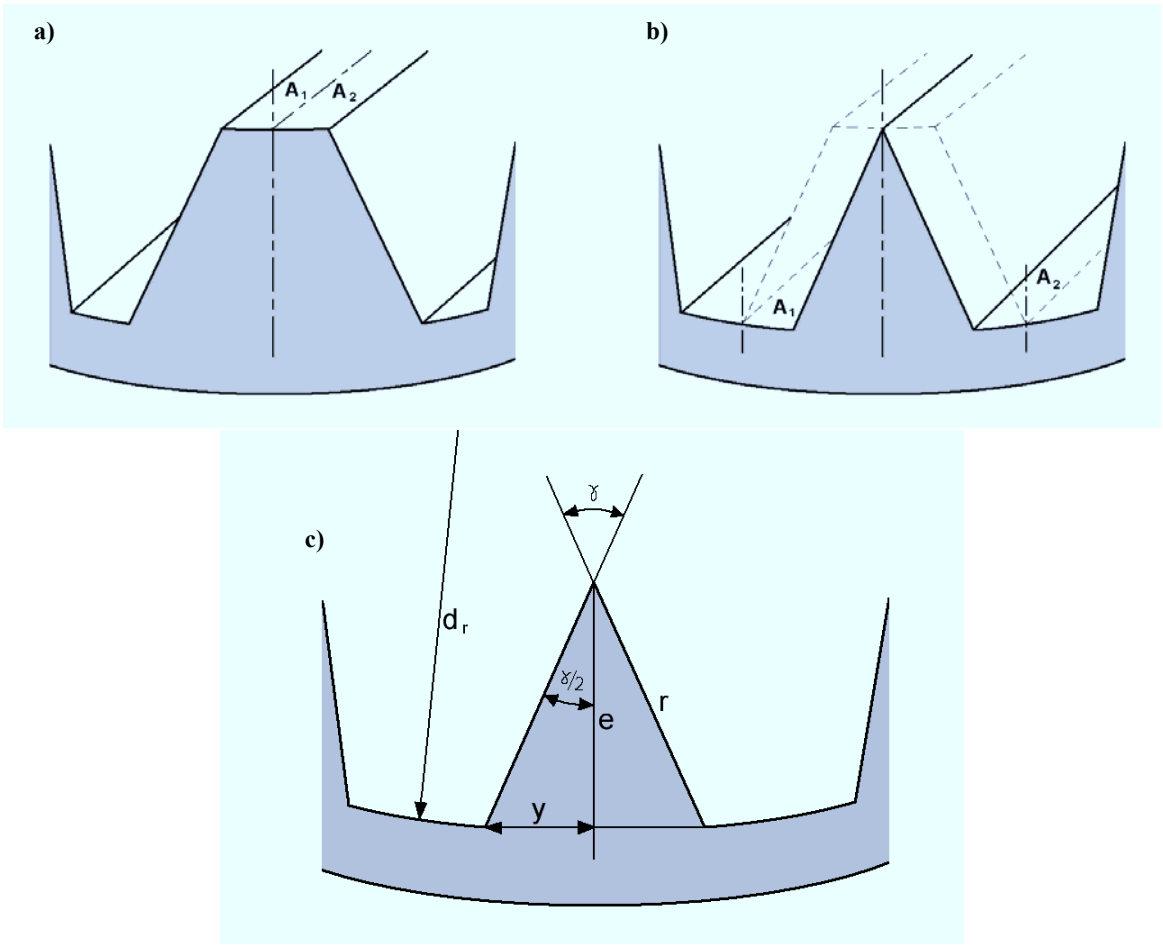

Figure A.1 a) Actual enhanced tube cross sectional area b) Simplified cross sectional area enhanced tube c) Detailed simplified cross sectional area (from Lambrechts (2003)).

and

$$\begin{aligned} A_z &= 2nerL \\ &= 2neL\sec(\gamma/2) \end{aligned} \tag{A.4}$$

The assumption made here is that the base of the fin is a straight line since its length is small compared to the perimeter of the tube.

Thus, from Equations (A.1) to (A.4)

$$\begin{aligned} A_e &= \pi d_r L - 2neL\tan(\gamma/2) + 2neL\sec(\gamma/2) \\ &= \pi d_r L + \frac{2neL}{\cos(\gamma/2)}(1-\sin(\gamma/2)) \end{aligned} \tag{A.5}$$

The same can be done for calculating the actual cross-sectional area by subtracting the cross-sectional area occupied by the fins from the maximum cross-sectional area (based on the root/nominal diameter). Thus,

$$A_{ce} = \frac{\pi}{4}d_r^2 - e^2 n\tan(\gamma/2) \tag{A.6}$$

Appendix B

Uncertainty Analysis

B.1 Introduction

To achieve the main objectives of this study, it was necessary to obtain inner-tube heat transfer and frictional coefficients. Therefore, a full uncertainty analysis was performed for these two parameters as well as for the non-dimensional parameters such as Reynolds and Nusselt numbers. Part of obtaining the heat transfer coefficient was the determination of the heat transferred, the energy balance obtained, wall temperature measurements and inlet and outlet temperatures, all of which will be analysed. For the friction factors, the main uncertainty would be from the differential pressure transducer and will be analysed accordingly.

B.2 Theory

Two components are generally regarded when it comes to uncertainty in a measurement: a fixed error and a random error. These errors are also called the bias, B, and the precision, P, respectively (Moffat, 1988).

Fixed errors, or bias, are errors that are repeatable and can in principle be accounted for. These errors arise from calibration, imperfection in the measuring equipment, theory, incorrect assumptions, etc. Random errors, or precision, are always present and arise from variations in the measurement process, electrical noise, changes in the measuring equipment, etc. (Nicholas and White, 1982). The magnitudes of the bias and precision errors will correspond to the 95% probability that the actual error will not be more than the estimate.

The uncertainty in a single measurement is given by:

$$\delta x_i = \left\{ (B_i)^2 + (P_i)^2 \right\}^{1/2} \tag{B.1}$$

x_i is a single observation and δx_i represents 2σ, with σ being the standard deviation.

The result R of an experiment is normally calculated from a set of measurements using a group of equations. Thus, the result R is a function of several variables and is given as (Moffat,

1988):

$$R = R\left(x_1, x_2, \ldots, x_n\right) \tag{B.2}$$

Assuming that the uncertainties of x_i are known, the uncertainty in R can be determined by

$$\delta R = \frac{\partial R}{\partial x_i}\delta x_i \tag{B.3}$$

The partial derivative of R is called the *sensitivity coefficient* of the result R with respect to x_i. The sensitivity coefficient is the effect that the uncertainty of a single measurement, with the measurement being in error, has on the overall uncertainty of the result. For several independent variables, the uncertainty of R can be found by means of the root sum squared method. This method has the effect of suppressing terms which are smaller than a third of the largest term. Thus, for several independent variables, the uncertainty of R is described by Moffat (1988) as:

$$\delta R = \left\{ \left(\frac{\partial R}{\partial x_1}\right)^2 \delta x_1 + \left(\frac{\partial R}{\partial x_2}\right)^2 \delta x_2 + \ldots + \left(\frac{\partial R}{\partial x_n}\right)^2 \delta x_n \right\} \tag{B.4}$$

Each term represents the contribution made by the uncertainty in one variable to the overall uncertainty in the result (Moffat, 1988).

B.3 Uncertainties

Instruments

Each of the three types of instruments used (thermocouples, Coriolis flow metres and pressure transducers) had a manufacturer-specified accuracy which was used as the bias. To obtain the precision of the instruments, 400 samples were captured, averaged and the standard deviation multiplied by two to fall within the 95% confidence region. Table B.1 shows the instruments with their ranges, bias, precision and total uncertainty obtained by using Equation (B.1).

B.3.1 Analysis

For this analysis, the two extremities of the flow were considered; the highest and the lowest flow rates. The lowest flow rates corresponded to an inner-tube Reynolds number of approximately 500, while the highest flow rate corresponded to an inner-tube Reynolds number of approximately 20 000. Further, the uncertainties of two of the methods used to calculate heat transfer coefficients will be calculated; one for the *LMTD* method and the other for the *Single-Stream Exchanger* method.

Table B.1 Ranges and accuracies of instruments to be used.

Instrument	Range	Bias	Precision	Uncertainty
Thermocouple	$-200 - 350$ °C	0.1 °C[a]	0.023°C	0.103°C
Coriolis Flow Meter				
Inner-Tube High	$0 - 0.667$ kg/s	0.1%	0.06%	0.117%
Inner-Tube Low	$0 - 0.04$ kg/s	0.1%	0.08%	0.131%
Annulus	$0 - 1.8$ kg/s	0.1%	0.02%	0.102%
Pressure Transducers				
Transducer 1	Diaphragm Selection[b]	0.25%FS[c]	0.9%	0.93%
Transducer 2	0-7 kPa	0.1%FS	1.6%	1.6%

[a] Calibrated with a Pt-100 which had an uncertainty of 0.01°C.

[b] This pressure transducer has multiple diaphragms that can be changed for the desired pressure drop range.

[c] FS = Full Scale.

The layout of the analysis will be as follows: First, the uncertainties of all the measurements used to calculate the heat transfer coefficient and the dimensionless properties of the inner fluid will be determined. Secondly, the uncertainties of the actual heat transfer coefficients as defined by the above mentioned methods will be determined. Lastly, the uncertainty of the friction factor will be determined.

Heat Transfer

In- and outlet temperatures

The in- and outlet temperatures of the inner tube and the annulus consisted of three thermocouples being placed at each of these positions, all three evenly spaced around the periphery of the tube. A representative temperature is then obtained by using the average of the three thermocouples, or

$$\bar{T}_{iin} = \frac{T_{iin1} + T_{iin2} + T_{iin3}}{3} \tag{B.5}$$

with its uncertainty being calculated by

$$\delta\bar{T}_{iin} = \left[\left(\frac{\delta T_{iin1}}{3}\right)^2 + \left(\frac{\delta T_{iin2}}{3}\right)^2 + \left(\frac{\delta T_{iin3}}{3}\right)^2\right]^{1/2} \tag{B.6}$$

Since the uncertainties in each of the thermcouples are the same, Equation (B.6) can be written as

$$\delta \bar{T}_{iin} = \sqrt{\frac{1}{3}} \delta T \tag{B.7}$$

This process is exactly the same for the other in- and outlets.

Fluid properties

All fluid properties and their uncertainties were calculated from the formulations obtained from Wagner and Pruß (2002), excluding the enthalpy uncertainties which were obtained from IAPWS (2003). The uncertainties of the properties are given in Table B.2.

Table B.2 Uncertainties of fluid properties.

Property	Uncertainty
Density	0.05%
Viscosity	1.00%
Specific Heat	0.10%
Thermal Conductivity	1.00%
Enthalpy	0.10%

Heat flux

The heat flux was calculated from

$$q_i = \frac{\dot{m}_i}{A_i} \left(h_{iin} - h_{iout} \right) \tag{B.8}$$

with its uncertainty given by

$$\delta q_i = \left[\left(\frac{\partial q_i}{\partial \dot{m}_i} \delta \dot{m}_i \right)^2 + \left(\frac{\partial q_i}{\partial A_i} \delta A_i \right)^2 + \left(\frac{\partial q_i}{\partial h_{iin}} \delta h_{iin} \right)^2 + \left(\frac{\partial q_i}{\partial h_{iout}} \delta h_{iout} \right)^2 \right]^{1/2}$$

$$\delta q_i = \left[\left(\frac{\delta \dot{m}_i}{A_i} (h_{iin} - h_{iout}) \right)^2 + \left(\frac{\dot{m}_i \delta A_i}{A_i^2} (h_{iin} - h_{iout}) \right)^2 + \left(\frac{\dot{m}_i \delta h_{iin}}{A_i} \right)^2 + \left(\frac{-\dot{m}_i \delta h_{iout}}{A_i} \right)^2 \right]^{1/2} \tag{B.9}$$

Heat transfer area

The uncertainties in the heat transfer areas for the inner fluid as well as the annulus are, respectively, given by Equations (B.11) and (B.13).

$$A_i = \pi D_i L_{hx} \tag{B.10}$$

$$\delta A_i = \left[\left(\frac{\partial A_i}{\partial D_i} \delta D_i \right)^2 + \left(\frac{\partial A_i}{\partial L_{hx}} \delta L_{hx} \right)^2 \right]^{1/2}$$

$$\delta A_i = \left[(\pi L_{hx} \delta D_i)^2 + (\pi D_i \delta L_{hx})^2 \right]^{1/2} \tag{B.11}$$

$$A_o = \pi D_o L_{hx} \tag{B.12}$$

$$\delta A_o = \left[\left(\frac{\partial A_o}{\partial D_o} \delta D_o \right)^2 + \left(\frac{\partial A_o}{\partial L_{hx}} \delta L_{hx} \right)^2 \right]^{1/2}$$

$$\delta A_o = \left[(\pi L_{hx} \delta D_o)^2 + (\pi D_o \delta L_{hx})^2 \right]^{1/2} \tag{B.13}$$

Inner-tube outer-wall temperatures

The wall temperatures were measured at nine different stations, each station having four thermocouples on the outer surface of the inner tube of which the average of the four was used for each station. The uncertainty of the average temperature for each station was 0.05°C.

The average wall temperature was then obtained by making use of a second-order curve fit through all nine stations and integrating over the total length of the heat exchanger, or

$$\bar{T}_{wo} = \frac{1}{L_{hx}} \int_0^{L_{hx}} \left(a_2 x^2 + a_1 x + a_0\right) \mathrm{d}x$$
$$\bar{T}_{wo} = \frac{1}{3} a_2 L_{hx}^2 + \frac{1}{2} a_1 L_{hx} + a_0 \tag{B.14}$$

The uncertainty in this averaged wall temperature is given by

$$\delta \bar{T}_{wo} = \left[\left(\frac{\partial \bar{T}_{wo}}{\partial L_{hx}} \delta L_{hx} \right)^2 + \left(\frac{\partial \bar{T}_{wo}}{\partial a_2} \delta a_2 \right)^2 + \left(\frac{\partial \bar{T}_{wo}}{\partial a_1} \delta a_1 \right)^2 + \left(\frac{\partial \bar{T}_{wo}}{\partial a_0} \delta a_0 \right)^2 \right]^{1/2} \tag{B.15}$$

To obtain the uncertainties of the constants, a_2, a_1 and a_0, a second-order regression analysis needs to be conducted, by

$$\begin{bmatrix} \sum_i y_i \\ \sum_i y_i x_i \\ \sum_i y_i x_i^2 \end{bmatrix} = \begin{bmatrix} n & \sum_i x_i & \sum_i x_i^2 \\ \sum_i x_i & \sum_i x_i^2 & \sum_i x_i^3 \\ \sum_i x_i^2 & \sum_i x_i^3 & \sum_i x_i^4 \end{bmatrix} \begin{bmatrix} a_o \\ a_1 \\ a_2 \end{bmatrix} \tag{B.16}$$

where n is the number of data points (in this case nine points), y_i the y-values of the data (or the wall temperatures of each station) and x_i the x-values (or the measured distances of each station). This equation can be written in a more compact form as

$$Y = AX \tag{B.17}$$

The regression constants, X, can be obtained by

$$A^{-1} Y = X \tag{B.18}$$

which are all now in terms of x_i and y_i. The uncertainties of these constants can now be obtained. This, however, is a tedious exercise and will not be shown here. This process is made easier by using software (Matlab with Simulink) specifically designed to calculate these partial differential equations.

In the end, though, the resulting uncertainty in the wall temperature is given as

$$\delta \bar{T}_{wo} = 0.032^{\circ}\mathrm{C} \tag{B.19}$$

This value, however, can be improved upon by rather using the *trapezoidal rule* instead of the curve-fitting method. The trapezoidal rule in mathematical form for the average wall temperatures is given by

$$\bar{T}_{wo} = \frac{1}{16} \left[\bar{T}_{wo_1} + 2\bar{T}_{wo_2} + \ldots + 2\bar{T}_{wo_8} + \bar{T}_{wo_9} \right] \tag{B.20}$$

where $\bar{T}_{wo_{1\ldots9}}$ are the average wall temperatures at each station. The uncertainty in the average wall temperature is then given by

$$\delta\bar{T}_{wo} = \left[\frac{1}{256}\left(\delta\bar{T}^2_{wo_1} + \delta\bar{T}^2_{wo_9}\right) + \frac{1}{64}\left(\delta\bar{T}^2_{wo_2} + \ldots + \delta\bar{T}^2_{wo_8}\right)\right]^{1/2} \tag{B.21}$$

By using this method, the uncertainty in the average wall temperature becomes 0.008°C, almost an order of magnitude improvement. The difference in the physical temperature value is at most less than 0.04°C.

Thermal conductivity

To obtain the inner-wall temperature of the inner tube, the thermal conductivity of the tube needs to be known. For a copper tube, the thermal conductivity is given by Abu-Eishah (2001) as

$$k_{cu} = aT^b_{w_{Cu}} e^{cT_{w_{Cu}} + d/T_{w_{Cu}}} \tag{B.22}$$

where the constants, a, b, c and d, are given by

$$\begin{aligned} a &= 82.56648 \\ b &= 0.262301 \\ c &= -4.06701 \times 10^{-4} \\ d &= 59.72934 \end{aligned}$$

The temperature, $T_{w_{Cu}}$, is in Kelvins with an initial value taken from the inner-tube outer-wall temperatures. With the heat transfer rate known, an inner-wall temperature is calculated from which the average of the inner- and outer-wall temperatures is used to recalculate the thermal conductivity. This process is repeated until the solution converges. The uncertainty in the thermal conductivity was given as 0.13%.

Wall resistance

The inner-tube wall resistance is defined as

$$R_w = \frac{\ln(D_o/D_i)}{2\pi k_{cu} L_{hx}} \tag{B.23}$$

with its uncertainty being given by

$$\delta R_w = \left[\left(\frac{\partial R_w}{\partial D_o} \delta D_o \right)^2 + \left(\frac{\partial R_w}{\partial D_i} \delta D_i \right)^2 + \left(\frac{\partial R_w}{\partial k_{cu}} \delta k_{cu} \right)^2 + \left(\frac{\partial R_w}{\partial L_{hx}} \delta L_{hx} \right)^2 \right]^{1/2} \tag{B.24}$$

$$\delta R_w = \left[\left(\frac{\delta D_o}{2\pi D_o k_{cu} L_{hx}} \right)^2 + \left(\frac{-\delta D_i}{2\pi D_i k_{cu} L_{hx}} \right)^2 + \left(\frac{-\ln(D_o/D_i)}{2\pi k_{cu}^2 L_{hx}} \delta k_{cu} \right)^2 + \left(\frac{-\ln(D_o/D_i)}{2\pi k_{cu} L_{hx}^2} \delta L_{hx} \right)^2 \right]^{1/2} \tag{B.25}$$

Inner-wall temperature

With the outer-wall temperature and thermal conductivity known, the inner-wall temperature of the inner tube could be calculated from

$$\bar{T}_{wi} = Q_i R_w + \bar{T}_{wo} \tag{B.26}$$

with its uncertainty being calculated from

$$\delta \bar{T}_{wi} = \left[\left(\frac{\partial \bar{T}_{wi}}{\partial Q_i} \delta Q_i \right)^2 + \left(\frac{\partial \bar{T}_{wi}}{\partial R_w} \delta R_w \right)^2 + \left(\frac{\partial \bar{T}_{wi}}{\partial \bar{T}_{wo}} \delta \bar{T}_{wo} \right)^2 \right]^{1/2}$$

$$\delta \bar{T}_{wi} = \left[(R_w \delta Q_i)^2 + (Q_i \delta R_w)^2 + \left(\delta \bar{T}_{wo} \right)^2 \right]^{1/2} \tag{B.27}$$

Overall heat transfer coefficient

The overall heat transfer coefficient is defined as

$$U = \frac{Q_i}{A T_{lmtd}} \tag{B.28}$$

To simplify calculations, it is better to write this equation in terms of Q_i and T_{lmtd} only, or

$$\mathrm{UA} = \frac{Q_i}{T_{lmtd}} \tag{B.29}$$

The uncertainty in UA is given by

$$\delta \mathrm{UA} = \left[\left(\frac{\partial \mathrm{UA}}{\partial Q_i} \delta Q_i \right)^2 + \left(\frac{\partial \mathrm{UA}}{\partial T_{lmtd}} \delta T_{lmtd} \right)^2 \right]^{1/2} \tag{B.30}$$

$$\delta \mathrm{UA} = \left[\left(\frac{\delta Q_i}{T_{lmtd}} \right)^2 + \left(\frac{-Q_i \delta T_{lmtd}}{T_{lmtd}^2} \right)^2 \right]^{1/2} \tag{B.31}$$

Log-mean temperature difference

The log-mean temperature difference is given as

$$T_{lmtd} = \frac{\left(\bar{T}_{iin} - \bar{T}_{oout}\right) - \left(\bar{T}_{iout} - \bar{T}_{oin}\right)}{\ln\left(\frac{\left(\bar{T}_{iin} - \bar{T}_{oout}\right)}{\left(\bar{T}_{iout} - \bar{T}_{oin}\right)}\right)} \tag{B.32}$$

with its uncertainty being determined by

$$\delta T_{lmtd} = \left[\left(\frac{\partial T_{lmtd}}{\partial \bar{T}_{iin}} \delta \bar{T}_{iin} \right)^2 + \left(\frac{\partial T_{lmtd}}{\partial \bar{T}_{oout}} \delta \bar{T}_{oout} \right)^2 + \left(\frac{\partial T_{lmtd}}{\partial \bar{T}_{iout}} \delta \bar{T}_{iout} \right)^2 + \left(\frac{\partial T_{lmtd}}{\partial \bar{T}_{oin}} \delta \bar{T}_{oin} \right)^2 \right]^{1/2} \tag{B.33}$$

$$\delta T_{lmtd} = \left[\left(\left\{ \frac{1}{\ln\left(\frac{\left(\bar{T}_{iin}-\bar{T}_{oout}\right)}{\left(\bar{T}_{iout}-\bar{T}_{oin}\right)}\right)} - \frac{\left(\bar{T}_{iin}-\bar{T}_{oout}\right)-\left(\bar{T}_{iout}-\bar{T}_{oin}\right)}{\ln\left(\frac{\left(\bar{T}_{iin}-\bar{T}_{oout}\right)}{\left(\bar{T}_{iout}-\bar{T}_{oin}\right)}\right)^2 \left(\bar{T}_{iin}-\bar{T}_{oout}\right)} \right\} \delta\bar{T}_{iin} \right)^2 + \left(\left\{ -\frac{1}{\ln\left(\frac{\left(\bar{T}_{iin}-\bar{T}_{oout}\right)}{\left(\bar{T}_{iout}-\bar{T}_{oin}\right)}\right)} + \frac{\left(\bar{T}_{iin}-\bar{T}_{oout}\right)-\left(\bar{T}_{iout}-\bar{T}_{oin}\right)}{\ln\left(\frac{\left(\bar{T}_{iin}-\bar{T}_{oout}\right)}{\left(\bar{T}_{iout}-\bar{T}_{oin}\right)}\right)^2 \left(\bar{T}_{iin}-\bar{T}_{oout}\right)} \right\} \delta\bar{T}_{oout} \right)^2 + \left(\left\{ -\frac{1}{\ln\left(\frac{\left(\bar{T}_{iin}-\bar{T}_{oout}\right)}{\left(\bar{T}_{iout}-\bar{T}_{oin}\right)}\right)} + \frac{\left(\bar{T}_{iin}-\bar{T}_{oout}\right)-\left(\bar{T}_{iout}-\bar{T}_{oin}\right)}{\ln\left(\frac{\left(\bar{T}_{iin}-\bar{T}_{oout}\right)}{\left(\bar{T}_{iout}-\bar{T}_{oin}\right)}\right)^2 \left(\bar{T}_{iout}-\bar{T}_{oin}\right)} \right\} \delta\bar{T}_{iout} \right)^2 + \left(\left\{ \frac{1}{\ln\left(\frac{\left(\bar{T}_{iin}-\bar{T}_{oout}\right)}{\left(\bar{T}_{iout}-\bar{T}_{oin}\right)}\right)} - \frac{\left(\bar{T}_{iin}-\bar{T}_{oout}\right)-\left(\bar{T}_{iout}-\bar{T}_{oin}\right)}{\ln\left(\frac{\left(\bar{T}_{iin}-\bar{T}_{oout}\right)}{\left(\bar{T}_{iout}-\bar{T}_{oin}\right)}\right)^2 \left(\bar{T}_{iout}-\bar{T}_{oin}\right)} \right\} \delta\bar{T}_{oin} \right)^2 \right]^{1/2} \tag{B.34}$$

Heat transfer coefficients

The uncertainties of the heat transfer coefficients for the single-stream heat exchanger model and the LMTD method will now be determined, respectively. For the single-stream model, the inner-fluid bulk temperature first needs to be determined before the heat transfer coefficient can be calculated. For the LMTD method, the calculation of the annulus heat transfer coefficient needs to be determined, and then combined with the overall heat transfer coefficient to obtain the inner-fluid heat transfer coefficient.

Single-stream method

The inner-fluid bulk temperature was obtained assuming a single-stream heat exchanger model. Experimentally, this was obtained by enforcing a constant wall temperature boundary condition. The inner-fluid temperature then has a logarithmic profile given by

$$T_i(x) = \bar{T}_{wi} + \left(\bar{T}_{iin} - \bar{T}_{wi}\right) e^{\frac{-UP}{\dot{m}_i c_{pi}} x} \tag{B.35}$$

Integrating over the length of the heat exchanger, the average inner-fluid temperature is then obtained from

$$\bar{T}_i = \bar{T}_{wi} - \frac{\left(\bar{T}_{iin} - \bar{T}_{wi}\right) \dot{m}_i c_{pi}}{\mathrm{UA}} e^{\frac{-\mathrm{UA}}{\dot{m}_i c_{pi}}} + \frac{\dot{m}_i c_{pi}}{\mathrm{UA}} \left(\bar{T}_{iin} - \bar{T}_{wi}\right) \tag{B.36}$$

The uncertainty in the inner-fluid temperature is then obtained by

$$\delta\bar{T}_i = \left[\left(\frac{\partial \bar{T}_i}{\partial \bar{T}_{wi}} \delta\bar{T}_{wi}\right)^2 + \left(\frac{\partial \bar{T}_i}{\partial \bar{T}_{iin}} \delta\bar{T}_{iin}\right)^2 + \left(\frac{\partial \bar{T}_i}{\partial \dot{m}_i} \delta\dot{m}_i\right)^2 + \left(\frac{\partial \bar{T}_i}{\partial c_{pi}} \delta c_{pi}\right)^2 + \left(\frac{\partial \bar{T}_i}{\partial \mathrm{UA}} \delta\mathrm{UA}\right)^2\right]^{1/2} \tag{B.37}$$

Therefore,

$$\delta\bar{T}_i = \left[\left(\left\{1+\frac{\dot{m}_i c_{pi}}{\mathrm{UA}}e^{\frac{-UA}{\dot{m}_i c_{pi}}}-\frac{\dot{m}_i c_{pi}}{\mathrm{UA}}\right\}\delta T_{wi}\right)^2+\left(\left\{\frac{\dot{m}_i c_{pi}}{\mathrm{UA}}e^{\frac{-UA}{\dot{m}_i c_{pi}}}+\frac{\dot{m}_i c_{pi}}{\mathrm{UA}}\right\}\delta\bar{T}_{iin}\right)^2+\left(\left\{\frac{-\left(\bar{T}_{iin}-\bar{T}_{wi}\right)c_{pi}}{\mathrm{UA}}e^{\frac{-UA}{\dot{m}_i c_{pi}}}+\frac{\left(\bar{T}_{iin}-\bar{T}_{wi}\right)c_{pi}}{\mathrm{UA}}-\frac{\left(\bar{T}_{iin}-\bar{T}_{wi}\right)}{\dot{m}_i}e^{\frac{-UA}{\dot{m}_i c_{pi}}}\right\}\delta\dot{m}_i\right)^2+\left(\left\{\frac{-\left(\bar{T}_{iin}-\bar{T}_{wi}\right)\dot{m}_i}{\mathrm{UA}}e^{\frac{-UA}{\dot{m}_i c_{pi}}}+\frac{\left(\bar{T}_{iin}-\bar{T}_{wi}\right)\dot{m}_i}{\mathrm{UA}}-\frac{\left(\bar{T}_{iin}-\bar{T}_{wi}\right)}{c_{pi}}e^{\frac{-UA}{\dot{m}_i c_{pi}}}\right\}\delta c_{pi}\right)^2+\left(\left\{\frac{\left(\bar{T}_{iin}-\bar{T}_{wi}\right)\dot{m}_i c_{pi}}{(\mathrm{UA})^2}e^{\frac{-UA}{\dot{m}_i c_{pi}}}-\frac{\left(\bar{T}_{iin}-\bar{T}_{wi}\right)\dot{m}_i c_{pi}}{(\mathrm{UA})^2}+\frac{\left(\bar{T}_{iin}-\bar{T}_{wi}\right)}{\mathrm{UA}}e^{\frac{-UA}{\dot{m}_i c_{pi}}}\right\}\delta\mathrm{UA}\right)^2\right]^{1/2} \tag{B.38}$$

The heat transfer coefficient is then obtained from

$$\alpha_i = \frac{q_i}{\bar{T}_i - \bar{T}_{wi}} \tag{B.39}$$

with its uncertainty being given by

$$\delta\alpha_i = \left[\left(\frac{\partial\alpha_i}{\partial q_i}\delta q_i\right)^2+\left(\frac{\partial\alpha_i}{\partial\bar{T}_i}\delta\bar{T}_i\right)^2+\left(\frac{\partial\alpha_i}{\partial\bar{T}_{wi}}\delta\bar{T}_{wi}\right)^2\right]^{1/2}$$

$$\delta\alpha_i = \left[\left(\frac{\delta q_i}{\bar{T}_i-\bar{T}_{wi}}\right)^2+\left(\frac{-q_i\delta\bar{T}_i}{\left(\bar{T}_i-\bar{T}_{wi}\right)^2}\right)^2+\left(\frac{q_i\delta\bar{T}_{wi}}{\left(\bar{T}_i-\bar{T}_{wi}\right)^2}\right)^2\right]^{1/2} \tag{B.40}$$

LMTD method

For the LMTD method, the annulus heat transfer coefficient needs to be obtained. Since the inner-tube outer-wall temperatures as well as the annulus wall temperatures are measured, this

heat transfer coefficient can easily be obtained from

$$\alpha_o = \frac{q_i}{\bar{T}_{wo} - \bar{T}_{woo}} \tag{B.41}$$

Since the annulus wall temperatures were measured at five different positions along the length of the tube, the average annulus wall temperature was obtained by using the same procedure followed to obtain the average temperature for the inner-tube's wall. The uncertainty of this temperature was found to be 0.022°C.

The uncertainty in the annulus heat transfer coefficient is then

$$\delta\alpha_o = \left[\left(\frac{\partial\alpha_o}{\partial q_i}\delta q_i\right)^2 + \left(\frac{\partial\alpha_o}{\partial\bar{T}_{wo}}\delta\bar{T}_{wo}\right)^2 + \left(\frac{\partial\alpha_o}{\partial\bar{T}_{woo}}\delta\bar{T}_{woo}\right)^2\right]^{1/2} \tag{B.42}$$

$$\delta\alpha_o = \left[\left(\frac{\delta q_i}{\bar{T}_{wo} - \bar{T}_{woo}}\right)^2 + \left(-\frac{q_i\delta\bar{T}_{wo}}{\left(\bar{T}_{wo} - \bar{T}_{woo}\right)^2}\right)^2 + \left(\frac{q_i\delta\bar{T}_{woo}}{\left(\bar{T}_{wo} - \bar{T}_{woo}\right)^2}\right)^2\right]^{1/2} \tag{B.43}$$

The inner-fluid heat transfer coefficient is then given as

$$\alpha_i = \frac{1}{A_i}\left[\frac{1}{\mathrm{UA}} - R_w - \frac{1}{\alpha_o A_o}\right]^{-1} \tag{B.44}$$

and its uncertainty being

$$\delta\alpha_i = \left[\left(\frac{\partial\alpha_i}{\partial A_i}\delta A_i\right)^2 + \left(\frac{\partial\alpha_i}{\partial \mathrm{UA}}\delta \mathrm{UA}\right)^2 + \left(\frac{\partial\alpha_i}{\partial R_w}\delta R_w\right)^2 + \left(\frac{\partial\alpha_i}{\partial\alpha_o}\delta\alpha_o\right)^2 + \left(\frac{\partial\alpha_i}{\partial A_o}\delta A_o\right)^2\right]^{1/2} \tag{B.45}$$

$$\begin{aligned}\delta\alpha_i = \Bigg[&\left(-\frac{\delta A_i}{A_i^2}\left[\frac{1}{\mathrm{UA}} - R_w - \frac{1}{\alpha_o A_o}\right]^{-1}\right)^2 + \\ &\left(\frac{\delta \mathrm{UA}}{A_i \mathrm{UA}^2}\left[\frac{1}{\mathrm{UA}} - R_w - \frac{1}{\alpha_o A_o}\right]^{-2}\right)^2 + \\ &\left(\frac{\delta R_w}{A_i}\left[\frac{1}{\mathrm{UA}} - R_w - \frac{1}{\alpha_o A_o}\right]^{-2}\right)^2 + \\ &\left(\frac{\delta\alpha_o}{A_i A_o \alpha_o^2}\left[\frac{1}{\mathrm{UA}} - R_w - \frac{1}{\alpha_o A_o}\right]^{-2}\right)^2 + \\ &\left(\frac{\delta A_o}{A_i A_o^2 \alpha_o}\left[\frac{1}{\mathrm{UA}} - R_w - \frac{1}{\alpha_o A_o}\right]^{-2}\right)^2\Bigg]^{1/2}\end{aligned} \tag{B.46}$$

Dimensionless Parameters

Since all fluid flows and heat transfer equations are in terms of dimensionless parameters, the uncertainties of these parameters need to be determined. The parameters mainly used are the Reynolds number, Prandtl number and Nusselt number. These are defined with their respective uncertainties as

$$Re = \frac{\dot{m} D_h}{A_c \mu} \tag{B.47}$$

$$\delta Re = \left[\left(\frac{\partial Re}{\partial \dot{m}} \delta \dot{m} \right)^2 + \left(\frac{\partial Re}{\partial A_c} \delta A_c \right)^2 + \left(\frac{\partial Re}{\partial D_h} \delta D_h \right)^2 + \left(\frac{\partial Re}{\partial \mu} \delta \mu \right)^2 \right]^{1/2} \tag{B.48}$$

$$\therefore \delta Re = \left[\left(\frac{D_h \delta \dot{m}}{A_c \mu} \right)^2 + \left(-\frac{\dot{m} D_h}{A_c^2 \mu} \delta A_c \right)^2 + \left(\frac{\dot{m} \delta D_h}{A_c \mu} \right)^2 + \left(-\frac{\dot{m} D_h}{A_c \mu^2} \delta \mu \right)^2 \right]^{1/2} \tag{B.49}$$

$$Pr = \frac{\mu c_p}{k} \tag{B.50}$$

$$\delta Pr = \left[\left(\frac{\partial Pr}{\partial \mu} \delta \mu \right)^2 + \left(\frac{\partial Pr}{\partial c_p} \delta c_p \right)^2 + \left(\frac{\partial Pr}{\partial k} \delta k \right)^2 \right]^{1/2} \tag{B.51}$$

$$\therefore \delta Pr = \left[\left(\frac{c_p \delta \mu}{k} \right)^2 + \left(\frac{\mu \delta c_p}{k} \right)^2 + \left(-\frac{\mu c_p \delta k}{k^2} \right)^2 \right]^{1/2} \tag{B.52}$$

$$Nu = \frac{\alpha D_h}{k} \tag{B.53}$$

$$\delta Nu = \left[\left(\frac{\partial Nu}{\partial \alpha} \delta \alpha \right)^2 + \left(\frac{\partial Nu}{\partial D_h} \delta D_h \right)^2 + \left(\frac{\partial Nu}{\partial k} \delta k \right)^2 \right]^{1/2} \tag{B.54}$$

$$\therefore \delta Nu = \left[\left(\frac{D_h \delta \alpha}{k} \right)^2 + \left(\frac{\alpha \delta D_h}{k} \right)^2 + \left(-\frac{\alpha D_h \delta k}{k^2} \right)^2 \right]^{1/2} \tag{B.55}$$

Friction Factors

The friction factors are calculated from its definition which is given as

$$f = \frac{2 D_i \Delta p}{\rho_i u_i^2 L_{\Delta p}} \tag{B.56}$$

The uncertainty in friction factor is then calculated as follows:

$$\delta f = \left[\left(\frac{\partial f}{\partial D_i} \delta D_i \right)^2 + \left(\frac{\partial f}{\partial \Delta p} \delta \Delta p \right)^2 + \left(\frac{\partial f}{\partial \rho_i} \delta \rho_i \right)^2 + \left(\frac{\partial f}{\partial u_i} \delta u_i \right)^2 + \left(\frac{\partial f}{\partial L_{\Delta p}} \delta L_{\Delta p} \right)^2 \right]^{1/2} \tag{B.57}$$

$$\delta f = \left[\left(\frac{2\Delta p \delta D_i}{\rho_i u_i^2 L_{\Delta p}} \right)^2 + \left(\frac{2D_i \delta \Delta p}{\rho_i u_i^2 L_{\Delta p}} \right)^2 + \left(-\frac{2D_i \Delta p \delta \rho_i}{\rho_i^2 u_i^2 L_{\Delta p}} \right)^2 + \left(-\frac{4D_i \Delta p \delta u_i}{\rho_i u_i^3 L_{\Delta p}} \right)^2 + \left(-\frac{2D_i \Delta p \delta L_{\Delta p}}{\rho_i u_i^2 L_{\Delta p}^2} \right)^2 \right]^{1/2} \tag{B.58}$$

B.4 Summary

The uncertainties of all the values discussed are given in Table B.3. Values for low and high Reynolds numbers are given.

Table B.3 Uncertainties of the equations used to obtain heat transfer and friction factors at low Reynolds numbers (≈ 500) and high Reynolds numbers ($\approx 15\ 000$).

Property	Low Re	High Re
$\dot{m}_i$	0.28%	0.10%
$\dot{m}_o$	0.10%	0.11%
$\bar{T}_{iin/iout}$ & $\bar{T}_{oin/oout}$	0.073°C	0.058°C
$\bar{T}_{woo}$	0.047°C	0.047°C
$\bar{T}_{wo}$	0.017°C	0.021°C
$\bar{T}_{wi}$	0.017°C	0.021°C
$\bar{T}_i$	0.389°C	0.111°C
T_{lmtd}	0.383°C	0.070°C
$\dot{Q}_i$	0.32%	0.24%
UA	3.9%	0.41%
Re	1.04%	1.01%
Nu	4.21%	1.15%
Pr	1.97%	1.42%
Δp	18%	0.12%
α_i	4.09%	0.57%
f	18%	0.30%

Appendix C

Wilson Plot Technique

The Wilson Plot method, first developed by Wilson (1915) and then modified by Briggs and Young (1969), is a method employed to obtain heat transfer coefficient data for heat exchangers when direct measurements are hard to obtain. It makes use of the experimentally determined overall heat transfer coefficient in a two-fluid exchanger and the individual resistances which it relates to. This relation has the form

$$\frac{1}{UA} = \frac{1}{\alpha_i A_i} + R_w + \frac{1}{\alpha_o A_o} \tag{C.1}$$

The heat transfer coefficient on the shell- and tube-side was obtained from the Sieder and Tate (1936) relations given by

$$Nu_o = C_o Re_o^d Pr_o^{0.4} \left(\frac{\mu_o}{\mu_{wo}}\right)^{0.14} \tag{C.2}$$

$$Nu_i = C_i Re_i^{0.8} Pr_i^{1/3} \left(\frac{\mu_i}{\mu_{wi}}\right)^{0.14} \tag{C.3}$$

Rearranging Equation (C.1) and employing Equations (C.2) and (C.3) for the heat transfer coefficients, the following expression is obtained:

$$\left[\frac{1}{UA} - R_w\right]\left[Re^d Pr^{0.4}\frac{kA}{D_h}\right]_o \left(\frac{\mu}{\mu_w}\right)_o^{0.14} = \frac{1}{C_i}\left\{\frac{\left[Re^d Pr^{0.4}\frac{kA}{D_h}\right]_o \left(\frac{\mu}{\mu_w}\right)_o^{0.14}}{\left[Re^{0.8} Pr^{1/3}\frac{kA}{D_h}\right]_i \left(\frac{\mu}{\mu_w}\right)_i^{0.14}}\right\} + \frac{1}{C_o} \tag{C.4}$$

Equation (C.4) has the form $y = mx + b$ where $m = \frac{1}{C_i}$ and $b = \frac{1}{C_o}$. The data is plotted on a graph, as shown in Figure C.1, and the slope and intersect are determined (due to the length

of Equation (C.4), the x- and y-axes in Figure C.1 are only shown as x and y). With the new values of C_i, a new heat transfer coefficient is determined from Equation (C.3). With this and the heat transfer rate obtained from experimental data known, a new wall temperature can be determined. This wall temperature is used to obtain the viscosity ratio of Equation (C.4). This process is repeated until C_i converges. For this process to have started, an appropriate initial value for d had to be chosen. A good value would be the value found in the Sieder and Tate (1936) equation, being $d = 0.8$.

Once C_i has converged, Equations (C.1), (C.2) and (C.3) are rearranged to obtain the following equation:

$$\left[\frac{1}{UA} - R_w - \frac{1}{C_i\left[Re^{0.8}Pr^{1/3}\frac{kA}{D_h}\right]_i\left(\frac{\mu}{\mu_w}\right)_i^{0.14}}\right] \times \left[Pr^{0.4}\frac{kA}{D_h}\right]_o\left(\frac{\mu}{\mu_w}\right)_o^{0.14} = \frac{1}{C_o Re_o^d} \tag{C.5}$$

Equation (C.5) can be rewritten in the form

$$\frac{1}{y_o} = C_o Re_o^d \tag{C.6}$$

$$\ln\left(\frac{1}{y_o}\right) = d\ \ln\left(Re_o\right) + \ln\left(C_o\right) \tag{C.7}$$

where y_o is the left side of Equation (C.5). Once again, this equation is in the form of $y = mx+b$ where $m = d$ is the slope and $b = \ln(C_o)$ the intersect. An example is given in Figure C.2. With the new value of d and C_o determined, the whole process is repeated. This continues until the constants, C_i, C_o and d, converge to a set limit.

The data required for the Wilson Plot method is obtained by capturing in- and outlet temperatures of both the inner tube and annulus as well as the flow rates for both. A requirement to obtain reasonable Wilson Plot results is that sufficient data be collected for the two main resistances, that is, the inner and annulus heat transfer coefficients. This is obtained by keeping one of the flows, say the annulus, constant while cycling through a set of inner-tube flow rates. After one cycle, the annulus flow is then changed to a next value and the process is repeated.

The results of the modified Wilson Plot method showed that with the experimental data, the following values for the constants were obtained:

$$\begin{aligned} C_i &= 0.021597 \\ C_o &= 0.019828 \\ d &= 0.86181 \end{aligned}$$

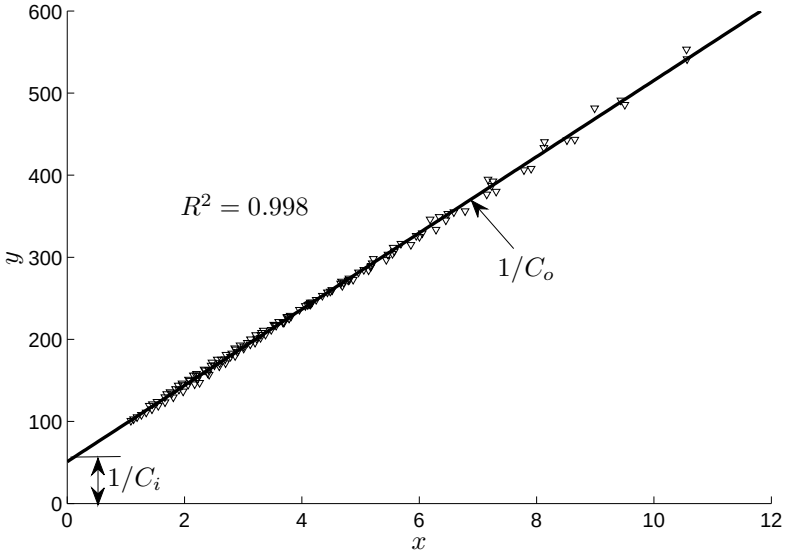

Figure C.1 Wilson Plot results for the inner tube.

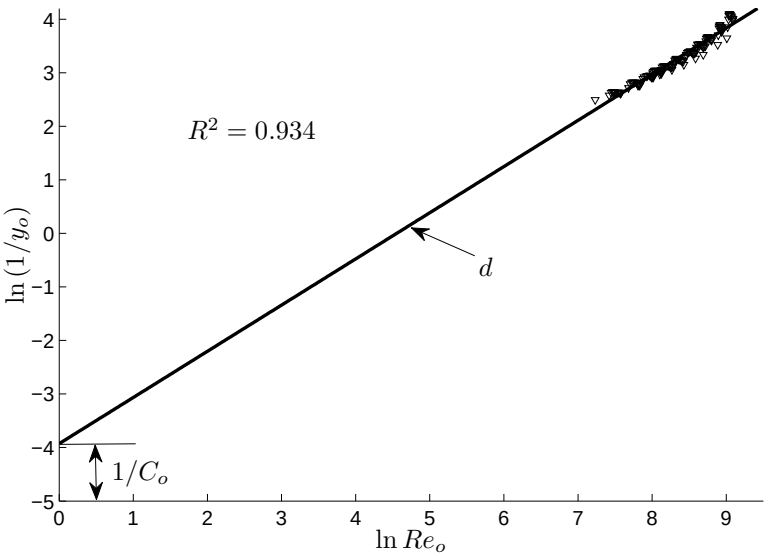

Figure C.2 Wilson Plot results for the annulus.

The data fits Equations (C.4) and (C.5) with an r-squared value of 0.998 and 0.934, respectively.

To summarise, the Sieder and Tate (1936) equations now have the following form:

$$Nu_o = 0.01983 Re_o^{0.8618} Pr_o^{0.4} \left(\frac{\mu_o}{\mu_{wo}}\right)^{0.14} \tag{C.8}$$

$$Nu_i = 0.02160 Re_i^{0.8} Pr_i^{1/3} \left(\frac{\mu_i}{\mu_{wi}}\right)^{0.14} \tag{C.9}$$